BEILSTEIN JOURNAL OF ORGANIC CHEMISTRY

Organic gelators and hydrogelators

Edited by Jean-Pierre Desvergne

Imprint

Beilstein Journal of Organic Chemistry
www.bjoc.org
ISSN 1860-5397
Email: journals-support@beilstein-institut.de

The *Beilstein Journal of Organic Chemistry* is published by the Beilstein-Institut zur Förderung der Chemischen Wissenschaften.

Beilstein-Institut zur Förderung der Chemischen Wissenschaften
Trakehner Straße 7–9
60487 Frankfurt am Main
Germany
www.beilstein-institut.de

Beilstein Journal of Organic Chemistry

Organic gelators and hydrogelators

Jean-Pierre Desvergne

Editorial

Open Access

Address:
Institut des Science Moléculaires, Université Bordeaux 1 - CNRS UMR 5255, 351 cours de la Libération, 33405 Talence Cedex, France

Email:
Jean-Pierre Desvergne - jp.desvergne@ism.u-bordeaux1.fr

Beilstein J. Org. Chem. **2010,** *6,* 846–847.
doi:10.3762/bjoc.6.99

Received: 27 July 2010
Accepted: 28 July 2010
Published: 21 September 2010

Guest Editor: J.-P. Desvergne

The design and control of molecular self-assembly is of great interest in the development of new molecular architectures with multiple desired functions or properties. In this context, the gelling systems formed by low molecular weight gelators are particularly promising and are the subject of an ever increasing number of studies.

A gel consists of one or more gelling agents and a fluid (organic solvent, water, supercritical liquid) which behaves as a viscoelastic material (soft matter) due to the immobilization of solvent molecules in a three-dimensional network. This network results from the self-assembly of the gelling agent into fibres via non-covalent interactions such as hydrogen bonding, π–π stacking, van der Waals and electrostatic interactions, coordination, and charge transfer. Additional non-covalent interactions lead to physical entanglement of the fibres, which creates a 3D network, the fluid being trapped in the nanoscale interstices. A very large quantity of solvent can be imprisoned in the supramolecular network (in the case of supergelators it is not rare to observe more than 10^4 molecules of solvent per molecule of gelator in the gel composition), thus creating extraordinary variations of the physical properties of the system. These physical gels are usually thermoreversible (reversible sol-gel transition by heating and cooling) and, depending on the molecular structure of the gelling agent and the fluid which is rigidified, it is possible to form nanoscale superstructures such as nanofibres, nanoribbons, nanosheets, nanoparticles, helical windings, etc., which are of interest for materials and nanoobject conception.

Thus, owing to their non-conventional behaviour, low molecular weight gelators are very attractive for applications in various areas, including supramolecular templates or matrices, transport and release of drugs, art conservation, cosmetics, sensors, optoelectronics, actuators, etc. However, despite numerous efforts to establish a structure-property relationship for the development of low molecular weight gelling agents, prediction of the gelling ability of a compound is not straightforward. A major challenge today is the rational design of small size molecular gelators coupled with an understanding of the mechanism of gelation. It is also important to develop future green gelators for eco-compatible applications.

This thematic series on organogels and hydrogels will address these various points with a particular emphasis on the molecular requirements on the gelling ability, the different approaches for producing molecular gelators, and some techniques used for the characterization and the properties of the gels.

It is my great pleasure to act as guest editor of this Thematic Series, which gathers a wide range of expertise to meet the

demands of this interdisciplinary field. I warmly thank all the authors who have enthusiastically accepted to contribute to this series which will give the reader a clear overview of this rapidly developing research field and will identify future growth areas.

Jean-Pierre Desvergne

Talence, July 2010

Beilstein Journal of Organic Chemistry

Chiral gels derived from secondary ammonium salts of (1*R*,3*S*)-(+)-camphoric acid

Tapas Kumar Adalder[1], N. N. Adarsh[1], Ravish Sankolli[2] and Parthasarathi Dastidar[*1]

Full Research Paper

Open Access

Address:
[1]Indian Association for the Cultivation of Science, Kolkata, India and [2]Indian Institute of Science, Bangalore, India

Email:
Tapas Kumar Adalder - tka.chem@yahoo.com;
N. N. Adarsh - ocann@iacs.res.in;
Parthasarathi Dastidar[*] - parthod123@rediffmail.com

* Corresponding author

Keywords:
crystal engineering; LMOG; single crystal X-ray diffraction; supramolecular gels; supramolecular synthon

Beilstein J. Org. Chem. **2010,** *6,* 848–858.
doi:10.3762/bjoc.6.100

Received: 01 July 2010
Accepted: 09 September 2010
Published: 21 September 2010

Guest Editor: J.-P. Desvergne

Abstract

In order to have access to chiral gels, a series of salts derived from (1*R*,3*S*)-(+)-camphoric acid and various secondary amines were prepared based on supramolecular synthon rationale. Out of seven salts prepared, two showed moderate gelation abilities. The gels were characterized by differential scanning calorimetry, table top rheology, scanning electron microscopy, single crystal and powder X-ray diffraction. Structure property correlation based on X-ray diffraction techniques remain inconclusive indicating that some of the integrated part associated with the gelation phenomena requires a better understanding.

Introduction

A gel is a two component system which is mainly liquid with a very little amount of solid. In gel state, gelator molecules form 3-D networks within which solvent molecules are trapped thus resulting in a gel. Depending on the nature of the network, gels can be of two kinds – chemical or polymeric and physical or supramolecular. While covalent bonds are responsible for the formation of 3-D networks in chemical gels, various non-covalent interactions such as hydrogen bonding, π-π stacking, hydrophobic, van der Waals forces etc. are required to form gel network in supramolecular gels. It is believed that in supramolecular gels, the gelator molecules self-assemble to form self-assembled fibrilar networks (SAFINs) which, by some means, are entangled to form 3-D gel networks within which the solvent molecules are immobilized via capillary force action to form gel. A gel with an organic solvent is called organogel whereas that obtained from water or an aqueous solvent mixture is known as a hydrogel. Among the various classes of supramolecular gelators, interest in low molecular mass organic gelators (LMOGs) [1-10] is a continuous expanding area on account of their various promising applications [11-13]. Broadly, LMOGs are used in cosmetics [14], tissue engineering [15], drug delivery and biomedical applications [16-19], art

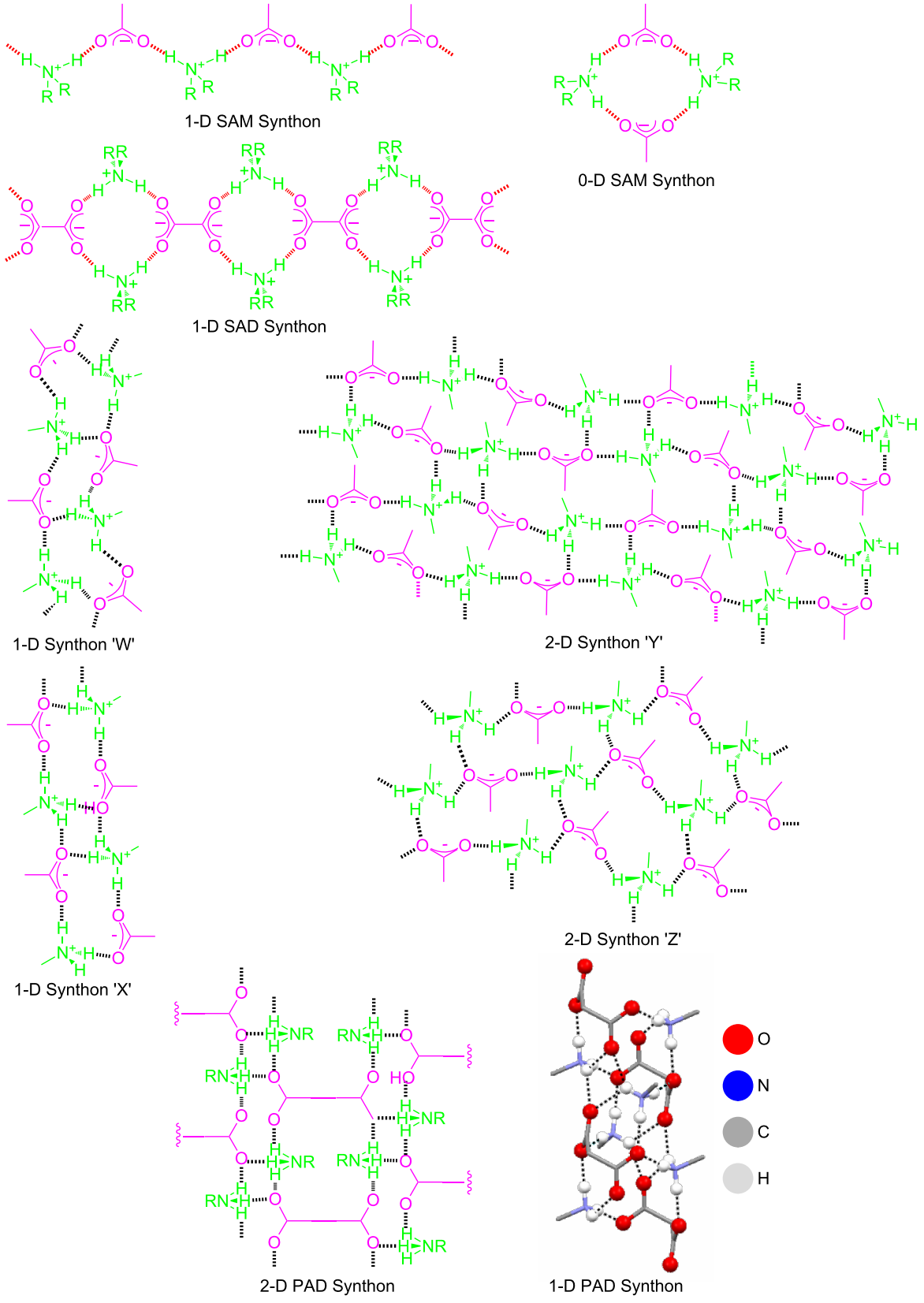

Scheme 1: Different types of 1-D and 2-D HBN forming supramolecular synthons.

conservation [20-22], templated synthesis of nanoparticles [23,24], capture and removal of pollutants [25], catalysis [26], sensors [27], electrooptics/photonics [28], structure-directing agents [29,30] etc. The gelator molecules form SAFINs typically when a hot solution containing a small amount of gelator is cooled below a critical temperature (sol-gel temperature); the SAFINs then start to entangle themselves to form a three dimensional network within which the solvent molecules are immobilized by capillary force interactions resulting in gel formation. The elegance of a LMOG lies in the reversible nature of the gel forming network and it is possible to tune the physical properties of the gel by applying external stimuli such as temperature, pH, sound waves [31], anions [32] etc.

The lack of understanding of the mechanism of gel formation at the molecular level makes it difficult to design a gelator. Most of gelling agents have been discovered serendipitously or derived from a known gelator scaffold. But recent advances in the supramolecular chemistry [33] and crystal engineering [34] has made it possible to design a gelator molecule in a rational manner by exploiting a supramolecular synthon [35] approach, at least for certain classes of gelling agents [3]. We have shown by correlating many single crystal structures of organic salts derived from various organic acids (both mono- and di-basic) and amines (both primary and secondary) with their gelling and non-gelling behavior that 1-D and 2-D forming supramolecular synthons such as secondary ammonium monocarboxylate (SAM) [36,37], secondary ammonium dicarboxylate (SAD) [38,39], primary ammonium monocarboxylate (PAM) [40,41] and primary ammonium dicarboxylate (PAD) [42,43] appear to play a crucial role in gel formation (Scheme 1).

In the present work we intend to exploit **SAD** synthons to make chiral gels. Supramolecular chirality is an important aspect in the development of chiral catalysts [26], chiro-optical switches [44], helical crystallization of proteins and inorganic replicas [45], chiral resolution [46] etc. For this purpose, we have reacted a dibasic acid such as (1*R*,3*S*)-(+)-camphoric acid with various secondary amines namely, dicyclohexylamine (DCHA), dipropylamine (DPA), dibutylamine (DBUA), diisobutylamine (DIBUA), dihexylamine (DHA), dibenzylamine (DBA) and di-*sec*-butylamine (DSBUA) in a 1:2 molar ratio (Scheme 2).

These salts were then used in gelation studies and the resulting gels characterized by table top rheology, differential scanning calorimetry (DSC), scanning electron microscopy (SEM), single- and powder X-ray diffraction (SXRD and PXRD, respectively). Single crystal structures of two gelators and one nongelator, i.e., DBUAMC **3,** DBAMC **6,** and DCHADC **1**, respectively were determined and discussed in the context of structure-property correlation.

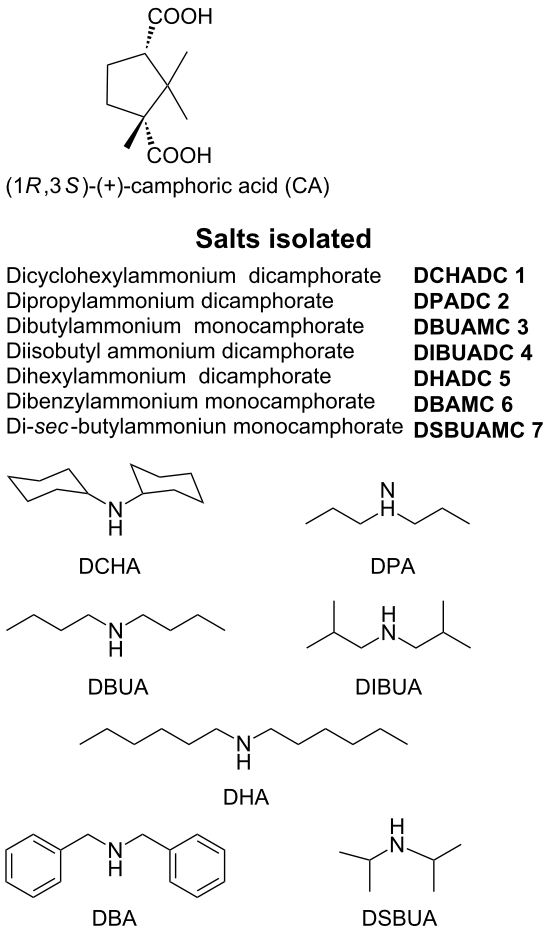

Scheme 2: Salts studied in the present report.

Results and Discussions

Synthesis

The salts were isolated as crystalline solids by the slow evaporation of a methanolic solution of the acid and the corresponding amine taken in an appropriate molar ratio. FT-IR spectra indicated that both the protons of the dicarboxylic acids were absent as was evident from the presence of the characteristic band of COO^- (1622–1635 cm^{-1}) and absence of COOH (1699 cm^{-1}) in salts **1**, **2**, **4** and **5**. However, the presence of FT-IR bands at 1701, 1631 cm^{-1} for salt **3**, 1705, 1548 cm^{-1} for salt **6** and 1701, 1620 cm^{-1} for salt **7** clearly indicated that 1:1 acid:amine salts were formed in these cases; satisfactory elemental analysis also support the formation of 1:1 salts **6** and **7** when the corresponding acid and the amines were deliberately reacted in a 1:1 molar ratio. However, that was not the case with salt **3** whose elemental analysis data did not match a 1:1 stoichiometry (see Experimental).

Gelation Studies

All the salts were scanned for gelation in various solvents. In a typical procedure, 20 mg of a salt was taken in a test tube

(10 mm × 100 mm) and dissolved in 0.5 ml of the solvent of choice by heating on a hot plate. The gel was obtained by keeping the solution undisturbed under ambient conditions (Table 1).

The salts DBUAMC **3** and DBAMC **6** gave stable gels with polar solvents such as nitrobenzene, and bromobenzene, chlorobenzene and 1,2-dichlorobenzene, respectively. The salt DBUAMC **3** also gave a partial gel (PG) with bromobenzene, chlorobenzene, 1,2-dichlorobenzene; a gel is called PG when the top layer of the solution becomes gel-like entrapping the flowing liquid underneath [47]. DHADC **5** gave a weak gel with nitrobenzene and 1,4 dioxane. Representative photomicrographs of the organogels are depicted in Figure 1.

To ascertain the thermoreversibility of the gel network, DSC was recorded on a selected gel sample derived from a ~4.0 wt % 1,2-dichlorobenzene solution of DBAMC **6** (Figure 2).

It is clear from the DSC data that the gelation was indeed thermoreversible. However, both the sol-gel and gel-sol transitions occur over a broad range of temperature making it difficult to assess the enthalpy change associated with this process. To get some idea about the enthalpy change associated with gel-sol, we carried out table top rheology [48] on some selected gels (Figure 3).

T_{gel} (gel-sol dissociation temperature) vs [gelator] plots on some selected gels displayed a steady increase of T_{gel} with the increase in [gelator] which indicated that, in the present cases,

Figure 1: Photomicrographs of the organogels (from left to right: nitrobenzene gel of DBUAMC **3**; 1,2-dichlorobenzene gel of DBAMC **6**; chlorobenzene gel of DBAMC **6**; bromobenzene gel of DBAMC **6**).

Table 1: Gelation data (CS = Clear solution, GP = Gelatinous precipitate, FC = Fibrous crystal, CP = crystalline precipitate, AP = Amorphous precipitate, WP = White precipitate, YP = Yellow precipitate, PG = Partial gel, WG = Weak gel, FGN = Fibrous gelatinous network, PLC = plate like crystal, WT = White turbidity).

Solvent	DCHDC 1	DPADC 2	DBUAMC 3	DIBUADC 4	DHADC 5	DBAMC 6	DSBUAMC 7
	MGC/Wt %	MGC/Wt %	MGC/Wt % (T_{gel}/°C)	MGC/Wt %	MGC/Wt %	MGC/Wt % (T_{gel}/°C)	MGC/Wt %
Bromobenzene	CS	FC	PG	FGP	WT	4.00 (98)	FC
Chlorobenzene	CS	WP	PG	FGP	WT	4.00 (110)	FC
1,2-Dichloro-benzene	CS	FC	PG	FC	WT	2.22 (106)	FC
Toluene	GP	CS	CS	CS	CS	AP	CS
o-Xylene	CS	CS	CS	CS	CS	AP	CS
m-Xylene	CS	CS	GP	CS	CS	CP	CS
p-Xylene	CS	CS	GP	CS	CS	CP	CS
Mesitylene	CS	CS	GP	CS	CS	WP	CS
Nitrobenzene	GP	YP	4.00 (78)	PLC	WG	YP	FC
1,4-Dioxane	FC	WP	FGN	FC	WG	AP	CS
Methylsalicylate	CS	CS	WG	PLC	CS	WP	SC
DMSO	FC	CS	FC	CS	FC	CS	CS
DMF	CP	CS	FC	CS	FC	CS	CS
EG	CS	CS	CS	CS	CS	FC	CS

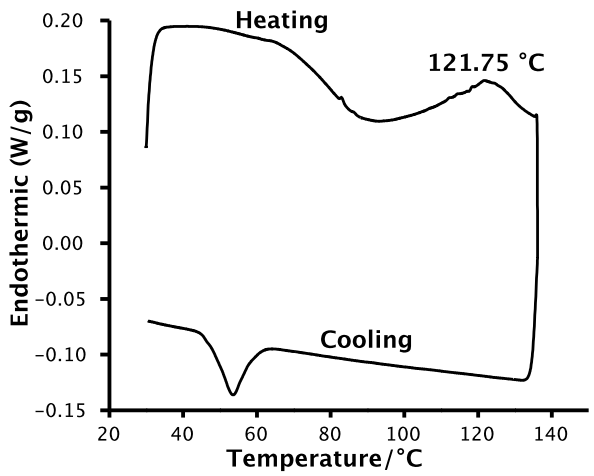

Figure 2: DSC of a 4.0 wt % 1,2-dichlorobenzene gel of DBAMC **6**.

self-assembly in the gel state was driven by strong supramolecular interactions such as hydrogen bonding. Application of the Schroeder-van Laar equation (Equation 1) resulted in a linear semilog plot (Figure 3), when the mole fraction of the gelator at each concentration was plotted against $1/T_{gel}$ K^{-1}.

$$\ln[gelator] = -(\Delta H_m / RT_{gel}) + const. \quad (1)$$

Where ΔH_m and T_{gel} are the enthalpy change and temperature associated with the gel-sol transition process, respectively and R is universal gas constant. Here it is considered that gel-sol transition is first order in nature on the assumption that the gel melts into an ideal solution wherein the exact amount of gel involved in the transition is known. The calculated ΔH value for DBAMC **6** is 60.9 kJ/mol and that of DBUAMC **3** is 56.5 kJ/mol, respectively which clearly indicates that 1,2-dichlorobenzene gel of DBAMC **6** is stronger than the nitrobenzene gel of DBUAMC **3**.

To see the morphological features of the gel fibers, some selected xerogels were subjected to SEM (Figure 4). Highly entangled networks of fibers were seen in the chlorobenzene and 1,2-dichlorobenzene xerogels of DBAMC **6**, whereas relatively short plate like morphology was observed in the nitrobenzene xerogel of DBUAMC **3**. Understandably, the solvent molecules are immobilized in these networks to form gel.

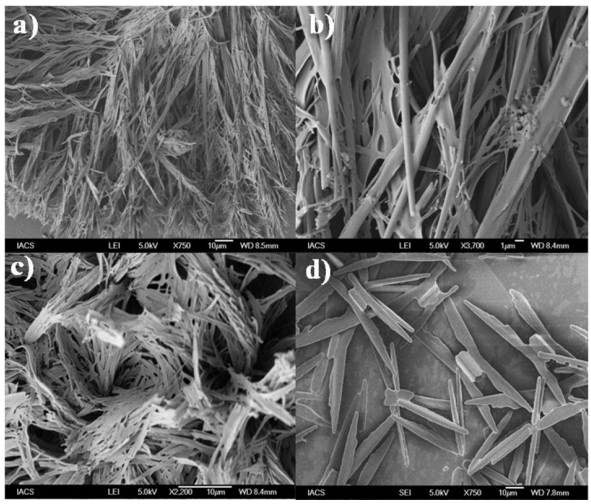

Figure 4: SEM micrographs of the xerogels. (a) & (b) 0.5 wt % 1,2-dichlorobenzene gel of DBAMC **6**; (c) 0.8 wt % chlorobenzene gel of DBAMC **6**; d) 0.5 wt % nitrobenzene gel of DBUAMC **3**.

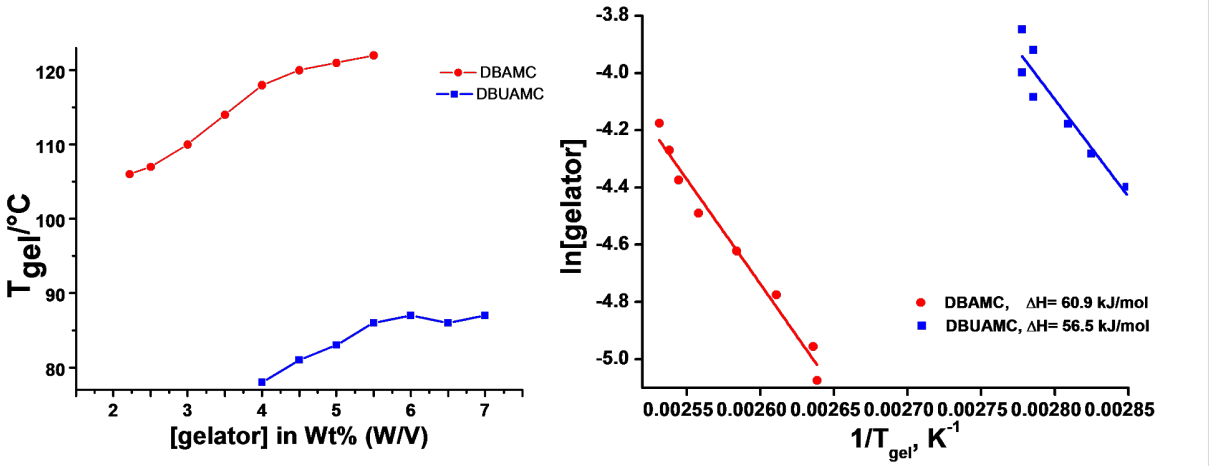

Figure 3: *Left* – T_{gel} vs [gelator] plot; *right* – semilog plot of mole fraction of the gelators against $1/T$; 1,2-Dichlorobenzene and nitrobenzene gels were used for DBAMC **6** and DBUAMC **3**, respectively.

To prove structure-property correlation in these gelators, we tried to crystallize as many salts as possible. However, our best efforts resulted in the crystallization of only three salts, DBUAMC **3**, DBAMC **6** and DCHADC **1**, which were examined by single crystal X-ray diffraction (Table 2).

The crystal of DBUAMC **3** isolated from ethylene glycol/methanol mixture belongs to the orthorhombic space group $P2_12_12_1$. The carboxylic acid moiety shows the C–O distances as 1.241(3)–1.272(3) and 1.197(4)–1.300(4) Å which is indicative of the presence of both COOH and COO^-. FT-IR data also support this observation (1701 and 1631 cm^{-1}). The presence of a secondary ammonium cation is also evident from the strong peak at 2960 cm^{-1} with multiple bands extending to 2411 cm^{-1}. In the crystal structure, the butylammonium cation is disordered over two positions. The strongest hydrogen bonding donor, the charge assisted secondary ammonium cation, form hydrogen bonds with the strongest hydrogen bonding acceptor COO^-; interestingly, the COO^- forms hydrogen bonding with two crystallographically equivalent dibutylammonium cations [N…O = 2.725(7)–3.040(6) Å]. On the other hand, the COOH moiety forms hydrogen bonding only with COO^- [O…O = 2.614(3) Å; ∠ O–H…O = 176.9°]. Such hydrogen bonding interactions lead to the formation of a 3-D hydrogen bonded network (Figure 5).

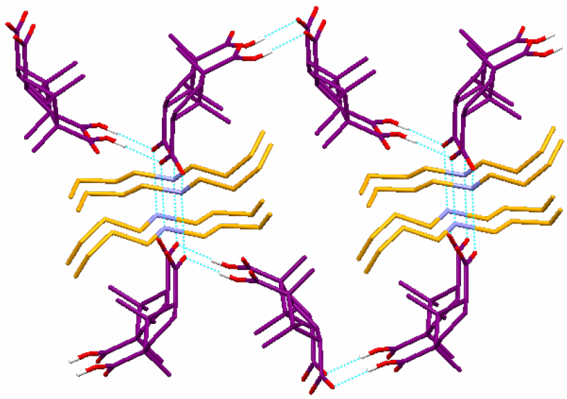

Figure 5: Crystal structure illustration of DBUAMC **3**; 3-D hydrogen bonded network; only one part of the disordered ammonium cation and hydrogen atom associated with carboxylic moiety are shown for clarity.

Crystals of DBAMC **6** suitable for single crystal X-ray diffraction study were grown from mesitylene. It crystallized in the non-centrosymmetric monoclinic space group $P2_1$. The C–O

Table 2: Crystallographic data.

Crystal parameters	DBUAMC 3	DBAMC 6	DCHADC 1
Empirical formula	$C_{18}H_{33}NO_4$	$C_{24}H_{31}NO_4$	$C_{34}H_{62}N_2O_4$
Formula weight	327.45	397.50	562.86
Crystal size/mm	0.46 × 0.38 × 0.28	0.24 × 0.19 × 0.12	0.28 × 0.16 × 0.12
Crystal system	Orthorhombic	Monoclinic	Monoclinic
Space group	$P2_12_12_1$	$P2_1$	$P2_1$
a / Å	8.6977(9)	6.6454(3)	12.2424(15)
b / Å	12.5877(13)	17.9624(9)	17.278(2)
c / Å	18.8825(19)	9.3062(4)	16.7260(19)
α / °	90.00	90.00	90.00
β / °	90.00	98.981(4)	98.199(2)
γ / °	90.00	90.00	90.00
Volume / $Å^3$	2067.3(4)	1097.24(9)	3501.8(7)
Z	4	2	4
F(000)	720	428	1248
μ MoKα / mm^{-1}	0.073	0.081	0.068
Temperature / K	298(2)	100(2)	298(2)
R_{int}	0.0368	0.0397	0.0453
Range of *h*, *k*, *l*	−10/10, −14/9, −17/22	−10/10, −7/7, −18/17	−12/13, −18/13, −17/16
θmin / max / °	1.94 /25.00	2.49/26.00	1.23 / 22.50
Reflections collected/unique/observed [I>2σ(I)]	8622 /3609 /3015	11570/4209/2685	11933/6369/5344
Data/restraints/parameters	3609/0/204	4209/1/266	6369/1/727
Goodness of fit on F^2	1.090	0.923	1.219
Final R indices [I>2σ(I)]	R_1 = 0.0724 wR_2 = 0.2043	R_1 = 0.0462 wR_2 = 0.1039	R_1 = 0.1042 wR_2 = 0.2406
R indices (all data)	R_1 = 0.0820 wR_2 = 0.2230	R_1 = 0.0845 wR_2 = 0.1153	R_1 = 0.1194 wR_2 = 0.2529

distances of the carboxylic acid moieties are 1.237(2)–1.270(3) Å and 1.193(3)–1.309(3) Å indicating that only one COOH group is deprotonated. This is also evident in the FT-IR spectra of **6** wherein bands characteristic of COOH (1705 cm^{-1}) and COO^- (1548 cm^{-1}) were observed. A strong band at 2974 cm^{-1} with multiple bands extending to 2445 cm^{-1} also supports the existence of secondary ammonium cation. In the crystal structure, the strongest hydrogen bonding donor, the charge assisted secondary ammonium cation, and the acceptor (the carboxylate anion) are involved in hydrogen bonding [N…O = 2.711(2)–2.752(2) Å; ∠ N^+–H…O = 161.3–168.6°] resulting in 1-D hydrogen bonded network. The COOH group bridges such 1-D chains by O–H…O hydrogen bonding [O…O = 2.570(2) Å; ∠ O–H…O = 161.38°] involving COOH and COO^- resulting into a overall 2-D hydrogen bonded sheet that runs along the c-axis. The 2-D sheets are further packed in a parallel fashion along the b-axis sustained by weak π-π stacking interactions (3.926 Å) involving the phenyl groups of the neighboring 2-D sheets (Figure 6).

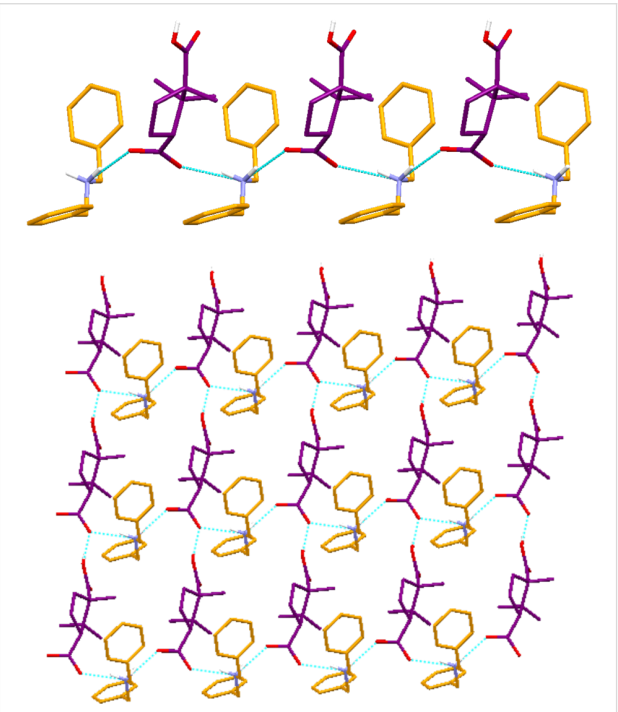

Figure 6: Crystal structure illustrations of DBAMC **6**; *top* – propagation 1-D network involving ammonium and carboxylate ions; *bottom* – overall 2-D hydrogen bonded network.

Crystals of DCHADC **1** was grown from m-xylene. It was crystallized in the non-centrosymmetric monoclinic space group $P2_1$. The C–O distance of the carboxylic acid moieties are 1.226(10)–1.259(10)) Å and 1.226(10)–1.233(11) Å indicating that both the COOH groups are deprotonated which is consistent with the FT-IR data. The appearance of one band at 1622 cm^{-1} and absence of COOH band at 1699 cm^{-1} for the parent acid suggest that both the carboxylic acid groups are deprotonated. A strong band at 2928 cm^{-1} with multiple bands extending to 2362 cm^{-1} also supports the existence of secondary ammonium cation. In the crystal structure, the strongest hydrogen bonding donor, the charge assisted secondary ammonium cation, and the acceptor – the carboxylate anion – undergo hydrogen bonding [N…O = 2.653(9)–2.742(10) Å; ∠ N^+–H…O = 159.5–169.1°] resulting in 1-D zigzag hydrogen bonded network. Because of the bifunctionality of the camphorate moiety, this network propagates in one direction, resulting in 1-D zigzag networks, which are arranged in a parallel fashion in the crystal lattice (Figure 7).

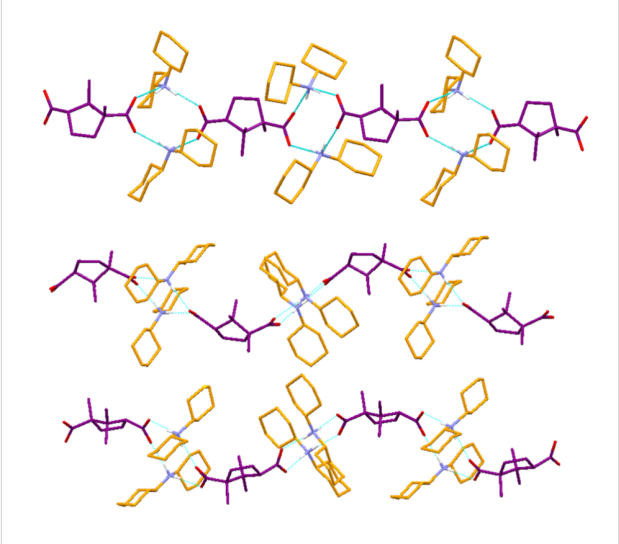

Figure 7: Illustration of crystal structure of DCHADC **1**; *top* – 1-D hydrogen bonded zigzag chain displaying SAD synthon; *bottom* – packing of such zigzag chains.

Thus, it is clear that both salts **3** and **6** are1:1 acid:base salts and obviously do not possess SAD moieties, whereas salt **1**, which is a 1:2 acid:amine salt, does indeed have a SAD synthon. However, salts **3** and **6** were able to gel a few solvents, whilst salt **1** failed to gel any of the solvents studied herein. It may be recalled here that 2-D hydrogen bonded networks (such as in the salts **3** and **6**) have been shown to play a crucial role in gelation [3]. The failure of the salt **1**, displaying 1-D SAD synthon, to form gels once again points to the need for a better understanding of gel fiber and solvent interactions.

To see if these crystal structures of **3** and **6** (as discussed above) truly represent the bulk solid as well as the xerogels, we undertook detailed PXRD studies. The comparison plot involving simulated, bulk and xerogel PXRDs for both the salts do not match which indicate the presence of other morphs in the bulk as well as in the corresponding xerogels. The single crystal

structure of the salt **1** also appears to be unrepresentative of its bulk as evident from the PXRD comparison plots of the simulated and bulk solid (Figure 8).

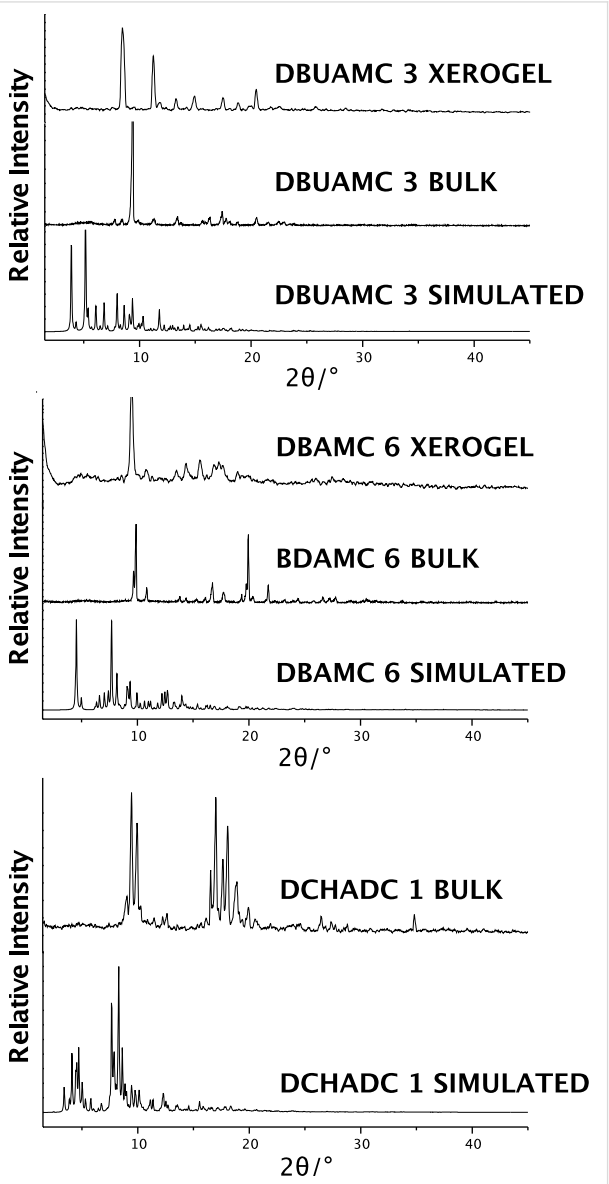

Figure 8: PXRD patterns of salts **3**, **6** and **1** under various conditions.

Conclusion

We have synthesized a series of secondary ammonium salts of (1*R*,3*S*)-(+)-camphoric acid following the rationale of supramolecular synthon in order to have an easy access to chiral gels. Out of seven salts prepared, four were 1:2 acid:amine salts, whereas the others were 1:1 salts. Two 1:1 salts, i.e., DBUAMC **3** and DBAMC **6** were found to be moderate gelling agents. The rest of the salts were either non-gelators or showed weak gelation abilities. Table top rheology data suggest that the 1,2-dichlorobenzene gel of DBAMC **6** is stronger than the nitrobenzene gel of DBUAMC **3**. Attempts to correlate the structure with gelling/non-gelling behavior based on various X-ray diffraction techniques was inconclusive as the PXRD patterns of the simulated, bulk and xerogel do not match in both the gelators. Moreover, salt **1** which displayed 1-D SAD synthon failed to gel any of the solvents studied herein indicating that many factors that might be crucial for gelation such as the nucleation of gel fiber, kinetics of gel fiber growth, their self-assembly to form SAFINs and their interactions with the solvent molecules etc. are needed for a deeper understanding. Although we were successful in achieving an easy access to few chiral gels following this supramolecular synthon approach, this study clearly indicates that some of the integrated parts associated with the gelation phenomena require to be better understood before a straightforward design strategy for synthesizing gelling agents can be formulated.

Experimental

Materials and physical measurements

All the reagents were obtained from various commercial sources (Sigma-Alrdrich, S. D. Fine Chemical,India etc.) and used as such without further purification. Solvents were of L. R. grade (Ranchem, Spectrochem, India etc.) and were used without further distillation. Melting points were determined by Veego programmable melting point apparatus, India. IR spectra were obtained on a FT-IR instrument (FTIR-8300, Shimadzu). The elemental compositions of the purified compounds were confirmed by elemental analysis (Perkin-Elmer Precisely, Series-II, CHNO/S Analyzer-2400). Scanning electron microscopy (SEM) was carried out with a JEOL, JMS-6700F, Field Emission Scanning Electro Microscope. Differential Scanning Calorimetry (DSC) was recorded with a Perkin-Elmer, Diamond DSC. Powder X-ray patterns were recorded on a Bruker AXS D8 Advance Powder (Cu Kα1 radiation, λ = 1.5406 Å) diffractometer.

General Synthetic Procedure

The salts were synthesized by reacting the acid and the corresponding amine in a 1:2 molar ratio (except for DBUAMC **3**, DBAMC **6** and DSBUAMC **7** where the stoichiometry of acid and amine were 1:1) in MeOH in a beaker. The resultant mixture was subjected to sonication for a few minutes to ensure the homogeneous mixing of the two components. The resulting mixture was then kept at room temperature from which a white solid was collected in near-quantitative yield after 1–2 days and then subjected to various physicochemical analyses and gelation test. All the salts were fully characterized by FT-IR and elemental analysis (except for DBUAMC **3** for which the elemental analysis data did match; however, other data such as FT-IR and single crystal X-ray indicated the formation of a 1:1 acid:amine salt).

T_{gel} Measurements

In a typical experiment, the salt was dissolved in the targeted solvent by heating. The solution was then allowed to cool to room temperature. Gel formation was confirmed by tube inversion. T_{gel} was measured by the dropping ball method; a glass ball weighing 242.0 mg was placed on a 0.5 mL gel in a test tube (10 × 100 mm). The tube was then immersed in an oil bath placed on a magnetic stirrer in order to ensure uniform heating. The temperature was noted when the ball touched the bottom of the tube.

Analytical data

DCHADC **1**: mp: 169–170 °C; FT-IR (cm^{-1}): 2928, 2854, 2793, 2725, 2698, 2667, 2521, 2440, 2422, 2362, 2343, 2206, 2104, 1622, 1535, 1498, 1452, 1386, 1354, 1311, 1282, 1267, 1236, 1215, 1172, 1124, 1068, 1053, 1033, 1010, 977, 922, 889, 848, 798, 750, 597, 559, 499, 449, 412; Elemental analysis calculated for $C_{34}H_{62}N_2O_4$: C, 72.55; H, 11.10; N, 4.98; Found: C, 72.42; H, 11.15; N, 5.05.

DPADC **2**: mp: 157–158 °C ; FT-IR (cm^{-1}): 2966, 2939, 2879, 2845, 2806, 2704, 2565, 2443, 1633, 1533, 1467, 1458, 1384, 1354, 1327, 1309, 1280, 1182, 1122, 1057, 916, 877, 798, 756, 690, 551, 532, 482, 434; Elemental analysis calculated for $C_{22}H_{46}N_2O_4$: C, 65.63; H, 11.52; N, 6.96; Found: C, 65.62; H, 11.36; N, 6.86.

DBUAMC **3:** mp: 167–168 °C ; FT-IR (cm^{-1}): 2960, 2933, 2874, 2837, 2785, 2580, 2478, 2411, 1701, 1631, 1537, 1462, 1383, 1354, 1329, 1311, 1284, 1259, 1172, 1124, 1080, 1057, 993, 914, 792, 754, 736, 476.

DIBUADC **4**: mp: 156–158 °C ; FT-IR (cm^{-1}): 2964, 2875, 2850, 2559, 2428, 2360, 2339, 1635, 1535, 1465, 1381, 1352, 1307, 1282, 1172, 1120, 1080, 1035, 993, 796,758, 682, 673, 476, 430; Elemental analysis calculated for $C_{26}H_{54}N_2O_4$: C, 68.08; H, 11.87; N, 6.11; Found: C,67.56; H,11.50; N, 5.77.

DHADC **5**: mp: 114–115 °C; FT-IR (cm^{-1}): 2958, 2931, 2860, 2575, 2459, 2418, 2364, 2341, 1631, 1539, 1464, 1381, 1354, 1327, 1313, 1280, 1215, 1170, 1122, 1080, 1062, 916, 796, 759, 729, 694, 547, 476; Elemental analysis calculated for $C_{33}H_{68}N_2O_4$: C, 71.17; H, 12.31; N, 5.03; Found: C,71.62; H,11.84; N, 4.97.

DBAMC **6**: mp: 184 °C; FT-IR (cm^{-1}): 3053, 3032, 2974, 2928, 2879, 2744, 2590, 2445, 1952, 1705, 1548, 1498, 1458, 1396, 1369, 1294, 1234, 1207, 1114, 1082, 1049, 1026, 983, 910, 881, 779, 742, 694, 484, 455. Elemental analysis calculated for $C_{24}H_{31}NO_4$: C, 72.52; H, 7.86; N, 3.52; Found: C, 72.27; H, 7.86; N, 3.37.

DSBUAMC **7**: mp: 116–117 °C; FT-IR (cm^{-1}): 2976, 2941, 2881, 2779, 2737, 2600, 2497, 2434, 1701, 1620, 1552, 1456, 1392, 1371, 1300, 1244, 1207, 1112, 1035,1008, 977, 792, 725, 547, 466, 435. Elemental analysis calculated for $C_{18}H_{35}NO_4$: C, 65.62; H, 10.71; N, 4.25; Found: C, 65.62; H, 10.14; N, 4.01.

X-ray single crystal data

Data were collected using MoKα (λ = 0.7107 Å) radiation on a BRUKER APEX II diffractometer equipped with CCD area detector. Data collection, data reduction, structure solution/ refinement were carried out using the software package of SMART APEX. All structures were solved by the direct method and refined in a routine manner. In most of the cases, non-hydrogen atoms were treated anisotropically. All the hydrogen atoms were geometrically fixed. CCDC (CCDC No. 782834–782836) contains the supplementary crystallographic data for this paper. These data can be obtained free of charge via http://www.ccdc.cam.ac.uk/conts/retrieving.html (or from the Cambridge Crystallographic Data Centre, 12 Union Road, Cambridge CB21EZ, UK; fax: (+44) 1223-336-033; or deposit@ccdc.cam.ac.uk).

Supporting Information

Supporting Information File 1

Cif file of crystal structure of **DBAMC 6**.
[http://www.beilstein-journals.org/bjoc/content/supplementary/1860-5397-6-100-S1.cif]

Supporting Information File 2

Cif file of crystal structure of **DBUAMC 3**.
[http://www.beilstein-journals.org/bjoc/content/supplementary/1860-5397-6-100-S2.cif]

Supporting Information File 3

Cif file of crystal structure of **DCHADC 1**.
[http://www.beilstein-journals.org/bjoc/content/supplementary/1860-5397-6-100-S3.cif]

Acknowledgements

TKA and PD thank CSIR, New Delhi for a JRF fellowship and financial grant, respectively.

References

1. Weiss, R. G.; Terech, P., Eds. *Molecular Gels. Materials with Self-Assembled Fibrillar Networks;* Springer: Dordrecht, The Netherlands, 2005.
2. Fages, F., Ed. *Low molecular mass gelators: Design, self-assembly, function;* Topics in Current Chemistry, Vol. 256; Springer: Berlin, Germany, 2005.

3. Dastidar, P. *Chem. Soc. Rev.* **2008,** *37,* 2699–2715. doi:10.1039/b807346e
4. Abdallah, D. J.; Weiss, R. G. *Adv. Mater.* **2000,** *12,* 1237–1247. doi:10.1002/1521-4095(200009)12:17<1237::AID-ADMA1237>3.0.CO;2-B
5. Terech, P.; Weiss, R. G. *Chem. Rev.* **1997,** *97,* 3133–3160. doi:10.1021/cr9700282
6. de Loos, M.; Feringa, B. L.; van Esch, J. H. *Eur. J. Org. Chem.* **2005,** 3615–3631. doi:10.1002/ejoc.200400723
7. Sangeetha, N. M.; Maitra, U. *Chem. Soc. Rev.* **2005,** *34,* 821–836. doi:10.1039/b417081b
8. Suzuki, M.; Hanabusa, K. *Chem. Soc. Rev.* **2009,** *38,* 967–975. doi:10.1039/b816192e
9. Estroff, L. A.; Hamilton, A. D. *Chem. Rev.* **2004,** *104,* 1201–1218. doi:10.1021/cr0302049
10. Piepenbrock, M. O. M.; Lloyd, G. O.; Clarke, N.; Steed, J. W. *Chem. Rev.* **2010,** *110,* 1960–2004. doi:10.1021/cr9003067
11. Hirst, A. R.; Escuder, B.; Miravet, J. F.; Smith, D. K. *Angew. Chem., Int. Ed.* **2008,** *47,* 8002–8018. doi:10.1002/anie.200800022
12. Smith, D. K. Molecular Gels - Nanostructured Soft Materials. In *Organic Nanostructures;* Atwood, J. L.; Steed, J. W., Eds.; Wiley-VCH: Weinheim, Germany, 2008.
13. Banerjee, S.; Das, R. K.; Maitra, U. *J. Mater. Chem.* **2009,** *19,* 6649–6687. doi:10.1039/b819218a
14. Wynne, A.; Whitefield, M.; Dixon, A. J.; Anderson, S. *J. Dermatol. Treat.* **2002,** *13,* 61–66. doi:10.1080/095466302317584403
15. Lee, K. Y.; Mooney, D. J. *Chem. Rev.* **2001,** *101,* 1869–1880. doi:10.1021/cr000108x
16. Bhuniya, S.; Seo, Y. J.; Kim, B. H. *Tetrahedron Lett.* **2006,** *47,* 7153–7156. doi:10.1016/j.tetlet.2006.08.002
17. Vemula, P. K.; Cruikshank, G. A.; Karp, J. M.; John, G. *Biomaterials* **2009,** *30,* 383–393. doi:10.1016/j.biomaterials.2008.09.045
18. Zhao, F.; Ma, M. L.; Xu, B. *Chem. Soc. Rev.* **2009,** *38,* 883–891. doi:10.1039/b806410p
19. Sreenivasachary, N.; Lehn, J.-M. *Chem.–Asian J.* **2008,** *3,* 134–139. doi:10.1002/asia.200700041
20. Carretti, E.; Dei, L. In *Molecular Gels. Materials with Self-Assembled Fibrillar Networks;* Weiss, R. G.; Terech, P., Eds.; Springer: Dordrecht, The Netherlands, 2005; pp 929–938.
21. Carretti, E.; Fratini, E.; Berti, D.; Dei, L.; Baglioni, P. *Angew. Chem., Int. Ed.* **2009,** *48,* 8966–8969. doi:10.1002/anie.200904244
22. Carretti, E.; Grassi, S.; Cossalter, M.; Natali, I.; Caminati, G.; Weiss, R. G.; Baglioni, P.; Dei, L. *Langmuir* **2009,** *25,* 8656–8662. doi:10.1021/la804306w
23. Palui, G.; Nanda, J.; Ray, S.; Banerjee, A. *Chem.–Eur. J.* **2009,** 6902–6909. doi:10.1002/chem.200900149
24. Ray, S.; Das, A. K.; Banerjee, A. *Chem. Commun.* **2006,** 2816–2818. doi:10.1039/b605498f
25. Adhikari, B.; Palui, G.; Banerjee, A. *Soft Matter* **2009,** *5,* 3452–3460. doi:10.1039/b905985g
26. Rodríguez-Llansola, F.; Miravet, J. F.; Escuder, B. *Chem. Commun.* **2009,** 7303–7305. doi:10.1039/b916250j
27. Murata, K.; Aoki, M.; Nishi, T.; Ikeda, A.; Shinkai, S. *J. Chem. Soc., Chem. Commun.* **1991,** 1715–1718. doi:10.1039/C39910001715
28. Ajayaghosh, A.; Praveen, V. K.; Vijayakumar, C. *Chem. Soc. Rev.* **2008,** *37,* 109–122. doi:10.1039/b704456a
29. van Bommel, K. J. C.; Friggeri, A.; Shinkai, S. *Angew. Chem., Int. Ed.* **2003,** *42,* 980–999. doi:10.1002/anie.200390284
30. Sreenivasachary, N.; Lehn, J.-M. *Proc. Natl. Acad. Sci. U. S. A.* **2005,** *102,* 5938–5943. doi:10.1073/pnas.0501663102
31. Cravotto, G.; Cintas, P. *Chem. Soc. Rev.* **2009,** *38,* 2684–2697. doi:10.1039/b901840a
32. Maeda, H. *Chem.–Eur. J.* **2008,** 11274–11282. doi:10.1002/chem.200801333
33. Lehn, J.-M. *Angew. Chem., Int. Ed.* **1988,** *27,* 89–112. doi:10.1002/anie.198800891
34. Desiraju, G. R. *Angew. Chem., Int. Ed.* **2007,** *46,* 8342–8356. doi:10.1002/anie.200700534
35. Desiraju, G. R. *Angew. Chem., Int. Ed.* **1995,** *34,* 2311–2327. doi:10.1002/anie.199523111
36. Trivedi, D. R.; Dastidar, P. *Cryst. Growth Des.* **2006,** *6,* 2114–2121. doi:10.1021/cg060325c
37. Trivedi, D. R.; Ballabh, A.; Dastidar, P. *J. Mater. Chem.* **2005,** *15,* 2606–2614. doi:10.1039/b504969e
38. Sahoo, P.; Kumar, D. K.; Trivedi, D. R.; Dastidar, P. *Tetrahedron Lett.* **2008,** *49,* 3052–3055. doi:10.1016/j.tetlet.2008.03.060
39. Trivedi, D. R.; Ballabh, A.; Dastidar, P. *Cryst. Growth Des.* **2006,** *6,* 763–768. doi:10.1021/cg050590i
40. Das, U. K.; Trivedi, D. R.; Adarsh, N. N.; Dastidar, P. *J. Org. Chem.* **2009,** *74,* 7111–7121. doi:10.1021/jo901463k
41. Ballabh, A.; Adalder, T. K.; Dastidar, P. *Cryst. Growth Des.* **2008,** *8,* 4144–4149. doi:10.1021/cg800613d
42. Sahoo, P.; Adarsh, N. N.; Chacko, G. E.; Raghavan, S. R.; Puranik, V. G.; Dastidar, P. *Langmuir* **2009,** *25,* 8742–8750. doi:10.1021/la9001362
43. Ballabh, A.; Trivedi, D. R.; Dastidar, P. *Org. Lett.* **2006,** *8,* 1271–1274. doi:10.1021/ol053000i
44. Guo, P.; Zhang, L.; Liu, M. *Adv. Mater.* **2006,** *18,* 177–180. doi:10.1002/adma.200501047
45. Ihara, H.; Takafuji, M.; Sakurai, T. In *Encyclopedia of Nanoscience and Nanotechnology;* Nalwa, H. S., Ed.; American Scientific Publishers: Stevenson Ranch, CA, 2004; Vol. 9, pp 473–495.
46. Bunzen, J.; Kiehne, U.; Benkhäuser-Schunk, C.; Lützen, A. *Org. Lett.* **2009,** *11,* 4786–4789. doi:10.1021/ol901958v
47. Yamanaka, M.; Fujii, H. *J. Org. Chem.* **2009,** *74,* 5390–5394. doi:10.1021/jo900894q
48. Raghavan, S. R.; Cipriano, B. H. In *Molecular Gels. Materials with Self-Assembled Fibrillar Networks;* Weiss, G.; Terech, P., Eds.; Springer: Dordrecht, The Netherlands, 2005; p 241.

Beilstein Journal of Organic Chemistry

Pyridinium based amphiphilic hydrogelators as potential antibacterial agents

Sayanti Brahmachari, Sisir Debnath, Sounak Dutta and Prasanta Kumar Das*

Full Research Paper

Open Access

Address:
Department of Biological Chemistry, Indian Association for the Cultivation of Science, Jadavpur, Kolkata – 700 032, India. Fax: +(91)-33-24732805

Email:
Prasanta Kumar Das* - bcpkd@iacs.res.in

* Corresponding author

Keywords:
antibacterial; bilayer structure; hydrogel; pyridinium; self-assembly

Beilstein J. Org. Chem. **2010,** *6,* 859–868.
doi:10.3762/bjoc.6.101

Received: 05 May 2010
Accepted: 15 July 2010
Published: 21 September 2010

Guest Editor: J.-P. Desvergne

Abstract

The numerous applications of hydrogelators have led to rapid expansion of this field. In the present work we report the facile synthesis of amphiphilic hydrogelators having a quaternary pyridinium unit coupled to a hydrophobic long alkyl chain through an amide bond. Different amphiphiles with various hydrophobic chain length and polar head groups were rationally designed and synthesized to develop a structure-property relation. A judicious combination of hydrophilic and hydrophobic segments led to the development of pyridinium based amphiphilic hydrogelators having a minimum gelation concentration of 1.7%, w/v. Field emission scanning electronic microscopy (FESEM), atomic force microscopy (AFM), photoluminescence, FTIR studies, X-ray diffraction (XRD) and 2D NOESY experiments were carried out to elucidate the different non-covalent interactions responsible for the self-assembled gelation. The formation of three-dimensional supramolecular aggregates originates from the interdigitated bilayer packing of the amphiphile leading to the development of an efficient hydrogel. Interestingly, the presence of the pyridinium scaffold along with the long alkyl chain render these amphiphiles inherently antibacterial. The amphiphilic hydrogelators exhibited high antibacterial activity against both Gram-positive and Gram-negative bacteria with minimum inhibitory concentration (MIC) values as low as 0.4 μg/mL. Cytotoxicity tests using MTT assay showed 50% NIH3T3 cell viability with hydrogelating amphiphile **2** up to 100 μg/mL.

Introduction

Gels are an outstanding group of soft materials lying at the interface of solid and liquid, and find numerous applications in various fields including tissue engineering, biosensors, food processing, cosmetics, photography, controlled drug delivery etc. [1-11]. Amongst the variety of gels, hydrogels (those that entrap water) are of special importance owing to their tremendous potential in biomedicine [12-16]. These hydrogels can be of natural origin [17] (collagens, polysaccharides) as well as of synthetic origin [18] (poly(acrylic acid) and derivatives, polypeptides and small molecules). This fascinating class of

materials results from the spontaneous self-assembly of polymeric/non-polymeric molecules that lead to the formation of supramolecular three dimensional (3D) networks with interstitial space for the immobilization of solvents. Low-molecular-weight-gelators (LMWG) have received more attention than their polymeric analogues for a number of scientific applications due to their thermo-reversible nature and their prompt response to external stimuli [19]. A critical balance between hydrophilic and hydrophobic interactions is mandatory for any gelation process. Non-covalent interactions such as hydrogen bonding, ionic interactions, π–π stacking or van der Waals forces play a pivotal role in self-assembled gelation [12]. Tuning the structure of gelator molecules leads to a better understanding of the contribution of the different interactive forces and an insight into the 3D-morphology of supramolecular aggregates [20-22]. In this context, low molecular weight hydrogels (LMWH) are of greater importance compared to polymeric ones as the former (i) can have diversified supramolecular morphology by varying the structure of its precursor molecules, (ii) have the ability for quick response to external stimuli, and (iii) are potentially biocompatible [12,23,24]. Thus, the huge range of applications of the hydrogels and the beneficial aspects of small molecule gelators including ease of preparation have synergistically led to a surge in the development of tailor-made LMWHs.

The presence of an aromatic ring (for example, phenyl, naphthalene, *N*-fluorenyl-9-methoxycarbonyl (Fmoc), indole, pyridine) in small molecule gelator is known to have crucial influence in inducing self-aggregation towards gelation. The planar aromatic moiety favors π–π stacking interactions between the molecules and leads to the formation of 3D networks of viscoelastic gels [25-27]. Interestingly, among all these aromatic rings, the positively charged pyridine (pyridinium) unit is well known to impart antibacterial properties to amphiphilic molecules [28-31]. The cationic charge of the amphiphile plays an instrumental role in disrupting the innate defense mechanism of microorganisms by disrupting the microbial cell membrane [32,33]. Hence, it would be interesting to develop amphiphilic hydrogelators that have pyridinium moieties in order to exploit its favorable π–π stacking interaction towards self-assembled gelation as well as an ability to kill bacteria. Furthermore, a very simple method of synthesizing such amphiphilic antibacterial hydrogelators with pyridinium units would definitely boost its importance and utility for a wide spectrum of applications.

In the present work, we report the facile synthesis of pyridinium based amphiphiles (**1**–**5**, Figure 1) of which amphiphiles **1** and **2** were efficient hydrogelators with minimum gelation concentrations (MGC) ≈1.7–2.0%, w/v. Modification of certain features of the amphiphiles such as the aliphatic chain length and the polar head group was systematically carried out to understand their influence on the self-assembled hydrogelation. The various factors involved in the formation of supramolecular aggregates leading to hydrogelation were studied using FTIR, XRD and fluorescence spectroscopy. The topographical features of the soft matter were visualized using different microscopic techniques (scanning electron microscopy (SEM), atomic force microscopy (AFM)). Interestingly, these compounds were found to show excellent antibacterial activity against Gram-positive and Gram-negative bacteria with minimum inhibitory concentration (MIC) values as low as 0.4 μg/mL for *Micrococcus luteus*. In addition, amphiphile **2** was investigated for cytotoxicity with mammalian cells (NIH3T3) and showed sufficient viability throughout a range of concentrations.

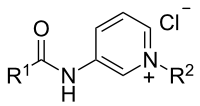

R^1	R^2	Amphiphile
$C_{17}H_{35}$	CH_3	**1**
$C_{15}H_{31}$	CH_3	**2**
$C_{13}H_{27}$	CH_3	**3**
$C_{15}H_{31}$	H	**4**
$C_{15}H_{31}$	C_2H_5	**5**

Figure 1: Structure of amphiphiles **1**–**5**.

Results and Discussion

Gelation is simply a macroscopic manifestation of the self-assembled aggregation at the molecular level due to the optimum combination of hydrophilic and hydrophobic interactions between molecules [12]. The formation, nature and morphology of these supramolecular 3D-networks are primarily dictated by the architecture of the gelating molecules. To establish the different nature of interactions taking place within the supramolecular assemblies, a structure-property correlation for the gelators is necessary. In the present work we have synthesized a series of amphiphilic compounds containing a quaternary pyridinium unit as the polar head group and varied the length of alkyl chain of the hydrophobic part (**1**–**5**, Figure 1) using very simple methodology (Scheme 1). Variation at the

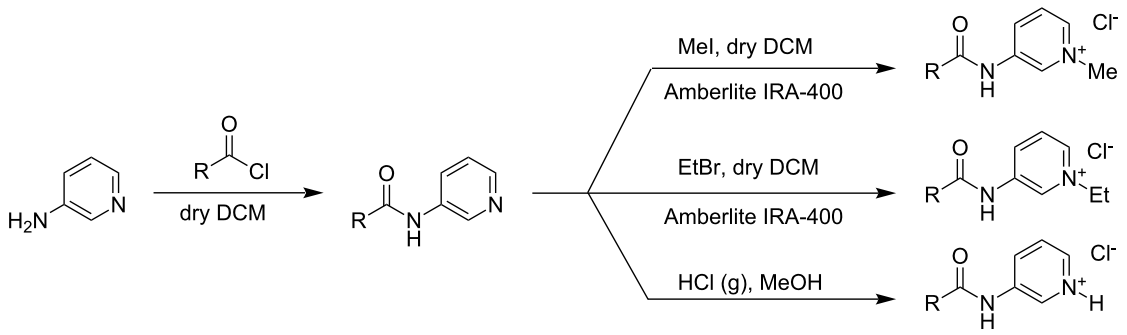

Scheme 1: Synthetic procedure of the amphiphiles.

hydrophilic as well as the hydrophobic segment was performed to understand the critical balance imperative for hydrogelation.

Amphiphile **1**, with a *N*-methylated pyridinium moiety as the polar head linked by a C-18 alkyl chain through an amide bond, exhibited efficient water gelation ability (MGC of 2.0%, w/v). The stable to inversion of container method confirmed the formation of gel. However, the hydrogel was not stable as the amphiphile precipitated from the gel after 4–5 h. It is possible that the C-18 alkyl chain is too hydrophobic to maintain the optimum hydrophilic–hydrophobic balance necessary for efficient gelation. Consequently, keeping all other segments identical as in **1**, the C-18 alkyl chain was replaced by a shorter alkyl chain, C-16 in case of amphiphile **2**. In accord with our expectations, amphiphile **2** exhibited better water gelation ability with a MGC of 1.7%, w/v. The transparent hydrogel of **2** was stable for several months. At this point, we were curious to know how the gelation efficiency would be affected by further lowering the alkyl chain length to C-14 (amphiphile **3**). However, compound **3** was found to be a non-gelator. A decrease in the hydrophobicity in amphiphile **3** possibly destroyed the hydrophilic–hydrophobic balance required for water gelation. Following the importance of the hydrophobic segment of the amphiphile in gelation, we were also interested to investigate the influence of the polar head group of the pyridinium-based amphiphiles in hydrogelation. To this end we made very minor modifications to the quaternized nitrogen of the pyridine moiety keeping other segments unaltered as in the efficient gelator **2**. *N*-methylated pyridinium of **2** was changed first of all to a simple protonated pyridinium moiety in amphiphile **4** and then to *N*-ethylated pyridinium group in the case of **5** (Figure 1). Neither of these amphiphiles exhibited any water gelation ability, which reiterates the importance of the optimum balance between hydrophilic and hydrophobic character within a molecule for gelation.

The gel-to-sol transition temperature (T_{gel}) for both the hydrogels was determined by placing the gel-containing glass vial (inner diameter = 10 mm) in a thermostated oil bath and raising the temperature slowly at a rate of 2 °C/min. T_{gel} is defined as the temperature (±0.5 °C) at which the gel melts and starts to flow from an inverted glass vial. Both hydrogels of **1** and **2** at their MGC showed T_{gel} at 35 and 36 °C, respectively. In agreement with the previous reports it was found that the T_{gel} of the hydrogels steadily increased with increase in gelator concentration (Figure 2) [34,35]. This clearly indicates the enhancement in the strength of the non-covalent intermolecular interaction in the aggregated state with increasing gelator concentration. Also the thermo-reversible nature of hydrogelation was established as the sol formed on heating returned to the gel state upon lowering the temperature. Interestingly, the T_{gel} curve of amphiphile **2** maintained a slightly higher profile throughout the range of the concentrations suggesting the comparatively better hydrogelation efficiency of **2** over that of **1**.

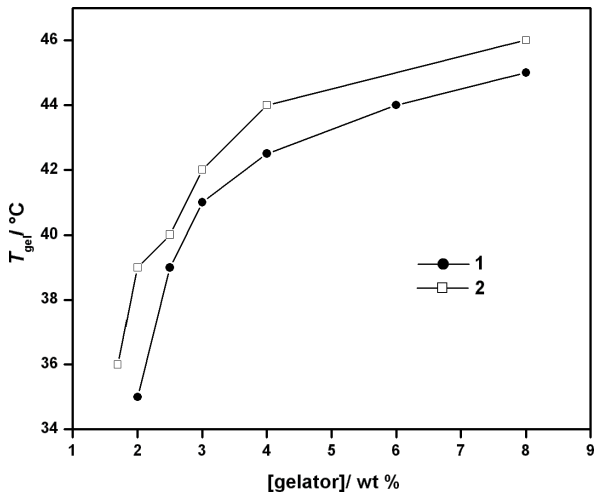

Figure 2: Variation of the T_{gel} with concentration of amphiphiles **1** and **2**.

The formation of three dimensional higher ordered structures during self-assembled hydrogelation was investigated by field

emission scanning electron microscopy (FESEM). Morphology of the dried xerogels showed the formation of different supramolecular structures that are involved in the gelation process of **1** and **2** (Figure 3). SEM image of hydrogel **1** showed an aggregated form of porous networks (Figure 3a), which were responsible for the entrapment of the solvent. In case of hydrogel **2**, formation of thin intertwined fibrillar networks of 200–300 nm dimensions (Figure 3b) was observed. The fibrillar architecture of **2** at the aggregated state was further confirmed by Atomic Force Microscopic (AFM) images. Two and three dimensional AFM images of xerogel **2** (Figure 3c, d) showed the involvement of fibrillar networks in self-assembled hydrogelation. The dimension of the fibril network observed in the AFM image was also in accord with the FESEM images.

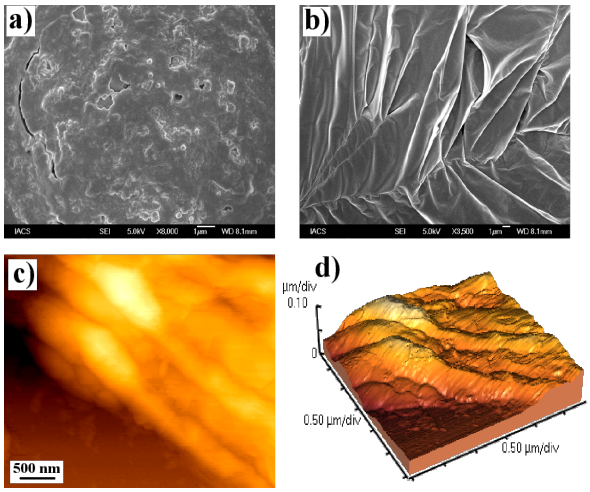

Figure 3: (a, b) FESEM images of the dried gels of **1** and **2**, respectively at their MGC. (c, d) Two- and three-dimensional AFM image of xerogel **2**.

The participation of the pyridinium ring in hydrogelation was investigated by taking the luminescence spectra of the efficient gelator **2** at various concentrations (0.01–3.0%, w/v) in water (Figure 4) at room temperature. The amphiphile **2** was excited at λ = 330 nm and the emission spectra were recorded between of 340–550 nm. At a very low concentrations (0.01%, w/v), **2** showed an emission peak at λ_{em} = 402 nm. With a gradual increase in the concentration of **2**, a steady increase in the fluorescence intensity was observed up to 0.035%, w/v. With further increase in the concentration of **2**, the fluorescence intensity decreased with a continuous red shift of the λ_{em} from 402 nm to 416 nm. The observed increase in the fluorescence intensity as well as continuous quenching of the signal after 0.035%, w/v to MGC and above is probably due to the interaction between the pyridinium ring and the cationic charge (Figure 4) [36]. Notably, the quenching in the emission of pyridine started at a concentration that is ≈50 times lower than the

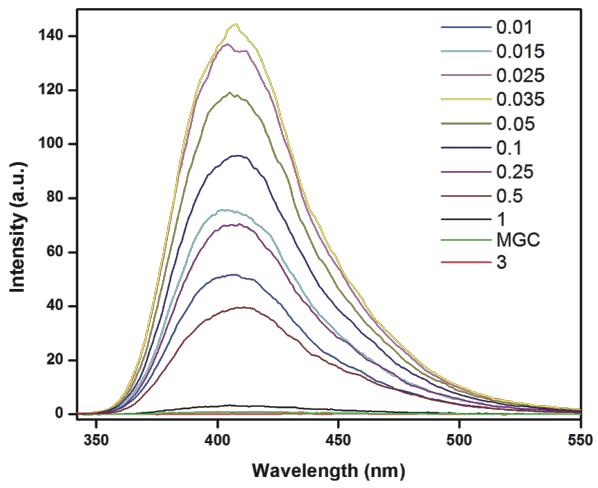

Figure 4: Luminescence spectra of **2** in water (λ_{ex} = 330 nm) at various concentrations and room temperature.

corresponding MGC which is also almost three times higher than its critical micellar concentration (0.011%, w/v). Hence, the amphiphile **2** began to self-assemble towards hydrogelation above 0.035%, w/v. Moreover, the red shifted emission peak up to MGC and above indicates that the intermolecular π–π interactions between the pyridine moieties plays an important role in gelation [28]. Consequently, the fluorescence quenching of pyridine by the cationic charge was due to the close proximity of the head groups during gelation.

To determine the involvement of intermolecular hydrogen bonding between the amide N–H and carbonyl oxygen we investigated both hydrogels by FTIR spectroscopy. As the presence of H_2O in FTIR spectroscopy may create difficulties in extracting information on intermolecular interactions, we measured the FTIR spectra of gelators **1** and **2** in D_2O (self-aggregated state) and in $CHCl_3$ (non-aggregated state). The absorption frequency for the C=O stretching band (amide I) in gels is always lower compared to that in $CHCl_3$. The transmission bands of C=O stretching for the gel **1** and **2** in D_2O appeared at 1660 and 1655 cm^{-1}, respectively, which is characteristic of hydrogen bonded amide groups (Figure 5). Whereas the corresponding amide I stretching frequency at 1700 and 1703 cm^{-1} for **1** and **2** in $CHCl_3$ demonstrates the existence of a non-hydrogen bonded amide group. Hydrogen bond formation is accompanied by a decrease in the bond order and hence the observed shift in the carbonyl stretching frequency to a lower value underlines the participation of intermolecular H-bonding in the gel state [37]. In addition, the N–H stretching frequency of amide for both gelators appeared at ≈3400 cm^{-1} in the gel state which was shifted to 3430 cm^{-1} in the non-aggregated form in $CHCl_3$. This shift in the N–H stretching confirms the

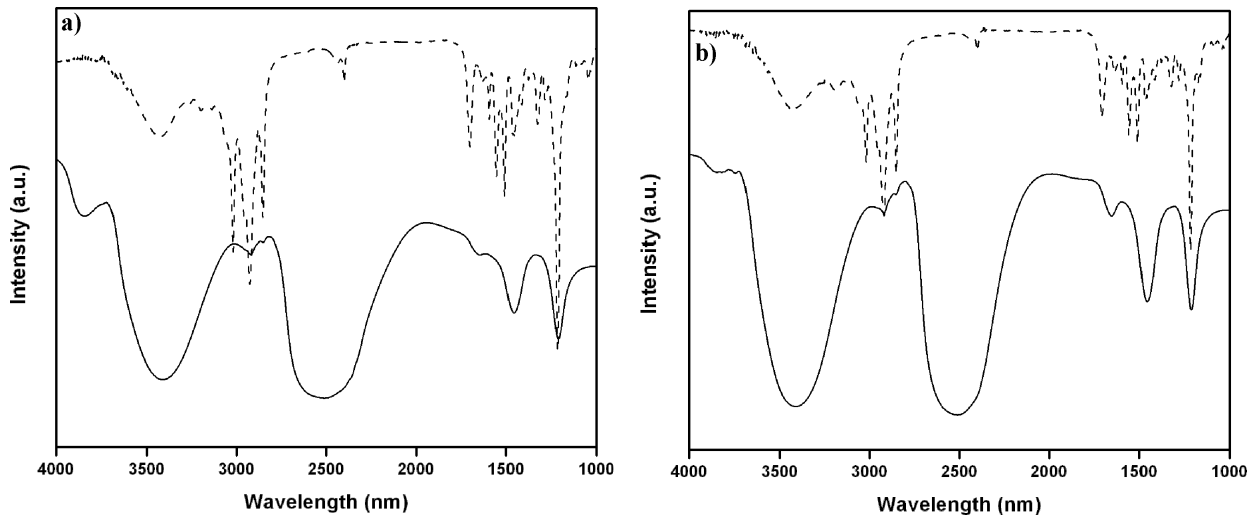

Figure 5: FTIR spectra of (a) **1** and (b) **2** in $CHCl_3$ solution (dashed line) and in D_2O at the gel state (solid line).

participation of the amide N-H in the intermolecular hydrogen bonding. Furthermore, the increase in intensity of the methylene scissoring vibration $\delta(CH_2)$ band at ≈1460 cm^{-1} for both the gelators (Figure 5) in D_2O indicates the high trans conformational packing of alkyl chain [38].

To establish further the intermolecular interaction between the gelators as noted above, we carried out 2D NOESY experiments for gelator **2** (2.0%, w/v) in the aggregated state in DMSO-d_6 in the presence of 70% water and also in the non self-assembled state of the amphiphile in neat DMSO-d_6. At 70% water content in DMSO-d_6, off-diagonal cross peaks were observed between the aromatic rings and the methyl group on the quaternized nitrogen of pyridine (Figure 6). The presence of off-diagonal peaks in the aggregated form clearly indicates the existence of through space interaction between the neighboring gelator molecules which plays a crucial role in gelation. No such off-diagonal peak was observed for **2** in neat DMSO-d_6 which is in accord with the absence of any kind of intermolecular interaction in the non-gelated state of the amphiphile.

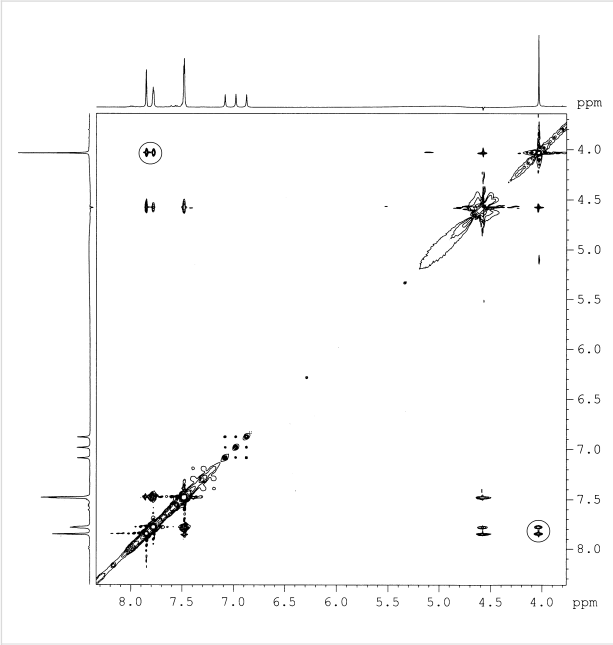

Figure 6: 2D-NOESY spectra of **2** (2%, w/v) in DMSO-d_6 with 70% water.

To investigate the molecular packing and orientation of the gelator molecules in the supramolecular self-assembled state, the xerogel of **2** was examined by X-ray diffraction (XRD). A sharp diffraction peak was obtained in the small angle region at $2\theta = 2.37°$ which corresponds to a *d*-spacing of 3.71 nm indicating an ordered arrangement of the molecules in the gel state (Figure 7). The observed *d*-spacing was greater than the length of a single surfactant molecule, 2.6 nm (calculated using MOPAC AMI method, CS Chem Office) but smaller than twice the fully extended molecular length of gelator **2** (5.2 nm).

Thus, on the basis of the aforementioned spectroscopic, microscopic studies as well as from the XRD results, it can be concluded that in the gelation process the amphiphiles are possibly forming repeating bilayers in which the molecules are connected by intermolecular hydrogen bonding and hydrophobic interaction. The probable interdigitated bilayer packing of the amphiphile **2** is represented in Figure 8 [39].

As noted earlier the pyridinium component is well known to impart antibacterial properties to a molecule [28-31]. Thus, we

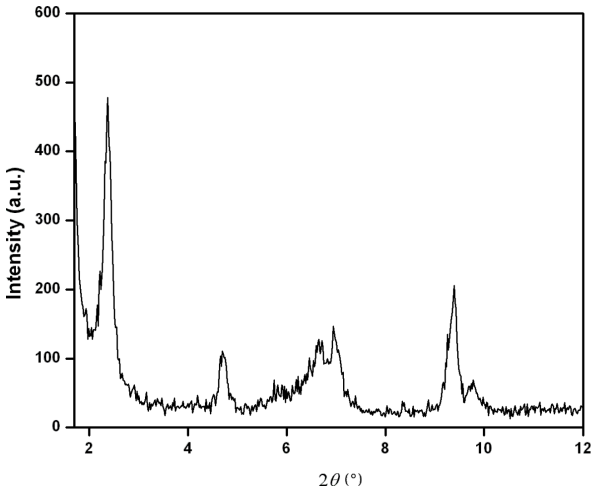

Figure 7: XRD diagram of the dried gel of **2**.

envisaged that it might be possible to develop inherently antibacterial soft matter based on amphiphilic pyridinium compounds. The antibacterial activities of both hydrogelating amphiphiles (**1** and **2**) were tested against two types of Gram-positive (*Bacillus subtilis* and *Micrococcus luteus*) and Gram-negative (*Escherichia coli* and *Klebsiella aerogenes*) bacteria. Minimum inhibitory concentrations (MIC), the lowest amphiphile concentration at which no viable bacterial cell is present, are presented in Table 1. Both **1** and **2** were found to be

Table 1: Antibacterial activities (MICs) of **1** and **2** in μg/mL.

Amphiphile	Gram-positive		Gram-negative	
	B. subtilis	*M. luteus*	*E. coli*	*K. aerogenes*
1	2.0	0.6	20.0	5.0
2	1.0	0.4	10.0	5.0

effective in killing bacteria with MIC values of 0.4–2.0 μg/mL for Gram-positive bacteria and 5.0–20.0 μg/mL for Gram-negative bacteria. However, **2** was found to have slightly better antibacterial activity than **1** with MIC values of only 0.4 μg/mL for Gram-positive *Micrococcus luteus* and 10 μg/mL for Gram-negative *Escherichia coli*. Interestingly, the pyridinium based amphiphilic hydrogelators showed antibacterial activity against both type of bacteria which is in contrast to the antibacterial activity of conventional quaternary cationic amphiphiles which are, in general, ineffective against Gram-negative bacteria. The positively charged amphiphiles are presumably adsorbed on the negatively charged cell membrane of microbes due to electrostatic interaction. This interaction is also entropically favorable as huge numbers of counterions are released. Next, the hydrophobic chain penetrates the hydrophobic cell membrane by 'self-promoted' transport resulting in release of the cytoplasmic constituents thus leading to the death of bacteria

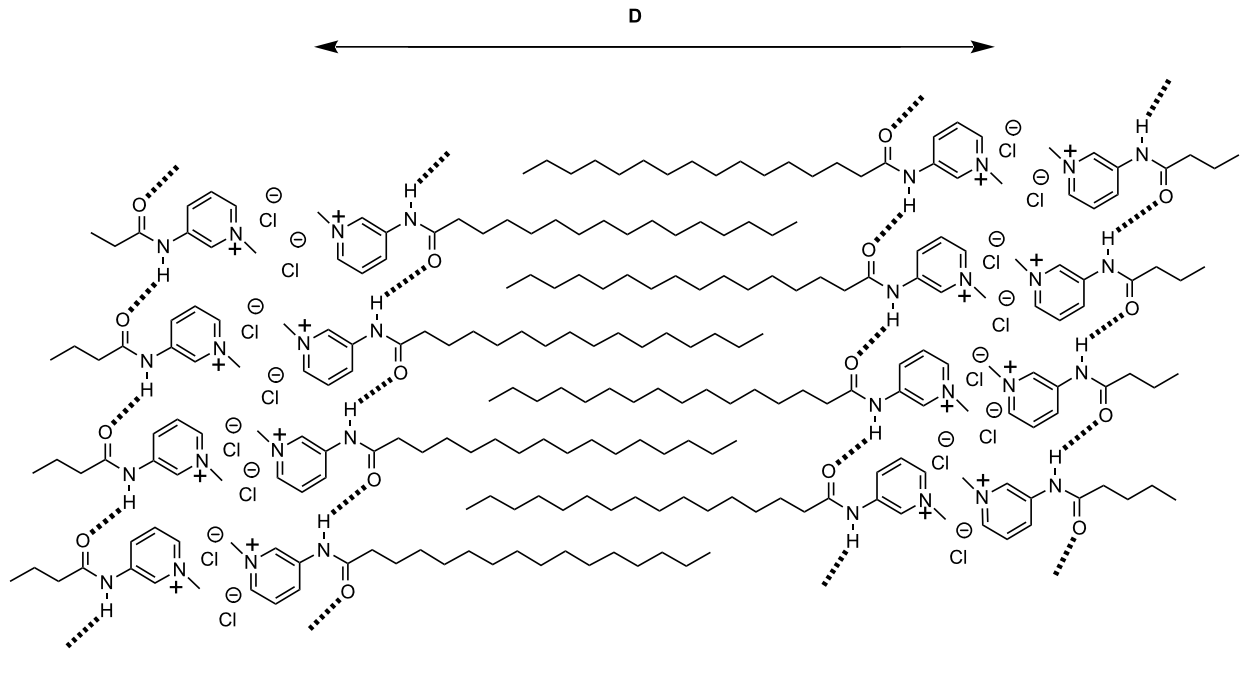

Figure 8: Schematic representation of the possible arrangement of molecules during hydrogelation of **2**.

[29,40]. The pyridinium-based amphiphiles **1** and **2** are structurally different from those studied earlier [29] and their antibacterial activity is similar to that of the reported pyridinium compounds. Most importantly, the hydrogelation ability along with the inherent antibacterial properties of the present amphiphiles make them interesting scaffolds for biomedicinal applications.

Application of antibacterial biomaterials becomes more versatile and significant only when they are also non-toxic to living cells. Consequently, the cytotoxicity of amphiphile **2** (as a representative example) in NIH3T3 cells was investigated using MTT based assay. Encouragingly, the molecule showed more than 96% viability up to a concentration of 20 μg/mL. However, as the concentration of the amphiphile increased, viability towards the cell decreased. Nevertheless, even up to a concentration of 100 μg/mL, greater than 50% viability was noted (Figure 9). Thus, the cationic amphiphiles are potentially lethal to bacteria, but encouragingly viable to mammalian cells. Such cell selectivity may originate from the difference in the lipid composition as well as in the membrane potential gradient between the target prokaryotic and the non-target eukaryotic cell membranes [41,42].

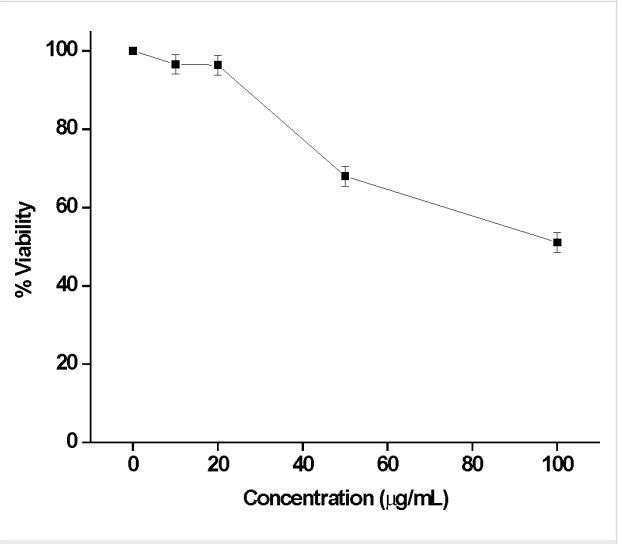

Figure 9: MTT assay based percent NIH3T3 cell viability as a function of concentration of amphiphile **2**.

Conclusion

We have utilized a combination of a quaternary pyridinium unit and hydrophobic long chain to build a scaffold, which can gelate water. The routes adopted for the synthesis of such molecules were extremely simple. Systematic variations of the structure of the amphiphile reveal that minute architectural changes at molecular level influences the self-assembling mechanism of the gelation process. The major responsible factors for the gelation process were found to be non-covalent interactions such as π–π stacking and intermolecular hydrogen bonding. These cationic amphiphilic molecules exhibited antibacterial activity against both Gram-positive and Gram-negative bacteria and were found to be viable towards mammalian cells. The antibacterial activity conjugated with low cytotoxicity and water gelation ability makes this class of compound an attractive target for the development of antibacterial biomaterials.

Experimental

Materials

Myristic acid, palmitic acid, stearic acid and ethyl bromide were purchased from SRL, India. Thionyl chloride, 3-aminopyridine, methyl iodide were purchased from Spectrochem, India. D_2O, DMSO-d_6 and $CDCl_3$ were obtained from Aldrich Chemical Co. Thin layer chromatography was performed on Merck precoated silica gel 60-F_{254} plates. All the material used in the cell culture study, such as Dulbecco's Modified Eagles' Medium (DMEM), heat inactivated fetal bovine serum (FBS), trypsin from porcine pancreas and MTT, were obtained from Sigma Aldrich Chemical Company. ^{1}H NMR spectra were recorded on an AVANCE 300 MHz (BRUKER) spectrometer. Mass spectrometric data were acquired by the electron spray ionization (ESI) technique on a Q-Tof-micro Quadruple mass spectrometer (Micromass). Fluorescence and FTIR spectra were measured on a Varian Cary Eclipse luminescence spectrometer and a Perkin Elmer Spectrum 100 FTIR spectrometer, respectively.

General synthetic procedure

Synthesis of amphiphiles 1–5

The acid (3 g) was refluxed with thionyl chloride (1 mL) for 4 h in an oil bath at 70 °C. The unreacted thionyl chloride was removed with a rotary-evaporator. The resulting compound (90% yield) was dissolved in dry dichloromethane (DCM) and then 3-aminopyridine (1.5 equiv dissolved in minimum quantity of dry DCM) added dropwise with stirring and ice cooling. The solution was stirred for 3–4 h, the DCM removed and the residue dissolved in ethyl acetate. The solution was washed with NaOH to remove excess acid and to convert the pyridinium salt to the free pyridine base. The organic layer was washed with brine until neutral. The ethyl acetate was then removed and the alkylated compound coupled through the amide linkage purified by column chromatography on 60–120 mesh silica gel with 1% methanol/chloroform mixture as eluent (75% yield). The compound thus obtained was stirred with methyl iodide (1.1 equiv) in dry DCM for 4–5 hours. After the reaction, the DCM was removed and the compound dissolved in ethyl acetate. The product was purified by column chromatography on 60–120 mesh silica gel with methanol/chloroform as eluent. The resulting iodide salt was subjected to ion

exchange on Amberlite IRA-400 chloride resin to produce the pure chloride salt. The overall yield was ≈50–60%. Amphiphile **5** was quaternized with ethyl bromide (2 equiv) and stirred for 36 h. The reaction mixture was taken in chloroform and washed with aqueous sodium thiosulphate and brine solutions. The organic layer was evaporated (rotary evaporator) and finally purified by column chromatography on 60–120 mesh silica gel with methanol/chloroform as the eluent. In order to synthesize compound **4** the corresponding coupled compound was dissolved in methanol (minimum quantity) and HCl gas was passed through it. The precipitate formed was filtered and collected. General synthetic scheme for the preparation of all the amphiphiles (**1**–**5**) is shown in Scheme 1.

Data for 1: ^{1}H NMR (300 MHz, $CDCl_3$, 25 °C): δ = 0.88 (t, 3H), 1.26 (br, 28H), 1.66–1.75 (m, 2H), 2.65 (t, 2H), 4.45 (s, 3H), 7.88–7.93 (m, 1H), 8.44–8.46 (d, 1H), 9.24–9.27 (d, 1H), 9.85 (s, 1H), 10.79 (br, 1H) ppm; ESI-MS: *m/z* calcd for $C_{24}H_{43}N_2O$ (the quaternary ammonium ion, 100%) 375.3370; found 375.3335 $[M]^+$; Elemental analysis calcd (%) for $C_{24}H_{43}N_2OCl$: C, 70.12 H, 10.54; N, 6.81; found: C, 69.86; H, 10.31; N, 6.53.

Data for 2: ^{1}H NMR (300 MHz, $CDCl_3$, 25 °C): δ = 0.87 (t, 3H), 1.25 (br, 24H), 1.65–1.74 (m, 2H), 2.67 (t, 2H), 4.44 (s, 3H), 7.88–7.93 (m, 1H), 8.44–8.46 (d, 1H), 9.24–9.27 (d, 1H), 9.85 (s, 1H), 10.80 (br, 1H) ppm; ESI-MS: *m/z* calcd for $C_{22}H_{39}N_2O$ (the quaternary ammonium ion, 100%) 347.3057, found 347.2011 $[M]^+$; Elemental analysis calcd (%) for $C_{22}H_{39}N_2OCl$: C, 68.99; H, 10.26; N, 7.31; found: C, 69.21; H, 10.15; N, 7.23.

Data for 3: ^{1}H NMR (300 MHz, $CDCl_3$, 25 °C): δ = 0.87 (t, 3H), 1.24 (br, 20H), 1.66–1.70 (m, 2H), 2.68 (t, 2H), 4.56 (s, 3H), 7.80–7.82 (m, 1H), 8.11 (br, 1H), 9.42–9.43 (d, 1H), 10.05 (s, 1H), 12.55 (br, 1H) ppm; ESI-MS: *m/z* calcd for $C_{20}H_{35}N_2O$ (the quaternary ammonium ion, 100%) 319.2744; found 319.1093 $[M]^+$; Elemental analysis calcd (%) for $C_{20}H_{35}N_2OCl$: C, 67.67; H, 9.94; N, 7.89; found: C, 67.49; H, 10.02; N, 8.07.

Data for 4: ^{1}H NMR (300 MHz, $CDCl_3$, 25 °C): δ = 0.87 (t, 3H), 1.26 (br, 24H), 1.59 (br, 2H), 2.29 (t, 2H), 7.53 (m, 1H), 7.69–7.73 (m, 2H), 7.81 (s, 1H), 8.19 (br, 1H) ppm; ESI-MS: *m/z* calcd for $C_{21}H_{37}N_2O$ (the quaternary ammonium ion, 100%) 333.2900; found 333.1956 $[M]^+$; Elemental analysis calcd (%) for $C_{21}H_{37}N_2OCl$: C, 68.36; H, 10.11; N, 7.59; found: C, 68.43; H, 9.98; N, 7.37.

Data for 5: ^{1}H NMR (300 MHz, $CDCl_3$, 25 °C): δ = 0.87 (t, 3H), 1.25 (br, 24H), 1.41–1.45 (m, 2H), 1.70–1.75 (t, 3H), 2.61 (t, 2H), 4.61–4.64 (q, 2H), 7.85 (s, 1H), 8.38 (s, 1H), 9.18–9.20 (d, 1H), 9.8 (s, 1H), 11.28 (s, 1H) ppm; ESI-MS: *m/z* calcd for $C_{23}H_{41}N_2O$ (the quaternary ammonium ion, 100%): 361.3213; found 361.1093 $[M]^+$; Elemental analysis calcd (%) for $C_{23}H_{41}N_2OCl$: C, 69.58; H, 10.41; N, 7.06; found: C, 69.36; H, 10.26; N, 7.12.

Preparation of hydrogel

The required amount of the amphiphile was added in 1 mL water at pH = 7.0 to a screw-capped vial with an internal diameter of 10 mm and heated slowly until the solid had completely dissolved. The solution was then cooled to room temperature without any disturbance. After 1 h, formation of gel was confirmed by stable to inversion of the glass vial.

Microscopic studies

FESEM was performed on JEOL-6700F microscope. A piece of hydrogel was mounted on a glass slide and dried for few hours under vacuum before imaging. The morphology of the dried gel of compound **2** was also studied using AFM (Veeco, model AP0100) in the non-contact mode. A piece of gel was mounted on a silicon wafer and dried for a few hours under vacuum before imaging.

Fluorescence spectroscopy

The emission spectra of the compound **2** were recorded on Varian Cary Eclipse luminescence spectrometer in the concentration range from 0.01%, w/v to above MGC (3%, w/v). A super stock solution of **2** was prepared and diluted as required. The compound was excited at λ_{ex} = 330 nm and emission recorded between 340–550 nm. The excitation and emission slit widths were 5 nm and 5 nm, respectively.

FTIR measurements

FTIR measurements of the gelators **1** and **2** in $CHCl_3$ solution and in D_2O (gel state) were taken in a Perkin Elmer Spectrum 100 FTIR spectrometer using KBr and CaF_2 windows, respectively with 1 mm Teflon spacers at their MGC.

NMR measurements

^{1}H NMR and 2D-NOESY spectra were recorded on AVANCE 300MHz (BRUKER) spectrometer at 2%, w/v for **2** in DMSO-d_6 and in water (70%) and DMSO-d_6 (30%).

X-ray diffraction (XRD)

XRD measurements were taken with Seifert XRD 3000P diffractometer. The source was Cu Kα radiation (λ = 0.15406 nm) with a voltage and current of 40 kV and 30 mA, respectively. The gel was mounted on a glass slide and dried under vaccum. The xerogel was scanned from 2Θ = 1–40°.

Microorganisms and culture conditions

The in vitro antimicrobial activity of the cationic amphiphiles was investigated against representative Gram-positive and Gram-negative bacteria. Gram-positive bacteria used in the present study were *Bacillus subtilis* and *Micrococcus luteus*. Gram-negative bacteria investigated include *Escherichia coli* and *Klebsiella aerogenes*. Investigations of antibacterial activities were performed by the broth dilution method. The LB medium (tryptone (10 g), yeast extract (5 g) and NaCl (10 g) in 1 L sterile distilled water at pH 7.0) was used as the liquid medium in all antibacterial experiments. All the microbial strains were purchased from Institute of Microbial Technology, Chandigarh, India. The stock solutions of all the amphiphiles as well as the required dilutions were made in autoclaved sterile water. Freeze-dried ampoules of all bacterial strains were opened and a loopful of culture was spread to give single colonies on the respective solid LB agar media and incubated for 24 h at 37 °C. A representative single colony was picked up with a wire loop and was spread on an agar slant to give single colonies. The slants were incubated at 37 °C for the respective time. These incubated cultures of all the bacteria were diluted as required to give a working concentration in the range of 10^6–10^9 colony forming units (cfu)/mL before every experiment.

Antimicrobial studies

Minimum inhibitory concentrations (MICs) of hydrogelating amphiphiles **1** and **2** were estimated by both the broth dilution and the spread plate method. MIC was measured using a series of test tubes containing the amphiphiles (0.05–200 μg/mL) in 5 mL liquid medium. Diluted microbial culture was added to each test tube at identical concentrations to obtain the working concentration of bacteria: for *B. subtilis* 7.5×10^7–1×10^8 cfu/mL, for *M. luteus* 5×10^6–7.5×10^6 cfu/mL, for *E. coli* 3.75×10^7–7.5×10^7 cfu/mL, for *K. aerogenes* 9×10^7–1.2×10^8 cfu/mL. All the test tubes were then incubated at 37 °C for 24 h. The optical density of all the solutions was measured at 650 nm before and after incubation. Liquid medium containing microorganisms was used as a positive control. All the experiments were performed in triplicate and repeated twice.

Cell cultures

Mouse embryonic fibroblast cell NIH3T3 were obtained from National Center for Cell Science (NCCS), Pune and maintained in DMEM medium supplemented with 10% FBS, 100 mg/L streptomycin and 100 IU/mL penicillin. Cells were grown in a 25 mL cell culture flask and incubated at 37 °C in a humidified atmosphere of 5% CO_2 to approximately 70–80% confluence. Media change was done after 2–3 days and subculture was performed every 7 days. After 7 days, media was removed to eliminate the dead cells. Next, the adherent cells were detached from the surface of the culture flask by trypsination. Cells were now in the exponential phase of growth for checking the viability of amphiphile **2**.

Cytotoxicity assay

The cytotoxicity of amphiphile **2** was assessed by the microculture MTT reduction assay as described in the literature. This assay is based on the reduction of a soluble tetrazolium salt by mitochondrial dehydrogenase of the viable cells to form an insoluble colored formazan product. The amount of formazan product formed can be measured spectrophotometrically after dissolution of the dye in DMSO. The activity of the enzyme and the amount of the formazan produced is proportional to the number of live cells. Reduction of the absorbance value can be attributed to the killing of the cells or inhibition of the cell proliferation by the molecule. 150 μL of cell solution were seeded (20,000 cells per well) in a 96-well microtiter plate for 18–24 h before the assay. A stock solution of the amphiphile **2** was prepared. Sequential dilution of this stock solution was carried out during the experiment to vary the concentrations of the amphiphile in the microtiter plate. The cells were incubated with the amphiphile solutions at different concentrations for 4 h at 37 °C under 5% CO_2. Then, 15μL of MTT stock solution (5 mg/mL) in phosphate buffer saline was added to the above mixture and the cells were further incubated for another 4 h. The precipitated formazan was dissolved in DMSO and absorbance at 570 nm was measured using BioTek® Elisa Reader. The number of surviving cells were expressed as percent viability = $[A_{570}$ (treated cells)−background/A_{570}(untreated cells)−background$] \times 100$.

Acknowledgements

P.K.D. is thankful to the Department of Science and Technology (DST), India for financial assistance through the Ramanna Fellowship (No. SR/S1/RFPC-04/2006). S.B., S.D. and S.D. acknowledge Council of Scientific and Industrial Research, India for Research Fellowships. We thank Anshupriya Shome for her help in antibacterial and cytotoxic studies.

References

1. Terech, P.; Weiss, R. G. *Chem. Rev.* **1997,** *97,* 3133–3160. doi:10.1021/cr9700282
2. George, M.; Weiss, R. G. *Acc. Chem. Res.* **2006,** *39,* 489–497. doi:10.1021/ar0500923
3. Sangeetha, N. M.; Maitra, U. *Chem. Soc. Rev.* **2005,** *34,* 821–836. doi:10.1039/b417081b
4. Jung, J. H.; Kobayashi, H.; Masuda, M.; Shimizu, T.; Shinkai, S. *J. Am. Chem. Soc.* **2001,** *123,* 8785–8789. doi:10.1021/ja010508h
5. Sone, E. D.; Zubarev, E. R.; Stupp, S. I. *Angew. Chem., Int. Ed.* **2002,** *41,* 1705–1709. doi:10.1002/1521-3773(20020517)41:10<1705::AID-ANIE1705>3.0.CO;2-M

6. Mitra, R. N.; Das, P. K. *J. Phys. Chem. C* **2008,** *112,* 8159–8166. doi:10.1021/jp712106d
7. Kobayashi, S.; Hamasaki, N.; Suzuki, M.; Kimura, M.; Shirai, H.; Hanabusa, K. *J. Am. Chem. Soc.* **2002,** *124,* 6550–6551. doi:10.1021/ja0260622
8. Bhattacharya, S.; Krishnan-Ghosh, Y. *Chem. Commun.* **2001,** 185–186. doi:10.1039/b007848o
9. Bieser, A. M.; Tiller, J. C. *J. Phys. Chem. B* **2007,** *111,* 13180–13187. doi:10.1021/jp074953w
10. Basit, H.; Pal, A.; Sen, S.; Bhattacharya, S. *Chem.–Eur. J.* **2008,** *14,* 6534–6545. doi:10.1002/chem.200800374
11. Bhat, S.; Maitra, U. *Molecules* **2007,** *12,* 2181–2189. doi:10.3390/12092181
12. Estroff, L. A.; Hamilton, A. D. *Chem. Rev.* **2004,** *104,* 1201–1218. doi:10.1021/cr0302049
13. Tiller, J. C. *Angew. Chem., Int. Ed.* **2003,** *42,* 3072–3075. doi:10.1002/anie.200301647
14. Heeres, A.; van der Pol, C.; Stuart, M.; Friggeri, A.; Feringa, B. L.; van Esch, J. *J. Am. Chem. Soc.* **2003,** *125,* 14252–14253. doi:10.1021/ja036954h
15. Mitra, R. N.; Shome, A.; Paul, P.; Das, P. K. *Org. Biomol. Chem.* **2009,** *7,* 94–102. doi:10.1039/b815368j
16. Su, W.-Y.; Chen, Y.-C.; Lin, F.-H. *Acta Biomater.* **2010,** *6,* 3044–3055. doi:10.1016/j.actbio.2010.02.037
17. Akiyoshi, K.; Deguchi, S.; Tajima, H.; Nishikawa, T.; Sunamoto, J. *Macromolecules* **1997,** *30,* 857–861. doi:10.1021/ma960786e
18. Das, D.; Dasgupta, A.; Roy, S.; Mitra, R. N.; Debnath, S.; Das, P. K. *Chem.–Eur. J.* **2006,** *12,* 5068–5074. doi:10.1002/chem.200501638
19. Godeau, G.; Barthélémy, P. *Langmuir* **2009,** *25,* 8447–8450. doi:10.1021/la900140b
20. Kar, T.; Debnath, S.; Das, D.; Shome, A.; Das, P. K. *Langmuir* **2009,** *25,* 8639–8648. doi:10.1021/la804235e
21. Mitra, R. N.; Das, D.; Roy, S.; Das, P. K. *J. Phys. Chem. B* **2007,** *111,* 14107–14113. doi:10.1021/jp076495x
22. Dutta, S.; Shome, A.; Debnath, S.; Das, P. K. *Soft Matter* **2009,** *5,* 1607–1620. doi:10.1039/b821272d
23. Xing, B.; Yu, C.-W.; Chow, K.-H.; Ho, P.-L.; Fu, D.; Xu, B. *J. Am. Chem. Soc.* **2002,** *124,* 14846–14847. doi:10.1021/ja028539f
24. Bhattacharya, S.; Srivastava, A.; Pal, A. *Angew. Chem., Int. Ed.* **2006,** *45,* 2934–2937. doi:10.1002/anie.200504461
25. Tang, C.; Smith, A. M.; Collins, R. F.; Ulijn, R. V.; Saiani, A. *Langmuir* **2009,** *25,* 9447–9453. doi:10.1021/la900653q
26. Samanta, S. K.; Gomathi, A.; Bhattacharya, S.; Rao, C. N. R. *Langmuir* **2010,** *26,* 12230–12236. doi:10.1021/la101150p
27. Ajayaghosh, A.; Praveen, V. K. *Acc. Chem. Res.* **2007,** *40,* 644–656. doi:10.1021/ar7000364
28. Debnath, S.; Shome, A.; Das, D.; Das, P. K. *J. Phys. Chem. B* **2010,** *114,* 4407–4415. doi:10.1021/jp909520w
29. Haldar, J.; Kondaiah, P.; Bhattacharya, S. *J. Med. Chem.* **2005,** *48,* 3823–3831. doi:10.1021/jm049106l
30. Sambhy, V.; Peterson, B. R.; Sen, A. *Angew. Chem., Int. Ed.* **2008,** *47,* 1250–1254. doi:10.1002/anie.200702287
31. Singh, S.; Bhadani, A.; Kataria, H.; Kaur, G.; Kamboj, R. *Ind. Eng. Chem. Res.* **2009,** *48,* 1673–1677. doi:10.1021/ie801737m
32. Makovitzki, A.; Shai, Y. *Biochemistry* **2005,** *44,* 9775–9784. doi:10.1021/bi0502386
33. Zasloff, M. *Nature* **2002,** *415,* 389–395. doi:10.1038/415389a
34. Menger, F. M.; Caran, K. L. *J. Am. Chem. Soc.* **2000,** *122,* 11679–11691. doi:10.1021/ja0016811
35. Mukhopadhyay, S.; Maitra, U.; Ira; Krishnamoory, G.; Schmidt, J.; Talmon, Y. *J. Am. Chem. Soc.* **2004,** *126,* 15905–15914. doi:10.1021/ja046788t
36. Lenz, T.; Bonnist, E. Y. M.; Pljevaljcic, G.; Neely, R. K.; Dryden, D. T. F.; Scheidig, A. J.; Jones, A. C.; Weinhold, E. *J. Am. Chem. Soc.* **2007,** *129,* 6240–6248. doi:10.1021/ja069366n
37. Suzuki, M.; Sato, T.; Kurose, A.; Shirai, H.; Hanabusa, K. *Tetrahedron Lett.* **2005,** *46,* 2741–2745. doi:10.1016/j.tetlet.2005.02.144
38. Kogiso, M.; Hanada, T.; Yase, K.; Shimizu, T. *Chem. Commun.* **1998,** 1791–1792. doi:10.1039/a803606c
39. Jung, J. H.; Shinkai, S.; Shimizu, T. *Chem.–Eur. J.* **2002,** *8,* 2684–2690. doi:10.1002/1521-3765(20020617)8:12<2684::AID-CHEM2684>3.0.CO;2-Z
40. Roy, S.; Das, P. K. *Biotechnol. Bioeng.* **2008,** *100,* 756–764. doi:10.1002/bit.21803
41. Matsuzaki, K.; Harada, M.; Handa, T.; Munakoshi, S.; Fujii, N.; Yajima, H.; Miyajima, K. *Biochim. Biophys. Acta* **1989,** *981,* 130–134. doi:10.1016/0005-2736(89)90090-4
42. Hansen, M. B.; Nielsen, S. E.; Berg, K. *J. Immunol. Methods* **1989,** *119,* 203–210. doi:10.1016/0022-1759(89)90397-9

License and Terms

Beilstein Journal of Organic Chemistry

Chain stopper engineering for hydrogen bonded supramolecular polymers

Thomas Pinault[1,2], Bruno Andrioletti[3] and Laurent Bouteiller[*1,2]

Full Research Paper

Open Access

Address:
[1]UPMC Université Paris 06, UMR 7610, Chimie des Polymères, F-75005 Paris, France, [2]CNRS, UMR 7610, Chimie des Polymères, F-75005 Paris, France and [3]Université Claude Bernard-Lyon 1, ICBMS-UMR 5246, 43 Boulevard du 11 Novembre 1918, F-69622 Villeurbanne Cedex, France

Email:
Laurent Bouteiller[*] - laurent.bouteiller@upmc.fr

* Corresponding author

Keywords:
chain stopper; gel; hydrogen bond; supramolecular polymer; urea

Beilstein J. Org. Chem. **2010,** *6,* 869–875.
doi:10.3762/bjoc.6.102

Received: 29 June 2010
Accepted: 13 September 2010
Published: 21 September 2010

Guest Editor: J.-P. Desvergne

Abstract

Supramolecular polymers are linear chains of low molar mass monomers held together by reversible and directional non-covalent interactions, which can form gels or highly viscous solutions if the self-assembled chains are sufficiently long and rigid. The viscosity of these solutions can be controlled by adding monofunctional compounds, which interact with the chain extremities: chain stoppers. We have synthesized new substituted ureas and thioureas and tested them as chain stoppers for a bis-urea based supramolecular polymer. In particular, the bis-thiourea analogue of the bis-urea monomer is shown not to form a supramolecular polymer, but a good chain stopper, because it is a strong hydrogen bond donor and a weak acceptor. Moreover, all substituted ureas tested reduce the viscosity of the supramolecular polymer solutions, but the best chain stopper is obtained when two hydrogen bond acceptors are placed in the same relative position as for the monomer and when no hydrogen bond donor is present.

Introduction

Supramolecular polymers are linear chains of low molar mass monomers held together by reversible and highly directional non-covalent interactions [1-3]. Because of their macromolecular architecture, they can display polymer-like rheological properties, and they can, in particular, form gels if the self-assembled chains are sufficiently long and rigid [4-9]. Compared to the well-known organogelators formed by the entanglement of usually crystalline fibers [10-13], supramolecular polymers display some specific features. In particular, hydrogen-bonded supramolecular polymers are often dynamic at room temperature, which means that they do not need to be heated and then cooled to form a gel. Moreover, the gels formed are usually visco-elastic, meaning that they show an elastic response only at high frequencies.

The chain length of a supramolecular polymer depends on the strength of the association between the monomers, which is highly dependent on their concentration, the temperature, the solvent, i.e., environmental factors, but also on the presence of additives. Chain-stoppers are monofunctional monomers able to

interact with monomers and therefore able to break polymer chains. They can be introduced in order to reduce the length of the supramolecular polymer (and thus reduce the viscosity of the solution) [14-16], but also in order to block the concentration dependence of the supramolecular polymers [17-19]. Chain stoppers can also be exploited to decorate the chain-ends with particular functional groups or labels [20,21]. The effectiveness of these schemes depends directly on the design of the chain-stopper: the interaction between chain-stopper and monomer should ideally be as strong as the interaction between monomers. It is therefore of interest to identify chain stoppers with an improved affinity toward a given supramolecular polymer. In this article, we investigate the efficiency of several new chain stoppers for a well-known bis-urea-based supramolecular polymer **EHUT** (Figure 1). This supramolecular polymer is particularly interesting, because it has been previously shown to self-assemble cooperatively into two competitive high molecular weight structures [22-24].

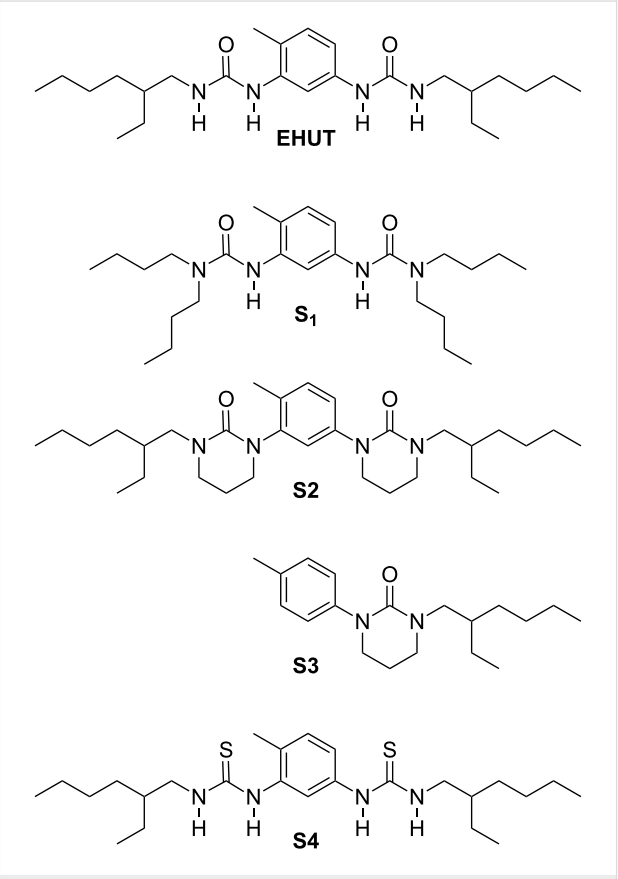

Figure 1: Structures of monomer **EHUT** and chain stoppers.

Results and Discussion

Design and synthesis

The bis-urea based monomer **EHUT** has been shown to self-assemble in non-polar solvents, into two supramolecular polymeric structures, the tube or the filament forms, which are in dynamic exchange [23,24]. The respective stability of each form depends on the solvent, the temperature and the concentration. The filament form contains a single molecule in its cross section [25-27], and is the most stable structure at concentrations above 10^{-3}mol/L and at room temperature, in solvents such as chloroform [22], carbon tetrachloride [28] and 1,3,5-trimethylbenzene [29]. The tube form contains three molecules in its cross section [6,30,31], and is the most stable structure at concentrations above 10^{-5}mol/L and at room temperature, in solvents such as toluene [32] and dodecane [5].

Chain stopper **S1**, with two NH groups replaced by *N*-butyl groups, was previously shown to be a good chain stopper for **EHUT** in carbon tetrachloride [17], i.e., a good chain stopper of the filament form. However, at high concentrations, the two remaining NH groups were shown to form hydrogen bonds [17], and therefore **S1** can also behave to some extent as a co-monomer of **EHUT**: a small proportion of **S1** molecules may be incorporated in the filament structure rather than at its extremities. Simple alkylation of the 2 remaining NH groups does not yield an efficient chain stopper [17]. This surprising result was tentatively attributed to the conformation of the tetra-substituted urea group, which may be ill-adapted to form hydrogen bonds to the urea groups of **EHUT** (Figure 2).

Hence, we introduced cyclic urea groups in the structure of chain stopper **S2**, by the alkylation of **EHUT** with 1,3-dibromopropane [33]. The rigidity of the cyclic ureas forbids any conformational rearrangement and should make it possible to probe whether the presence of NH functions in **S1** significantly affects the chain stopper efficiency. In order to see if both urea carbonyls in **S2** interact cooperatively with **EHUT** assemblies ,the mono-urea stopper **S3** was also prepared. Finally, chain stopper **S2** can only interact with bis-urea assemblies as a hydrogen bond acceptor through its carbonyl groups. It is therefore of interest to try and design a potentially complementary chain stopper, which would interact with bis-urea assemblies as a hydrogen bond donor. For this purpose, we synthesized the bis-thiourea **S4**, from the corresponding bis-thioisocyanate, because thioureas are known to be strong hydrogen bond donors and weak hydrogen bond acceptors [34,35].

Before evaluating the chain stopper efficiency of these compounds, i.e., their interaction with **EHUT**, their self-association was probed.

Self-association of bis-thiourea

Chain stoppers **S2** and **S3** cannot self-associate because they contain only hydrogen bond acceptors, however this is not the case for **S4**, and it is of interest to determine the conditions

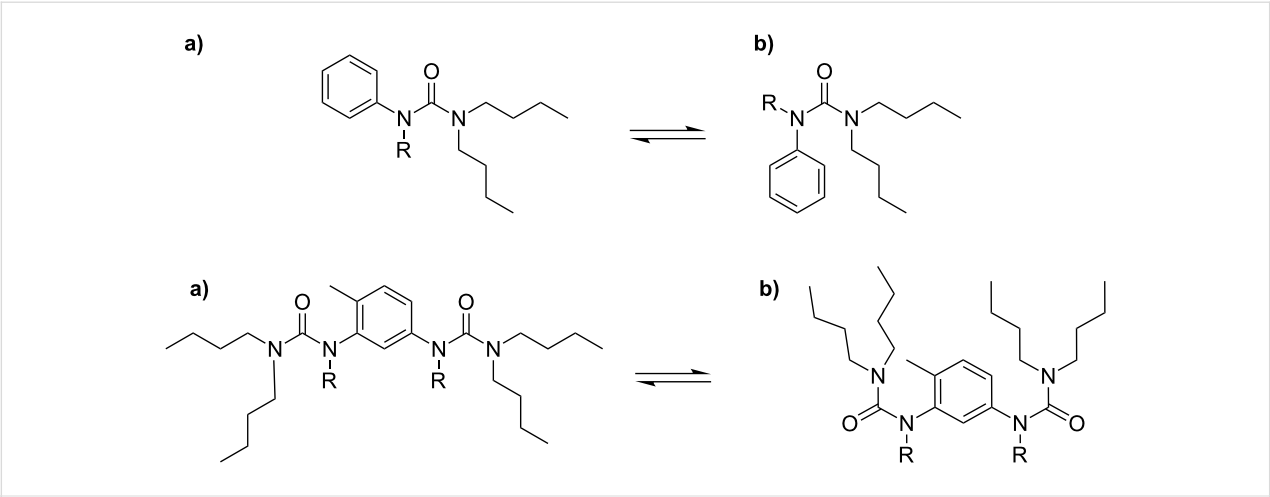

Figure 2: Substituted urea conformation. If R is alkyl, the most stable conformation is b); if R = H, the most stable conformation is a) [37].

under which **S4** can be considered not to associate with itself. Figure 3a shows the FTIR spectra of **S4** at several concentrations in chloroform. At concentrations below 53 mM, a single band is visible in the region corresponding to the N–H stretching vibration. This band (3405 cm^{-1}) can be attributed to free NH groups. Only at a high concentration (0.5 mol/L) does a band characteristic for hydrogen bonded NH groups appear (3250 cm^{-1}). The very weak hydrogen bonding propensity of bis-thiourea **S4** is particularly obvious when compared to bis-urea **EHUT** (Figure 3b): at the same concentration (9 mM), the bis-urea is nearly fully associated, whereas the bis-thiourea is virtually not associated. The respective behaviour of the bis-urea and the bis-thiourea was also probed by Small Angle Neutron Scattering (SANS) in toluene. Figure 4 shows the previously established q^{-1} dependence of **EHUT**, which is characteristic for long and rigid fibrillar scatterers [23]. In contrast, the low intensity and flat profil for **S4** at small angles is characteristic for small globular scatterers. A fit was performed with the form factor of a sphere, and yields a diameter of 22 Å, which is comparable to the largest dimension of the fully extended molecule (25 Å). In conclusion, bis-thiourea **S4** does not self-assemble significantly at concentrations below 12 mM in toluene or 53 mM in chloroform.

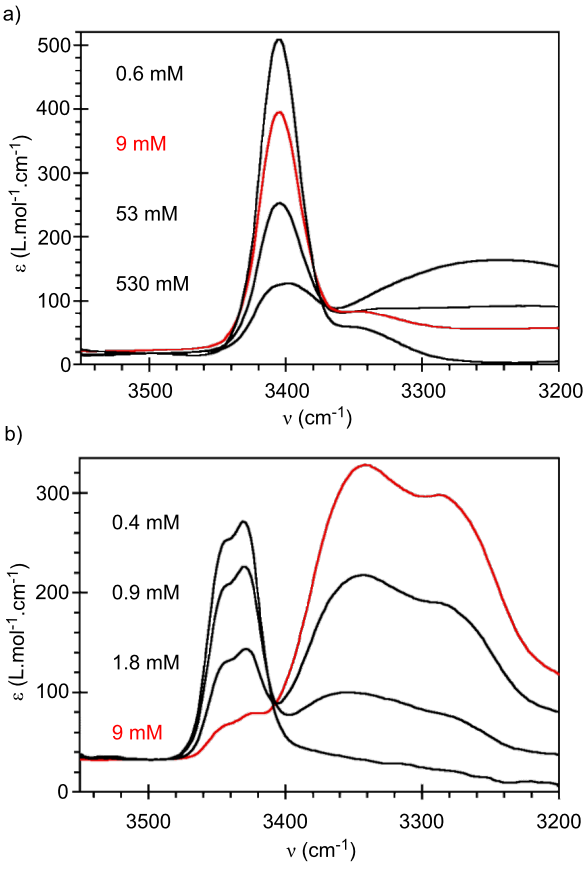

Figure 3: FTIR spectra, at 20 °C, for $CDCl_3$ solutions of **S4** (a) or **EHUT** (b), at several concentrations.

Chain stopper effect on the EHUT filament structure

Viscosimetry is certainly the most sensitive technique to probe the efficiency of a chain stopper on supramolecular polymers. Therefore, we measured the viscosity of solutions of **EHUT** at a fixed concentration (20 mM) with increasing amounts of chain stopper. For this, 1,3,5-trimethylbenzene was chosen as the solvent because it is known to favor the formation of **EHUT** filaments at room temperature [29]. Figure 5 shows that all four compounds strongly reduce the relative viscosity of **EHUT**, which decreases from a value of 7.6 in the absence of stopper to a value close to 1 (i.e. the solution has approximately the same viscosity as the solvent) for a molar fraction ratio of stopper to monomer of 0.1. However, there are some significant differ-

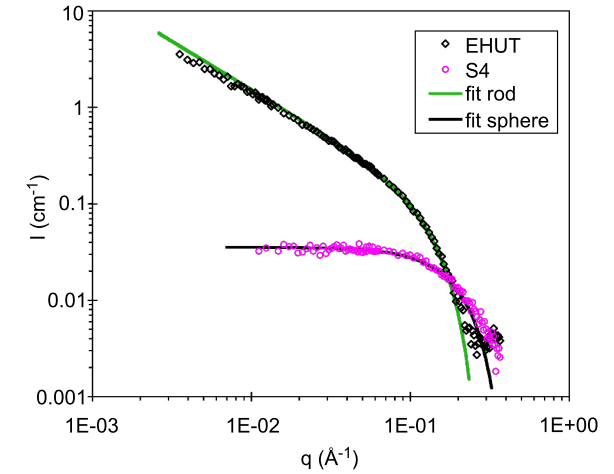

Figure 4: SANS intensity versus scattering vector for 12 mM solutions of **EHUT** or **S4** in d_8-toluene, at 22 °C. The plain curves are fits according to a model for infinitely long rigid rods of diameter 26 Å (green), or for spheres of diameter 22 Å (black).

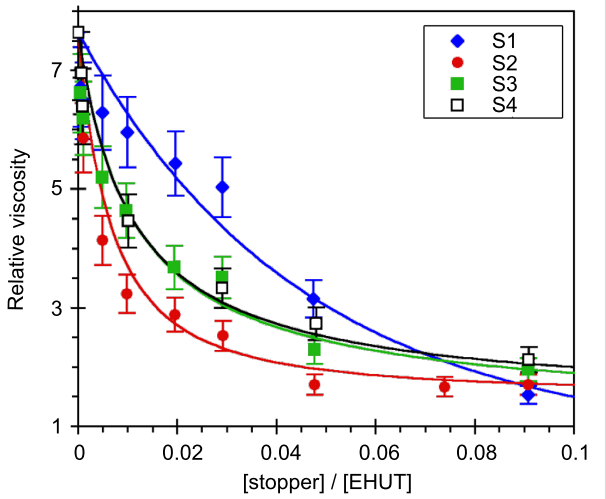

Figure 5: Relative viscosity for solutions of **EHUT** (20 mM) in 1,3,5-trimethylbenzene at 25 °C, with increasing molar fraction of chain stoppers. The lines are a guide for the eye only.

ences between the stoppers: their efficiency increases in the order **S1** < **S3** ≈ **S4** < **S2**. Several conclusions can be derived from this result. First, the lower viscosity of solutions containing **S2** than those containing **S1** means that the remaining two NH groups of **S1** do participate in hydrogen bonding and reduce the efficiency of the stopper. Secondly, the lower viscosity of solutions containing **S2** than those containing **S3** indicates that both carbonyls are probably involved in the association between **S2** and an **EHUT** filament. Finally, bis-thiourea **S4** is a reasonably good chain stopper. The fact that it is not as good as **S2** is perhaps due to some marginal hydrogen bonding involving the thiocarbonyl groups.

Chain stopper effect on the EHUT tube structure

For the above, toluene was chosen as the solvent, because it is known to favor the formation of **EHUT** tubes at room temperature [32] and has a similar polarity as 1,3,5-trimethylbenzene. Figure 6 shows that all four compounds also reduce the relative viscosity of **EHUT** in toluene, but the situation is more complex than in trimethylbenzene. If we consider first the part of the curves with a stopper to monomer fraction lower than 0.05, the efficiency of the chain stoppers increases in the order **S3** < **S1** ≈ **S4** < **S2**. Therefore, the same conclusions for the interactions with the **EHUT** tubes can be derived as for the interactions with the **EHUT** filaments: i) the lower viscosity of solutions containing **S2** than those containing **S1** means that the remaining two NH groups of **S1** participate in hydrogen bonding and reduce the efficiency of the stopper; ii) the lower viscosity of solutions containing **S2** than those containing **S3** indicates that both carbonyl groups are involved in the association between **S2** and an **EHUT** tube; and iii) bis-thiourea **S4** is a reasonably good chain stopper, but not as good as **S2** probably due to some marginal hydrogen bonding involving the thiocarbonyls. If we consider now the part of the curves with a stopper to monomer fraction larger than 0.05, it is surprising to see that instead of the value decreasing to 1, the relative viscosity reaches a plateau at a value of 5 and 4 in the cases of **S1** and **S2**, respectively. To our knowledge, such a saturating effect is unprecedented, and may indicate that an additional mechanism is involved in the interaction between the bis-urea tubes and **S1** or **S2**. For example, we can hypothesize that at sufficiently high concentrations, **S1** or **S2** do not only interact with the extremities of the tubes, but also anywhere along them,

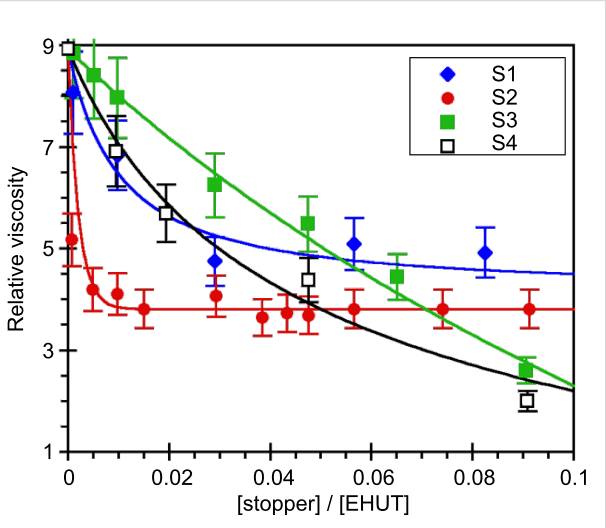

Figure 6: Relative viscosity for solutions of **EHUT** (1.1 mM) in toluene at 25 °C, with increasing molar fraction of chain stoppers. The lines are a guide for the eye only.

without breaking them. However, additional characterizations will be required to test this interpretation [36].

Conclusion

We have synthesized new substituted ureas and thioureas and tested them as chain stoppers for a bis-urea based supramolecular polymer. Depending on the solvent used, the bis-urea either forms filaments with a single monomer in the cross-section or tubes with three monomers in the cross-section. For both supramolecular architectures, similar conclusions can be derived: while all compounds tested reduce the viscosity of the supramolecular polymer solutions, the best chain stopper is obtained when two hydrogen bond acceptors are placed in the same relative position as for the monomer, and when no hydrogen bond donor is present.

Moreover, we have shown that a bis-thiourea with the same structure as the bis-urea monomer does not to form a supramolecular polymer, but acts as a good chain stopper, because it is a strong hydrogen bond donor and a weak acceptor.

Experimental

Synthesis

The synthesis of **EHUT** [32] and chain stopper **S1** [17] have previously been reported.

Chain stopper S2. NaH (9 g) was placed in a three necked round bottomed flask and washed with pentane (25 mL) under a nitrogen atmosphere. An **EHUT** solution (4.32 g, 10 mmol) in dry THF (400 mL) was added and the mixture stirred for 1 h. 1,3-Dibromopropane (20.5 mL, 200 mmol) in dry THF (100 mL) was then added, and the solution heated under reflux for 24 h. After cooling, ice was slowly added and the solvent evaporated. Chloroform (200 mL) was added and the organic phase washed successively with brine (300 mL) and water (2 × 300 mL), dried over magnesium sulfate and concentrated. Silica gel column chromatography (ethyl acetate) followed by recrystallization from pentane afforded 1.9 g of a white solid (37%). ^{1}H NMR (200 MHz, DMSO-d_6): δ (ppm) = 7.2 (d, J = 1.5 Hz, 1H, Ar-*H*), 7.12 (d, J = 8.1 Hz, 1H, Ar-*H*), 7.06 (dd, J = 8.1 Hz, J = 1.5, 1H, Ar-*H*), 3.74–3.02 (m, 12H, N-CH_2), 2.21 (s, 3H, Ar-CH_3), 2.07 (m, 4H, CH_2), 1.66 (m, 2H, C*H*), 1.36 (m, 16H, CH_2), 0.92 (t, 12H, CH_3). ^{13}C NMR (50 MHz, DMSO-d_6): δ (ppm) = 153.7/153.2 (*C*=O), 136.3/136.2/129.9/129.7/108.3/103.2 (*Ar*), 51.7/51.5/50.3/50.2/47.7/46.9 (N-*C*H$_2$), 37.4 (*C*H), 31.5/31.3/27.9/27.7/24.2/24.1/22.3 (*C*H$_2$), 17.2 (Ar-*C*H$_3$), 14/13.8/11.5/11.4 (*C*H$_3$).

Chain stopper S3. NaH (1.5 g) was placed in a three necked round bottomed flask and washed with pentane (5 mL) under a nitrogen atmosphere. A solution of *N*-(2-ethylhexyl)-*N*′-(4-methylphenyl)urea [22] (1 g, 3.8 mmol) in dry THF (25 mL) was added and the mixture stirred for 1 h. 1,3-Dibromopropane (3.9 mL, 38 mmol) in dry THF (50 mL) was then added, and the solution heated under reflux for 24 h. After cooling, ice was slowly added and the solvent evaporated. Chloroform (50 mL) was added and the organic phase washed successively with brine (70 mL) and water (2 × 70 mL), dried over magnesium sulfate and concentrated. Silica gel column chromatography (ethyl acetate/dichloromethane and then ethyl acetate) followed by recrystallization from pentane afforded 0.66 g of a white solid (57%). ^{1}H NMR (200 MHz, DMSO-d_6): δ (ppm) = 7.42/7.17 (2d, 4H, Ar-*H*), 3.21 (m, 6H, N-CH_2), 2.15 (s, 3H, Ar-CH_3), 1.78 (m, 3H, CH_2(cycle) + C*H*) , 1.32 (m, 8H, CH_2), 0.93 (t, 6H, CH_3).

Chain stopper S4. 2-Ethylhexylamine (8.8 mL, 52 mmol) in dichloromethane (50 mL) was added slowly under a nitrogen atmosphere to a stirred solution of 2,4-toluene diisothiocyanate (5.06 g, 24.5 mmol) in dichloromethane (200 mL, distilled over calcium hydride). After 24 h, the solvent was evaporated. Recrystallization from ethanol/water afforded 7.74 g of a white solid (68%). ^{1}H NMR (250 MHz, DMSO-d_6, δ (ppm)): 9.47/9.04 (2s, 2H, Ar-N*H*), 7.52/7.37 (2s, 2H, CH$_2$-N*H*), 7.32 (s, 1H, Ar-*H*), 7.21–7.11 (m, 2H, Ar-*H*), 3.40 (m, 4H, N-CH_2), 2.14 (s, 3H, Ar-CH_3), 1.59 (m, 2H, C*H*), 1.25 (m, 16H, CH_2), 0.84 (m, 12H, CH_3). ^{13}C NMR (62.5 MHz, DMSO-d_6, δ (ppm)): 181.2/180.4 (*C*=S), 137.0/130.6/130.0/122.6/121.1 (*Ar*), 47.4/47.1 (N-*C*H$_2$), 38.4/38.3 (*C*H), 30.5/28.4/23.8/22.6 (*C*H$_2$), 17.1 (Ar-*C*H$_3$), 14.0/10.7 (*C*H$_3$). MS (ESI) = [M-H] 463.4

Viscometry

Solutions were prepared by stirring at room temperature for at least 1 day prior to use. Capillary viscosity was measured at 25 ± 0.1 °C with an automatic Anton-Paar AMVn viscometer (capillary internal diameter 1.8 mm; ball diameter 1.5 mm). The measurements were performed with an angle of 20° and repeated six times.

FTIR spectroscopy

Infrared spectra were recorded on a Nicolet Avatar 320 spectrometer in KBr cells of 0.3 to 2.5 cm path length.

SANS

Measurements were made at the LLB (Saclay, France) on the Paxy instrument, at three distance-wavelength combinations to cover the 3 10^{-3} to 0.3 Å^{-1} q-range, where the scattering vector q is defined as usual, assuming elastic scattering, as $q = (4\pi/\lambda)\sin(\theta/2)$, where θ is the angle between incident and scattered beam. The sample diaphragm was 7.6 mm. Collimation was achieved with a diaphragm of 22 mm for a sample – detector distance of 1.5 m, or 16 mm for a sample – detector

distance of 3.2 and 6.7 m. Data were corrected for the empty cell signal and the solute and solvent incoherent background. A light water standard was used to normalize the scattered intensities into cm^{-1} units.

Acknowledgements

O. Bénaud is acknowledged for his contribution to this project. We thank François Boué (LLB, Saclay) for assistance with SANS experiments.

References

1. Ciferri, A., Ed. *Supramolecular Polymers;* Marcel Dekker: New York, 2005.
2. Brunsveld, L.; Folmer, B. J. B.; Meijer, E. W.; Sijbesma, R. P. *Chem. Rev.* **2001,** *101,* 4071–4097. doi:10.1021/cr990125q
3. Bouteiller, L. *Adv. Polym. Sci.* **2007,** *207,* 79–112. doi:10.1007/12_2006_110
4. van der Gucht, J.; Besseling, N. A. M.; Knoben, W.; Bouteiller, L.; Cohen Stuart, M. A. *Phys. Rev. B* **2003,** *67,* 051106. doi:10.1103/PhysRevE.67.051106
5. Ducouret, G.; Chassenieux, C.; Martins, S.; Lequeux, F.; Bouteiller, L. *J. Colloid Interface Sci.* **2007,** *310,* 624–629. doi:10.1016/j.jcis.2007.01.059
6. Shikata, T.; Nishida, T.; Isare, B.; Linares, M.; Lazzaroni, R.; Bouteiller, L. *J. Phys. Chem. B* **2008,** *112,* 8459–8465. doi:10.1021/jp800495v
7. van Gorp, J. J.; Vekemans, J. A. J. M.; Meijer, E. W. *J. Am. Chem. Soc.* **2002,** *124,* 14759–14769. doi:10.1021/ja020984n
8. Ogata, D.; Shikata, T.; Hanabusa, K. *J. Phys. Chem. B* **2004,** *108,* 15503–15510. doi:10.1021/jp0486604
9. Sakamoto, A.; Ogata, D.; Shikata, T.; Hanabusa, K. *Macromolecules* **2005,** *38,* 8983–8986. doi:10.1021/ma051489p
10. Terech, P.; Weiss, R. G. *Chem. Rev.* **1997,** *97,* 3133–3159. doi:10.1021/cr9700282
11. van Esch, J. H.; Feringa, B. L. *Angew. Chem., Int. Ed.* **2000,** *39,* 2263–2266. doi:10.1002/1521-3773(20000703)39:13<2263::AID-ANIE2263>3.0.CO;2-V
12. Sangeetha, N. M.; Maitra, U. *Chem. Soc. Rev.* **2005,** *34,* 821–836. doi:10.1039/b417081b
13. George, M.; Weiss, R. G. *Acc. Chem. Res.* **2006,** *39,* 489–497. doi:10.1021/ar0500923
14. Folmer, B. J. B.; Cavini, E.; Sijbesma, R. P.; Meijer, E. W. *Chem. Commun.* **1998,** 1846–1848.
15. Ercolani, G. *Chem. Commun.* **2001,** 1416–1417. doi:10.1039/b101678b
16. Pinault, T.; Cannizzo, C.; Andrioletti, B.; Ducouret, G.; Lequeux, F.; Bouteiller, L. *Langmuir* **2009,** *25,* 8404–8407. doi:10.1021/la804138u
17. Lortie, F.; Boileau, S.; Bouteiller, L.; Chassenieux, C.; Lauprêtre, F. *Macromolecules* **2005,** *38,* 5283–5287. doi:10.1021/ma050168a
18. Knoben, W.; Besseling, N. A. M.; Cohen Stuart, M. A. *Macromolecules* **2006,** *39,* 2643–2653. doi:10.1021/ma0518914
19. Knoben, W.; Besseling, N. A. M.; Bouteiller, L.; Cohen Stuart, M. A. *Phys. Chem. Chem. Phys.* **2005,** *7,* 2390–2398. doi:10.1039/b503463a
20. Hirschberg, J. H. K.; Ramzi, A.; Sijbesma, R. P.; Meijer, E. W. *Macromolecules* **2003,** *36,* 1429–1432. doi:10.1021/ma025723c
21. Dudek, S. P.; Pouderoijen, M.; Abbel, R.; Schenning, A. P. H. J.; Meijer, E. W. *J. Am. Chem. Soc.* **2005,** *127,* 11763–11768. doi:10.1021/ja052054k
22. Simic, V.; Bouteiller, L.; Jalabert, M. *J. Am. Chem. Soc.* **2003,** *125,* 13148–13154. doi:10.1021/ja037589x
23. Bouteiller, L.; Colombani, O.; Lortie, F.; Terech, P. *J. Am. Chem. Soc.* **2005,** *127,* 8893–8898. doi:10.1021/ja0511016
24. Bellot, M.; Bouteiller, L. *Langmuir* **2008,** *24,* 14176–14182. doi:10.1021/la802367r
25. Vonau, F.; Suhr, D.; Aubel, D.; Bouteiller, L.; Reiter, G.; Simon, L. *Phys. Rev. Lett.* **2005,** *94,* 066103. doi:10.1103/PhysRevLett.94.066103
26. Vonau, F.; Aubel, D.; Bouteiller, L.; Reiter, G.; Simon, L. *Phys. Rev. Lett.* **2007,** *99,* 086103. doi:10.1103/PhysRevLett.99.086103
27. Vonau, F.; Linares, M.; Isare, B.; Aubel, D.; Habar, M.; Bouteiller, L.; Reiter, G.; Geskin, V.; Zerbetto, F.; Lazzaroni, R.; Simon, L. *J. Phys. Chem. C* **2009,** *113,* 4955–4959. doi:10.1021/jp809552j
28. Boileau, S.; Bouteiller, L.; Lauprêtre, F.; Lortie, F. *New J. Chem.* **2000,** *24,* 845–848. doi:10.1039/b006742n
29. Pinault, T.; Isare, B.; Bouteiller, L. *ChemPhysChem* **2006,** *7,* 816–819. doi:10.1002/cphc.200500636
30. Isare, B.; Linares, M.; Lazzaroni, R.; Bouteiller, L. *J. Phys. Chem. B* **2009,** *113,* 3360–3364. doi:10.1021/jp810236z
31. Isare, B.; Linares, M.; Zargarian, L.; Fermandjian, S.; Miura, M.; Motohashi, S.; Vanthuyne, N.; Lazzaroni, R.; Bouteiller, L. *Chem.–Eur. J.* **2010,** *16,* 173–177. doi:10.1002/chem.200902399
32. Lortie, F.; Boileau, S.; Bouteiller, L.; Chassenieux, C.; Demé, B.; Ducouret, G.; Jalabert, M.; Lauprêtre, F.; Terech, P. *Langmuir* **2002,** *18,* 7218–7222. doi:10.1021/la0255166
33. Katz, H. E.; Cram, D. J. *J. Am. Chem. Soc.* **1984,** *106,* 4977–4987. doi:10.1021/ja00329a058
34. Laurence, C.; Berthelot, M.; Le Questel, J.-Y.; El Ghomari, M. J. *J. Chem. Soc., Perkin Trans. 2* **1995,** 2075–2079. doi:10.1039/p29950002075
35. Masunov, A.; Dannenberg, J. J. *J. Phys. Chem. B* **2000,** *104,* 806–810. doi:10.1021/jp993078e
36. SANS experiments have been performed for **EHUT** solutions in d_8-toluene, in the presence of chain stopper **S1** or **S2** ([**EHUT**] = 11 mM; [stopper]/[**EHUT**] = 0.2). In the q-range investigated ($3.16\ 10^{-3}$ – $3.14\ 10^{-1}$ $Å^{-1}$), the scattering curves are virtually the same as without chain-stopper (data not shown). This indicates that the local structure is not significantly affected.
37. Nowick, J. S.; Powell, N. A.; Martinez, E. J.; Smith, E. M.; Noronha, G. *J. Org. Chem.* **1992,** *57,* 3763–3765. doi:10.1021/jo00040a007

Beilstein Journal of Organic Chemistry

Oxalyl retro-peptide gelators. Synthesis, gelation properties and stereochemical effects

Janja Makarević, Milan Jokić, Leo Frkanec, Vesna Čaplar, Nataša Šijaković Vujičić and Mladen Žinić*

Full Research Paper

Open Access

Address:
Laboratory for Supramolecular and Nucleoside Chemistry, Ruđer Bošković Institute, P.O.B. 180, HR-10002 Zagreb, Croatia

Email:
Mladen Žinić* - zinic@irb.hr

* Corresponding author

Keywords:
chiral; organogel; oxalamide; retro-peptide; self-assembly

Beilstein J. Org. Chem. **2010,** *6,* 945–959.
doi:10.3762/bjoc.6.106

Received: 30 June 2010
Accepted: 23 August 2010
Published: 04 October 2010

Guest Editor: J.-P. Desvergne

Abstract

In this work we report on gelation properties, self-assembly motifs, chirality effects and morphological characteristics of gels formed by chiral retro-dipeptidic gelators in the form of terminal diacids (**1a–5a**) and their dimethyl ester (**1b–5b**) and dicarboxamide (**1c–5c**) derivatives. Terminal free acid retro-dipeptides (*S,S*)-bis(LeuLeu) **1a**, (*S,S*)-bis(PhgPhg) **3a** and (*S,S*)-bis(PhePhe) **5a** showed moderate to excellent gelation of highly polar water/DMSO and water/DMF solvent mixtures. Retro-peptides incorporating different amino acids (*S,S*)-(LeuPhg) **2a** and (*S,S*)-(PhgLeu) **4a** showed no or very weak gelation. Different gelation effectiveness was found for racemic and single enantiomer gelators. The heterochiral (*S,R*)**-1c** diastereoisomer is capable of immobilizing up to 10 and 4 times larger volumes of dichloromethane/DMSO and toluene/DMSO solvent mixtures compared to homochiral (*S,S*)-**1c.** Based on the results of ^{1}H NMR, FTIR, CD investigations, molecular modeling and XRPD studies of diasteroisomeric diesters (*S,S*)**-1b**/(*S,R*)**-1b** and diacids (*S,S*)**-1b**/(*S,R*)**-1a**, a basic packing model in their gel aggregates is proposed. The intermolecular hydrogen bonding between extended gelator molecules utilizing both, the oxalamide and peptidic units and layered organization were identified as the most likely motifs appearing in the gel aggregates. Molecular modeling studies of (*S,S*)-**1a**/(*S,R*)**-1a** and (*S,S*)-**1b**/(*S,R*)**-1b** diasteroisomeric pairs revealed a decisive stereochemical influence yielding distinctly different low energy conformations: those of (*S,R*)-diastereoisomers with lipophilic *i*-Bu groups and polar carboxylic acid or ester groups located on the opposite sides of the oxalamide plane resembling bola amphiphilic structures and those of (*S,S*)-diasteroisomers possessing the same groups located at both sides of the oxalamide plane. Such conformational characteristics were found to strongly influence both, gelator effectiveness and morphological characteristics of gel aggregates.

Introduction

Reversible processes of peptide, protein and nucleic acids self-assembly are of paramount importance in biotic systems and are central to vital biological functions. On the other hand, some pathological changes leading to diseases such as Alzheimer's, Parkinson's and prion diseases, type II diabetes, etc. are associated with anomalous self-assembly of smaller peptides into

amyloid fibrils which finally result in the formation of amyloid plaques [1-4]. During the last two decades there has been a growing interest in self-organization of small peptide models capable of self-assembling into highly organized supramolecular structures with potential use as novel bio- or nanomaterials possessing advanced properties and functions [5-10]. It has been shown that even short peptides, such as dipeptides, tripeptides or tetrapeptides, themselves or incorporated into more complex structures, are capable of self-assembling into fibers or fibrils [11-15]. In a number of cases such organization results in formation of gels consisting of self-assembled fibrous aggregates usually containing a large volume of solvent [16]. In gels, the fibers are heavily entangled into 3-dimensional networks which immobilize the solvent and prevent fluidity in the system [17-23]. In the last 15 years many low molecular weight gelling molecules of wide structural diversity, including a variety of amino acid and small peptide derivatives, have been prepared and studied [24-41]. These investigations revealed that gelator assemblies of various morphologies, including fibers and fiber bundles of diverse diameters, helical fibers or ribbons, tapes and nano-tubules, sometimes simultaneously present with micelles or vesicles, could be found [17-23]. For many gel systems evidence for hierarchical organisation was provided which determined the final morphological appearance of the aggregates [26]. It appears that gelation induced by aggregation of small abiotic or bio-inspired organic molecules represents an advantageous experimental system allowing in depth studies of the self-assembly as a general phenomenon. Such studies should ultimately result in revealing the relationship between gelator structures, self-assembly motifs and apparent morphologies of final assemblies as well as assisting in the elucidation of the role of solvent, which has been largely neglected in the majority of studies carried out to date. However, such an understanding of gelation is still out of reach; it is still hardly possible to predict gelation capability on the basis of the structure of a candidate molecule and it is even more difficult to predict which solvents and how effectively they would be gelled [42,43]. Hence, systematic studies of gels formed by structurally diverse small gelator molecules comprising elucidation of their self-assembly motifs, gelation effectiveness toward solvents of different structure and physical characteristics, estimation of solvation and stereochemical effects and their influence on the morphological characteristics of final gel assemblies may be rewarding, and should provide a much better understanding of the self-assembly processes involved in gelation.

In this work we report on gelation properties, self-assembly motifs, chirality effects and morphological characteristics of gels formed by chiral bis(dipeptide)oxalamides. Structurally, such gelators belong to the group of retro-peptides, which have been intensively studied as peptidomimetics due to their higher proteolytic stability and bioavailability compared to natural counterparts [44-47]. Despite very promising biomedicinal properties, very little is known about the self-assembly potential of this class of compounds in solution. Computer simulations of some malonamide retro-peptides have shown that the extended conformations are less stable than the helical ones [48,49]. Nevertheless, the crystal structure of the retro–inverso peptide Bz–S–gAla–R–mAla–NHPh revealed it's unidirectional self-assembly by intermolecular β-sheet type of hydrogen bonding so that malonamide retro-peptides could be considered as potential candidates for development of new gelator molecules [50]. The oxalamide based retro-peptides are relatively rare and much less studied than the more flexible malonamide retro-peptides [51-54]. In contrast to the malonamide group, the planar and much more rigid oxalamide fragment is self-complementary and exhibit a strong tendency for intermolecular hydrogen bonding both in the solid state and in the solution [55-60]. Hence, the oxalyl retro-peptides are expected to preferably form extended conformations capable of intermolecular oxalamide–oxalamide hydrogen bonding and the formation of unidirectional assemblies the latter being a necessary condition for gelation [24-31,58-60]. Herein, we provide experimental and molecular modeling evidence that the oxalamide retro-peptides indeed tend to form unidirectional hydrogen bonded assemblies of gelator molecules that adopt fully extended conformations. We also present the evidence that for the (*S,R)*-bis(LeuLeu) **1a** and (*S,S)*-bis(LeuLeu) **1a** retro-peptidic gelators, the stereochemistry has a decisive impact on their gelation effectiveness and final gel morphology in their water/DMSO gels.

Results and Discussion

Synthesis of oxalyl retro-dipeptidic gelators

A series of chiral bis(dipeptide)oxalamides was prepared as outlined in Scheme 1. The synthesis and analytical characterization of the prepared compounds are collected in the Supporting Information. Two sets of bis(dipeptide)oxalamides were prepared: the first incorporating a single amino acid and variable terminal groups such as carboxylic acid, methyl ester and carboxamide, namely (*S*,*S*)-bis(LeuLeu) **1a**, **b**, **c**; (*S,S*)-bis(PhgPhg) **3a**, **b**, **c** and (*S,S*)-bis(PhePhe) **5a**, **b**, **c** and, the second containing two different amino acids, (*S,S*)-bis(LeuPhg) **2a**, **b**, **c** and (*S,S*)-bis(PhgLeu) **4a**, **b**, **c** (configurations of only two of the four stereogenic centers are denoted corresponding to that of oxalamide α- and β-amino acid, respectively, as depicted in Scheme 1).

Compared to the previously studied bis(amino acid)-oxalamide gelators (Figure 1), the retro-dipeptidic gelators, in addition to the oxalamide hydrogen bonding unit, also contain two peptidic

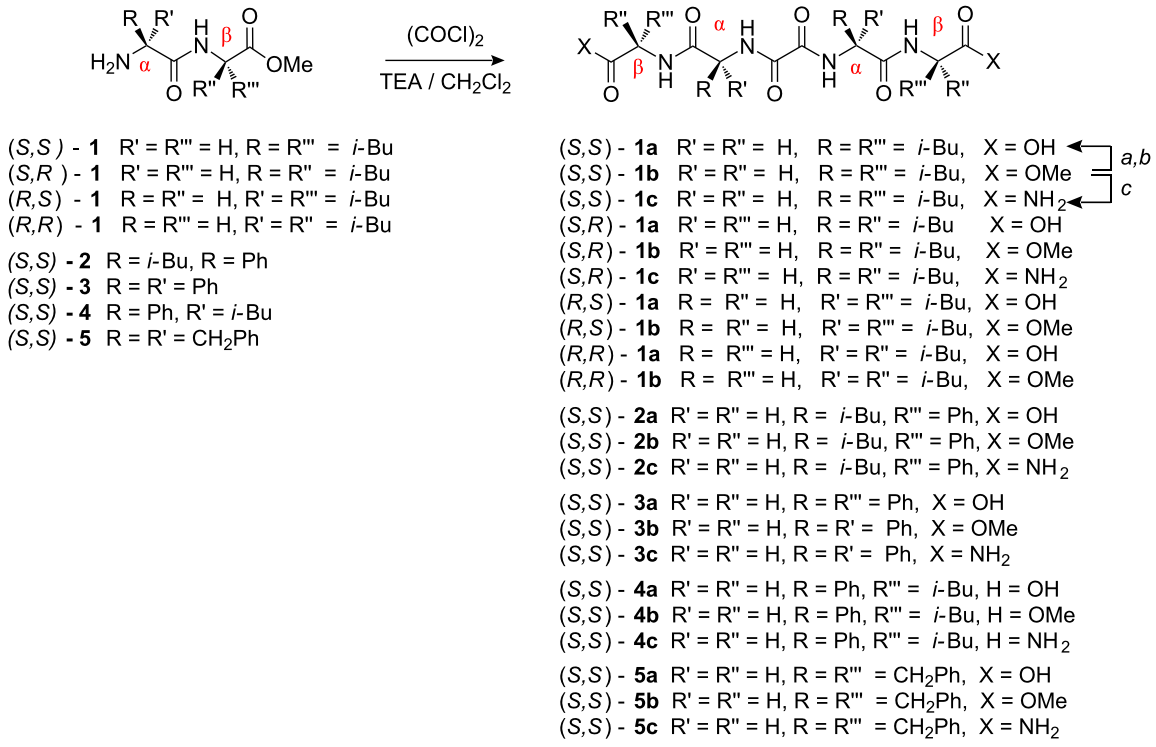

(*S,S*) - **1** R' = R''' = H, R = R''' = *i*-Bu
(*S,R*) - **1** R' = R''' = H, R = R'' = *i*-Bu
(*R,S*) - **1** R = R'' = H, R' = R''' = *i*-Bu
(*R,R*) - **1** R = R''' = H, R' = R'' = *i*-Bu

(*S,S*) - **2** R = *i*-Bu, R = Ph
(*S,S*) - **3** R = R' = Ph
(*S,S*) - **4** R = Ph, R' = *i*-Bu
(*S,S*) - **5** R = R' = CH_2Ph

(*S,S*) - **1a** R' = R'' = H, R = R''' = *i*-Bu, X = OH
(*S,S*) - **1b** R' = R'' = H, R = R''' = *i*-Bu, X = OMe
(*S,S*) - **1c** R' = R'' = H, R = R''' = *i*-Bu, X = NH_2
(*S,R*) - **1a** R' = R''' = H, R = R'' = *i*-Bu X = OH
(*S,R*) - **1b** R' = R''' = H, R = R'' = *i*-Bu, X = OMe
(*S,R*) - **1c** R' = R''' = H, R = R'' = *i*-Bu, X = NH_2
(*R,S*) - **1a** R = R'' = H, R' = R''' = *i*-Bu, X = OH
(*R,S*) - **1b** R = R'' = H, R' = R''' = *i*-Bu, X = OMe
(*R,R*) - **1a** R = R''' = H, R' = R'' = *i*-Bu, X = OH
(*R,R*) - **1b** R = R''' = H, R' = R'' = *i*-Bu, X = OMe

(*S,S*) - **2a** R' = R'' = H, R = *i*-Bu, R''' = Ph, X = OH
(*S,S*) - **2b** R' = R'' = H, R = *i*-Bu, R''' = Ph, X = OMe
(*S,S*) - **2c** R' = R'' = H, R = *i*-Bu, R''' = Ph, X = NH_2

(*S,S*) - **3a** R' = R'' = H, R = R''' = Ph, X = OH
(*S,S*) - **3b** R' = R'' = H, R = R' = Ph, X = OMe
(*S,S*) - **3c** R' = R'' = H, R = R' = Ph, X = NH_2

(*S,S*) - **4a** R' = R'' = H, R = Ph, R''' = *i*-Bu, H = OH
(*S,S*) - **4b** R' = R'' = H, R = Ph, R''' = *i*-Bu, H = OMe
(*S,S*) - **4c** R' = R'' = H, R = Ph, R''' = *i*-Bu, H = NH_2

(*S,S*) - **5a** R' = R'' = H, R = R''' = CH_2Ph, X = OH
(*S,S*) - **5b** R' = R'' = H, R = R''' = CH_2Ph, X = OMe
(*S,S*) - **5c** R' = R'' = H, R = R''' = CH_2Ph, X = NH_2

Scheme 1: Oxalyl retro-dipetide gelators; each **b** to **a**, (*a*) LiOH/MeOH, H_2O; (*b*) H^+; each **b** to **c**: (*c*) NH_3/MeOH.

units with specifically oriented hydrogen bond donor and acceptor sites and amino acid lipophilic substituents. Such structural characteristics enable multiple structural and stereochemical variations of the basic gelator structure and subsequent studies of structural and stereochemical influences on gelation properties, self-assembly motifs and gel morphology.

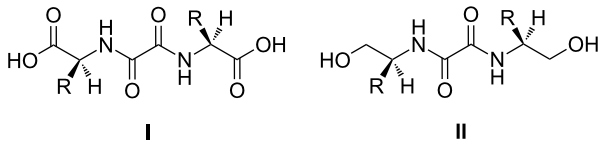

I **II**

Figure 1: Chiral bis(amino acid)-(**I**) and bis(amino alcohol)-(**II**)-oxalamide gelators.

The influence of stereochemistry on self-aggregation and morphology was studied with **1a–c** combining different configurations of Leu: (*S,R*)-**1a**, **b**, **c** and (*R,S*)-**1a**, **b**, **c**. Gelation properties of pure enantiomers (*S,S*)-**1b** and (*S,R*)-**1b** are compared with those of (*S,S*)-**1b**/(R,R)-**1b** and (*S,R*)-**1b**/(*R,S*)-**1b** racemic mixtures (Scheme 1).

Gelation properties

Terminal diacid retro-dipeptides

Gelation observed for selected gelator–solvent pairs is expressed by gelator effectiveness (G_{eff}, mL) corresponding to the maximal volume of solvent that could be immobilized by 10 mg of the gelator (Table 1). The oxalamides **1a**, **3a** and **5a** were insoluble in water but showed moderate to excellent gelation of water/DMSO and water/DMF solvent mixtures. The Leu containing gelator **1a** appeared more than 2 times more effective in gelation of water/DMSO or DMF mixtures than the aromatic acid containing gelators **3a** and **5a**. However, **3a** and **5a** also gelled small to moderate volumes of EtOH and *rac*-2-octanol, whilst Leu incorporating **1a** formed gels with the more lipophilic solvents, decalin and tetralin. The retro-dipeptides containing two different amino acids showed no or only weak gelation; (*S,S*)-(LeuPhg) **2a** lacked any gelation ability toward the tested solvents, while (*S,S*)-(PhgLeu) **4a** showed only weak gelation of water/DMSO, dichloromethane and toluene. Apparently, the retro-peptides incorporating aliphatic and aromatic amino acids are less versatile gelators compared to retro-peptides containing identical amino acid fragments. The latter points to the importance of intermolecular lipophilic interactions for the stabilization of gel assemblies being stronger in the

Table 1: Gelator effectivenesses (G_{eff}, mL) of retro-dipeptides **1a**–**5a** and bis(Leu)oxalamide **I** in gelation of various solvents and solvent mixtures (sol.: soluble; ins.: insoluble; cr.: crystallization; [A] gel/sol mixture).

Solvent	**I**	(*S,S*)-**1a**	(*S,R*)-**1a**	(*S,R*)-**1a**/(*R,S*)-**1a**	(*S,S*)-**1a**/(*R,R*)-**1a**	**2a**	**3a**	**4a**	**5a**
H_2O	0.4	ins.	ins.	ins.	ins.	ins.	ins.	ins.	ins.
H_2O/DMSO	0.8+0.4	5.09+2.98	15.0+4.5	5.3+5.3	cr.	cr.	2.3+1.6	1.0+1.0	1.1+0.5
H_2O/DMF	cr.	5.84+3.25	7.5+2.0	2.8+1.7	cr.	cr.	2.5+1.1	cr.	2.8+0.7
EtOH	1.5	sol.	cr.	cr.	cr.	sol.	cr.	sol.	1.1
±2-octanol	10.95	ins.	sol.		cr.	sol.	1.25	cr.	5.75
THF	0.4	sol.	sol.	sol.	sol.	sol.	sol.	sol.	sol.
CH_2Cl_2	1.5+0.05[a]	ins.	cr.	ins.	ins.	ins.	ins.	0.25	ins.
CH_3CN	0.95	cr.	cr.	cr.	cr.	sol.	cr.	ins.	7.0
toluene	1.95	cr.	cr.	0.25	cr.	ins.	ins.	0.5	sol.
p-xylene	2.45	ins.	ins.		0.25	ins.	ins.	[A]	cr.
decalin	0.2	0.2	0.8	1.7	jelly	ins.	ins.	ins.	ins.
tetralin	3.0	1.8	jelly	0.5	0.2	sol.	ins.	jelly	4.0

[a]DMSO.

case of identical amino acids either lipophilic or aromatic, and weaker for mixed aromatic-lipophilic amino acid fragments present in the gelator molecule.

Interestingly, the (*S,R*)-bis(LeuLeu) retro-peptide **1a**, the diastereomer of (*S,S*)-**1a**, exhibited an increased G_{eff} for the water/DMSO mixture and decalin which however is absent for water/DMF solvent mixture (Table 1). The latter exemplifies the strong stereochemical influence on gelator effectiveness in certain solvents.

In many cases of chiral gelators, pure enantiomers were found more effective gelators than the racemates, although several exceptions were observed showing that the racemic form could be a more effective gelator of certain solvents than the corresponding pure enantiomer [60-68]. Therefore, we also compared gelation properties of selected enantiomers and racemates and found that the (*S,R*)-**1a**/(*R,S*)-**1a** racemate was considerably less effective in gelation of both, water/DMSO and water/DMF solvent mixtures compared to the pure enantiomer (*S,R*)-**1a**, while the racemate (*S,S*)-**1a**/(*R,R*)-**1a** lacked any gelation ability and tended to crystallize from both solvent mixtures.

Generally, it can be concluded that the retro-dipeptides are less effective and less versatile gelators compared to the previously studied bis(amino acid)oxalamides. Table 1 shows that bis(Leu)oxalamide **I** is much more versatile and a more efficient gelator compared to (*S,S*)-**1a** and (*S,R*)-**1a**, and is capable of gelling water and various solvents of medium and low polarity. However, **I** is considerably less efficient in gelation of highly polar water/DMSO and water/DMF solvent mixtures compared to both **1a** diasteroisomers. Hence, the presence of more hydrogen bonding sites and lipophilic groups in the retro-dipeptides appears less favorable for gelation of water and solvents of medium and low polarity presumably due to decreased solubility and increased crystallization tendency compared to bis(amino acid)oxalamides. However, their efficient gelation of water/DMSO and water/DMF solvent mixtures presents a striking difference where DMSO and DMF co-solvents could sufficiently increase their solubility up to the point necessary for aggregation into sufficiently long fibers capable of networking.

Terminal dimethyl ester retro-dipeptides

In the previously studied series of bis(amino acid)oxalamide gelators transformation of terminal carboxylic acid groups into methyl esters resulted in the complete loss of gelation ability [59]. In the retro-dipeptide series the gelation properties of methyl ester derivatives **1b**–**5b**, were not significantly different from those of the respective diacid derivatives **1a**–**5a** except that the diester derivatives appear slightly more versatile exhibiting gelation also with some lipophilic solvents (Table 1 and Table 2). This could be explained by the increased lipophilicity of the diester derivatives and, consequently increased solubility in more lipophilic solvents compared to the diacid gelators. It should be noted that the diester racemates (*S,R*)-**1b**/(*R,S*)-**1b** and (*S,S*)-**1b**/(*R,R*)-**1b** showed significantly increased effectiveness in gelation of water/DMSO and water/DMF solvent mixtures compared to the respective free acid racemates (*S,R*)-**1a**/(*R,S*)-**1a** and (*S,S*)-**1a**/(*R,R*)-**1a** (Table 1), respectively. Also, in contrast to the free acid gelators, the diester racemates were up to two times more efficient in the gelation of water/DMF and water/DMSO mixtures than their pure enantiomer counterparts (*S,R*)-**1b** and (*S,S*)-**1b** (Table 2). The latter provides additional

Table 2: Gelator effectiveness (G_{eff}, mL) of bis(dipeptide)oxalamide dimethyl esters **1b**–**5b** in gelation of various solvents and solvent mixtures (sol.: soluble; ins.: insoluble; cr.: crystallization; [A] gel/sol mixture; (F): cotton-like fiber aggregates; ** the mixture of crystals and gel.).

Solvent	(*S*,*S*)-**1b**	(*S*,*R*)-**1b**	(*S*,*R*)-**1b**/ (*R*,*S*)-**1b**	(*S*,*S*)-**1b**/ (*R*,*R*)-**1b**	**2b**	**3b**	**4b**	**5b**
H_2O	ins.	ins.	ins.	ins.	ins.	ins.	ins.	ins.
H_2O/DMSO	3.95+6.75	9.7+10.0	13.2+9.65	13.8+9.1	0.15+0.5	1.1+2.7	0.2+0.5	cr.
H_2O/DMF	5.1+4.8	11.5+11.7	13.1+7.8	5.4+3.4	cr.	cr.	cr.	cr.
EtOH	cr.	cr.	cr.	cr.	cr.	2.00	(F1.3)	0.9
±2-octanol	cr.	cr.	cr.	cr.	1.85	cr.	(F0.5)	2.05
THF	sol.	cr.	sol.	sol.	sol.	sol.	sol.	cr.
CH_2Cl_2	sol.	sol.	sol.	sol.	sol.	ins.	sol.	cr.
CH_3CN	cr.	cr.	cr.	cr.	cr.	cr.	cr	cr.
toluene	[A]	0.15	**	0.55	1.1	ins.	1.25	2.0
p-xylene	[A]	0.5	**	1.3	1.1	ins.	1.1	2.5
decalin	2.3	0.8	1.75	5.6	2.0	ins.	4.8	1.7
tetralin	cr.	0.2	sol.	sol.	0.6	0.4	0.9	0.5

examples that in some cases racemates could be more effective gelators than the pure enantiomers. Hence, in the search for highly effective gelators for targeted solvents, the racemic form of a chiral gelator must be tested.

Terminal dicarboxamide retro-dipeptides

The diamide derivatives bis(LeuLeuNH_2) **1c**, bis(PhgPhgNH_2) **3c** and bis(PhePheNH_2) **5c** appeared more versatile being capable of gelling a larger set of tested solvents compared to the respective dicarboxylic acid (**1a**, **3a**, and **5a**) and dimethyl ester derivatives (**1b**, **3b** and **5b**) (Tables 1–3). The influence of stereochemistry on gelator versatility and effectiveness can be illustrated by the considerably improved gelation properties of the heterochiral (*S,R*)-**1c** diastereoisomer compared to homochiral (*S,S*)-**1c**; the former is capable of immobilizing up to 10 and 4 times larger volumes of dichloromethane and toluene solvent mixtures containing a little DMSO, respectively (Table 3). Also the bis(LeuPhgNH_2) **2c** and bis(PhgLeuNH_2) **4c** incorporating different amino acids appeared more versatile than the corresponding diacids (**2a**, **4a**) and diesters (**3b**, **4b**). It appears that the increased hydrogen bonding potential of terminal diamide derivatives provides somewhat more versatile gelators capable of gelating solvents of medium and low polarity where intermolecular hydrogen bonding is favored.

TEM and DSC investigations

As reported previously, TEM investigations of bis(amino acid)oxalamide gels revealed in most cases formation of very dense networks consisting of heavily entangled tiny fibers with diameters in the range of 10–20 nm [58-60]. A similar

Table 3: Gelation effectiveness (G_{eff}, mL) of bis(amino acid and dipeptide-$CONH_2$)oxalamides **1c**–**5c** in gelation of various solvents and solvent mixtures (sol.: soluble, ins.: insoluble; cr.: crystalline; [A] gel/sol mixture).

Solvent	(*S*,*S*)-**1c**	(*S*,*R*)-**1c**	**2c**	**3c**	**4c**	**5c**
H_2O	ins.	ins.	ins.	ins.	ins.	ins.
H_2O/DMSO	0.55+1.4	0.8+1.2	1.8+2.9[a]	cr.	4.7+5.0	1.3+1.6
H_2O/DMF	0.45+0.75	0.8+0.6	1.05+11[a]	cr.	1.7+1.8	2.7+3.0
EtOH	cr.	[A]	ins.	ins.	3.4	ins.
±2-octanol	ins.	3.0	5.0+0.1[a]	ins.	cr.	ins.
THF	ins.	ins.	1.1+0.05[a]	ins.	ins.	ins.
CH_2Cl_2	1.05+0.2[a]	11.0+0.84[a]	2.0+0.1[a]	ins.	1.5+0.4	ins.
CH_3CN	ins.	0.5+0.04[a]	ins.	ins.	ins.	ins.
toluene	1.05+0.2[a]	4.0+0.4[a]	2.2+0.2[a]	ins.	0.75+0.1[a]	ins.
p-xylene	ins.	7.5+0.4[a]	6.9+0.2[a]	ins.	0.95+0.08[a]	ins.
decalin	ins.	ins.	0.8	ins.	ins.	0.5(ins.)
tetralin	7.3	sol.	2.0	ins.	1.0	2.0

[a]DMSO.

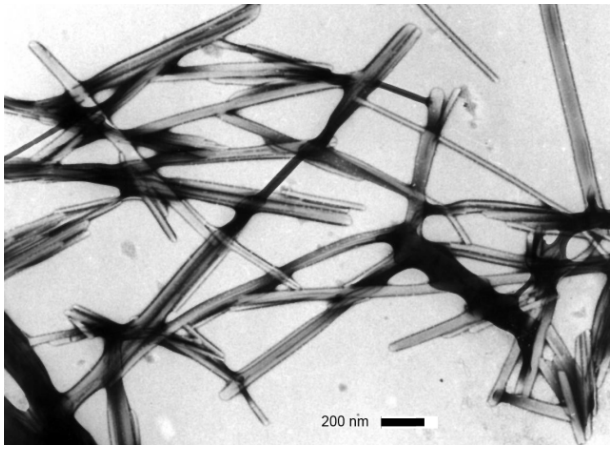

Figure 2: TEM images (PWK staining) of: (*S*,*S*)-**1a** H_2O/DMSO gel.

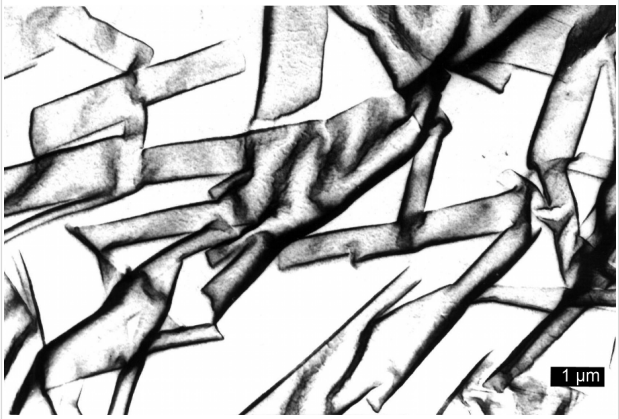

Figure 4: TEM images (PWK staining) of: (*S*,*R*)-**1b** toluene gel showing the presence of short tape like aggregates.

morphology was observed for the bis(PhePhe)-**5a**-EtOH gel (fiber *d*'s 6–20 nm) and bis(PhgLeu) **4a** water/DMSO gel (fiber *d*'s 5–15 nm) (see Supporting Information File 1, Figure S1a,b). TEM images of diastereomeric (*S*,*S*)-**1a** and (*S*,*R*)-**1a** water/DMSO gels (Figure 2 and Figure 3) show highly distinct morphology of gel networks. In the first gel rather straight fibers and fiber bundles with diameters in the range of 40–100 nm could be observed. However, the (*S*,*R*)-**1a** network showed a lower bundling tendency (Figure 3) and contained mostly fibers with diameters between 20–40 nm. In contrast to water/DMSO gels, the TEM image of the methyl ester derivative (*S*,*R*)-**1b** gel with toluene had a totally different morphology characterized by the presence of short and very wide tapes (Figure 4). As observed earlier for other gel systems, gelator effectiveness G_{eff} depends not only solubility but also depends on the thickness of fibers constituting the network [43,59,60]. Since solvent is entrapped by capillary forces, the formation of a dense network composed of thin fibers should possess smaller compartments and hence a higher solvent immobilization capacity compared to those less dense formed by thick fibers.

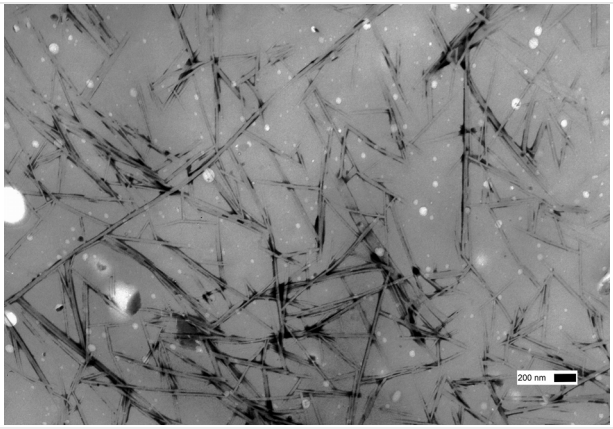

Figure 3: TEM images (PWK staining) of: (*S*,*R*)-**1a** H_2O/DMSO gel.

The TEM observed thicknesses of gel aggregates existing in water/DMSO and toluene gels could be also correlated with gelator effectiveness (G_{eff}, mL, see Table 1 and Table 2). It appears that (*S*,*R*)-**1b** (G_{eff} 19.5 mL, water/DMSO gel) organized in thinner fibers is more than twice effective a gelator than its diasteroisomer (*S*,*S*)-**1a** (G_{eff} 8.0 mL, water/DMSO gel) which forms thicker fiber bundles. In the toluene gel, (*S*,*R*)-**1b** organizes into wide and short tapes with low networking capacity which is reflected in a very low (G_{eff} 0.15 mL) gelator effectiveness.

DSC investigation of the highly efficient (*S*,*R*)-**1a** gelator of water/DMSO solvent mixture showed only one transition in the heating (T_m) and cooling (T_c) cycle with gelation enthalpy changes of 37.70 and −38.20 kJ/mol, respectively (Table 4). The (*S*,*R*)-**1a**/(*R*,*S*)-**1a** racemic mixture being almost two times less effective in gelation of the same solvent mixture compared to (*S*,*R*)-**1a**, showed two transitions in the DCS heating and cooling cycle neither of which corresponded to those observed with (*S*,*R*)-**1a**. Moreover, the racemate showed considerably lower enthalpy changes compared to pure enantiomer gel (Table 4). The latter observations for the racemate gel indicate higher complexity of such systems and suggest possible interactions of enantiomers that lead to diasteromeric assemblies with a certain level of organization.

Table 4: Δ*H* and transition temperatures for selected retropeptide DMSO/water obtained from DSC heating and cooling cycles.

Gelator/solvent	T_m °C	ΔH_m kJ/mol	T_c °C	ΔH_c kJ/mol
(*S*,*R*)-**1a**/water/DMSO	93.2	37.70	82.6	−38.20
(*S*,*R*)-**1a**/(*R*,*S*)-**1a**/ water/DMSO	97.6 137.0	20.36 2.32	78.2 123.2	−23.95 −2.80

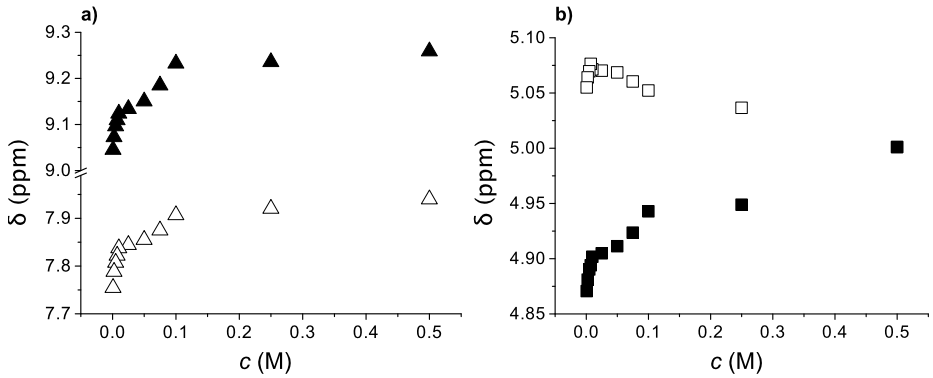

Figure 5: The concentration dependence of NH and C*H chemical shifts in (*S,R*)-**1b** toluene-d_8 gel samples (concentration range 0.001–0.1 M): a) oxalamide-NH protons (▲); Leu-NH's (Δ) and b) oxalamide-α-Leu-C*H (■) and oxalamide-β-Leu-C*H (□) protons.

FTIR, ^{1}H NMR and CD investigations

To identify supramolecular interactions that stabilize gel assemblies, the selected gels were studied by ^{1}H NMR, FTIR and CD spectroscopy. Valuable information on the self-assembly of gelator molecules in the pre-gelation state and in the gel could be obtained by analysis of the concentration and temperature dependent ^{1}H NMR and FTIR spectra. It was previously reported that the planar and self-complementary oxalamide unit persistently forms intermolecular hydrogen bonds and represents the major organizational element in the gel assemblies of both, bis(amino acid)- and bis(amino alcohol)oxalamides, and also has the major influence on their organization in the solid state [55-60]. In addition, the latter gelators tend to exhibit layered organization in their gel assemblies due to their structural resemblance to bola-amphiphiles.

In the FTIR spectra of (*S,S*)-**1b** and (*S,R*)-**1b** toluene gels one wide band or two poorly resolved NH bands, respectively, appear in the region of 3260–3320 cm^{-1} corresponding to a hydrogen bonded NH. In addition, the ester carbonyl and amide I bands are located at 1750 and 1653 cm^{-1}, respectively, the position of the latter being in accord with its participation in hydrogen bonding.

^{1}H NMR investigation showed significant concentration dependence of N–H and C*H proton shifts in the (*S,R*)-**1b** (Figure 5), (*S,S*)-**1b** and its racemate (*S,S*)-**1b**/(*R,R*)-**1b** (Figure 6) toluene-d_8 gel samples. In the first case the oxalamide NH and Leu-NH protons were downfield shifted by 1.6 and 1.8 ppm, respectively, for a gelator concentration increase from 0.001–0.1 mol dm^{-3}. The oxalamide-α-Leu methine protons (C*H) were also significantly downfield shifted ($\Delta\delta_{C*H}$ = 0.566 ppm) while the β-Leu-C*H proton shifts were less significant. Strong downfield shifts of the oxalamide- and Leu-NH protons as well as the α-Leu-C*H proton closest to the oxalamide unit suggest simultaneous participation of both

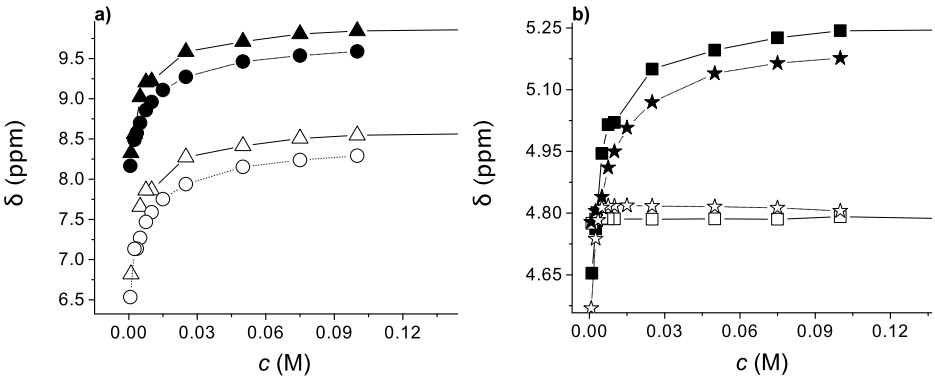

Figure 6: The concentration dependence of NH and C*H chemical shifts in (*S,S*)-**1b** and its racemate (*S,S*)-**1b**/(*R,R*)-**1b** toluene-d_8 gels (concentration range 0.001–0.1 mol dm^{-3}): a) (*S,S*)-**1b** oxalamide-NH protons (▲) and Leu-NH protons (Δ); the racemate oxalamide-NH protons (●) and Leu-NH protons (O); b) (*S,S*)-**1b** oxalamide-α-Leu-C*H (■);(*S,S*)-**1b** oxalamide-β-Leu-C*H (□); the racemate oxalamide-α-Leu-C*H (★); racemate oxalamide-β-Leu-C*H (☆).

the oxalamide and Leu-NH protons in intermolecular hydrogen bonding. A comparison of the magnitudes of concentration induced shifts for diastereomeric gelators (*S,R*)-**1b** (Figure 5; oxalamide-NH protons Δδ 0.25 ppm; Leu-NH protons Δδ 0.17 ppm; α-Leu-C*H Δδ 0.13 ppm) and (*S,S*)-**1b** (Figure 6, oxalamide-NH protons Δδ 1.50 ppm; Leu-NH protons Δδ 1.55 ppm; α-Leu-C*H Δδ 0.53 ppm) shows large differences. The monitored protons of (*S,S*)-**1b** are more strongly downfield shifted than the corresponding protons of (*S,R*)-**1b** for the same concentration range. Similar trends of NH and C*H concentration induced shifts are observed for (*S,S*)-**1b** and its racemate (*S,S*)-**1b**/(*R,R*)-**1b** toluene-d_8 gels (Figure 6). Again the magnitudes of the NH and C*H concentration induced shifts are higher for the (*S,S*)-**1b** than for the racemate gel. It should be noted that the higher concentration induced shifts are observed for (*S,S*)-**1b** which forms sol–gel mixture in toluene compared to both (*S,R*)-**1b** and the racemate (*S,S*)-**1b**/(*R,R*)-**1b** forming stable toluene gels (Table 2).

The concentration induced shift curves show that for the examined gelators, the self-assembly equilibrium is reached at different gelator concentrations; for (*S,S*)-**1b** and its racemate (*S,S*)-**1b**/(*R,R*)-**1b**, the saturation point is reached at the same concentration of 0.03 mol dm^{-3} (Figure 6a,b) which corresponds to the experimentally determined minimal gelation concentration (*MGC*) for the racemate of 0.034 mol dm^{-3}. If the racemate were organized in the conglomerate as separate enantiomeric (*S,S*)-**1b** and (*R,R*)-**1b** assemblies, the magnitudes of the concentration induced shifts should be similar to those measured the for (*S,S*)-**1b** assemblies. Since this was not observed (Figure 6a, b) the results suggest formation of racemic gel assemblies composed of both enantiomers. The latter also points to the lack of any resolution at the supramolecular level which was found to occur for some racemic gelators and specific solvents [60]. The observation that (*S,S*)-**1b** with toluene gives a sol/gel mixture while the racemate gives a stable gel implies that the enantiomer forms insufficiently long assemblies incapable of efficient networking and of forming of self-supported gel, while the opposite holds for the racemic assemblies which are capable of forming the gel network

The discontinuous concentration induced shift curves obtained for (*S,R*)-**1b** diasteroisomer may indicate the presence of different assemblies at lower and higher gelator concentrations. It appears that the first saturation point is reached at a concentration around 0.03 mol dm^{-3} and the second at 0.12 mol dm^{-3}, the latter corresponding nicely to the experimentally determined *MGC* of 0.116 mol dm^{-3}. It should be noted that in the low and high concentration ranges downfield shifts of oxalamide- and Leu-NH protons are observed indicating that both assemblies are formed by intermolecular hydrogen bonding. The determined higher saturation point and *MGC* of 0.12 mol dm^{-3} for (*S,R*)-**1b** compared to the saturation point of the (*S,S*)-**1b** diastereoisomer (0.03 mol dm^{-3}) could be explained by the increased solubility of the (*S,R*)-**1b** assemblies in toluene compared to those formed by the second diastereoisomer [69]. However, despite of the lower saturation point and lower solubility, the (*S,S*)-**1b** assemblies cannot form the gel which points toward possible solvation effects taking a decisive role in the self-assembly of the diastereoisomers. Recently, Meijer et al. [70] presented convincing evidence that co-organization of solvent at the periphery of the gel aggregates plays a direct role in the assembly processes evident, even during the formation of the pre-aggregates. The influence of solvent structure on the length of the aggregates was clearly demonstrated. Hence, different solvation effects of toluene operating in the self-assembly of (*S,S*)-**1b** and (*S,R*)-**1b** may be responsible for the formation of insufficiently long aggregates of the first diastereoisomer resulting in the formation of the sol–gel mixture, and sufficiently long assemblies of the second one being capable of networking and the formation of a self-supported gel.

The variations of oxalamide NH, Leu-NH, α- and β-Leu-C*H proton chemical shifts with increasing temperature in the toluene-d_8 gel samples of the diastereomeric (*S,R*)-**1b** and (*S,S*)-**1b** (concentrations of 0.5 mol dm^{-3}) are shown in Figure 7. For the (*S,R*)-**1b** gel, a temperature increase from 20–50 °C induced only slight downfield shifts of both the oxalamide- and Leu-NH protons as well as the α- and β-Leu-C*H protons; in the higher temperature interval (50–90 °C) all protons were downfield shifted in accord with the breaking of intermolecular hydrogen bonds involving both the oxalamide and Leu NH protons. In contrast, the respective protons of the (*S,S*)-**1b** are continuously shifted downfield with increasing temperature (Figure 7c). Hence, a clear difference in the thermal behavior of (*S,S*)-**1b** weak gel and (*S,R*)-**1b** gels was observed. Similar discontinuous temperature variation curves to those observed for (*S,R*)-**1b** were also found for bis(amino acid)oxalamide gelators which were shown to exhibit the layered type of organization in their gel assemblies [59,60]. Small downfield shifts of the oxalamide- and LeuNH protons observable in the low temperature regime (Figure 7a) were explained by the less energy demanding disassembly that occurred at lipophilic sites of the interacting bilayers resulting in small deshielding of these protons. In the higher temperature regime the downfield shifts of the same protons indicate the breaking of intermolecular hydrogen bonds. This conclusion is supported by molecular modeling (see the respective paragraph) which showed that the low energy conformation of (*S,R*)-**1b** is similar to those found for bis(amino acid)oxalamides and that both show a strong resemblance to bola-amphiphiles which are known to organize into bilayers [71].

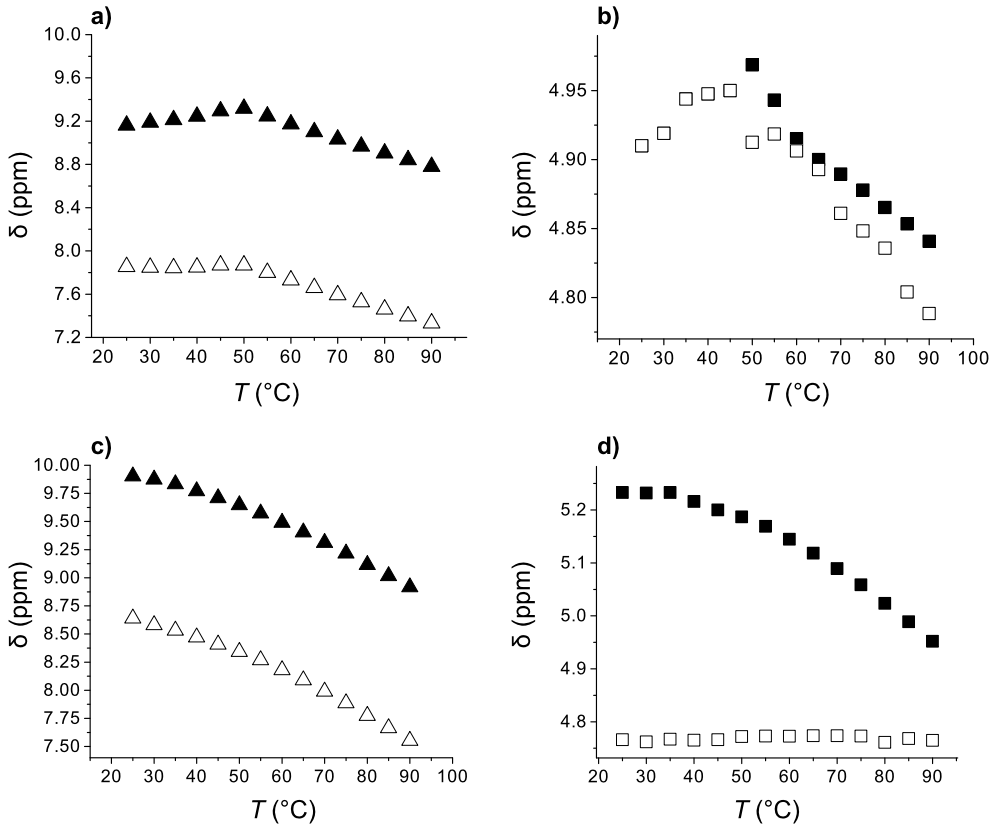

Figure 7: Temperature dependence of: a) oxalamide NH protons (▲), Leu-NH protons (Δ) and b) oxalamide-α-Leu-C*H (■) and oxalamide-β-Leu-C*H (□) chemical shifts in 0.5 mol dm^{-3} (*S,R*)-**1b** toluene-d_8 gel sample; c) and d) induced shifts of the respective protons in (*S,S*)-**1b** toluene-d_8 gel.

The temperature dependence of CD spectra of decalin gels formed by diastereoisomeric methyl esters (*S,R*)-**1b** and (*S,S*)-**1b** (Figure 8a, b, respectively) was also investigated. At room temperature (*S,R*)-**1b** shows negative Cotton effect at λ = 245 nm of moderate intensity which decreases on increasing temperature from 20 to 50 °C. Further temperature increase of the gel sample resulted in the appearance of a new negative CD peak at λ = 234 nm corresponding to the shoulder band in the gelator UV spectrum (Figure 8e); the intensity of the band increased with increasing temperature (Figure 8a). As reported for the self-assembled alanine based gelators, the CD signal at around 232 nm can be ascribed to the n,π^*-transition of the amide carbonyl [72-74]. Hence, the λ = 234 nm band that appeared at 60 °C could be ascribed to the intrinsic chirality of disassembled gelator molecules. Although the origin of the λ = 245 nm CD band is not clear, it could be the consequence of circular differential scattering which was shown to contribute to the CD spectra of large aggregated biomolecules [75].

By contrast, the CD spectra of the (*S,S*)-**1b** gel showed a negative CD band at λ_{min} 238.6 nm (Figure 8b) corresponding to its electronic absorption band (Figure 8f), but similarly to (*S,R*)-**1b** the intensity of CD band increased with increasing temperature.

It should be noted that the temperature induced changes in the CD spectra of both, (*S,R*)-**1b** and (*S,S*)-**1b** decalin gels are different to those obtained for **5a** ethanol and bis(Leu)oxalamide 1-butanol gels (Figure 8c, d). With these latter gels a decrease of CD peak intensities with increasing temperature was observed in accord with the disassembly of the chiral gel aggregates which has also been observed for some other chiral gels [76]. Consequently, the CD results described for the (*S,R*)-**1b** and (*S,S*)-**1b** gels, characterized by the increase of CD signals with increasing gel temperature, indicate that in these systems there is no aggregation increased chirality as observed for some other gels of the chiral gelators.

XRPD, molecular modeling and packing model

The X-ray powder diffraction (XRPD) pattern of (*S,S*)-**1b** xerogel showed strong peaks corresponding to periodic distance *d* of 16.1 and 13.4 Å and a weaker peaks corresponding to *d's* of 15.1 and 8.6 Å (Figure 9b).

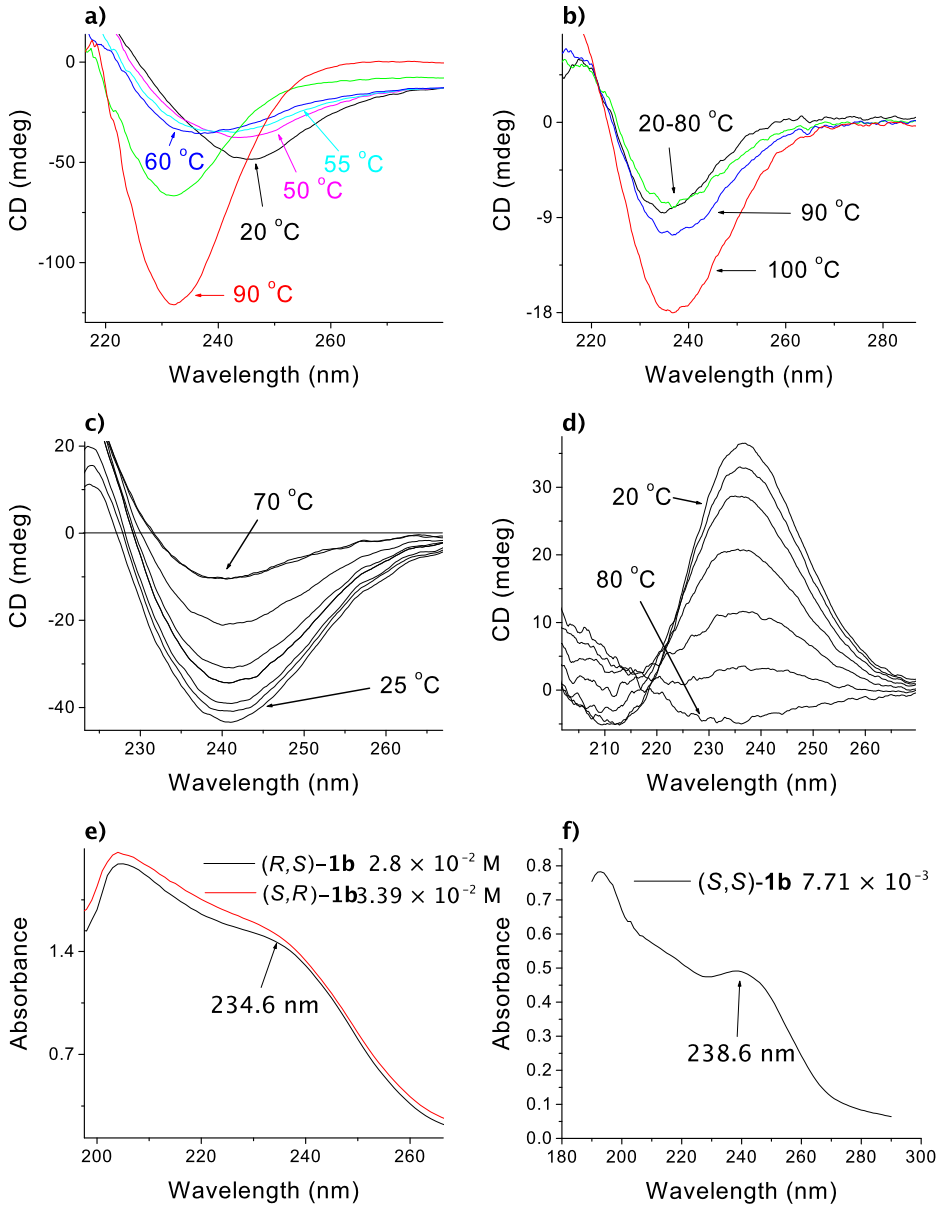

Figure 8: Temperature dependent CD spectra of: a) (*S*,*R*)-**1b** decalin gel (c = 3.4·10^{-2} M); b) (*S*,*S*)-**1b** decalin gel (c =7.6·10^{-3} M); c) **5a** ethanol gel (c =1·10-2 M) and d) (*S*,*S*)-bis(Leu)oxalamide **I** 1-butanol gel (c = 2.8·10^{-2} M); e), f) UV spectra of (*S*,*R*)-**1b** (red curve), (*R*,*S*)-**1b** and (*S*,*S*)-**1b** taken in decalin at specified concentrations.

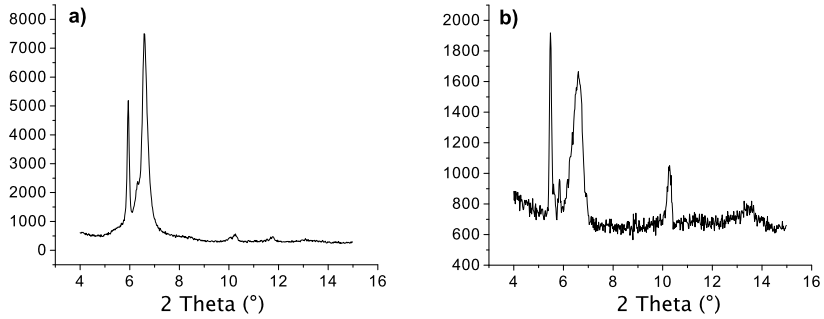

Figure 9: X-ray powder diffractograms of (a) (*S*,*R*)-**1b** and (b) (*S*,*S*)-**1b** xerogels prepared from their toluene gels.

For the (*S,R*)-**1b** xerogel, strong peaks corresponding to *d*'s of 14.9 and 13.4 Å and smaller peaks to *d*'s of 13.98, 8.6 and 7.5 Å could be observed (Figure 9a). Molecular modeling of (*S,R*)-**1b** and (*S,S*)-**1b** yields low energy extended conformations with lengths of 15.1 and 15.9 Å, respectively (Figure 10a) [77].

The measured extended conformation lengths correspond nicely to the largest periodic distances of 14.9 and 16.1 Å obtained by XRP diffraction of (*S,R*)-**1b** and (*S,S*)-**1b** xerogels indicative of the formation of assemblies of the extended gelator molecules. However, the low energy conformations of (*S,R*)-**1b** and (*S,S*)-**1b** are distinctly different with all *i*-Bu groups *cis*-oriented in (*S,R*)-**1b**, while the *i*-Bu groups in α- and β-Leu of (*S,S*)-**1b** have the *trans*-arrangement with respect to the plane containing the amide and oxalamide groups (Figure 10a). Conformational analysis reveals why such arrangements of *i*-Bu groups occur (Figure 10b, Newman projections of two stereogenic centers only). Our earlier results based on single crystal X-ray analysis of bis(amino acid)oxalamides showed that their most stable conformations are characterized by vicinal positioning of the methine proton at the stereogenic centre and oxalamide carbonyl oxygen atom which produces the lowest steric repulsion. Similarly, in the conformation A of (*S,R*)-**1b** with *cis*-arrangement of the *i*-Bu groups, the smallest group (H) of the β-Leu chiral centre is located close to amide carbonyl; the conformations with *trans*-arrangement of *i*-Bu groups should be less stable due to increased steric repulsion between the amide carbonyl oxygen and either the *i*-Bu or carboxymethyl group. Among the conformations of (*S,S*)-**1b** denoted B, C and D with *trans*-, *cis*- and *trans*-arrangement of *i*-Bu groups, respectively, the conformation D appears the most stable due to the vicinal position of the smallest group (H) and amide carbonyl oxygen atom. These conclusions are supported by molecular modeling (Figure 10a); the lowest energy conformations of (*S,R*)-**1b** and (*S,S*)-**1b** generated by systematic search of their conformational space correspond to A and D of Figure 10b, respectively. In support, the values of the vicinal NH-Cα-H coupling constants $J_{NH\text{-}CH}$ for the (*S,R*)-**1b** oxalamide NH-Leu Cα-H and Leu NH-Leu Cα-H (8.63 and 8.48 Hz) and (*S,S*)-**1b** (8.63 and 8.33 Hz) obtained from their ^{1}H NMR spectra taken in $CDCl_3$ correspond to dihedral angles close to *trans*-coplanar positioning of NH and Cα-H protons in both groups

The low energy conformations of (*S,R*)-**1b** and (*S,S*)-**1b** were used for docking calculations to generate the hydrogen bonded dimers of extended gelator molecules involving both, the oxalamide and Leu-NH protons (Supporting Information File 1, Figure S3). The thicknesses of such dimers estimated from models are between 7.5 and 8.6 Å (Figure 11) which correspond well to periodic distance *d* of 8.6 Å found in their XRP diffractograms. The thickness of the (*S,R*)-**1b** dimer generated

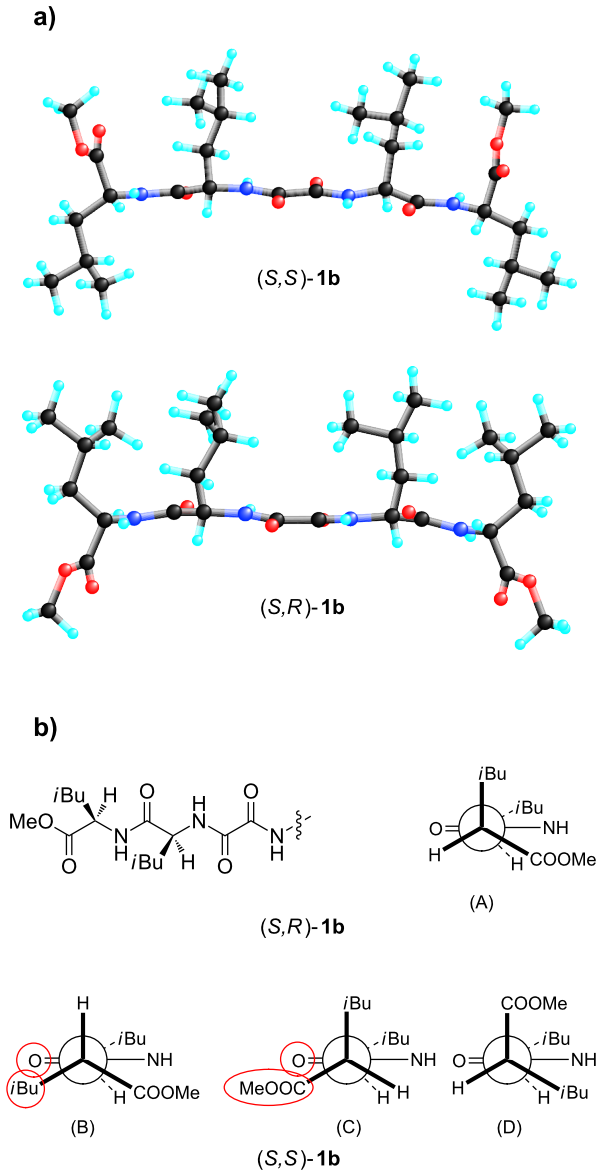

Figure 10: (a) Fully minimized the lowest energy conformations of (*S,S*)-**1b** (top) and (*S,R*)-**1b** generated by systematic conformational search (SYBYL package; second graphic); (b) Partial Newman projections of two stereogenic centers of (*S,R*)-**1b** and (*S,S*)-**1b** showing conformations with *cis*-arrangement of *i*-Bu groups in the former (A) and *trans*- (B, D) and *cis*- (C)-arrangements of *i*-Bu groups in the latter.

by lipophilic interactions is 13.4 Å corresponding exactly to *d* of 13.4 Å found in its XRPD. The (*S,S*)-**1b** model of the dimer formed by lipophilic packing gives a thickness of 13.9 Å. Based on these results and those of the FTIR and ^{1}H NMR studies, which suggested intermolecular hydrogen bonding between gelator molecules involving both the oxalamide and Leu amide units, a basic packing model for (*S,S*)-**1b** and (*S,R*)-**1b** can be proposed which consists of layers of hydrogen bonded gelator molecules (Figure 11).

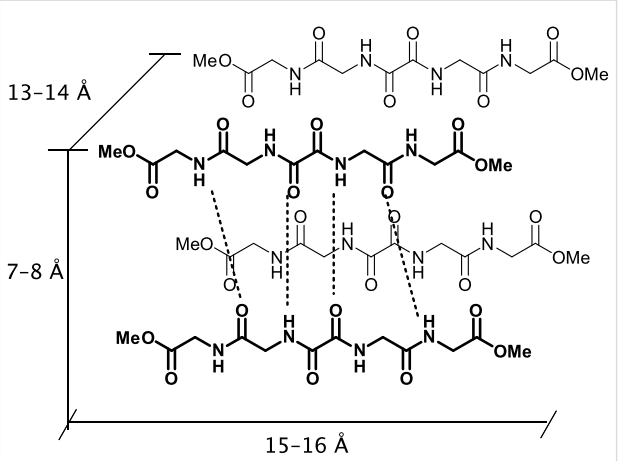

Figure 11: Schematic presentation of the proposed (*S,S*)-**1b** and (*S,R*)-**1b** basic packing model based on XRPD, ^{1}H NMR, FTIR and molecular modeling results.

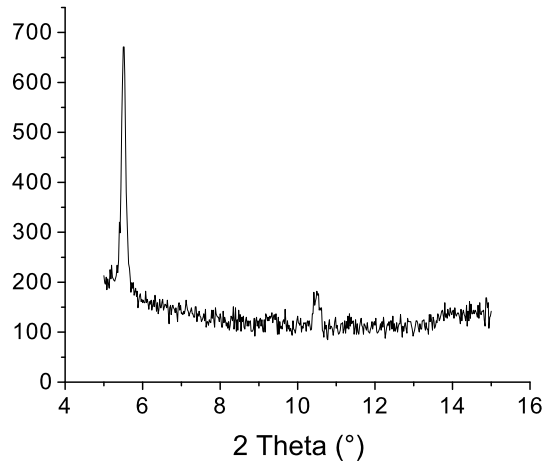

Figure 12: X-ray powder diffraction (XRPD) diagram of (*S,R*)-**1a** water/DMSO xerogel.

In contrast to the diester gelators (*S,R*)-**1b** and (*S,S*)-**1b** a detailed spectroscopic investigation of (*S,S*)-**1a** and (*S,R*)-**1a** organization in their water/DMSO gel assemblies was not possible due to solvent unsuitability.

Nevertheless, the FTIR spectrum of the (*S,R*)-**1b** xerogel prepared from its water/DMSO gel was found to differ from that of the crystalline sample; the positions of NH stretching, carboxylic acid and amide I carbonyl stretching, and NH bending amide II bands in the spectra of crystalline and xerogel samples appear at 3281.2 1724.4 1655.6 1543.6 1510.4 cm^{-1} and 3303.4 3273.5 1728.5 1651.6 1534.2 1510.5 cm^{-1}, respectively. The positions of the xerogel bands are similar to those found in the spectrum of previously studied bis(Leu)oxalamide water/DMSO gel assemblies (3300 1729 1658 1515 cm^{-1}) and which was shown to organize by intermolecular hydrogen bonding between oxalamide units and lateral carboxylic acid hydrogen bonding [59]. The appearance of two NH stretching and amide II bands in the (*S,R*)-**1b** xerogel spectrum (3303.4 3273.5 1534.2 1510 cm^{-1}) can be attributed to the intermolecular hydrogen bonds formed by Leu amide units. The XRPD of (*S,R*)-**1a** water/DMSO gel (Figure 12) showed two diffraction peaks at 2θ = 5.509 and 10.501 corresponding to periodic distances *d* of 16.04 and 8.42 Å which also suggests formation of hydrogen bonded assemblies between extended forms of gelator molecules as in the cases of the diester derivatives (*S,S*)-**1b** and (*S,R*)-**1b** (Figure 11).

These results indicate that the dicarboxylic retro-dipeptides (*S,S*)-**1a** and (*S,R*)-**1a** also show similar basic organization as their dimethyl ester counterparts (*S,S*)-**1b** and (*S,R*)-**1b** (Figure 11). Also molecular modeling of (*S,S*)-**1a** and (*S,R*)-**1a** generated very similar low energy conformations to those of (*S,S*)-**1b** and (*S,R*)-**1b** shown in Figure 10a, b. In both cases, the major organizational driving force is provided by extensive intermolecular hydrogen bonding. In lipophilic solvents, where such types of intermolecular interactions are highly favored, formation of wide and relatively short tapes could be observed (TEM, (*S,R*)-**1b** toluene gel, Figure 4) possibly due to the enhanced self-assembling in the direction of intermolecular hydrogen bonds. In contrast, gelling of the highly polar and hydrogen bond competitive water/DMSO solvent mixture (TEM, (*S,S*)-**1a** and (*S,R*)-**1a** water/DMSO gels, Figure 2 and Figure 3) results in the formation of tiny fibers or fiber bundles due to less favored self-assembly in the direction of intermolecular hydrogen bonding and more pronounced intermolecular lipophilic interactions.

Conclusion

A series of chiral bis(dipeptide)oxalamides was prepared representing a novel family of retro-peptidic gelators. Their gelation properties towards a defined set of solvents was assessed and, their conformational characteristics, organization in gel assemblies and thermal and morphological characteristics of selected gels were studied by molecular modeling, ^{1}H NMR, FTIR, CD, DCS, TEM and XRPD. Gelation experiments have shown that the group of terminal free acid retro-dipeptides (*S,S*)-bis(LeuLeu) **1a**, (*S,S*)-bis(PhgPhg) **3a** and (*S,S*)-bis(PhePhe) **5a** showed moderate to excellent gelation of polar water/DMSO and water/DMF solvent mixtures and were much less efficient in gelating solvents of medium and low polarity. Interestingly, the free acid gelators incorporating different amino acids (*S,S*)-(LeuPhg) **2a** and (*S,S*)-(PhgLeu) **4a** had no or very weak gelating ability. The observed difference in gelation between retro-peptides incorporating identical or two different amino acids is intriguing. It seems that the intermolecular lipophilic

interactions that stabilize gel assemblies in polar solvents are more favorable for identical amino acid fragments (lipophilic or aromatic) and less favorable when aromatic–lipophilic amino acid fragments are present in the gelator molecule. Gelation properties of methyl ester derivatives **1b**–**5b**, were not significantly different to those of the respective diacid derivatives **1a**–**5a** except that the former appear slightly more versatile and were capable of gelating some lipophilic solvents presumably due to increased solubility (Table 1 and Table 2). The diamide derivatives bis(LeuLeuNH_2) **1c**, bis(PhgPhgNH_2) **3c** and bis(PhePheNH_2) **5c** were even more versatile and were capable of gelating a larger set of tested solvents compared to the respective dicarboxylic acid (**1a**, **3a**, and **5a**) and dimethyl ester derivatives (**1b**, **3b** and **5b**) (Tables 1–3). It appears that the increased hydrogen bonding potential of terminal diamide derivatives gives somewhat more versatile gelators which could also gel solvents of medium and low polarity where intermolecular hydrogen bonding is favored. Stereochemical influences on gelation properties are exemplified by the following observations: (i) the racemate (*S,R*)-**1a**/(*R,S*)-**1a** exhibited considerably lower gelation effectiveness than the pure enantiomer (*S,R*)-**1a** while the (*S,S*)-**1a**/(*R,R*)-**1a** racemate had no gelation ability and tended to crystallize, (ii) terminal diester racemates (*S,R*)-**1b**/(*R,S*)-**1b** and (*S,S*)-**1b**/(*R,R*)-**1b** were two times more efficient in the gelation of water/DMF and water/DMSO mixtures, respectively, than the pure enantiomers (*S,R*)-**1b** and (*S,S*)-**1b**; the latter provides additional examples that some racemates could be more effective gelators of specific solvents than the pure enantiomers; (iii) among the terminal carboxamide gelators the heterochiral (*S,R*)-**1c** diastereoisomer is capable of immobilizing up to 10 and 4 times larger volumes of dichloromethane and toluene solvent mixtures containing a little DMSO, respectively, compared to homochiral (*S,S*)-**1c**. The combined results of ^{1}H NMR, FTIR, XRPD and molecular modeling studies of terminal diester (*S,S*)-**1b** and (*S,R*)-**1b** and terminal free acid (*S,S*)-**1a** and (*S,R*)-**1a** derivatives gave a consistent picture of their basic organization in gel assemblies. In lipophilic solvents and also in the highly polar water/DMSO mixture, the intermolecular hydrogen bonding between extended gelator molecules utilizing both, the oxalamide and Leu amide hydrogen bonding functionalities represents the major organizational driving force for aggregation. The TEM investigations have shown that in the highly lipophilic solvents the extensive intermolecular hydrogen bonding may lead to the formation of wide and relatively short tapes giving a gel network of low solvent immobilization capacity. Molecular modeling studies revealed that the homochiral (*S,S*)-**1a** and (*S,S*)-**1b** form the low energy conformations with *cis*-*trans*-arrangement of *i*-Bu groups in contrast to the heterochiral (*S,R*)-**1a** and (*S,R*)-**1b** conformations possessing the all-*cis*-arrangement of *i*-Bu groups with respect to the oxalamide plane. Such conformational differences were found to strongly influence both, gelation effectiveness and the morphology characteristics of gel network.

Supporting Information

Supporting Information File 1

Full experimental procedures and characterization details for all new compounds, molecular modeling and TEM images.
[http://www.beilstein-journals.org/bjoc/content/supplementary/1860-5397-6-106-S1.pdf]

Acknowledgements

The authors thank L. Horvat, B.sc and Dr. N. Ljubešić for TEM investigations. The financial support from the Croatian Ministry of Science, Education and Sports (Projects No. 098-0982904-2912) and EU COST Action D31 is gratefully acknowledged.

References

1. Barta-Szalai, G.; Borza, I.; Bozó, É.; Kiss, C.; Ágai, B.; Proszenyák, Á.; Keserű, G. M.; Gere, A.; Kolok, S.; Galgóczy, K.; Horváth, C.; Farkasa, S.; Domány, G. *Bioorg. Med. Chem. Lett.* **2004,** *14,* 3953–3956. doi:10.1016/j.bmcl.2004.05.053
2. Di Stefano, A.; Mosciatti, B.; Cingolani, G. M.; Giorgioni, G.; Ricciutelli, M.; Cacciatore, I.; Sozioa, P.; Claudi, F. *Bioorg. Med. Chem. Lett.* **2001,** *11,* 1085–1088. doi:10.1016/S0960-894X(01)00140-8
3. Medou, M.; Priem, G.; Quélever, G.; Camplo, M.; Kraus, J. K. *Tetrahedron Lett.* **1998,** *39,* 4021–4024. doi:10.1016/S0040-4039(98)00680-7
4. Jadhav, P. K.; Man, H.-W. *Tetrahedron Lett.* **1996,** *37,* 1153–1156. doi:10.1016/0040-4039(96)00013-5
5. Zhang, S.; Marini, D. M.; Hwang, W.; Santoso, S. *Curr. Opin. Chem. Biol.* **2002,** *6,* 865–871. doi:10.1016/S1367-5931(02)00391-5
6. Zhao, X.; Zhang, S. *Trends Biotechnol.* **2004,** *22,* 470–476. doi:10.1016/j.tibtech.2004.07.011
7. Zhang, S. *Biotechnol. Adv.* **2002,** *20,* 321–339. doi:10.1016/S0734-9750(02)00026-5
8. Llusar, M.; Sanchez, C. *Chem. Mater.* **2008,** *20,* 782–820. doi:10.1021/cm702141e
9. Vintiloiu, A.; Leroux, J. C. *J. Controlled Release* **2008,** *125,* 179–192. doi:10.1016/j.jconrel.2007.09.014
10. Yang, Y.; Khoe, U.; Wang, X.; Horii, A.; Yokoi, H.; Zhang, S. *Nano Today* **2009,** *4,* 193–210. doi:10.1016/j.nantod.2009.05.001
11. Zhang, S. *Nat. Biotechnol.* **2003,** *21,* 1171–1178. doi:10.1038/nbt874
12. Gao, X. Y.; Matsui, H. *Adv. Mater.* **2005,** *17,* 2037–2050. doi:10.1002/adma.200401849
13. Bong, D. T.; Clark, T. D.; Granja, J. R.; Ghadiri, M. R. *Angew. Chem., Int. Ed.* **2001,** *40,* 988–1011. doi:10.1002/1521-3773(20010316)40:6<988::AID-ANIE9880>3.0.CO;2-N

14. Valery, C.; Paternostre, M.; Robert, B.; Gulik-Krzywicki, T.; Narayanan, T.; Dedieu, J. C.; Keller, G.; Torres, M. L.; Cherif-Cheikh, R.; Calvo, P.; Artzner, F. *Proc. Natl. Acad. Sci. U. S. A.* **2003,** *100,* 10258–10262. doi:10.1073/pnas.1730609100
15. Aggeli, A.; Nyrkova, I. A.; Bell, M.; Harding, R.; Carrick, L.; McLeish, T. C. B.; Semenov, A. N.; Boden, N. *Proc. Natl. Acad. Sci. U. S. A.* **2001,** *98,* 11857–11862. doi:10.1073/pnas.191250198
16. Fages, F.; Vögtle, F.; Žinić, M. *Top. Curr. Chem.* **2005,** *256,* 77–131.
17. Terech, P.; Weiss, R. G., Eds. *Molecular Gels: Materials with Self-Assembled Fibrillar Networks;* Springer: Dordrecht, 2006.
18. Smith, D. K. Chapter 5. In *Organic Nanostructures;* Steed, J. W.; Atwood, J. L., Eds.; Wiley-VCH: Weinheim, 2008.
19. Fages, F. *Top. Curr. Chem.* **2005,** *256,* 1–273.
20. Terech, P.; Weiss, R. G. *Chem. Rev.* **1997,** *97,* 3133–3160. doi:10.1021/cr9700282
21. van Esch, J. H.; Feringa, B. L. *Angew. Chem., Int. Ed.* **2000,** *39,* 2263–2266. doi:10.1002/1521-3773(20000703)39:13<2263::AID-ANIE2263>3.0.CO;2-V
22. de Loos, M.; Feringa, B. L.; van Esch, J. H. *Eur. J. Org. Chem.* **2005,** 3615–3631. doi:10.1002/ejoc.200400723
23. Estroff, L. A.; Hamilton, A. D. *Chem. Rev.* **2004,** *104,* 1201–1218. doi:10.1021/cr0302049
24. Percec, V.; Ungar, G.; Peterca, M. *Science* **2006,** *313,* 55–56. doi:10.1126/science.1129512
25. Huang, X.; Terech, P.; Raghavan, S. R.; Weiss, R. G. *J. Am. Chem. Soc.* **2005,** *127,* 4336–4344. doi:10.1021/ja0426544
26. Aggeli, A.; Nyrkova, I. A.; Bell, M.; Harding, R.; Carrick, L.; McLeish, T. C. B.; Semenov, A. N.; Boden, N. *Proc. Natl. Acad. Sci. U. S. A.* **2001,** *98,* 11857–11862. doi:10.1073/pnas.191250198
27. de Loos, M.; van Esch, J.; Kellogg, R. M.; Feringa, B. L. *Angew. Chem., Int. Ed.* **2001,** *40,* 613–616. doi:10.1002/1521-3773(20010202)40:3<613::AID-ANIE613>3.0.CO;2-K
28. Arnaud, A.; Bouteiller, L. *Langmuir* **2004,** *20,* 6858–6863. doi:10.1021/la049365d
29. Simic, V.; Bouteiller, L.; Jalabert, M. *J. Am. Chem. Soc.* **2003,** *125,* 13148–13154. doi:10.1021/ja037589x
30. Bouteiller, L.; Colombani, O.; Lortie, F.; Terech, P. *J. Am. Chem. Soc.* **2005,** *127,* 8893–8898. doi:10.1021/ja0511016
31. Webb, J. E. A.; Crossley, M. J.; Turner, P.; Thordarson, P. *J. Am. Chem. Soc.* **2007,** *129,* 7155–7162. doi:10.1021/ja0713781
32. Ellis-Behnke, R. G.; Liang, Y.-X.; You, S.-W.; Tay, D. K. C.; Zhang, S.; So, K.-F.; Schneider, G. E. *Proc. Natl. Acad. Sci. U. S. A.* **2006,** *103,* 5054–5059. doi:10.1073/pnas.0600559103
33. Silva, G. A.; Czeisler, C.; Niece, K. L.; Beniash, E.; Harrington, D. A.; Kessler, J. A.; Stupp, S. I. *Science* **2004,** *303,* 1352–1355. doi:10.1126/science.1093783
34. Liang, Z.; Yang, G.; Ma, M.; Abbah, A. S.; Lu, W. W.; Xu, B. *Chem. Commun.* **2007,** 843–845.
35. Sada, K.; Takeuchi, M.; Fujita, N.; Numata, M.; Shinkai, S. *Chem. Soc. Rev.* **2007,** *36,* 415–436. doi:10.1039/b603555h
36. Fukushima, T.; Asaka, K.; Kosaka, A.; Aida, T. *Angew. Chem., Int. Ed.* **2005,** *44,* 2410–2413. doi:10.1002/anie.200462318
37. Puigmarti-Luis, J.; Laukhin, V.; Perez del Pino, A.; Vidal-Gancedo, J.; Rovira, C.; Laukhina, E.; Amabilino, D. B. *Angew. Chem., Int. Ed.* **2007,** *46,* 238–241. doi:10.1002/anie.200602483
38. Vemula, P. K.; John, G. *Chem. Commun.* **2006,** 2218–2220. doi:10.1039/b518289a
39. Yang, Z.; Xu, B. *Chem. Commun.* **2004,** 2424–2425. doi:10.1039/b408897b
40. Tiller, J. C. *Angew. Chem., Int. Ed.* **2003,** *42,* 3072–3075. doi:10.1002/anie.200301647
41. Vinogradov, S. V.; Bronich, T. K.; Kabanov, A. V. *Adv. Drug Delivery Rev.* **2002,** *54,* 135–147. doi:10.1016/S0169-409X(01)00245-9
42. van Esch, J. H. *Langmuir* **2009,** *25,* 8392–8394. doi:10.1021/la901720a
43. Frkanec, L.; Žinić, M. *Chem. Commun.* **2010,** *46,* 522–537. doi:10.1039/b920353m
44. Fletcher, M. D.; Campbell, M. M. *Chem. Rev.* **1998,** *98,* 763–795. doi:10.1021/cr970468t
45. Chorev, M.; Goodman, M. *Trends Biotechnol.* **1995,** *13,* 438–445. doi:10.1016/S0167-7799(00)88999-4
46. Chorev, M.; Goodman, M. *Acc. Chem. Res.* **1993,** *26,* 266–273. doi:10.1021/ar00029a007
47. Ceretti, S.; Luppi, G.; De Pol, S.; Formaggio, F.; Crisma, M.; Toniolo, C.; Tomasini, C. *Eur. J. Org. Chem.* **2004,** 4188–4196. doi:10.1002/ejoc.200400242
48. Stern, P. S.; Chorev, M.; Goodman, M.; Hagler, A. T. *Biopolymers* **1983,** *22,* 1885–1900. doi:10.1002/bip.360220806
49. Stern, P. S.; Chorev, M.; Goodman, M.; Hagler, A. T. *Biopolymers* **1983,** *22,* 1901–1917. doi:10.1002/bip.360220807
50. Carotti, A.; Carrieri, A.; Cellamare, S.; Fanizzi, F. P.; Gavuzzo, E.; Mazza, F. *Biopolymers* **2001,** *60,* 322–332. doi:10.1002/1097-0282(2001)60:4<322::AID-BIP9993>3.0.CO;2-Y
51. Ranganathan, D.; Vaish, N. K.; Shah, K.; Roy, R.; Madhusudanan, K. P. *J. Chem. Soc., Chem. Commun.* **1993,** 92–94.
52. Karle, I.; Rangahathan, D.; Shah, K.; Vaish, N. K. *Int. J. Pept. Protein Res.* **1994,** *43,* 160–165. doi:10.1111/j.1399-3011.1994.tb00517.x
53. Karle, I.; Rangahathan, D. *Int. J. Pept. Protein Res.* **1995,** *46,* 18–23. doi:10.1111/j.1399-3011.1995.tb00577.x
54. Karle, I.; Rangahathan, D. *Biopolymers* **1995,** *36,* 323–331. doi:10.1002/bip.360360307
55. Coe, S.; Kane, J. J.; Nguyen, T. L.; Toledo, L. M.; Wininger, E.; Fowler, W.; Lauher, J. W. *J. Am. Chem. Soc.* **1997,** *119,* 86–93. doi:10.1021/ja961958q
56. Nguyen, T. L.; Fowler, F. W.; Lauher, J. W. *J. Am. Chem. Soc.* **2001,** *123,* 11057–11064. doi:10.1021/ja016635v
57. Nguyen, T. L.; Scott, A.; Dinkelmeyer, B.; Fowler, F. W.; Lauher, J. W. *New J. Chem.* **1998,** *22,* 129–135. doi:10.1039/a707642h
58. Jokić, M.; Makarević, J.; Žinić, M. *J. Chem. Soc., Chem. Commun.* **1995,** 1723–1724.
59. Makarević, J.; Jokić, M.; Perić, B.; Tomišić, V.; Kojić-Prodić, B.; Žinić, M. *Chem.–Eur. J.* **2001,** *7,* 3328–3341. doi:10.1002/1521-3765(20010803)7:15<3328::AID-CHEM3328>3.0.CO;2-C
60. Makarević, J.; Jokić, M.; Raza, Z.; Štefanić, Z.; Kojić-Prodić, B.; Žinić, M. *Chem.–Eur. J.* **2003,** *9,* 5567–5580. doi:10.1002/chem.200304573
61. D'Aléo, A.; Pozzo, J.-L.; Fages, F.; Schmutz, M.; Mieden-Gundert, G.; Vögtle, F.; Čaplar, V.; Žinić, M. *Chem. Commun.* **2004,** 190–191. doi:10.1039/b307846a
62. Čaplar, V.; Žinić, M.; Pozzo, J.-L.; Fages, F.; Mieden-Gundert, G.; Vögtle, F. *Eur. J. Org. Chem.* **2004,** 4048–4059. doi:10.1002/ejoc.200400105

63. Luo, X.; Liu, B.; Liang, Y. *J. Chem. Soc., Chem. Commun.* **2001,** 1556–1557. doi:10.1039/b104428c
64. Hanabusa, K.; Kobayashi, H.; Suzuki, M.; Kimura, M.; Shirai, H. *Colloid Polym. Sci.* **1998,** *276,* 252–259. doi:10.1007/s003960050236
65. Hanabusa, K.; Okui, K.; Karaki, K.; Kimura, M.; Shirai, H. *J. Colloid Interface Sci.* **1997,** *195,* 86–93. doi:10.1006/jcis.1997.5139
66. Bhattacharya, S.; Acharya, S. N. G.; Raju, A. R. *Chem. Commun.* **1996,** 2101–2102. doi:10.1039/cc9960002101
67. Fuhrhop, J.-H.; Schneider, P.; Rosenberg, J.; Boekema, E. *J. Am. Chem. Soc.* **1987,** *109,* 3387–3390. doi:10.1021/ja00245a032
68. Terech, P.; Rodriguez, V.; Barnes, J. D.; McKenna, G. B. *Langmuir* **1994,** *10,* 3406–3418. doi:10.1021/la00022a009
69. Hirst, A. R.; Coates, I. A.; Boucheteau, T. R.; Miravet, J. F.; Escuder, B.; Castelletto, V. I.; Hamley, W.; Smith, D. K. *J. Am. Chem. Soc.* **2008,** *130,* 9113–9121. doi:10.1021/ja801804c
70. Jonkheijm, P.; van der Schoot, P.; Schenning, A. P. H. J.; Meijer, E. W. *Science* **2006,** *313,* 80–83. doi:10.1126/science.1127884
71. Fuhrhop, J.-H.; Wang, T. *Chem. Rev.* **2004,** *104,* 2901–2937. doi:10.1021/cr030602b
72. Lee, S. J.; Kim, E.; Seo, L. M.; Do, Y.; Lee, Y.-A.; Lee, S. S.; Jung, J. H.; Kogiso, M.; Shimizu, T. *Tetrahedron* **2008,** *64,* 1301–1308. doi:10.1016/j.tet.2007.11.062
73. Jung, J. H.; John, G.; Yoshida, K.; Shimizu, T. *J. Am. Chem. Soc.* **2002,** *124,* 10674–10675. doi:10.1021/ja020752o
74. Sreerama, N.; Woody, R. W. *Circular Dichroism: Principles and Applications*. 2nd ed.; Berova, N.; Nakanishi, K.; Woody, R. W., Eds.; John Wiley & Sons: New York, NY, 2000; pp 601–620.
75. Bustamante, C.; Tinoco, I., Jr.; Maestre, M. F. *Proc. Natl. Acad. Sci. U. S. A.* **1983,** *80,* 3568–3572. doi:10.1073/pnas.80.12.3568
76. Cai, W.; Wang, G.-T.; Du, P.; Wang, R.-X.; Jiang, X.-K.; Li, Z.-T. *J. Am. Chem. Soc.* **2008,** *130,* 13450–13459. doi:10.1021/ja8043322
77. *SYBYL®,* Version 7.3; TRIPOS Inc.: St. Louis, MO, 2007.

License and Terms

Beilstein Journal of Organic Chemistry

Towards racemizable chiral organogelators

Jian Bin Lin, Debarshi Dasgupta, Seda Cantekin and Albertus P. H. J. Schenning*

Letter

Open Access

Address:
Functional Organic Materials and Devices and Laboratory of Macromolecular and Organic Chemistry, Eindhoven University of Technology, PO Box 513, 5600MB Eindhoven, The Netherlands

Email:
Jian Bin Lin - j.b.lin@tue.nl; Debarshi Dasgupta - d.dasgupta@tue.nl; Seda Cantekin - s.cantekin@tue.nl; Albertus P. H. J. Schenning* - a.p.h.j.schenning@tue.nl

* Corresponding author

Keywords:
chirality; organogels; racemization; self-assembly

Beilstein J. Org. Chem. **2010,** *6,* 960–965.
doi:10.3762/bjoc.6.107

Received: 12 July 2010
Accepted: 20 September 2010
Published: 06 October 2010

Guest Editor: J.-P. Desvergne

Abstract

A chiral organogelator has been synthesized that can be racemized and self-assembled in apolar solvents whilst at higher concentrations organogels are formed. Field emission scanning and transmission electron microscopy revealed the formation of bundle fibrils that are able to gelate the solvent. ^{1}H NMR studies showed hydrogen-bond interactions between the peptide head groups of neighbouring organogelator molecules. The enantiomerically pure organogelator can be racemized by the base DBU (1,8-diazabicyclo[5.4.0]undec-7-ene) as was evident from chiral high-performance liquid chromatography analysis.

Introduction

Gelation represents a macroscopic manifestation of self-assembled molecules. Impressive supramolecular architectures have been reported in which the self-assembled molecules immobilize solvent to produce a gel phase. Carefully designed self complementary building blocks with co-added organizational information can make these gels responsive. In recent years, much effort has been devoted to the design and characterization of chiral self-assembled fibrillar networks that form organogels [1,2]. In such systems the chirality within a molecular building block is transcribed to nano- or mesoscale fibrous assemblies. These chiral structures represent excellent models for studying the emergence of specific shapes at a macroscopic level through cooperative interactions between molecules. In addition, helical assemblies possess a potential for applications in advanced materials and constrained media for chiral synthesis and separation [3-5].

The development of systems where the chiral supramolecular assembly responds to specific triggers, should facilitate the design of smart functional materials in which subtle molecular-scale changes have an impact on the macroscopic behavior. Most of the earliest stimuli-responsive gels undergo a

UV-induced transformation, which can be reversed by visible light. For example, Shinkai and coworkers demonstrated that *trans-cis* isomerization of gelator compounds by UV/visible light could induce a gel-sol transition [6]. Feringa and coworkers have reported a chiral gelator in which the supramolecular organization of the chiral assemblies can be switched using UV/visible light combined with heating and cooling [7]. Chiral gels that respond to other stimuli such as metal ions [8], guest molecules [9] and temperature [10] have also been reported.

In recent years, racemic gel fibers assembled from mixtures of enantiomeric building blocks have been described [11-14]. In most cases, the racemates were less efficient gelators than the pure enantiomers, and sometimes lead to crystallization [7]. Interestingly, Higashi and coworkers have observed that the separate enantiomers assemble into fibers with opposite helicity while the racemic mixture yield nanoscale, spherical structures [15]. In order to create chiral response materials based on such systems, it would be interesting to develop organogelators that can be racemized by a stimulus [16,17]. In the current manuscript we report our attempt to synthesize a racemizable chiral organogelator (Scheme 1). The molecular design of our organogelator (**3**) is based on a finding that the imine of 2-methylbenzaldehyde and phenylglycinamide can be racemized in the presence of the base DBU (1,8-diazabicyclo[5.4.0]undec-7-ene). Interestingly, a single solid chiral state from a nearly racemic mixture of this phenylglycinamide derivative was observed by so-called attrition-enhanced solid-phase enantioenrichment [18]. In order to obtain a molecule that is able to form a gel, 3,4-didodecyloxybenzaldehyde [19] was used in place of 2-methylbenzaldehyde.

Results and Discussion

Synthesis

The synthesis of ***R*-3** and ***S*-3** is outlined in Scheme 1. First, concentrated aqueous ammonia was added to ester **1** to yield pure phenylglycinamide **2** [18]. Reaction of **2** with 3,4-didodecyloxybenzaldehyde [19] led to compound **3** in 50% yield (Scheme 1). Both ***R*-3** and ***S*-3** were purified by recrystallization and fully characterized. Chiral high-performance liquid chromatography (HPLC) showed an ee of more than 99% for the enantiomers. Interestingly, ^{1}H NMR spectroscopy in chloroform revealed that the two amide protons of **3** behave differently at different concentration (Figure 1). The signal from one of the amide protons remains the same, even on the addition of a small amount DMSO-d_6, indicating intramolecular hydrogen bonding. The other amide proton signal was downfield shifted

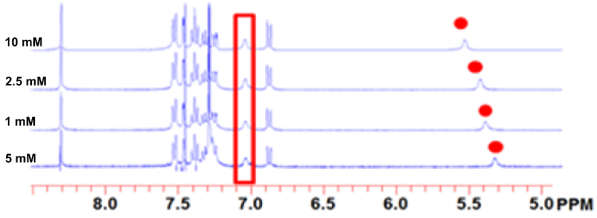

Figure 1: Concentration-dependent ^{1}H NMR spectra of ***R*-3** in chloroform ($CDCl_3$). The red colours indicate the hydrogen resonances of the amide unit.

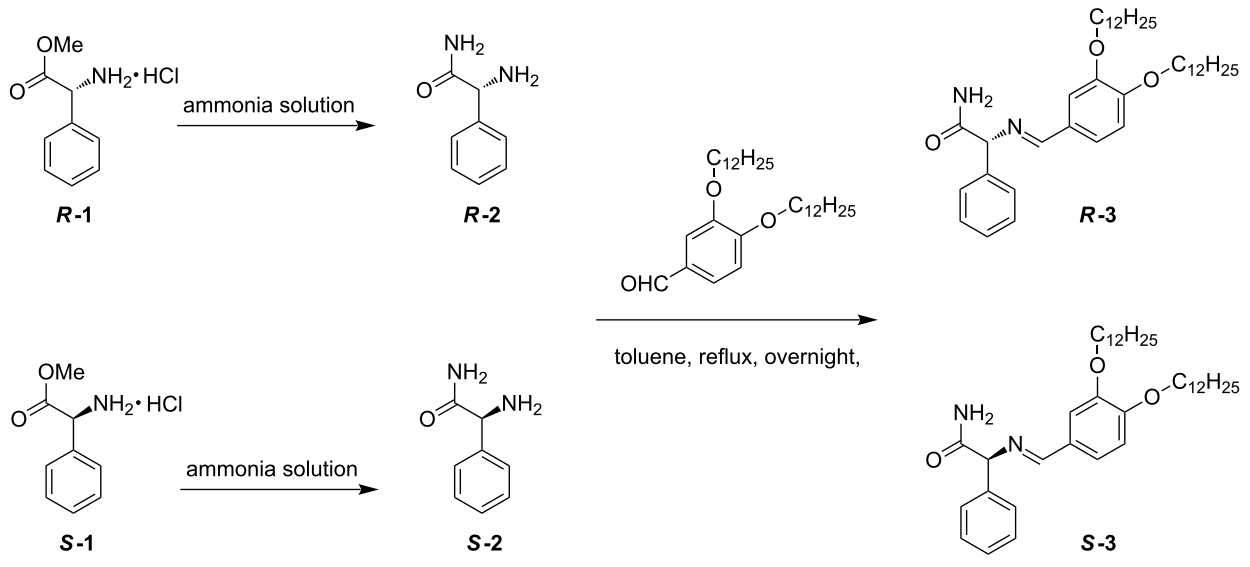

Scheme 1: Synthesis of ***R*-3** and ***S*-3**.

upon increasing the concentration, in accord with intermolecular hydrogen bonding.

Gel formation

The gelation ability of ***R*-3**, ***S*-3** and racemic **3** was investigated using the "inverse flow" method. At room temperature, ***R*-3** and ***S*-3** were insoluble in octane. However, on heating at 80 °C, both ***R*-3** and ***S*-3** became soluble in octane and when cooled to room temperature, a stable self-supporting semi-transparent gel was formed (Figure 2a). For all the samples, the thermoreversible gelation process was followed at 0 °C, since the gelation time becomes much longer at lower concentrations at 20 °C. For ***R*-3**, the critical gelation concentration (CGC) was detected by the failure of the whole mass to flow when the vial was turned upside down. The CGC value was 2.3 mM for ***R*-3**, which means that ***R*-3** can immobilize approximately 2700 molecules of octane per gelator molecule. The gel is thermoreversible, indicating that the first order phase transition is associated with gel melting and/or gel formation. When the racemate (***R*-3** = ***S*-3** = 2.5 mM) was heated and cooled to room temperature, precipitation was observed (Figure 2b).

The morphology of the organogel was further characterized by field emission scanning electron microscopy (FESEM) as well as with transmission electron microscopy (TEM). The TEM image (Figure 2c), of the dried ***R*-3** gel in octane (1 mM) exhibited entangled fibrillar network formation although the concentration stays well below the CGC value (2.3 mM) in this solvent. The critical gelation concentration indicates the threshold at which, infinite percolation is achieved within a network system, although microgel network structures can still be observed below the CGC. The fibers have an average diameter is 60 ± 10 nm and lengths of tens of micrometers suggesting effective anisotropic growth. The morphology of the ***R*-3** organogel in octane at a higher concentration (about 15 mM) also revealed a fibrillar structure, but in this case the fibrils were much bigger in size (nearly 150 nm in diameter) and in some parts they seemed to form two dimensional sheet like lamellar structures (FESEM image, Figure 2d).

In order to investigate the molecular arrangement of the fibers in apolar solvent, variable concentration ^{1}H NMR measurement were carried out in cyclohexane-d_{12}. In contrast to the observations in chloroform, in cyclohexane solution upon increasing the concentration the observed chemical shifts of both the N–H protons were downfield shifted (Figure 3), consistent with an increased degree of intermolecular hydrogen bonding suggesting the formation of intermolecular hydrogen-bond interactions between the amide units. Most likely hydrogen bonded dimers or tetramers are formed in this apolar solvent. Our data suggest that these hydrogen-bonded dimers or tetramers subsequently stack via π-π interaction and via van der Waals interactions into bundled fibers.

Racemization

The racemization of ***R*-3** was investigated by chiral HPLC. After adding 1 equivalent of DBU to a solution of ***R*-3** in octane at room temperature, samples were collected over time and the enantiomeric purity was measured. Racemization was not observed in the gel state (5 mM) after 18 hours, whilst after heating and cooling precipitation was observed. At a concentration of 1 mM, where self-assembled fibers are present, the ee of the solution decreased in time. Figure 4 shows a plot of ln(ee × 100) versus time for the racemization of ***R*-3** [18]. The first order kinetics expression: ln($ee(t)$) = ln($ee(0)$) + kt could be used to fit the experimental results and gave a $t_{1/2}$ of about

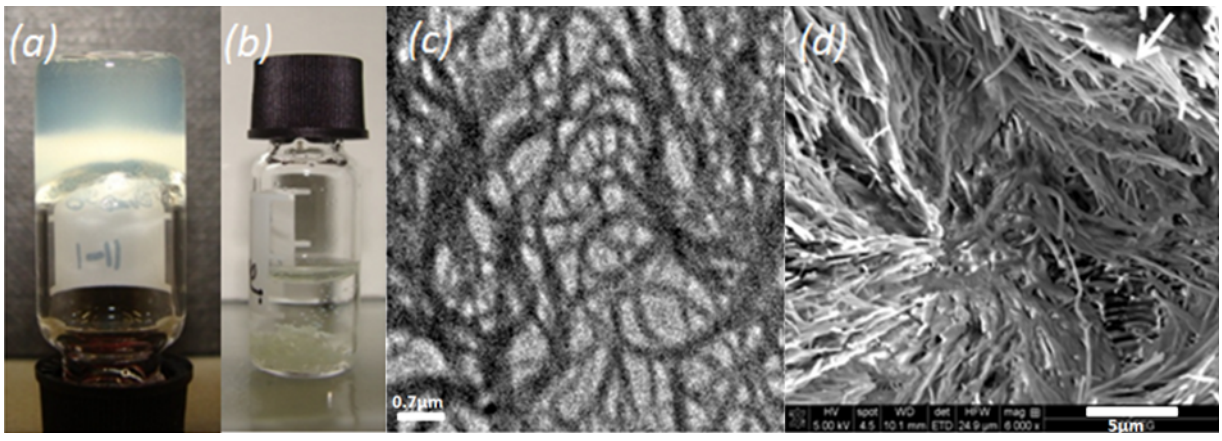

Figure 2: a) ***R*-3** gel in octane (5 mM); b) octane solution containing a mixture of ***R*-3** (2.5 mM) and ***S*-3** (2.5 mM) after cooling from 80 °C to room temperature; c) TEM image of the xerogel of ***R*-3** in octane; d) the surface morphology of the dried gel obtained from ***R*-3** in octane (15 mM) observed by FESEM.

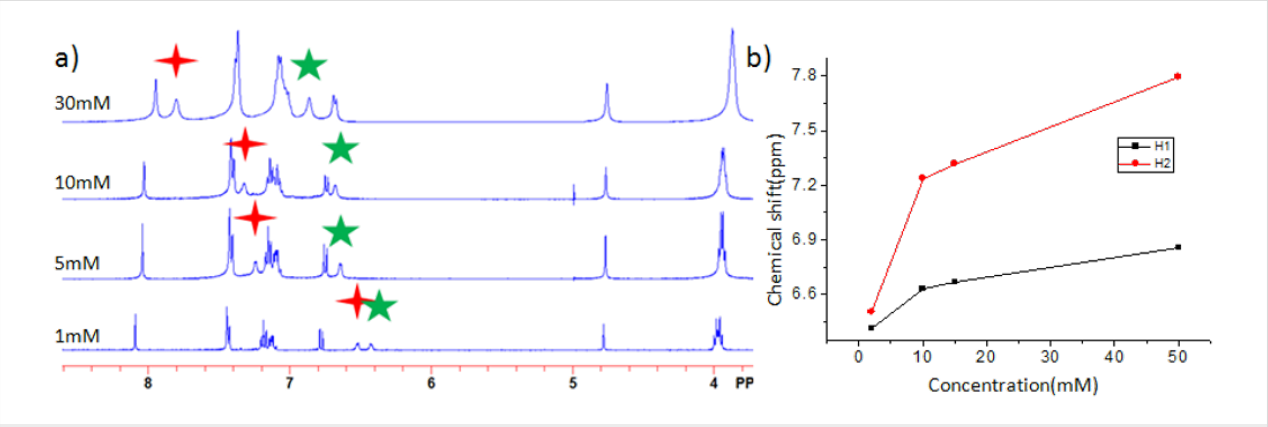

Figure 3: a) Concentration-dependent ^{1}H NMR spectra of ***R*-3** in cyclohexane-d_{12} and b) the shift of N–H signal of amide group versus concentration.

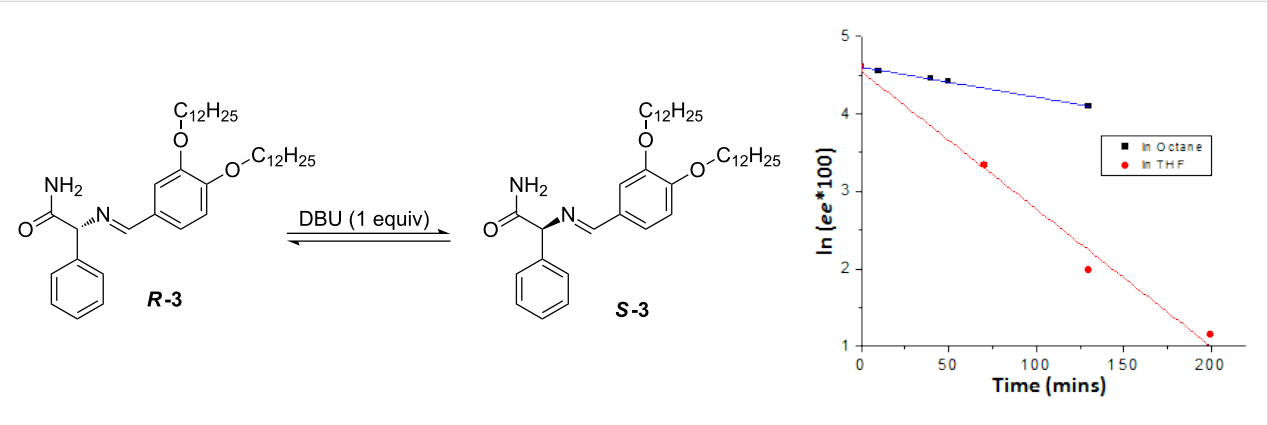

Figure 4: The evolution of ln(*ee* × 100) for the racemization of ***R*-3** (1 mM) in the presence of 1 equivalent of DBU in octane and THF.

177 min. Under the same conditions, the racemization rate in THF is much faster with a $t_{1/2}$ of about 37 min. This difference between the two solvents is most likely due to the difference in polarity and the fact that ***R*-3** is self-assembled in octane and molecularly dissolved in the more polar THF.

Conclusion

This work demonstrates a route towards racemizable chiral organogelators. Remarkably, our pure enantiomeric gelator could not be racemized in the gel phase, while racemization takes place in the self-assembled fiber state. We are currently studying this class of organogelator for the creation of responsive gels and attrition-enhanced solid-phase enantioenrichment phenomena [20].

Experimental

General

All chemicals were purchased from Aldrich. Non-deuterated solvents were purchased from Biosolve. All other solvents and chemicals were used as received. Deuterated solvents were obtained from Cambridge Isotope Laboratories, United States. NMR spectra were recorded with a Varian Mercury NMR Spectrometer. IR spectra were measured on a Perkin Elmer 1600 FT-IR. MALDI-TOF MS spectra were measured on a Perseptive DE Voyager Mass Spectrometer with α-cyano-4-hydroxycinnamic acid as the matrix.

Synthesis

Phenylglycinamide ***R*-2**, ***S*-2**: The ester salt ***R*-1**, ***S*-1** (5.04 g, 25 mmol) was stirred with concentrated ammonia solution (20 mL) at room temperature overnight. Subsequently, the product was precipitated, filtered, and washed with cold water. The resulting white solid was recrystallized from ethanol to afford 2.65 g of colourless crystals (71%) of ***R*-2**, ***S*-2**. ^{1}H NMR ($CDCl_3$, 400 MHz): 7.43 (m, 2H, ArH); 7.31 (m, 3H, ArH); 4.84 (br, 4H, NH_2); 4.44 (s, 1H, COCH). MALDI-TOF MS (calc MW = 150.08, $C_8H_{10}N_2O$): 150.97 $[M + H]^+$. IR ν (cm^{-1}): 3339; 3073; 1660; 1454; 1405; 1271; 869; 699.

***R*-3**, ***S*-3**: To a solution of 3,4-didodecyloxybenzaldehyde (237 mg, 0.5 mmol) in toluene, was added compound ***R*-2**, ***S*-2** (75 mg, 0.5 mmol) and the mixture was refluxed overnight. After

the reaction was complete, the solvent was removed. The resulting yellow solid was washed with methanol and *n*-hexane to yield 150 mg ***R*-3**, ***S*-3** (50%). ^{1}H NMR ($CDCl_3$, 400 MHz): 8.19 (s, 1H, CH=N); 7.48 (m, 2H, ArH); 7.42 (d, J = 1.2 Hz, 1H, ArH); 7.34 (m, 2H, ArH); 7.30 (m, 1H, ArH); 7.23 (dd, ^1J = 6.3Hz, ^2J = 1.2Hz, 1H, ArH); 7.03 (d, J = 2.8Hz, 1H, $CONH_2$); 6.89 (d, J =6.3Hz, 1H, ArH); 5.49 (d, J = 2.8 Hz, 1H, $CONH_2$); 4.95 (s, 1H, COCH); 4.05 (m, 4H, OCH_2, OCH_2); 1.83 (m, 4H, CH_2) ; 1.58 (m, 4H, CH_2) ; 1.46 (m, 4H, CH_2) ; 1.83 (m, 32H, CH_2) ; 1.83 (m, 6H, CH_3). ^{13}C NMR ($CDCl_3$, 100 MHz): 199.20; 174.34; 162.90; 152.33; 149.32; 144.98; 139.45; 128.65; 128.43; 127.83; 127.25; 123.52; 112.46; 111.78; 69.35; 69.07; 31.90; 29.62; 29.42; 29.34; 29.25; 29.08; 26.03; 25.96; 22.66; 14.09. MALDI-TOF MS (calc MW = 606.48, $C_{39}H_{62}N_2O_3$): 607.51 $[M + H]^+$. IR ν (cm^{-1}): 3403; 2918; 2849; 1652; 1514; 1263; 1120; 719. M.p. 80.5 °C. (*R*)-enantiomer: $[\alpha]^{25}_D$ 4.8 (*c* 0.01, $CHCl_3$), (*S*)-enantiomer: $[\alpha]^{25}_D$ −4.4 (*c* 0.01, $CHCl_3$).

ee Determination by HPLC [18]: The octane solution (2 mL) of the imine (1 mM) and DBU (1 equiv) was mixed with 1 mL of 0.25 M HCl solution and the aqueous solution extracted two times with 1 mL of $CHCl_3$. The remaining aqueous solution of phenylglycine amide HCl salt was used as such for the ee determination by the following HPLC method. Column; crownether Cr (+) 150 x 4.6 mm ID, eluent; aqueous $HClO_4$ pH = 1.2 / methanol 90/10 v/v %, flow: 1 mL/min, temperature, 25 °C, detection: λ = 220 nm, detection limit: 0.01 area %.

Electron Microscopy: The field emission scanning electron microscopy was performed on dried gel samples. The samples (15 mM in octane) were first coated with gold by the sputtering technique and then observed under a FEI Quanta 3D FEG microscope. The transmission electron microscopy was carried out by drop casting a solution (1 mM in octane) on a carbon coated copper grid and viewed under FEI Tecnai 20. TEM grids (R2/2 Quantifoil Jena) were purchased from Quantifoil.

Acknowledgements

We gratefully acknowledge Anja Palmans, Bert Meijer, Wim Noorduin, Bernard Kaptein and Richard M. Kellogg for stimulating discussions and comments. We are grateful to Sabrina van Oerle for her help with the synthesis of the starting materials and X. Lou for the help with the chiral HPLC measurements. This research was supported by a Small Scale Collaborative Project grant: Bottom-up Resolution of Functional Enantiomers from Self-Organised Monolayers (Project acronym: RESOLVE) seventh framework number: NMP4-SL-2008-214340.

References

1. Brizard, A.; Oda, R.; Huc, I. *Top. Curr. Chem.* **2005,** *256,* 167–218. doi:10.1007/b107174
2. Smith, D. K. *Chem. Soc. Rev.* **2009,** *38,* 684–694. doi:10.1039/B800409A
3. Cardolaccia, T.; Li, Y.; Schanze, K. S. *J. Am. Chem. Soc.* **2008,** *130,* 2535–2545. doi:10.1021/ja0765316
4. Zinic, M.; Vogtle, F.; Fages, F. *Top. Curr. Chem.* **2005,** *256,* 39–76. doi:10.1007/b107171
5. de Jong, J. J. D.; Tiemersma-Wegman, T. D.; van Esch, J. H.; Feringa, B. L. *J. Am. Chem. Soc.* **2005,** *127,* 13804–13805. doi:10.1021/ja055268a
6. Murata, K.; Aoki, M.; Suzuki, T.; Harada, T.; Kawabata, H.; Komori, T.; Ohseto, F.; Ueda, K.; Shinkai, S. *J. Am. Chem. Soc.* **1994,** *116,* 6664–6676. doi:10.1021/ja00094a023
7. de Jong, J. J. D.; Lucas, L. N.; Kellogg, R. M.; van Esch, J. H.; Feringa, B. L. *Science* **2004,** *304,* 278–281. doi:10.1126/science.1095353
8. Ihara, H.; Sakurai, T.; Yamada, T.; Hashimoto, T.; Takafuji, M.; Sagawa, T.; Hachisako, H. *Langmuir* **2002,** *18,* 7120–7123. doi:10.1021/la025535f
9. Chen, X.; Huang, Z.; Chen, S.-Y.; Li, K.; Yu, X.-Q.; Pu, L. *J. Am. Chem. Soc.* **2010,** *132,* 7297–7299. doi:10.1021/ja102480t
10. Huang, Z.; Lee, E.; Kim, H.-J.; Lee, M. *Chem. Commun.* **2009,** 6819–6821. doi:10.1039/b913286d
11. Messmore, B. W.; Sukerkar, P. A.; Stupp, S. I. *J. Am. Chem. Soc.* **2005,** *127,* 7992–7993. doi:10.1021/ja051183y
12. Hirst, A. R.; Huang, B. Q.; Castelletto, V.; Hamley, I. W.; Smith, D. K. *Chem.–Eur. J.* **2007,** *13,* 2180–2188. doi:10.1002/chem.200601665
13. Makarevic, J.; Jokic, M.; Raza, Z.; Stefanic, Z.; Kojic-Prodic, B.; Zinic, M. *Chem.–Eur. J.* **2003,** *9,* 5567–5580. doi:10.1002/chem.200304573
14. Hirst, A. R.; Smith, D. K.; Feiters, M. C.; Geurts, H. P. M. *Chem.–Eur. J.* **2004,** *10,* 5901–5910. doi:10.1002/chem.200400502
15. Koga, T.; Matsuoka, M.; Higashi, N. *J. Am. Chem. Soc.* **2005,** *127,* 17596–17597. doi:10.1021/ja0558387
16. Boettcher, C.; Schade, B.; Fuhrhop, J. H. *Langmuir* **2001,** *17,* 873–877. doi:10.1021/la001054p
17. Hanabusa, K.; Yamada, M.; Kimura, M.; Shirai, H. *Angew. Chem., Int. Ed.* **1996,** *35,* 1949–1951. doi:10.1002/anie.199619491
18. Noorduin, W. L.; Izumi, T.; Millemaggi, A.; Leeman, M.; Meekes, H.; Van Enckevort, W. J. P.; Kellogg, R. M.; Kaptein, B.; Vlieg, E.; Blackmond, D. G. *J. Am. Chem. Soc.* **2008,** *130,* 1158–1159. doi:10.1021/ja7106349
19. Meier, H.; Prass, E.; Zerban, G.; Kosteyn, F. *Z. Naturforsch., B* **1988,** *43,* 889–896.
20. Noorduin, W. L.; Vlieg, E.; Kellogg, R. M.; Kaptein, B. *Angew. Chem., Int. Ed.* **2009,** *48,* 9600–9606. doi:10.1002/anie.200905215

Beilstein Journal of Organic Chemistry

Differences between β-Ala and Gly-Gly in the design of amino acids-based hydrogels

Andreea Pasc[1], Firmin Obounou Akong[1], Sedat Cosgun[2] and Christine Gérardin[*1]

Full Research Paper

Open Access

Address:
[1]LERMAB - EA 4370, Nancy-Université, BP 70239, F-54506 Vandoeuvre-lès-Nancy, France and [2]Department of Chemistry, Fatih University, 34500 Buyukcekmece-Istanbul, Turkey

Email:
Andreea Pasc - Andrea.Pasc@lermab.uhp-nancy.fr; Firmin Obounou Akong - firmin.obounou-akong@lermab.uhp-nancy.fr; Sedat Cosgun - sedatcosgun@fatih.edu.tr; Christine Gérardin* - christine.gerardin@lermab.uhp-nancy.fr

* Corresponding author

Keywords:
amino acid; histidine; hydrogel; peptide-based surfactant; soft matter; supramolecular

Beilstein J. Org. Chem. **2010,** *6,* 973–977.
doi:10.3762/bjoc.6.109

Received: 09 July 2010
Accepted: 17 September 2010
Published: 11 October 2010

Guest Editor: J.-P. Desvergne

Abstract

Despite the continuous interest in organogels and hydrogels of low molecular weight gelators (LMWG), establishing the relationship between the molecular structure and the gelation mechanism is still a challenge. In this paper our interest focuses on the consequences of slight molecular modifications on the self-assembling behaviour of β-Ala vs Gly-Gly-based hydrogelators. Previously, in our group, amino acid based amphiphiles i.e. Gly-Gly-His-EO_2-Alk, a trimodular amphiphile (containing three domains: H-bond donor and acceptor/hydrophilic/hydrophobic domain, respectively) were reported to act as hydrogelators and that the gelation properties were related to hydrogen bonding, hydrophobic interactions and π-π stacking. Herein, β-Ala-His-EO_2-Alk was fully characterised by FT-IR, NMR, SAXS and SEM and the gelation mechanism is discussed. It appears that the number of amide groups determines the self-assembling behaviour into 1D or 2D/3D networks as a result of intimate interactions between gelator molecules.

Introduction

Hydrogels continue to attract much interest due to their versatile applications in tissue engineering, biosensing, drug or gene delivery and water pollution control [1-7]. For some of these applications, i.e., drug controlled-release systems or bioseparation, hydrogels are required to respond to external stimuli such as temperature, pH and ions. They have been traditionally constructed with high molecular weight polymers, physically or chemically cross-linked, but in the recent past, their construction by low molecular weight (LMW) compounds has been explored. With respect to polymeric hydrogels, supramolecular gels of LMWGs (low molecular weight gelators) are assembled by non-covalent forces, such as electrostatic, hydrogen bonding, dipole–dipole, π–π stacking and hydrophobic/van der Waals interactions. Since the cross-links between fibres are non-cova-

lent in nature, LMWHs exhibit thermoreversibility, rapid response to external stimuli (i.e., stirring, sonication). Among these LMWHs, amino acid-based amphiphiles have been received much attention in the recent past on account of their biocompatibility and eco-friendly nature.

Biologically inspired His-based surfactants are of particular interest not only for their antioxidant properties and their potential therapeutic effects, but also as building blocks for supramolecular architectures such as gels [8,9]. The structure of the surfactant is a major factor for their gelator properties. As reported in the literature [1], unless the molecules remain in solution, when a hot, homogeneous solution of the gelator, is cooled, the molecules start to condense and three outcomes are possible: (1) a highly ordered aggregation giving rise to crystals; (2) a random aggregation resulting in an amorphous precipitate, or (3) an aggregation process intermediate between these two, yielding a gel. The result seems to depend on the balance between hydrophilic and hydrophobic modules, as well as the number of H-donor and H-acceptor centers, or π–π stacking. Therefore the appropriate balance between all these factors must be determined.

As a part of the ongoing research carried out in our laboratory on the self-assembled systems of amino acids-based amphiphiles, we have recently shown that Gly-Gly-His and β-Ala-His-amphiphiles act as efficient hydrogelators [10]. The histidine moiety seems to play a key role in hydrogel formation, developing not only π-π stacking interactions but also by H-bonding; by replacing histidine by phenylalanine no hydrogel formation occurred (results to be published elsewere). His-based amphiphiles are surface active at low pH (< 7) and are able to complex Cu(II) ions to form metallosurfactants. Herein, the self-organisation within hydrogels (pH > 7) was investigated in order underline the role of slight variations of the molecular structure in supramolecular self-assembling, i.e., the number of H-bond donor and acceptor amide moieties (3 in β-Ala-His-amphiphile vs 4 Gly-Gly-His-amphiphile) and consequently, to obtain further insights on the gelation mechanism. The hydrogels were characterised by a number of techniques including, NMR, FT-IR, scanning electron microscopy, SAXS/WAXS.

Results and Discussion

Molecular design

A hydrogelator generally contains three functional domains: a hydrogen or electron donor and acceptor domain as the main organiser, a hydrophilic domain to adjust the solubility in water or in organic solvents, and a hydrophobic domain for van der Waals or hydrophobic interactions (Figure 1). They are able to entrap a large number of solvent molecules per one gelator molecule.

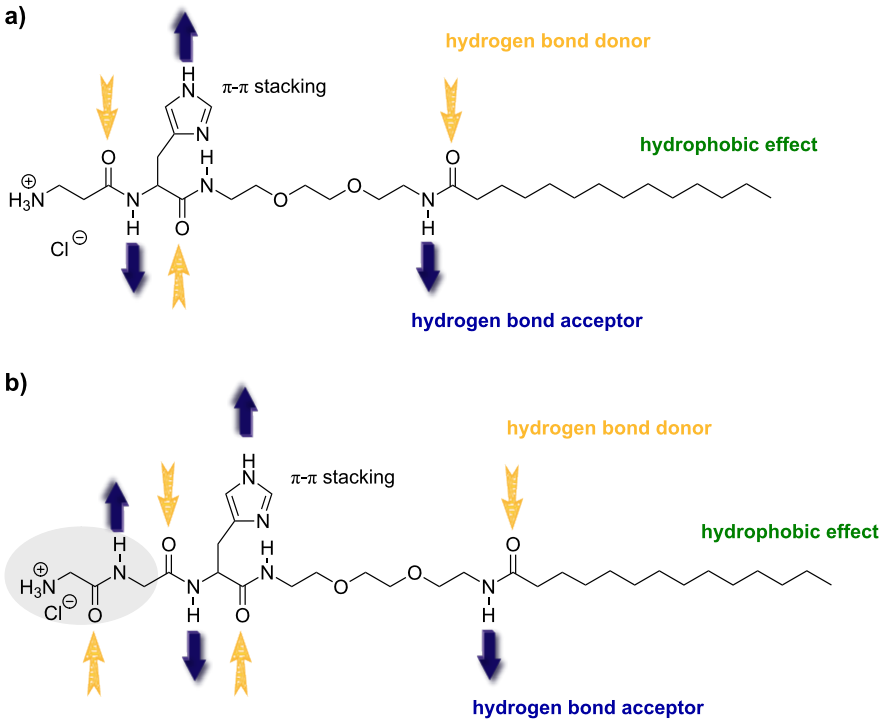

Figure 1: Molecular structures of β-Ala-His-EO_2-C_{14} (a) and Gly-Gly-His-EO_2-C_{14} (b).

Herein the gelators were designed as AA-His-EO_2-Alk, bearing i) an hydrophobic alkyl group, ii) a polar peptide group with complexing properties (AA = β-Ala or Gly–Gly) and iii) a flexible hydrophilic junction module, allowing for HLB control. Their synthesis is reported elsewere [11].

Gelation behaviour of amphiphiles

In previous studies, we showed that amphiphilic compounds designed as AA-His-EO_2-C_n, with n = 12, 14 and AA = β-Ala or Gly-Gly, respectively, formed hydrogels [10,11]. Gly-Gly-His-EO_2-C_{14} formed lamellar phases, the gels were transparent and the gel-to-sol transition temperatures were lower with respect to the β-Ala-derivative. In order to understand better the differences between the two compounds, NMR, X-ray and FT-IR measurements were performed on β-Ala-His-EO_2-C_{14}. The FT-IR measurements were made in order to evaluate the driving forces for the hydrogelation.

As expected ATR measurements (Figure 2) show the presence of H-bonding of the amides. The absorptions frequencies in the gel are always lower than in the free powder. The free individual IR frequencies of amide **I**-**III** were identified from the corresponding IR spectra of H_2N-EO_2-C_{14} (amide **I**, 1633 cm^{-1}), His-EO_2-C_{14} (amide **II**, 1643 cm^{-1}) and β-Ala-His-EO_2-C_{14} (amide **III**, 1681 cm^{-1}), respectively. In the xerogel, only one absorption band was observed at 1644 cm^{-1}, whereas in the D_2O hydrogel a weak and broad absorption band appeared at 1635 cm^{-1}, demonstrating the existence of H-bonded amide groups.

Furthermore, the increase in intensity of the methylene scissoring vibration δ(CH_2) at 1454 cm^{-1} indicates the high conformational packing of alkyl chain.

The ^1H NMR spectra of β-Ala-His-EO_2-C_{14} D_2O hydrogel (2% w/v) was carried out in order to both determine the sol-to-gel transition temperature and to see what group is implicated in the construction of the gel. In the gel state (below 30 °C) all gelator signals were poorly resolved; whereas above 35 °C they were more distinct and slightly right shifted.

The structure of the gel was studied by simultaneous small and wide-angle X-ray scattering (SAXS and WAXS) measurements (Figure 3). At low concentrations of the gelator (2% w/v) only the scattering profile was observed. However, when the concentration of the gelating compound was increased to 50% w/v, a broad diffraction peak appeared in the low-angle region suggesting the presence of a poorly ordered micellar phase with a periodicity distance of 6.9 nm. The observed d-spacing was slightly larger than twice the fully extended length of a single surfactant molecule, 2 × 3.4 nm (calculated using MOPAC method, CS Chem Office). Upon heating, the intensity of the

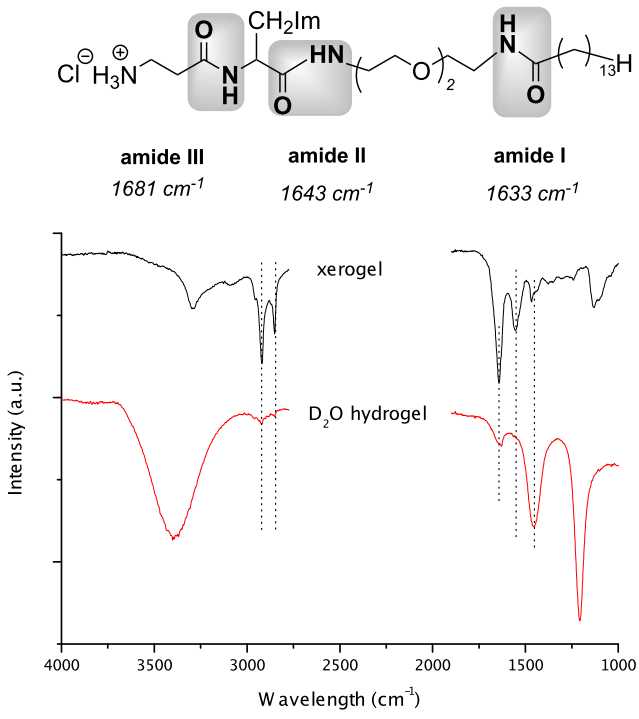

Figure 2: ATR spectra of β-Ala-His-EO_2-C_{14} in xerogel and D_2O hydrogel, respectively.

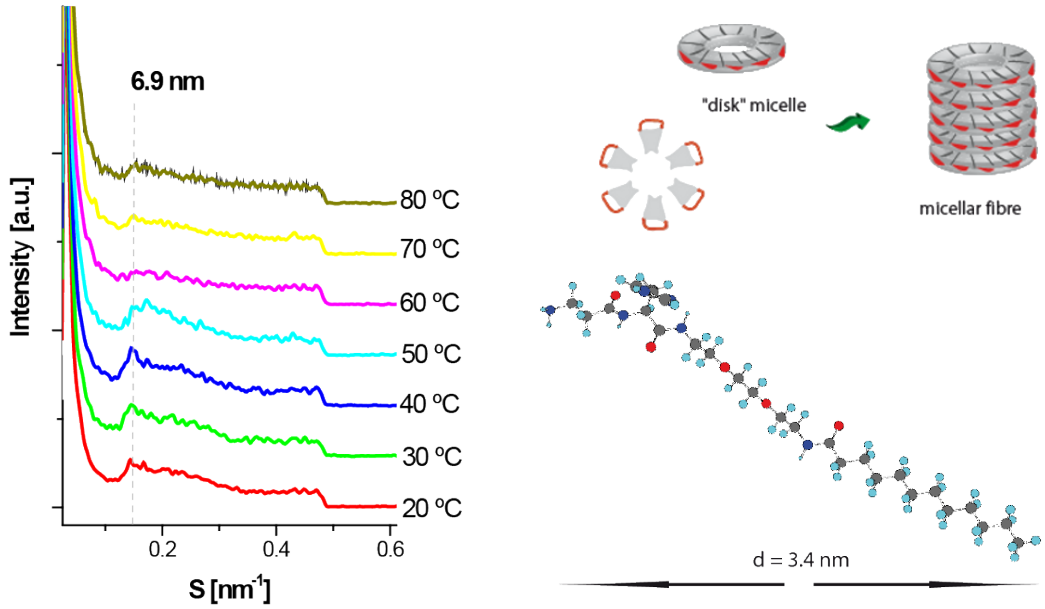

Figure 3: SAXS profile of concentrated gel of β-Ala-His-EO_2-C_{14} at different temperatures (where S = 2π/q and q is the scattering vector).

peak decreased drastically which can be attributed to a phase transition between 50 and 60 °C. The phase transition temperature was in agreement with the one observed by the dropping ball method at the same concentration, and was higher than the sol-to-gel transition temperature of the 2% w/v sample. On drying, the fibres aggregate to form larger fibre bundles as shown in Figure 4.

The morphology of the gel was observed by scanning electron microscopy (SEM, Figure 4). The micrographs show bundles tens of micrometers long and more than 1 μm wide containing thin fibres (less than 300 nm). Upon gelation, it appears that self-assembly of the 3D fibres of these low molecular weight molecules results in the formation of fibrous networks.

All these results appear to suggest the following gelation mechanism. On reducing the temperature to a certain value, amphiphilic molecules start to interact with each other by H-bonding to form micellar networks. The hydrophobicity of the 1D system is proportional to its length. Once the micellar fibre is too long, and thus too hydrophobic to be solubilised by water, it tends to interact with others fibres to produce 2D/3D networks (Figure 5).

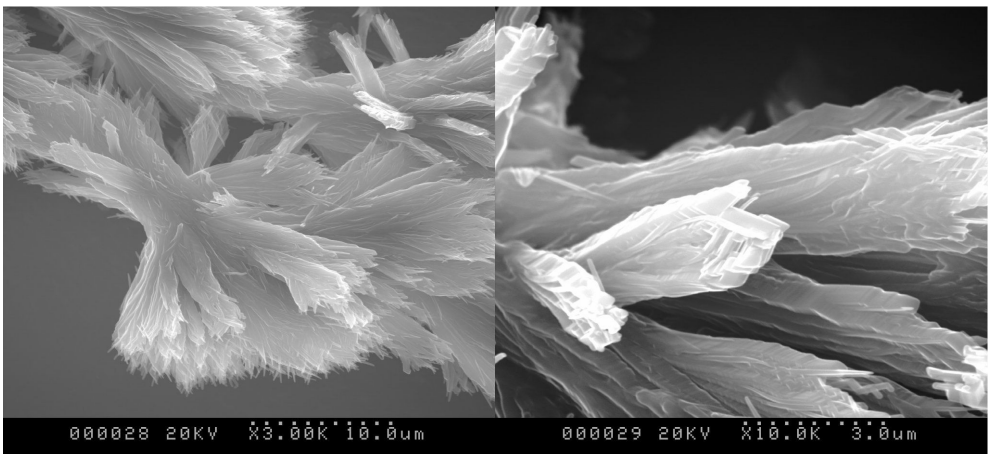

Figure 4: SEM micrographs of β-Ala-His-EO_2-C_{14} hydrogels after drying.

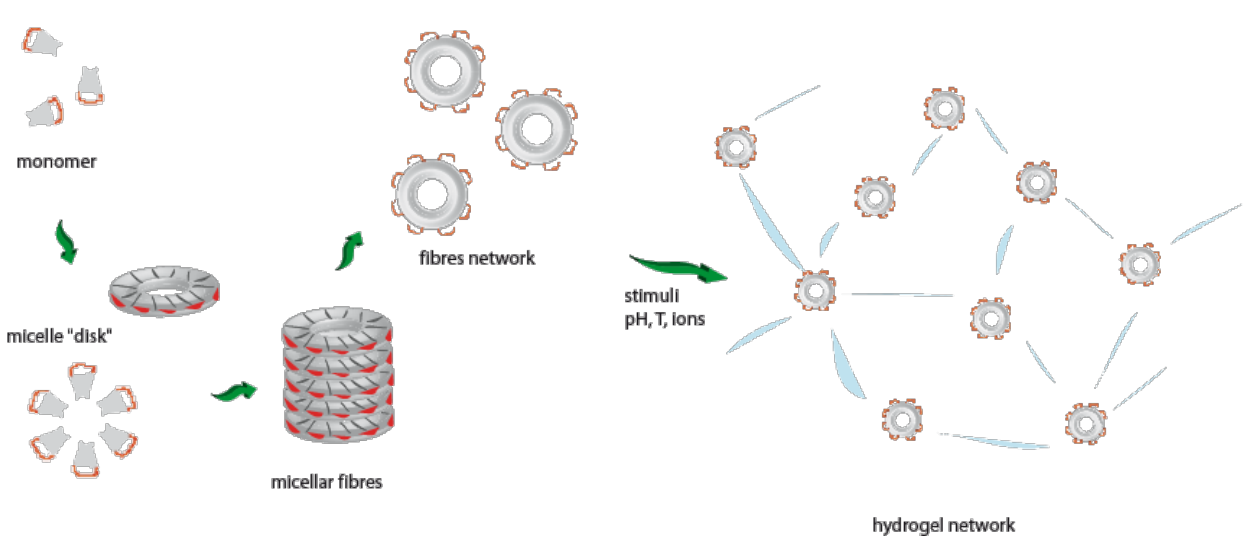

Figure 5: 2D/3D self assembling of β-Ala-His-EO_2-C_{14}.

Due to their complexing properties, these compounds are suitable candidates for selective binding of biologically relevant cations such as Cu^{2+} or Ni^{2+}, and therefore they offer a straightforward approach for the design of bioactive formulations, and, in particular, for oxidation stress problems. Moreover, these chiral hydrogels could potentially serve as general matrices to host various chiral compounds, either hydrophobic or hydrophilic, and could be used as an enantiomeric sensor or as a separation device for a range of chiral molecules.

Acknowledgements

We thank Salveco and region Lorraine for financial support, Mehdi Yemloul for his contribution to the NMR spectra and Dr. S. Funari and HASYLAB/DESY, Hamburg for the beamtime (A2 beamtime).

References

1. Sangeetha, N. M.; Maitra, U. *Chem. Soc. Rev.* **2005,** *34,* 821–836. doi:10.1039/b417081b
2. Estroff, L. A.; Hamilton, A. D. *Chem. Rev.* **2004,** *104,* 1201–1217. doi:10.1021/cr0302049
3. de Loos, M.; Feringa, B. L.; van Esch, J. H. *Eur. J. Org. Chem.* **2005,** 3615–3631. doi:10.1002/ejoc.200400723
4. Suzuki, M.; Sato, T.; Kurose, A.; Shirai, H.; Hanabusa, K. *Tetrahedron Lett.* **2005,** *46,* 2741–2745. doi:10.1016/j.tetlet.2005.02.144
5. Suzuki, M.; Owa, S.; Kimura, M.; Kurose, A.; Shirai, H.; Hanabusa, K. *Tetrahedron Lett.* **2005,** *46,* 303–306. doi:10.1016/j.tetlet.2004.11.027
6. Suzuki, M.; Yumoto, M.; Shirai, H.; Hanabusa, K. *Org. Biomol. Chem.* **2005,** *3,* 3073–3078. doi:10.1039/b507540h
7. Stendahl, J. C.; Rao, M. S.; Guler, M. O.; Stupp, S. I. *Adv. Funct. Mater.* **2006,** *16,* 499–508. doi:10.1002/adfm.200500161
8. Patra, T.; Pal, A.; Dey, J. *Langmuir* **2010,** *26,* 7761–7767. doi:10.1021/la904540x
9. Pal, A.; Shrivastava, S.; Dey, J. *Chem. Commun.* **2009,** 6997–6999. doi:10.1039/b914665b
10. Pasc, A.; Gizzi, P.; Dupuy, N.; Parant, S.; Ghanbaja, J.; Gerardin, C. *Tetrahedron Lett.* **2009,** *50,* 6183–6186. doi:10.1016/j.tetlet.2009.08.093
11. Gizzi, P.; Pasc, A.; Dupuy, N.; Parant, S.; Henry, B.; Gerardin, C. *Eur. J. Org. Chem.* **2009,** 3953–3963. doi:10.1002/ejoc.200900137

License and Terms

Beilstein Journal of Organic Chemistry

Insights into the mechanical properties of a silicone oil gel with a 'latent' gelator, 1-octadecylamine, and CO_2 as an 'activator'

Emiliano Carretti[*1], Mathew George[2,3] and Richard G. Weiss[*2]

Full Research Paper

Open Access

Address:
[1]Department of Chemistry & CSGI Consortium, University of Florence, via della Lastruccia, 3, I-50019 Sesto Fiorentino (Florence), Italy, [2]Department of Chemistry, Georgetown University, Washington, DC 20057-1227, USA and [3]Sepax Technologies, Inc., Newark, DE 19711, USA

Email:
Emiliano Carretti[*] - carretti@csgi.unifi.it; Richard G. Weiss[*] - weissr@georgetown.edu

* Corresponding author

Keywords:
ammonium carbamate; damping factor; gel-sol transition; rheology; viscosity

Beilstein J. Org. Chem. **2010,** *6,* 984–991.
doi:10.3762/bjoc.6.111

Received: 19 June 2010
Accepted: 30 September 2010
Published: 15 October 2010

Guest Editor: J.-P. Desvergne

Abstract

A detailed study of the rheological properties of silicone oil gels, made from a low-molecular-mass organic gelator, a combination of 1-octadecylamine (a latent gelator) and carbon dioxide (an 'activating' molecule), is reported. Information gleaned from the mechanical measurements is used to characterize the gel networks and how they respond to temperature and strain. It is shown, for example, that very precise measurements of the gel-to-sol transitions can be obtained from plots of viscosity versus temperature.

Introduction

During the last two decades, research efforts have increased enormously to understand the range of structures and processes of self-assembly of 'small' molecules such as low-molecular-mass organogelators (LMOGs), which gelate large volume fractions of a liquid. The structures of the assemblies almost always consist of one-dimensional objects (usually fibers, rods or nanotubes) that interact to form three-dimensional self-assembled fibrillar networks (SAFINs) [1-3]. This interest is motivated by the search for fundamental information on the basis for anisotropic self-assembly and recognition of the potential applications for such gels [4-6] – most can be reverted thermally to their solution (or sol) states – as models for several important biological aggregates (e.g., that are involved with neurodegenerative and other diseases, such as Alzheimer's, mad cow disease, and sickle cell anemia) that are much more complex structurally. Previously, we described simple methods by which 'latent' LMOGs (i.e., molecules that do not aggregate into SAFINs efficiently, or at all, unless a chemical stimulant, such as an acid [7] or a triatomic gas [8,9], especially carbon dioxide [10,11], is added).

Although the structures of SAFINs and rheological properties of their gels made with 'normal' LMOGs have been extensively investigated [2,12], the mechanical properties of gels made from latent LMOGs have not received much attention because their rheological measurements are fraught with experimental difficulties. Many of the gels from latent LMOGs are mechanically fragile and difficult to make in a manner that ensures a reasonable degree of reproducibility. Here, we describe a detailed rheological study of gels made from a latent LMOG, 1-octadecylamine (**ODA**), and a triatomic molecular 'activator', carbon dioxide, with silicone oil, tetramethyltetraphenyltrisiloxane, as the liquid component [10,11]. This liquid has been selected because its very low vapor pressure avoids a potential complication, i.e., evaporation of a portion of the liquid during long-term measurements.

Results and Discussion

General considerations. In previous work, we have reported the properties of these gels and others made with a variety of amine latent LMOGs, other triatomic gases, and a wide range of liquids [8-11]. The basic process to form the gels is simple: bubbling CO_2 through a solution of the amine and the liquid for a minute or longer (to ensure complete reaction). The CO_2 adds to one amino functionality, forming a carbamate, while a proton of the amine is transferred to a second amine molecule (Scheme 1) [13]. The resultant ammonium carbamate from **ODA**, $C_{18}H_{37}NHCO_2^{-}\ ^{+}H_3NC_{18}H_{37}$ (**ODA-C**), is held together much more strongly, by electrostatic forces, than uncharged latent LMOG molecules. Especially in liquids of low polarity, the electrostatic forces and ion pairing are very strong and they are the basis for the induced self-assembly leading to one-dimensional objects and SAFINs. The concentrations of the latent LMOG can be very low, <1 wt %. For the purposes of this work, somewhat higher concentrations were employed to ensure that the rheological measurements probe viscoelasticity and not simple Newtonian viscosity effects of the liquid.

It is known that the fibers constituting the SAFINs of the **ODA-C**/silicone oil gels are crystalline, and that the molecules of **ODA-C** are in extended conformations in lamellae with their long axes normal to the lamellar planes [10]. In addition, molecules of silicone oil are not inside the fibers [14] because the powder diffraction patterns of the neat **ODA-C** powder and the SAFIN structures in the gel are the same (i.e., the **ODA-C** molecules pack in the same morph in the absence and presence of silicone oil).

Flow curves. The rheological behavior of the gels was explored over a torque range from 5×10^{-4} to 100 mN m while increasing the torque logarithmically. This procedure ensures that the same protocol for increasing torque is applied to all the samples. Figure 1 shows the flow curves of **ODA-C**/silicone oil gels made from 1, 2, 4, 5, 7, and 8 wt % **ODA**. The shapes are similar and typical of viscoelastic shear thinning materials. The 'lower Newtonian region', indicated as η_0, corresponds to the value of the horizontal asymptote (Table 1) and is plotted as a function of **ODA** concentration in Figure 2.

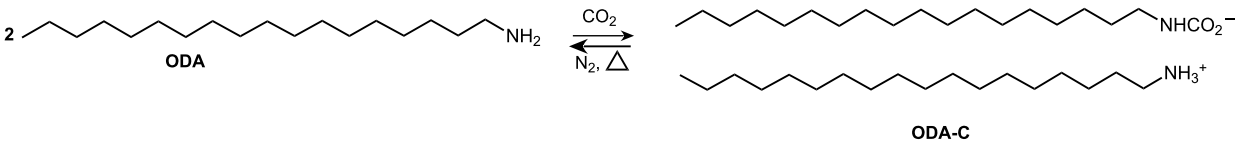

Scheme 1: Reversible reaction of octadecylamine with carbon dioxide.

Table 1: Values of η_0 from Figure 1 and T_g[a] from Figure 3. The activation energies (E_a)[b] have been calculated from Arrhenius fits of the data in Figure 3, plotting ln(η) versus 1/T for points above and below T_g. The numbers in parentheses are the E_a values normalized for LMOG content by dividing the gross numbers by the weight fraction of **ODA**.

Gelator wt %	η_0 (Pa·s)	T_g (°C)	E_a above T_g (kJ mol^{-1})	E_a below T_g (J mol^{-1})
1	1330 ± 430	43.0 (48)	0.10 (0.001)	0.091 (9.1 × 10^{-4})
2	3290 ± 50	50.4 (59–60)	5.01 (0.025)	38.9 (0.20)
4	14700 ± 100	64.2 (79)	12.0 (0.030)	919 (2.3)
5	40800 ± 8300	70.3 (80)	21.5 (0.043)	961 (1.9)
7	169000 ± 45000	74.5	42.6 (0.061)	520 (0.74)
8	810000 ± 105000	82.3	24.9 (0.031)	529 (0.66)

[a]Values in parentheses from the falling drop method [11].
[b]The numbers in parentheses are the E_a values normalized for LMOG content by dividing the gross numbers by the weight fraction of **ODA**.

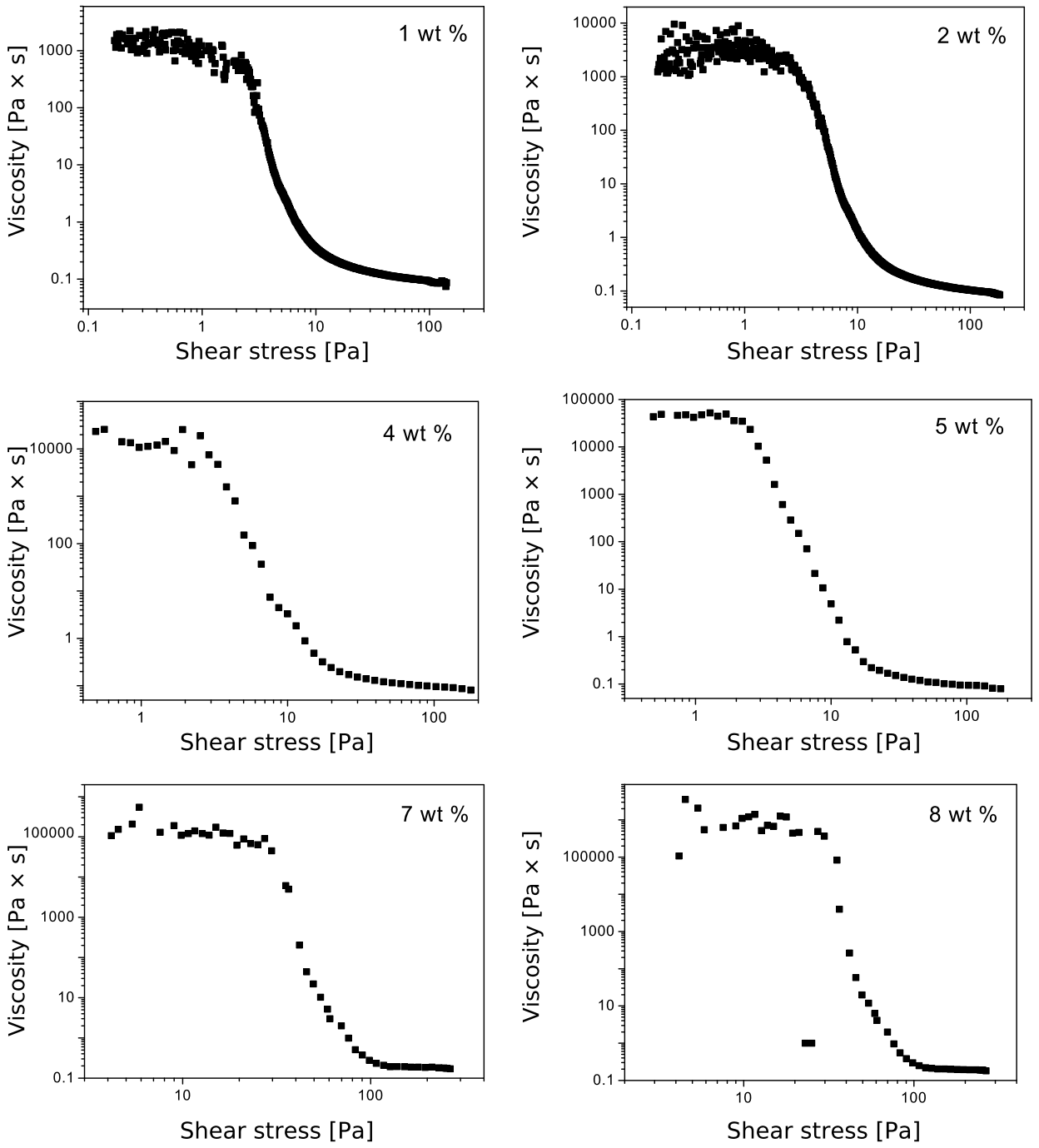

Figure 1: Flow curves of **ODA-C**/silicone oil gels at 25 °C and increasing stress.

Temperature effects. In our previous study with these gels [10], the values of the sol–gel transition temperatures (T_g) were measured by the 'falling drop' method [2,15,16]. This crude test has become a standard method, although it does not yield a value that is reproducible between laboratories – the thickness of the gel sample, the diameter of the vial, and the surface of the vial are variables that can alter the T_g measured in this way. By contrast, rheological measurements, when conducted in the linear viscoelastic regions, provide T_g values that should be reproducible in any laboratory provided the samples are prepared in the same way. However, it must be recognized that because the gels are under some shear stress, their T_g values

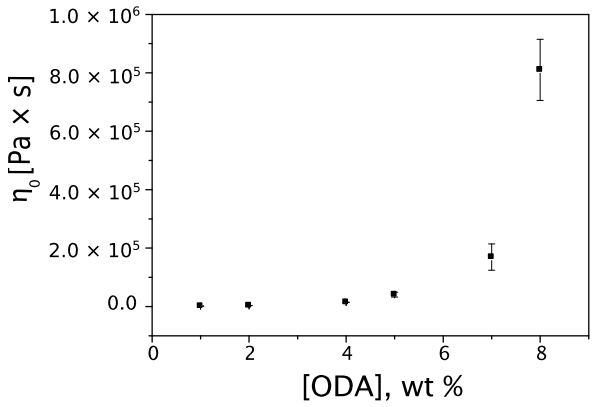

Figure 2: η_0 values as a function of **ODA** concentration.

may be slightly affected. In the experiments conducted here, the mechanical effects of shear on T_g are expected to be very small because the stress applied to the samples is in the lower Newtonian region, where the dependence of the viscosity on applied shear stress is minimized and the gelator network structures (i.e., self-assembled fibrillar networks or SAFINs) are pre-established to avoid shear alignment. Also, the very low solubility of the ammonium carbamate salt in silicone oil indicates that a very high fraction of **ODA-C** remains part of the SAFIN structure even at elevated temperatures that approach T_g [13].

From the intersection between the straight lines drawn from the linear portions of the data points in Figure 3, very precise values of T_g can be determined at each gelator concentration. Note that, as expected, the viscosities decrease much more precipitously upon increasing temperature above T_g. On comparison, the T_g values obtained rheologically and by the falling drop method [11] follow the same trend, but those from the data in Figure 3 are always lower (Table 1). Regardless, those values determined rheologically are closer to instrumentally independent parameters because, unlike the values from the falling drop method (which depend on the diameter of the container and the height of the gel) [16], they do not depend as acutely on the geometry of contact with the sample holder.

All viscosities were fit reasonably to the Arrhenius model to obtain activation energies for viscous flow. Such energies of very complex fluids (e.g., honey) are usually expressed per mole [17] and we have done so here. However, it is probably not correct to do so for a micro-separated 2-phase system such as a gel. Even with our careful attempts to prepare the gels so that they can be made reproducibly, the activation energy data indicate that we have only been partially successful. The rough trends in the activation energies indicate that the SAFINs of the gels differ at the microscopic level for reasons other than differing LMOG concentrations; there are inherent inhomogeneities that are a result of stochastic nucleation and microscopic growth effects. Although two gels made by the same protocol from aliquots of the same sol may appear to be the same macroscopically, they must differ in important ways on small length scales. Regardless, it is clear that the activation energies associated with fluidity changes increase as the **ODA** concentration increases; the effect is not linear. Furthermore, the influence of the SAFIN on viscous flow is apparent in the >100-fold higher activation energies in the gel phases than in the corresponding sol phases. Thus, more macroscopic measures of the gel properties, such as T_g, do follow smooth trends with LMOG concentration, and the T_g values, especially as measured by the falling drop method [2], are much more reproducible than the absolute values of the viscosities.

Optical microscopy. Optical micrographs of 2 wt % gel samples were recorded before and after the application of a constant and continuous stress of 10 Pa for 10 min. The micrograph in Figure 4A is typical of those previously reported [11]. As can be seen, aggregates before the application of the stress are more elongated and fiber-like than those after the perturbation (Figure 4B). The changes can be attributed to the partial breaking of the SAFIN that occurs when a large stress is applied to the system. Although the network is 'damaged', it is not destroyed even after this treatment: the viscosity of the perturbed sample remains significantly higher than that of neat silicone oil. In fact, the appearance of the gel in Figure 4B is very similar to that reported for an **ODA**/silicone oil gel (i.e., in the absence of CO_2) [11].

The changes are attributed to irreversible breaking of fibers as well as cleavage of some of their junction zones. Unlike non-crystalline SAFINs, such as those from giant worm-like micelles, only in exceptional cases are crystalline SAFINs able to 'heal' without being melted (i.e., transformed into the sol phase) and then reformed by cooling.

Amplitude sweep. The stability of the structures of viscoelastic substances is determined by their response to increasing strain and is measured as the limit of the linear viscoelastic strain range, the point where both G' and G'' values begin to decrease with increasing strain; usually, G' begins to decrease at lower strain values compared to G''. Beyond the strain limit, the SAFIN is damaged and eventually destroyed. Thus, the behavior of G' and G'' as a function of the angular frequency must be determined at a strain value within the linear viscoelastic range. For the amplitude sweep experiments shown in Figure 5, a 2 wt % **ODA-C**/silicone oil gel and a 1 Hz frequency of oscillation were chosen.

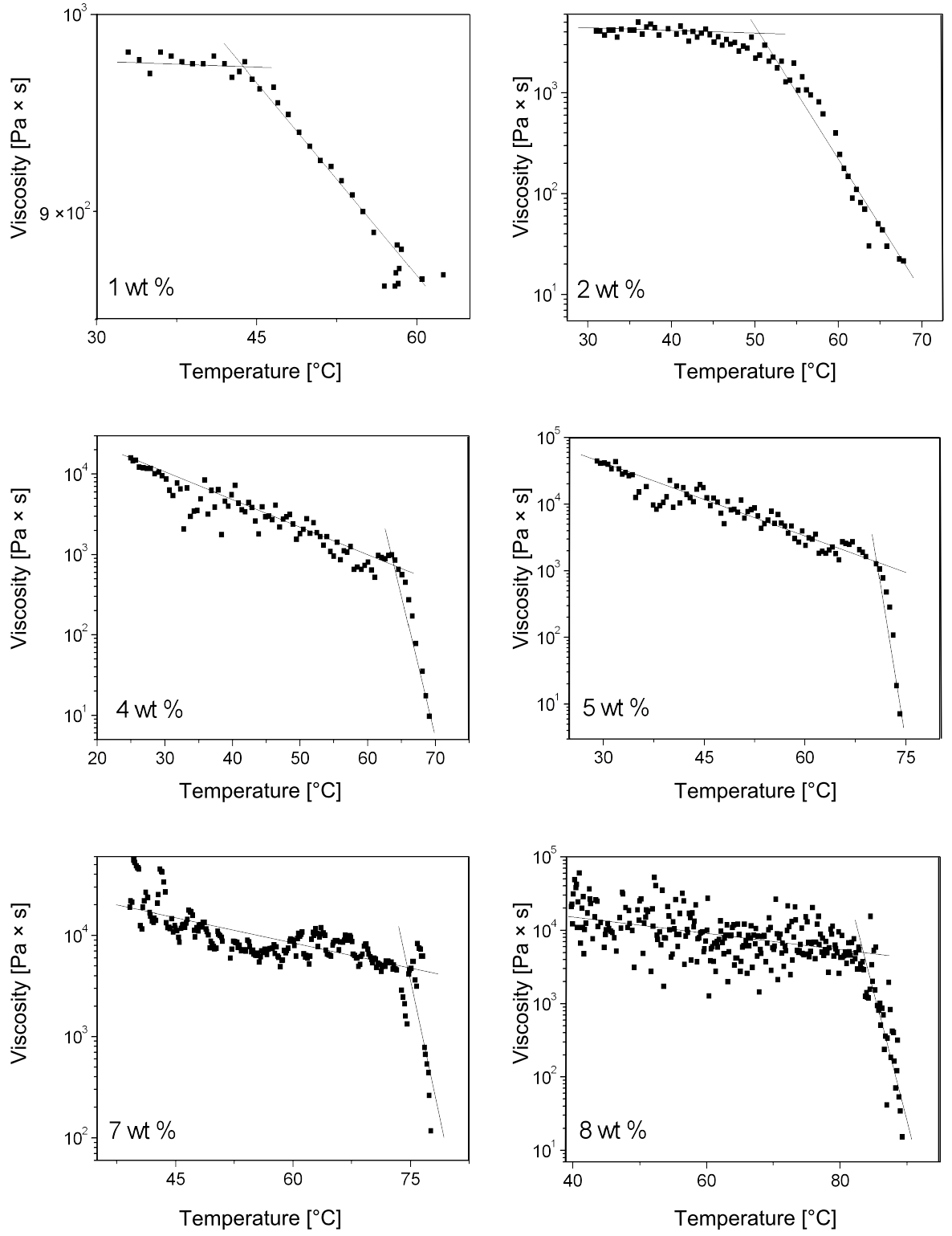

Figure 3: Dependence of viscosity of **ODA-C**/silicone oil gels on temperature at a shear stress of 1 Pa. From top left to bottom right: [**ODA**] = 1, 2, 4, 5, 7, and 8 wt %. Note that the viscosities of the 1 wt % sample have been plotted linearly and those at the other concentrations are plotted semi-logarithmically.

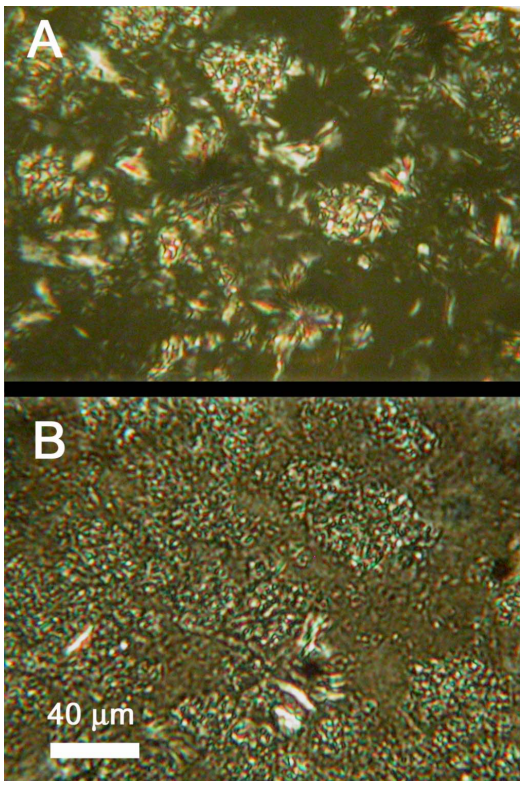

Figure 4: Optical micrographs of a 2 wt % **ODA-C**/silicone oil gel before (A) and after (B) the application of 10 Pa shear stress for 10 min at 25 °C. The space bar applies to both micrographs.

Frequency sweep. The behaviors of G' and G'' as a function of the frequency for 2, 4, and 8 wt % **ODA-C**/silicone oil gels are shown in Figure 6. The oscillation amplitudes are in the linear viscoelastic regions as determined from experiments (Figure 5).

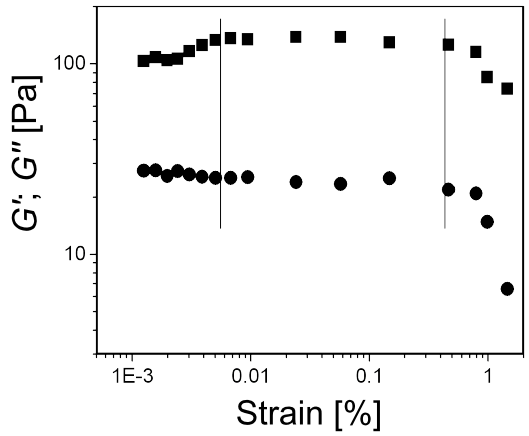

Figure 5: Amplitude sweep test of a 2 wt % **ODA-C**/silicone oil gel showing G' (■) and G'' (●). The vertical lines mark the range of the linear viscoelastic region.

The data are typical of a solid-like material: G' remains larger than G'' over a very broad range of frequencies; there is no crossover between the loss and shear moduli within the range of the accessible frequencies. These results indicate that the physical junctions in the **SAFIN**s behave as permanent crosslinks (i.e., they have long lifetimes), typical of other self-assembled systems [18]. The assessment that the gel networks are solid-like is also supported by the fact that both G' and G'' are more or less independent of frequency within the range investigated and increasing the **ODA-C** concentration leads to large increases in G', G'', and η^* (Figure 6). These conclusions are supported as well by the damping factors (DF = G''/G') of the gels, which remain less than 1, as expected for a solid-like material, over the total frequency ranges examined (Figure 7).

Furthermore, because the G' values for all the gel samples are nearly independent of the frequency of the applied perturbation, the average values of G' can be considered equal to the intrinsic elastic shear modulus, G [19], which can be correlated with the entanglement density, ρ_e, by the expression, $G = \rho_e k_B T$ [20]. In these cases, the frequency of junction zones (i.e., where fibers of a SAFIN are joined [1]) may contribute to ρ_e as well. Thus, an increase in the elastic modulus G' is indicative of an increase in the entanglement (or junction) density of the SAFIN fibers, even if the gross rheological behavior remains the same.

Conclusion

Silicone solutions of the latent gelator, **ODA**, treated with CO_2 gas produce viscoelastic materials that are true gels according to rheological criteria. The crystalline SAFINs are destroyed partially when exposed to excessive strain. It has been shown that very precise values of T_g are obtained by plotting the viscosities versus temperature and that these values should be more easily reproduced in other laboratories than those based on the falling drop method. The same data sets, when plotted in an Arrhenius fashion, yield activation energies for viscous flow within the gel and sol phases. As expected, the activation energies within the gel phases are at least one order of magnitude higher than those of the corresponding sol phases and, in some cases, more than 2 orders of magnitude higher. However, the rheological properties of the gels do not change linearly with latent LMOG concentration because the SAFIN structures must differ in subtle ways that cannot be understood by rheological measurements alone, but can be sensed acutely by them. Thus, rheology provides an extremely valuable tool to investigate the network structures of gels containing LMOGs.

Experimental

Dry CO_2 gas was bubbled through solutions of **ODA** (from Aldrich; distilled twice under vacuum and stored under a nitrogen atmosphere) in tetramethyltetraphenyltrisiloxane (Dow

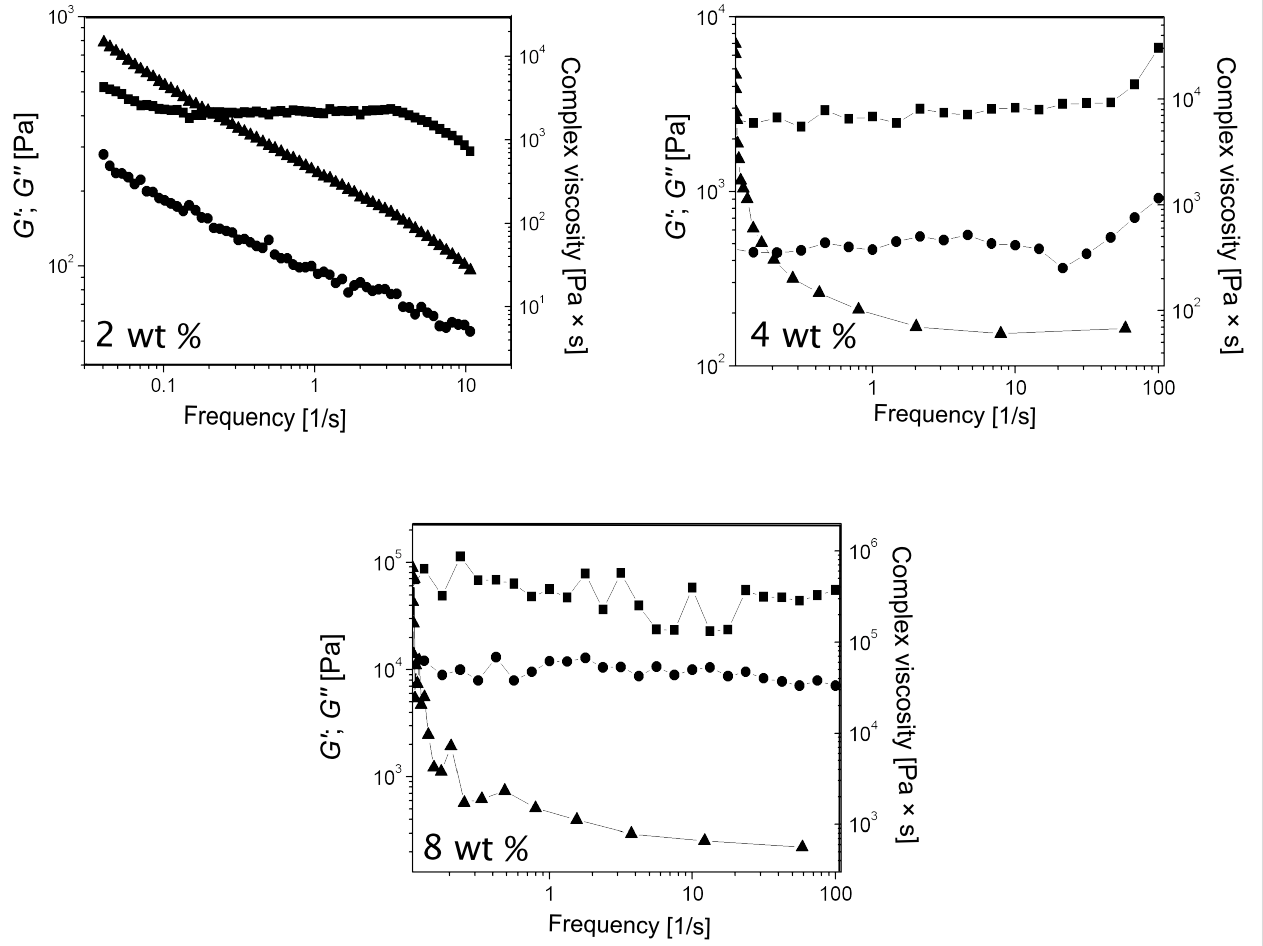

Figure 6: Frequency sweep tests and dynamic mechanical measurements of 2, 4, and 8 wt % **ODA-C**/silicone oil gels. *G′* (■), *G″* (●), and the complex viscosity, η^* (▲; right axes) as a function of frequency, ω.

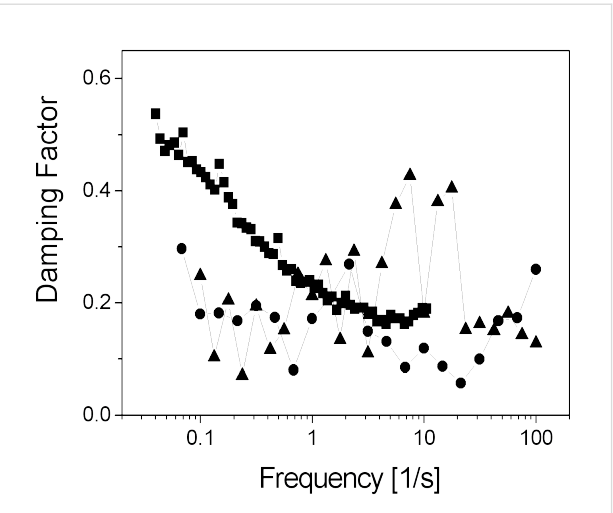

Figure 7: Damping factors of 2 (■), 4 (●) and 8 wt % (▲) gels at different frequencies.

silicone oil 704 from Dow Chemical Company, Midland, MI) for several minutes to prepare 1-octadecylammonium 1-octadecylcarbamate (**ODA-C**) and the fibrillar structures of the gels derived from it [10]. Under a dry CO_2 atmosphere and in sealed vials, the samples were heated to 75 °C for 5 min and slowly cooled (ca. 1 °C/min) to room temperature 3 times. This procedure yielded transparent sols that were cooled rapidly after the 4th heating by plunging the vials into a cold water bath at 2–3 °C. The resultant opaque, birefringent gels were then used for the rheological measurements.

Aliquots of the samples were heated again to 75 ± 2 °C and rapidly transferred onto the surface of the rheometer plate (initially at 10 °C above T_g [10] for 15 min). Then, the temperature of the plate was rapidly reduced (ca. 4 °C/min) to 25 °C; this annealing cycle was repeated 3 times prior to conducting the experiments at 25 °C. Virtually identical rheological data were obtained when aliquots of gel samples were transferred to the plate with a spatula at room temperature.

Rotational and oscillatory shear measurements were carried out with a plate–plate geometry (10 mm diameter) on a Paar Physica UDS 200 rheometer working in controlled shear stress. The dependencies of the storage modulus (G') and the loss modulus (G'') on the oscillation frequency were obtained from the phase lag between the applied shear stress and the related flow and from the ratio between the amplitudes of the imposed oscillation and the response of the gel. The complex viscosity was also calculated from Equation 1.

$$|\eta^*| = \sqrt{\frac{G'^2(\omega) + G''^2(\omega)}{\omega^2}} \quad (1)$$

G' and G'' were measured over a 0.001–100 s^{-1} frequency range. The values of the stress amplitude were examined by amplitude sweep tests in order to ensure that all measurements were performed within the linear viscoelastic region. All flow curve and oscillatory measurements were made at 25.0 ± 0.1 °C (Peltier temperature control system). Experiments to examine the viscosity at increasing temperatures were performed at a rate of 0.2 °C/min.

Optical micrographs were collected in the transmission mode by means of a Reichert Zetopan optical microscope equipped with an 11× objective and an 8× ocular using crossed Nicol polarizers.

Acknowledgments

MG and RGW thank the US National Science Foundation and EC thanks MIUR, Italy (PRIN 2006), to the Consorzio Interuniversitario per lo sviluppo dei Sistemi a Grande Interfase (CSGI-Firenze) for their financial support of this research.

References

1. Terech, P.; Weiss, R. G. *Chem. Rev.* **1997,** *97,* 3133–3160. doi:10.1021/cr9700282
2. Weiss, R. G.; Terech, P., Eds. *Molecular Gels. Materials with Self-Assembled Fibrillar Networks;* Springer: Dordrecht, 2006.
3. George, M.; Weiss, R. G. *Acc. Chem. Res.* **2006,** *39,* 489–497. doi:10.1021/ar0500923
4. Banerjee, S.; Das, R. K.; Maitra, U. *J. Mater. Chem.* **2009,** *19,* 6649–6687. doi:10.1039/B819218A
5. Fages, F., Ed. *Low Molecular Mass Gelators: Design, Self-Assembly, Function;* Springer-Verlag: Berlin, 2005.
6. Sangeetha, N. M.; Maitra, U. *Chem. Soc. Rev.* **2005,** *34,* 821–836. doi:10.1039/b417081b
7. Wang, C.; Robertson, A.; Weiss, R. G. *Langmuir* **2003,** *19,* 1036–1046. doi:10.1021/la026631j
8. George, M.; Weiss, R. G. *Langmuir* **2003,** *19,* 1017–1025. doi:10.1021/la026639t
9. Yu, T.; Cristiano, R.; Weiss, R. G. *Chem. Soc. Rev.* **2010,** *39,* 1435–1447. doi:10.1039/b821320h
10. George, M.; Weiss, R. G. *J. Am. Chem. Soc.* **2001,** *123,* 10393–10394. doi:10.1021/ja016819+
11. George, M.; Weiss, R. G. *Langmuir* **2002,** *18,* 7124–7135. doi:10.1021/la0255424
12. Terech, P. *Ber. Bunsen-Ges. Phys. Chem.* **1998,** *102,* 1630–1643.
13. George, M.; Weiss, R. G. *Langmuir* **2003,** *19,* 8168–8176. doi:10.1021/la0343829
14. Wang, R.; Geiger, C.; Chen, L.; Swanson, B.; Whitten, D. G. *J. Am. Chem. Soc.* **2000,** *122,* 2399–2400. doi:10.1021/ja993991t
15. Takahashi, A.; Sakai, M.; Kato, T. *Polym. J.* **1980,** *12,* 335–341. doi:10.1295/polymj.12.335
16. Weiss, P. G.; Terech, P., Eds. *Molecular Gels. Materials with Self-Assembled Fibrillar Networks;* Springer: Dordrecht, 2006. Chapter 8.
17. Cohen, I.; Weihs, D. J. *Food Eng.* **2010,** *100,* 366–371. doi:10.1016/j.jfoodeng.2010.04.023
18. Hyde, S. T.; Ninham, B. W.; Zemb, T. *J. Phys. Chem.* **1989,** *93,* 1464–1471. doi:10.1021/j100341a056
19. Raghavan, S. R.; Kaler, E. W. *Langmuir* **2001,** *17,* 300–306. doi:10.1021/la0007933
20. Schubert, B. A.; Kaler, E. W.; Wagner, N. J. *Langmuir* **2003,** *19,* 4079–4089. doi:10.1021/la020821c

License and Terms

Beilstein Journal of Organic Chemistry

Expanding the gelation properties of valine-based 3,5-diaminobenzoate organogelators with *N*-alkylurea functionalities

Hak-Fun Chow*[1,2,3] and Chin-Ho Cheng[1]

Full Research Paper

Open Access

Address:
[1]Department of Chemistry, The Chinese University of Hong Kong, Shatin, NT, Hong Kong SAR, [2]The Center of Novel Functional Molecules, The Chinese University of Hong Kong, Shatin, NT, Hong Kong SAR and [3]Institute of Molecular Functional Materials, Areas of Excellence Scheme, University Grants Committee, Hong Kong SAR

Email:
Hak-Fun Chow* - hfchow@cuhk.edu.hk

* Corresponding author

Keywords:
amino acids; hydrophobic effect; organogelators; self-assembly; urea

Beilstein J. Org. Chem. **2010,** *6,* 1015–1021.
doi:10.3762/bjoc.6.114

Received: 29 June 2010
Accepted: 12 October 2010
Published: 26 October 2010

Guest Editor: J.-P. Desvergne

Abstract

A new family of valine-containing 3,5-diaminobenzoate derivatives **2** with *N*-alkylurea moieties attached to the valine moieties was prepared. By appending these two new *N*-alkylurea chains to the molecular structure, their organogelating properties were extended from only aromatic solvents, to a wide range of other types of solvents such as alicyclic hydrocarbons, alcohols and polar solvents such as DMSO and DMF. It was also found that a longer *N*-alkylurea chain conferred improved gelation power and higher thermal stability as compared to those of the shorter ones.

Introduction

Organic gelators are an interesting group of molecules that are able to form a non-covalent three dimensional network with a particular solvent system. The ultimate result is the immobilization of solvent molecules. These molecules possess many potential applications in biomedical science, environmental and separation technology [1-6].

One key problem in the design and synthesis of organogelators lies in the difficulty in predicting their gelation properties beforehand. Most often a subtle change of the substituents of the organgelator can lead to substantial modification in its gelating properties. This is because gelation is the result of a delicate balance of various driving forces. If the binding interactions between the organogelator molecules are too strong, precipitation or crystallization will take place. On the other hand, if the interactions are too weak, dissolution of the organogelator will result. In addition, non-specific interactions such as hydrophobic and van der Waals interactions are diffi-

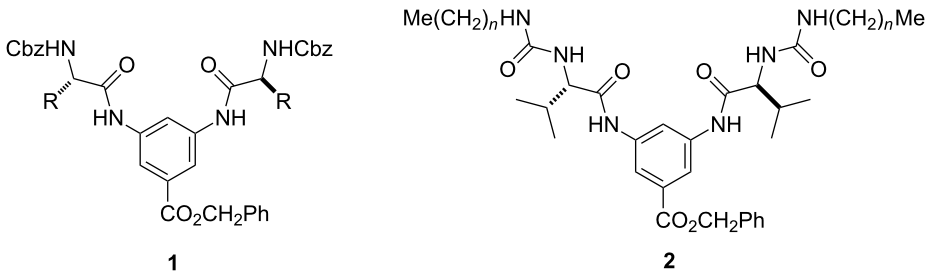

Figure 1: Amino acid based organogelators **1** and **2**.

cult to quantify, yet they can play very important roles on a cumulative scale when such interactions actually involve a large ensemble of solvent and gelator molecules.

Our group has been interested in the synthesis and self-assembled gelating properties of amino acid-containing non-dendritic [7,8] and dendritic molecules [9,10]. We recently showed that the organogelation strength in aromatic solvents of a series of α-amino acid-based low molecular weight organogelators **1** (Figure 1) could be enhanced by appending additional aromatic-containing substituents [7]. Both the Cbz protecting group and the benzyl ester functionality were responsible for the enhanced gelating power in aromatic solvents. However, they are poor organogelators in non-aromatic solvents such as alkanes, alcohols, acetone, acetonitrile and DMSO. In order to further expand their gelating power in other solvents, we decided to further modify the appending Cbz groups with other functionalities. One particular interesting moiety is the urea group, which can act simultaneously as a donor and an acceptor of hydrogen bonds and is known to be a key structural element in many organogelators [11-14]. Herein we report that the organogelating properties of **1** could be expanded to include alicyclic hydrocarbon, alcohols and even polar aprotic solvents such as DMSO and DMF by replacing the Cbz group with an *N*-alkylurea functionality (e.g., **2**). In addition, the length of the alkyl chain $-(CH_2)_nMe$ also exhibited some interesting effects on their gelation ability [15].

Results and Discussion

Synthesis

In our earlier report it was shown that, amongst the many α-amino acids used, valine-based **1** (R = $CHMe_2$) possessed much better organogelating properties. Hence in the present study we focused only on valine derivatives **2**. A homologous series of *N*-alkylurea side chain derivatives **2** (*n* = 3–6, 9, 10, 12, 15, 18 and 20) was prepared in order to evaluate effect of the length of the alkyl side chain on the resulting gelation properties.

The target organogelators were prepared according to Scheme 1. The known Boc protected benzyl ester **3** [7] was converted into the corresponding diamino compound **4** in 98% yield by treatment with trifluoroacetic acid (TFA) followed by neutralization with $NaHCO_3$. The *N*-alkylurea derivatives **2** were then obtained in 88–94% as white solids by coupling compound **4** with various *O*-succinimidyl alkylcarbamates **6**,

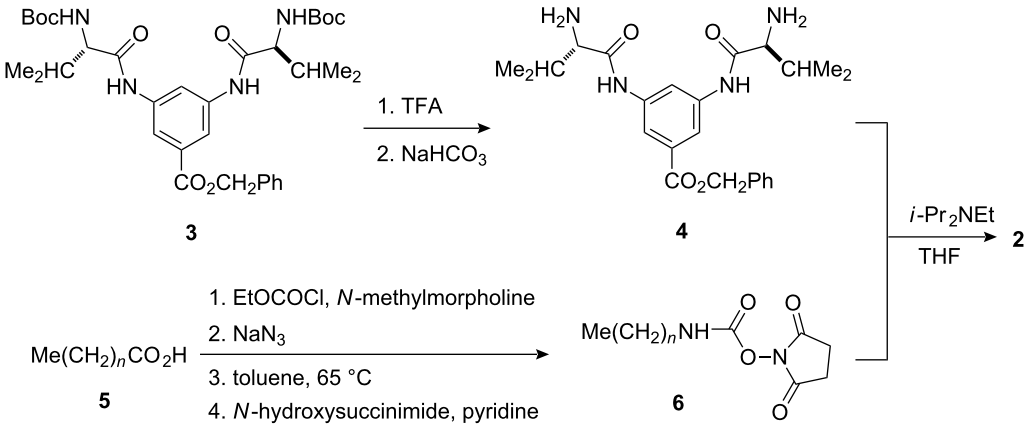

Scheme 1: Synthesis of organogelators **2**.

prepared from the corresponding alkanoic acids **5** according to a literature procedure [16], in the presence of *N*-diisopropylethylamine.

Structural characterization

All synthesized compounds were characterized by ^{1}H and ^{13}C nuclear magnetic resonance spectroscopy, mass spectrometry, elemental analysis, and optical polarimetry. Due to the poor solubilities of the target organogelators **2** in chloroform and acetone, their ^{1}H and ^{13}C NMR spectra were recorded in DMSO-d_6. In addition, the ^{1}H and ^{13}C NMR spectra of analogues with thirteen or more carbon atoms in the aliphatic hydrocarbon chains were recorded at 100 °C to avoid gelation of the solvent. The ^{1}H NMR spectra of compounds **2** showed the presence of the aliphatic hydrocarbon chains and the urea moieties. The methyl group of the aliphatic chains appeared as a triplet at ~ δ 0.86, while the methylenes of the aliphatic chains were located in close proximity to the signals of the valine side chain. On the other hand, the signals from the isopropyl group of the valine residue overlapped with those of the methylenes of the aliphatic chains. The two NH protons of the urea groups were different and appeared as a doublet at δ 6.04 and a triplet at δ 6.07. The benzyl ester group appeared as a singlet at δ 5.24 and a set of multiplets at δ 7.35–7.47. Finally, the aromatic protons of the 3,5-diaminobenzoate moiety appeared as two singlets at δ 7.98 and δ 8.26.

The ^{13}C NMR signals of the target molecules **2** could be grouped into three separate regions. First, in the downfield region, the ^{13}C signals located at δ 157, 165 and 171 were attributed to the urea, ester and anilide C=O groups, respectively. Second, the ^{13}C signals of the central 3,5-diamino-substituted aromatic core were scattered between δ 110–140, while the aromatic signals due to the benzyl ester were found at ~ δ 127–135. Finally, the ^{13}C signals of the valine side chain and the aliphatic hydrocarbon side chain were located in a range of δ 12–66. Specifically, the ^{13}C signal situated at δ 58 corresponded to the valine α-carbon. The benzylic carbon appeared at δ 66. The remaining aliphatic ^{13}C signals due to the aliphatic carbons and some of the resonance peaks overlapped with each other. Hence, the number of the observed signals was sometimes less than theoretically predicted. One ^{13}C signal (CH_2NH) was located at δ 39 and was often buried within the residual solvent signals of DMSO-d_6. For organogelators with longer aliphatic chains, this signal was too weak to be observed and assignment could only be made based on the chemical shift value of other homologues where this signal could be observed.

High-resolution mass spectra were recorded for all synthesized compounds. The experimental determined M^+ results were in accordance with the theoretical values. Generally, the abundance of the M^+ decreased with increasing length of the alkyl hydrocarbon side chain.

Gelation properties

The gelation behavior of bis(*N*-alkylurea valine) benzyl esters **2** were examined at a concentration of 2% w/v in various solvents (Table 1). Most organogelators **2** were found to be insoluble in common non-aromatic organic solvents at room temperature. In contrast, they were soluble in aromatic solvents and organic solvents of high polarity such as 1,4-dioxane, DMF and DMSO upon warming. Interestingly, homologues having shorter aliphatic chain (n < 10) were poor organogelators, while the longer aliphatic chain analogues ($n \geq 10$) formed transparent gels in aromatic solvents and translucent gels in 1,4-dioxane, DMF and DMSO. Most interestingly, it was observed that organogelator **2** (n = 20) with the longest hydrocarbon chain also formed opaque gels in alcoholic solvents and translucent gels in alicyclic hydrocarbon solvents, respectively. Hence, the range of the solvents that these new compounds can gel was significantly expanded by replacing the Cbz group with an *N*-alkylurea functionality.

Based on these experiments, organogelators **2** with longer aliphatic hydrocarbon chains ($n \geq 10$) were found to exhibit better gelation behavior in aromatic solvents. However, it was interesting to note that compounds with less than or equal to eight carbon atoms in the side chain failed to induce gelation. The effect of aliphatic hydrocarbon chain length (n = 10, 12, 15, 18 and 20) on their gelation power was then compared by the determination of their minimum gelation concentration (MGC) and gel-sol transition temperature (T_g) in different solvents (Table 2). It was found that the longer the alkyl chain, the lower the MGC but the higher the T_g value. Hence, the cumulative hydrophobic interaction between organogelator molecules with longer aliphatic chains must be stronger than that of the shorter ones, and this factor should contribute to the higher thermal stability of the longer chain organogels. In addition, the presence of the long aliphatic chain also prevented the organogelators from crystallizing by imposing a higher degree of local disorder.

Fourier transform infrared spectroscopy (FT-IR) was employed to elucidate the extent of intermolecular hydrogen bonding in the different macroscopic phases of organogelator **2** (n = 20) in *o*-xylene (Table 3). In 1% w/v hot *o*-xylene solution (100 °C), two peaks at 3342 and 3247 cm^{-1} in the ν_{N-H} regions were identified. These two signals could be assigned to the stretching bands of urea N–H and anilide N–H, respectively. The two peaks at 1729 and 1629 cm^{-1} in the $\nu_{C=O}$ region were found and they were attributed to the anilide C=O and urea C=O, respectively. Signal assignments of the urea C=O and N–H were

Table 1: Gelation behavior of bis(*N*-alkylurea valine) compounds **2** at 2% w/v [a].

Solvent	**2** (*n* = 3–6)	**2** (*n* = 9)	**2** (*n* = 10)	**2** (*n* = 12)	**2** (*n* = 15)	**2** (*n* = 18)	**2** (*n* = 20)
THF	I	P	P	P	P	P	P
acetone	I	I	I	I	I	I	I
chloroform	I	I	I	I	I	I	I
dichloromethane	I	I	I	I	I	I	I
ethyl acetate	I	I	I	I	I	I	I
ethylene glycol	I	I	I	I	I	I	I
1-butanol	–	–	–	–	–	–	OG
1-heptanol	–	–	–	–	–	–	OG
1-dodecanol	–	–	–	–	–	–	OG
cyclooctanol	–	–	–	–	–	–	TG
hexane	I	I	I	I	I	I	I
cyclohexene	–	–	–	–	–	–	TG
cyclooctene	–	–	–	–	–	–	TG
1,4-dioxane	S	S	S	TG	TG	TG	TG
DMF	S	S	S	TG	TG	TG	TG
DMSO	S	S	TG	TG	TG	TG	TG
anisole	S	S	CG	CG	CG	CG	CG
benzene	S	S	S	CG	CG	CG	CG
benzyl alcohol	S	CG	CG	CG	CG	CG	CG
o-dichlorobenzene	S	CG	CG	CG	CG	CG	CG
nitrobenzene	S	S	TG	TG	TG	TG	TG
toluene	S	CG	CG	CG	CG	CG	CG
o-xylene	S	CG	CG	CG	CG	CG	CG

[a]I = insoluble; P = precipitation; S = soluble; CG = clear transparent gel; OG = opaque gel; TG = translucent gel.

based on the spectral data of a model compound, namely 1,3-didodecylurea. In the FT-IR spectrum of **2** (*n* = 20) (1% w/v) in *o*-xylene gel at 25 °C, the corresponding peaks were identified at 3335, 3268, 1728 and 1628 cm^{-1}, respectively. Hence, there was little difference in terms of the stretching frequencies both in solution and in the gel state. Furthermore, both sets of values are very similar to those of **2** (*n* = 20) in solid KBr, where the C=O and N–H moieties are known to form extensive intermolecular hydrogen bonds. Hence, it is very likely that compound **2** exists as aggregates via intermolecular hydrogen bonding in solution state due to the extremely strong hydrogen bonding property of the urea moiety. In addition, broadening of absorption signals in the gel state was observed which suggests that further intermolecular hydrogen bonding occurred during gel formation.

Conclusion

We have reported the synthesis of novel valine-containing 3,5-diaminobenzoate derivatives **2** with additional *N*-alkylurea functionality at the *N*-terminal of the valine residues. The resulting organogelators were found to possess gelating ability that covered a wider range of organic solvents, including alco-

Table 2: Minimum gelation concentration and gel-to-sol transition temperature of compounds **2** (*n* = 10, 12, 15, 18 and 20).

Solvent	**2** (*n* = 10)		**2** (*n* = 12)		**2** (*n* = 15)		**2** (*n* = 18)		**2** (*n* = 20)	
	MGC[a]	T_g[b]	MGC	T_g	MGC	T_g	MGC	T_g	MGC	T_g
benzyl alcohol	1.8	—	1.8	70	1.5	79	1.2	88	1.0	94
o-dichlorobenzene	1.5	—	1.2	109	1.3	113	1.0	116	0.8	120
o-xylene	1.6	—	1.5	75	1.5	80	1.0	83	1.0	86

[a]In w/v%; [b]In °C as determined by inverted tube method.

Table 3: FT-IR data of compound **2** (*n* = 20) and 1,3-di(dodecyl)urea[a].

Samples	urea N–H	anilide N–H	anilide C=O	urea C=O
2 (*n* = 20) in *o*-xylene solution at 100 °C	3342	3247	1729	1629
2 (*n* = 20) in *o*-xylene gel at 25 °C	3335	3268	1728	1628
2 (*n* = 20) in solid in KBr pellet	3348	3248	1730	1629
1,3-di(dodecyl)urea in solid KBr pellet	3340	—	—	1622

[a]in cm^{-1}.

holic, aromatic, alicyclic hydrocarbon and polar solvents. Furthermore, attachment of longer aliphatic chains not only enhanced hydrophobic interactions between the organogelators, but also prevented crystallization of the self assembled aggregates during gelation, producing gels with a higher T_g and a lower MGC value.

Experimental

General. Optical rotation measurements were conducted in DMSO (unless otherwise stated) and below the MGC to avoid molecular aggregation or gelation and were measured with a Perkin Elmer 341 polarimeter. The starting materials **6** were prepared according to a literature procedure [16]. General procedures, yields and characterization data of compounds **6** (*n* = 3–20) can be found in Supporting Information File 1.

Compound 4. Trifluoroacetic acid (50 mL, 60 mmol) was added to a solution of the benzyl ester **3** [2] (6.40 g, 10.0 mol) in CH_2Cl_2 (100 mL) at 25 °C. The progress of deprotection was monitored by TLC. Upon complete deprotection (~ 12 h), the solvent was removed on a rotary evaporator. The crude product was made alkaline by the addition of aqueous $NaHCO_3$ solution to pH 8. The mixture was extracted with CH_2Cl_2 (50 mL × 3), the combined organic layers were washed with saturated NaCl solution (100 mL × 2), dried ($MgSO_4$), filtered and concentrated in vacuo to give compound **4** as a pale yellow liquid (4.3 g, 98%). $[\alpha]_D^{20}$ −177.6 (*c* 0.50, $CHCl_3$). ^{1}H NMR (DMSO-d_6): δ 0.85 (6H, d, *J* = 6.9, CH(C*H*$_3$)Me), 0.91 (6H, d, *J* = 6.9, CH(Me)C*H*$_3$), 1.85–1.99 (2H, m, C*H*(CH$_3$)$_2$), 3.12 (2H, d, *J* = 5.7, H$_2$NC*H*CH), 3.2–3.5 (6H, brs, NH), 5.35 (2H, s, PhC*H*$_2$), 7.36–7.49 (5H, m, Ar*H*), 7.98 (2H, d, *J* = 1.8, Ar*H*), 8.35 (1H, t, *J* = 1.8, Ar*H*). ^{13}C NMR (DMSO-d_6): δ 17.4, 19.5, 31.8, 60.8, 66.4, 114.4, 114.7, 128.2, 128.4, 128.6, 130.3, 136.1, 139.6, 165.4, 174.1. MS (FAB): 441 (M + H$^+$, 30%). HRMS (LSIMS): calcd for $C_{24}H_{32}N_4O_4$, 441.2496; found, 441.2505. Anal. found: C, 65.63; H, 7.50; N, 12.71. $C_{24}H_{32}N_4O_4$ requires C, 65.43; H, 7.32; N, 12.71.

General procedure for the preparation of bis-(*N*-alkylurea) benzyl esters 2. A mixture of *O*-succinimidyl carbamate **6** (10.0 mmol) and diisopropylethylamine (1.8 mL, 10.0 mmol) was added to a THF solution (100 mL) of the diamino benzyl ester **4** (2.2 g, 5.0 mmol). The reaction mixture was stirred at 25 °C for 4 h. The insoluble crude solid product was filtered and washed successively with boiling *n*-hexane (100 mL), acetone (100 mL) and THF (100 mL) to afford the title compound.

2 (*n* = 3). The product was obtained as a white solid (3.0 g, 94%) from *O*-succinimidyl butylcarbamate **6** (*n* = 3) (2.2 g, 10.0 mmol). $[\alpha]_D$ = +62.4 (*c* 1.01). mp 221–222 °C. ^{1}H NMR (DMSO-d_6): δ 0.83–0.90 (18H, m, CH(C*H*$_3$)$_2$ and CH$_2$CH$_2$C*H*$_3$), 1.22–1.36 (8H, m, aliphatic *H*), 1.92–1.94 (2H, m, CHC*H*(CH$_3$)$_2$), 2.99 (4H, q, *J* = 6, NHC*H*$_2$CH$_2$), 4.18 (2H, dd, *J* = 8.7 and 6.6, NHC*H*CH), 5.34 (2H, s, PhC*H*$_2$), 6.05 (2H, d, *J* = 4.2, urea N*H*), 6.09 (2H, t, *J* = 5.6, urea N*H*), 7.35–7.47 (5H, m, Ar*H*), 7.99 (2H, s, Ar*H*), 8.28 (1H, s, Ar*H*), 10.30 (2H, s, CON*H*Ar). ^{13}C NMR (DMSO-d_6): δ 13.7, 17.9, 19.3, 19.5, 31.2, 32.1, 38.9, 58.7, 66.4, 114.4, 114.8, 128.2, 128.4, 128.6, 130.3, 136.0, 139.6, 157.9, 165.4, 171.8. MS (FAB) 639 (M + H$^+$, 12%). HRMS (LSIMS): calcd for $C_{34}H_{50}N_6O_6$, 639.3865; found, 639.3854. Anal. found: C, 63.75; H, 7.95; N, 13.08. $C_{34}H_{50}N_6O_6$ requires C, 63.93; H, 7.89; N, 13.15.

2 (*n* = 4). The compound was obtained as a white solid (3.1 g, 94%) from *O*-succinimidyl pentylcarbamate **6** (*n* = 4) (2.3 g, 10.0 mmol). $[\alpha]_D$ = +57.9 (*c* 1.08). mp 224–225 °C. ^{1}H NMR (DMSO-d_6): δ 0.82–0.90 (18 H, m, CH(C*H*$_3$)$_2$ and CH$_2$CH$_2$C*H*$_3$), 1.20–1.39 (12 H, m, aliphatic *H*), 1.91–1.95 (2H, m, CHC*H*(CH$_3$)$_2$), 2.97 (4H, q, *J* = 6, NHC*H*$_2$CH$_2$), 4.16 (2H, dd, *J* = 9.0 and 6.6, NHC*H*CH), 5.34 (2H, s, PhC*H*$_2$), 6.05 (2H, d, *J* = 4.5, urea N*H*), 6.08 (2H, t, *J* = 5.6, urea N*H*), 7.38–7.48 (5H, m, Ar*H*), 7.98 (2H, s, Ar*H*), 8.26 (1H, s, Ar*H*), 10.30 (2 H, s, CON*H*Ar). ^{13}C NMR (DMSO-d_6): δ 13.9, 17.9, 19.3, 21.9, 28.6, 29.6, 31.2, 39.2, 58.7, 66.4, 114.4, 114.8, 128.1, 128.2, 128.6, 130.3, 136.0, 139.6, 157.9, 165.3, 171.8. MS (FAB) 667 (M + H$^+$, 10%). HRMS (LSIMS): calcd for $C_{36}H_{54}N_6O_6$, 667.4178; found, 667.4185. Anal. found: C, 64.77; H, 8.20; N, 12.53. $C_{36}H_{54}N_6O_6$ requires C, 64.84; H, 8.16; N, 12.60.

2 (*n* = 5). The product was obtained as a white solid (3.2 g, 91%) from *O*-succinimidyl hexylcarbamate **6** (*n* = 5) (2.4 g,

10.0 mmol). $[\alpha]_D$ = +63.6 (*c* 0.99). mp 225–226 °C. ^{1}H NMR (DMSO-d_6): δ 0.79–0.89 (18H, m, CH(CH_3)$_2$ and CH$_2$CH$_2$CH_3), 1.21–1.35 (16H, m, aliphatic *H*), 1.89–1.96 (2H, m, CHC*H*(CH$_3$)$_2$), 2.95 (4H, q, *J* = 6, NHCH_2CH$_2$), 4.17 (2H, dd, *J* = 8.4 and 6.6, NHC*H*CH), 5.31 (2H, s, PhCH_2), 6.00 (2H, d, *J* = 9, urea N*H*), 6.04 (2H, t, *J* = 5.6, urea N*H*), 7.32–7.44 (5H, m, Ar*H*), 7.96 (2H, s, Ar*H*), 8.24 (1H, s, Ar*H*), 10.20 (2H, s, CON*H*Ar). ^{13}C NMR (DMSO-d_6): δ 13.9, 17.9, 19.3, 22.1, 26.1, 29.9, 31.0, 31.2, 39, 58.7, 66.4, 114.4, 114.8, 128.1, 128.4, 128.5, 130.3, 136.0, 139.6, 157.9, 165.4, 171.8. MS (FAB) 695 (M + H$^+$, 12%). HRMS (LSIMS): calcd for $C_{38}H_{58}N_6O_6$, 695.4491; found, 695.4501. Anal. found: C, 65.26; H, 8.43; N, 11.81. $C_{38}H_{58}N_6O_6$ requires C, 65.68; H, 8.41; N, 12.09.

2 (*n* = 6). The product was obtained as a white solid (3.4 g, 94%) from *O*-succinimidyl heptylcarbamate **6** (*n* = 6) (2.6 g, 10.0 mmol). $[\alpha]_D$ = +59.7 (*c* 1.05). mp 227–228 °C. ^{1}H NMR (DMSO-d_6): δ 0.81–0.91 (18H, m, CH(CH_3)$_2$ and CH$_2$CH$_2$CH_3), 1.23–1.37 (20H, m, aliphatic *H*), 1.90–1.97 (2H, m, CHC*H*(CH$_3$)$_2$), 2.98 (4H, q, *J* = 6, NHCH_2CH$_2$), 4.18 (2H, dd, *J* = 9.0 and 6.6, NHC*H*CH), 5.34 (2H, s, PhCH_2), 6.04 (2H, d, *J* = 9.3, urea N*H*), 6.07 (2H, t, *J* = 5.7, urea N*H*), 7.35–7.48 (5H, m, Ar*H*), 7.99 (2H, s, Ar*H*), 8.27 (1H, s, Ar*H*), 10.26 (2H, s, CON*H*Ar). ^{13}C NMR (DMSO-d_6): δ 13.9, 17.9, 19.3, 22.0, 26.3, 28.4, 30.0, 31.2, 31.3, 39, 58.7, 66.3, 114.4, 114.8, 128.1, 128.4, 128.5, 130.3, 136.0, 139.6, 157.9, 165.3, 171.8. MS (FAB) 723 (M + H$^+$, 5%). HRMS (LSIMS): calcd for $C_{40}H_{62}N_6O_6$, 723.4804; found, 723.4819. Anal. found: C, 66.42; H, 8.68; N, 11.63. $C_{40}H_{62}N_6O_6$ requires C, 66.45; H, 8.64; N, 11.62.

2 (*n* = 9). The product was obtained as a white solid (3.7 g, 92%) from *O*-succinimidyl decylcarbamate **6** (*n* = 9) (3.0 g, 10.0 mmol). $[\alpha]_D$ = +53.9 (*c* 1.00). mp 230–231 °C. ^{1}H NMR (DMSO-d_6): δ 0.82–0.91 (18H, m, CH(CH_3)$_2$ and CH$_2$CH$_2$CH_3), 1.22–1.35 (32H, m, aliphatic *H*), 1.91–1.97 (2H, m, CHC*H*(CH$_3$)$_2$), 2.98 (4 H, q, *J* = 6, NHCH_2CH$_2$), 4.18 (2H, dd, *J* = 9.0 and 6.6, NHC*H*CH), 5.34 (2H, s, PhCH_2), 6.03 (2H, d, *J* = 8.7, urea N*H*), 6.06 (2H, t, *J* = 3.8, urea N*H*), 7.35–7.47 (5H, m, Ar*H*), 7.99 (2H, s, Ar*H*), 8.26 (1H, s, Ar*H*), 10.23 (2 H, s, CON*H*Ar). ^{13}C NMR (DMSO-d_6): δ 13.9, 17.9, 19.3, 22.1, 26.4, 28.7, 28.8, 28.9, 29.0, 30.0, 31.3, 39, 58.7, 66.3, 114.4, 114.8, 128.1, 128.2, 128.5, 130.3, 136.0, 139.5, 157.9, 165.3, 171.8. MS (FAB) 808 (M + H$^+$, 5%). HRMS (LSIMS): calcd for $C_{46}H_{74}N_6O_6$, 807.5743; found, 807.5730. Anal. found: C, 67.97; H, 9.24; N, 10.39. $C_{46}H_{74}N_6O_6$ requires C, 68.45; H, 9.24; N, 10.41.

2 (*n* = 10). The product was obtained as a white solid (3.8 g, 91%) from *O*-succinimidyl undecylcarbamate **6** (*n* = 10) (3.1 g, 10.0 mmol). $[\alpha]_D$ = +52.3 (*c* 1.02). mp 232–233 °C. ^{1}H NMR (DMSO-d_6): δ 0.81–0.90 (18H, m, CH(CH_3)$_2$ and CH$_2$CH$_2$CH_3), 1.22–1.34 (36H, m, aliphatic *H*), 1.91–1.97 (2H, m, CHC*H*(CH$_3$)$_2$), 2.97 (4 H, q, *J* = 6, NHCH_2CH$_2$), 4.18 (2H, dd, *J* = 8.7 and 6.6, NHC*H*CH), 5.34 (2H, s, PhCH_2), 6.04 (2H, d, *J* = 5.4, urea N*H*), 6.07 (2H, t, *J* = 5.3, urea N*H*), 7.35–7.47 (5H, m, Ar*H*), 7.98 (2H, s, Ar*H*), 8.26 (1H, s, Ar*H*), 10.27 (2H, s, CON*H*Ar). ^{13}C NMR (DMSO-d_6): δ 14.0, 18.0, 19.4, 22.2, 26.5, 28.8, 28.9, 29.1, 29.2, 30.1, 30.8, 31.3, 31.4, 39, 58.9, 66.5, 114.6, 114.9, 128.2, 128.3, 128.7, 130.4, 136.1, 139.7, 158.1, 165.5, 171.9. MS (FAB) 836 (M + H$^+$, 5%). HRMS (LSIMS): calcd for $C_{48}H_{78}N_6O_6$, 835.6056; found, 835.6041. Anal. found: C, 68.67; H, 9.45; N, 10.05. $C_{48}H_{78}N_6O_6$ requires C, 69.03; H, 9.41; N, 10.06.

2 (*n* = 12). The product was obtained as a white solid (4.0 g, 90%) from *O*-succinimidyl tridecylcarbamate **6** (*n* = 12) (3.4 g, 10.0 mmol). $[\alpha]_D$ = +53.9 (*c* 0.99). mp 235–236 °C. ^{1}H NMR (DMSO-d_6, 100 °C): δ 0.82–0.90 (18 H, m, CH(CH_3)$_2$ and CH$_2$CH$_2$CH_3), 1.23–1.35 (44H, m, aliphatic *H*), 1.91–1.98 (2H, m, CHC*H*(CH$_3$)$_2$), 2.99 (4H, q, *J* = 7, NHCH_2CH$_2$), 4.18 (2H, dd, *J* = 9.0 and 6.6, NHC*H*CH), 5.34 (2H, s, PhCH_2), 6.02 (2H, d, *J* = 9.6, urea N*H*), 6.05 (2H, t, *J* = 6.2, urea N*H*), 7.35–7.47 (5H, m, Ar*H*), 7.98 (2H, s, Ar*H*), 8.26 (1H, s, Ar*H*), 10.20 (2H, s, CON*H*Ar). ^{13}C NMR (DMSO-d_6, 100 °C): δ 13.0, 17.3, 18.5, 21.3, 25.8, 27.9, 28.1, 28.3, 29.3, 30.4, 30.6, 39, 58.7, 65.7, 114.9, 115.0, 127.2, 127.4, 127.8, 130.0, 135.7, 138.9, 157.4, 164.9, 171.0. MS (FAB) 892 (M + H$^+$, 3%). HRMS (LSIMS): calcd for $C_{52}H_{86}N_6O_6$, 891.6682; found, 891.6691. Anal. found: C, 69.95; H, 9.79; N, 9.47. $C_{52}H_{86}N_6O_6$ requires C, 70.08; H, 9.73; N, 9.42.

2 (*n* = 15). The product was obtained as a white solid (4.2 g, 89%) from *O*-succinimidyl hexadecylcarbamate **6** (*n* = 15) (3.8 g, 10.0 mmol). $[\alpha]_D$ = +50.5 (*c* 1.05). mp 239–240 °C. ^{1}H NMR (DMSO-d_6, 100 °C): δ 0.86 (6H, t, *J* = 3.5, CH$_2$CH$_2$CH_3), 0.91 (6H, d, *J* = 6.9, CH(CH_3)Me), 0.94 (6H, d, *J* = 6.9, CHMe(CH_3)), 1.26–1.40 (56H, m, aliphatic *H*), 1.90–2.15 (2H, m, CHC*H*(CH$_3$)$_2$), 2.95–3.06 (4H, m, NHCH_2CH$_2$), 4.19 (2H, dd, *J* = 6.3 and 9, NHC*H*CH), 5.36 (2H, s, PhCH_2), 5.86 (2H, d, *J* = 9, urea N*H*), 5.93 (2H, t, *J* = 5.4, urea N*H*), 7.37–7.47 (5H, m, Ar*H*), 7.95 (2H, d, *J* = 2.1, Ar*H*), 8.26 (1H, t, *J* = 2.1, Ar*H*), 9.90 (2H, s, CON*H*Ar). ^{13}C NMR (DMSO-d_6, 100 °C): δ 13.0, 17.3, 18.6, 21.3, 25.8, 28.0, 28.2, 28.4, 29.4, 30.5, 30.6, 39, 58.6, 65.7, 114.87, 114.93, 127.3, 127.4, 127.9, 130.0, 135.7, 139.0, 157.5, 164.9, 171.0. MS (FAB) 976 (M + H$^+$, 5%). HRMS (LSIMS): calcd for $C_{58}H_{98}N_6O_6$, 975.7621; found, 975.7626. Anal. found: C, 71.46; H, 9.94; N, 8.35. $C_{58}H_{98}N_6O_6$ requires C, 71.42; H, 10.13; N, 8.61.

2 (*n* = 18). The product was obtained as a white solid (4.7 g, 88%) from *O*-succinimidyl nonadecylcarbamate **6** (*n* = 18) (4.3 g, 10.0 mmol). $[\alpha]_D$ = +52.5 (*c* 1.01). mp 243–244 °C. ^{1}H NMR (DMSO-d_6, 100 °C): δ 0.84–0.93 (18H, m, CH(CH_3)$_2$ and $CH_2CH_2CH_3$), 1.25–1.37 (68H, m, aliphatic *H*), 1.95–1.99 (2H, m, CHC*H*$(CH_3)_2$), 2.95–3.06 (4H, m, NHCH_2CH_2), 4.19 (2H, dd, *J* = 8.4 and 6.6, NHC*H*CH), 5.35 (2H, s, PhCH_2), 5.92 (2H, d, *J* = 8.7, urea N*H*), 5.98 (2H, t, *J* = 5.6, urea N*H*), 7.35–7.47 (5H, m, Ar*H*), 7.96 (2H, s, Ar*H*), 8.24 (1H, s, Ar*H*), 10.04 (2H, s, CON*H*Ar). ^{13}C NMR (DMSO-d_6, 100 °C): δ 13.0, 17.3, 18.6, 21.3, 25.8, 28.0, 28.2, 28.4, 29.4, 30.5, 30.6, 39, 58.6, 65.7, 114.87, 114.93, 127.3, 127.4, 127.9, 130.0, 135.7, 139.0, 157.5, 164.9, 171.0. MS (FAB) 1060 (M + H$^+$, 3%). HRMS (LSIMS): calcd for $C_{64}H_{110}N_6O_6$, 1069.8560; found, 1069.8550. Anal. found: C, 72.53; H, 10.57; N, 7.81. $C_{64}H_{110}N_6O_6$ requires C, 72.55; H, 10.46; N, 7.93.

2 (*n* = 20). The product was obtained as a white solid (4.8 g, 86%) from *O*-succinimidyl heneicosylcarbamate **6** (*n* = 20) (4.5 g, 10.0 mmol). $[\alpha]_D$ = +53.1 (*c* 1.00). mp 249–250 °C. ^{1}H NMR (DMSO-d_6, 100 °C): δ 0.86 (6H, t, *J* = 6.9, $CH_2CH_2CH_3$), 0.92 (6H, d, *J* = 6.9, CH(CH_3)Me), 0.95 (6H, d, *J* = 6.9, CHMe(CH_3)), 1.28–1.43 (76H, m, aliphatic *H*), 1.95–2.12 (2H, m, CHC*H*$(CH_3)_2$), 3.00 (4H, q, *J* = 6, NHCH_2CH_2), 4.19 (2H, dd, *J* = 8.1 and 6.6, NHC*H*CH), 5.36 (2H, s, PhCH_2), 5.82 (2H, d, *J* = 9, urea N*H*), 5.88 (2H, t, *J* = 5.6, urea N*H*), 7.37–7.47 (5H, m, Ar*H*), 7.94 (2H, d, *J* = 2.1, Ar*H*), 8.19 (1H, t, *J* = 1.8, Ar*H*), 9.80 (2H, s, CON*H*Ar). ^{13}C NMR (DMSO-d_6, 100 °C): δ 13.0, 17.3, 18.5, 20.2, 21.3, 25.8, 27.9, 28.1, 28.3, 29.3, 30.4, 30.6, 39, 58.7, 65.7, 114.9, 115.0, 127.2, 127.4, 127.8, 130.0, 135.7, 138.9, 157.5, 164.9, 171.0. MS (FAB) 1116 (M + H$^+$, 100%). HRMS (LSIMS): calcd for $C_{68}H_{118}N_6O_6$, 1115.9186; found, 1115.9192. Anal. found: C, 73.17; H, 10.53; N, 7.45. $C_{68}H_{118}N_6O_6$ requires C, 73.20; H, 10.66; N, 7.53.

Supporting Information

General procedure, yields and characterization data of compounds 6 (*n* = 3–20).

Supporting Information File 1

Experimental Part.
[http://www.beilstein-journals.org/bjoc/content/supplementary/1860-5397-6-114-S1.pdf]

References

1. Terech, P.; Weiss, R. G. *Chem. Rev.* **1997,** *97,* 3133–3159. doi:10.1021/cr9700282
2. van Esch, J. H.; Feringa, B. L. *Angew. Chem., Int. Ed.* **2000,** *39,* 2263–2266. doi:10.1002/1521-3773(20000703)39:13<2263::AID-ANIE2263>3.0.CO;2-V
3. Gronwald, O.; Snip, E.; Shinkai, S. *Curr. Opin. Colloid Interface Sci.* **2002,** *7,* 148–156. doi:10.1016/S1359-0294(02)00016-X
4. Sangeetha, N. M.; Maitra, U. *Chem. Soc. Rev.* **2005,** *34,* 821–836. doi:10.1039/b417081b
5. Dastidar, P. *Chem. Soc. Rev.* **2008,** *37,* 2699–2715. doi:10.1039/b807346e
6. Vintiloiu, A.; Leroux, J.-C. *J. Controlled Release* **2008,** *125,* 179–192. doi:10.1016/j.jconrel.2007.09.014
7. Chow, H.-F.; Zhang, J.; Lo, C.-M.; Cheung, S.-Y.; Wong, K.-W. *Tetrahedron* **2007,** *63,* 363–373. doi:10.1016/j.tet.2006.10.066
8. Chow, H.-F.; Wang, G.-X. *Tetrahedron* **2007,** *63,* 7407–7418. doi:10.1016/j.tet.2007.02.037
9. Chow, H.-F.; Zhang, J. *Chem.–Eur. J.* **2005,** *11,* 5817–5831. doi:10.1002/chem.200500174
10. Chow, H.-F.; Zhang, J. *Tetrahedron* **2005,** *61,* 11279–11290. doi:10.1016/j.tet.2005.08.006
11. Steed, J. W. *Chem. Soc. Rev.* **2010,** *39,* 3686–3699. doi:10.1039/b926219a
12. van Esch, J.; Kellogg, R. M.; Feringa, B. L. *Tetrahedron Lett.* **1997,** *38,* 281–284. doi:10.1016/S0040-4039(96)02292-7
13. van Esch, J.; de Feyter, S.; Kellogg, R. M.; de Schryver, F.; Feringa, B. L. *Chem.–Eur. J.* **1997,** *3,* 1238–1243. doi:10.1002/chem.19970030811
14. van de Laan, S.; Feringa, B. L.; Kellogg, R. M.; van Esch, J. *Langmuir* **2002,** *18,* 7136–7140. doi:10.1021/la025561d
15. George, M.; Tan, G.; John, V. T.; Weiss, R. G. *Chem.–Eur. J.* **2005,** *11,* 3243–3254. doi:10.1002/chem.200401066
16. Guichard, G.; Semetey, V.; Didierjean, C.; Aubry, A.; Briand, J. P.; Rodriguez, M. *J. Org. Chem.* **1999,** *64,* 8702–8705. doi:10.1021/jo990092e

License and Terms

Beilstein Journal of Organic Chemistry

Self-assembly and semiconductivity of an oligothiophene supergelator

Pampa Pratihar[1], Suhrit Ghosh[1,2], Vladimir Stepanenko[1], Sameer Patwardhan[3], Ferdinand C. Grozema[3], Laurens D. A. Siebbeles[3] and Frank Würthner[*1]

Full Research Paper

Open Access

Address:
[1]Universität Würzburg, Institut für Organische Chemie, 97074 Würzburg, Germany, [2]Indian Association for the Cultivation of Science, Polymer Science Unit, Kolkata-700032, India (present address) and [3]Opto-Electronic Materials Section, Delft Chem Tech, Delft University of Technology, Julianalaan 136, 2628 BL Delft, The Netherlands

Email:
Frank Würthner* - wuerthner@chemie.uni-wuerzburg.de

* Corresponding author

This work is dedicated to Prof. Henning Hopf on the occasion of his 70th birthday.

Keywords:
charge transport; hydrogen bonding; oligothiophene; organogel; self-assembly

Beilstein J. Org. Chem. **2010,** *6,* 1070–1078.
doi:10.3762/bjoc.6.122

Received: 15 June 2010
Accepted: 05 August 2010
Published: 16 November 2010

Guest Editor: J.-P. Desvergne

Abstract

A bis(trialkoxybenzamide)-functionalized quaterthiophene derivative was synthesized and its self-assembly properties in solution were studied. In non-polar solvents such as cyclohexane, this quaterthiophene π-system formed fibril aggregates with an H-type molecular arrangement due to synergistic effect of hydrogen bonding and π-stacking. The self-assembled fibres were found to gelate numerous organic solvents of diverse polarity. The charge transport ability of such elongated fibres of quaterthiophene π-system was explored by the pulse radiolysis time resolved microwave conductivity (PR-TRMC) technique and moderate mobility values were obtained. Furthermore, initial AFM and UV-vis spectroscopic studies of a mixture of our electron-rich quaterthiophene derivative with the electron acceptor [6,6]-phenyl-C_{61}-butyric acid methyl ester (PCBM) revealed a nanoscale segregated assembly of the individual building blocks in the blend.

Introduction

Self-assembly provides a spontaneous pathway to generate higher-order structures from suitably designed building blocks by virtue of specific intra and intermolecular non-covalent interactions [1]. The development of such building blocks containing various functional π-systems has attracted much interest in the recent past due to their potential applications as active components in a variety of organic electronic devices [2]. Organogels are a special class of self-assembled materials in

which small building blocks generate fibrous structures due to intermolecular non-covalent interactions, and these elongated fibres form interpenetrating network in which the solvent molecules are trapped [3,4]. Organogels based on various π-systems such as oligophenylenevinylenes [5] and thienylenevinylenes [6] oligophenyleneethylenes [7], phthalocyanines [8], porphyrins [9], naphthalene and perylene bisimides [10-12], acenes [13,14] and merocyanines [15,16] have been studied in recent years. Self-assembly of various oligothiophene derivatives have been extensively investigated on account of their semiconducting and optoelectronic properties [17]. Feringa and co-workers reported organogels based on bisurea derivatives of bithiophene chromophores and demonstrated a significant charge carrier mobility as a result of self-assembly ($\Sigma\mu_{min} = 5 \times 10^{-3}$ cm^2 V^{-1} s^{-1}) [18]. However, the building blocks were made only from mono and bithiophene units. Later, Shinkai and co-workers reported the gelation ability of quaterthiophene and hexathiophene derivatives with peripheral amide-linked cholesterol moieties [19]. We recently reported [12] the self-assembly of perylene bisimide (PBI) π-systems that are functionalized with trialkoxybenzamide moiety and have shown that they possess much superior and versatile gelation and self-assembly properties compared to those of cholesterol-linked PBI gelators reported earlier [10]. We also have demonstrated that the trialkoxybenzamide units provide a unique opportunity to tune the mode of self-assembly (H-type vs. J-type) of PBIs by systematically varying the steric crowding in the peripheral alkyl groups [20,21]. These recent findings on PBI gelators prompted us to explore the utility of similar supramolecular design on the self-assembly of other functional π-systems.

Herein we describe the synthesis, self-assembly, gelation, and charge-carrier mobility studies of trialkoxybenzamide-functionalized quaterthiophene derivative **T1** (Scheme 1). We also present our initial results on the morphology of blends of this electron-rich p-type semiconducting **T1** with the well-known n-type semiconductor [6,6]-phenyl-C_{61}-butyric acid methyl ester (PCBM).

Results and Discussions

Synthesis

The synthetic route to the newly designed quaterthiophene derivative **T1** is depicted in Scheme 2. Compounds **4** [22] and **5** [20] were synthesized from commercially available starting materials in a few synthetic steps by literature methods, and then coupled together to produce the thiophene-containing building block **6** in 78% yield. 2, 2′-Bithiophene was converted to the corresponding tributyltin derivative **8** by the reported procedure [19] and then coupled with compound **6** in the presence of a Pd-catalyst to give the desired oligothiophene derivative **T1** in 82% yield. The new compounds **6** and **T1** were characterized by ^{1}H NMR and UV-vis spectroscopy, HRMS (ESI) and elemental analysis, while those synthetic intermediates already reported in the literature were characterized by ^{1}H NMR and UV-vis spectroscopy.

Gelation tests

The gelation properties of **T1** were examined in various organic solvents (Table 1) at a concentration of 3.5 mM. At room temperature **T1** was soluble only in chloroform, dichloromethane, and tetrahydrofuran among other tested solvents. However, at elevated temperatures this quaterthiophene could be dissolved in all the tested solvents and when the hot solution was cooled down to room temperature, spontaneous gelation was observed (see Figure 1A, inset) in most cases within 5–10 minutes. For example, aromatic hydrocarbons (toluene, benzene), aliphatic hydrocarbons (methylcyclohexane, cyclohexane, *n*-heptane, *n*-hexane), chlorinated hydrocarbons (chlorobenzene, tetrachloroethylene, 1,2-dichloroethane), ethers (dibutyl ether, THF, dioxan), hydrogen-bonding donor molecules (triethylamine, acetone), and even highly polar solvents such as DMF and ethanol could be gelated with **T1**. The only exceptions were acetonitrile and DMSO for which no gelation was observed. Critical gelation concentrations (CGC) were determined for all the solvents gelated with **T1** and found to be below 0.3 wt %. This CGC value is much lower compared to those of the previously reported quaterthiophene gelators containing cholesteryl amide peripheral groups [19]. It is interesting to note that in aliphatic hydrocarbons (methylcyclohexane (MCH), cyclohexane, *n*-hexane, *n*-heptane) and in tetrachloroethylene the CGC values are even less than 0.1 wt %. Organogelators with such low CGC values are classified as supergelators [4], and thus the present quaterthiophene gelator **T1** belongs to this category. The ability of **T1** to gelate such a wide range of solvents and its significantly low CGC values can be attributed to the favourable balance between the self-

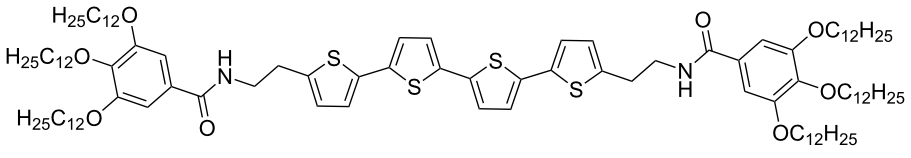

Scheme 1: Structure of the quarterthiophene derivative **T1**.

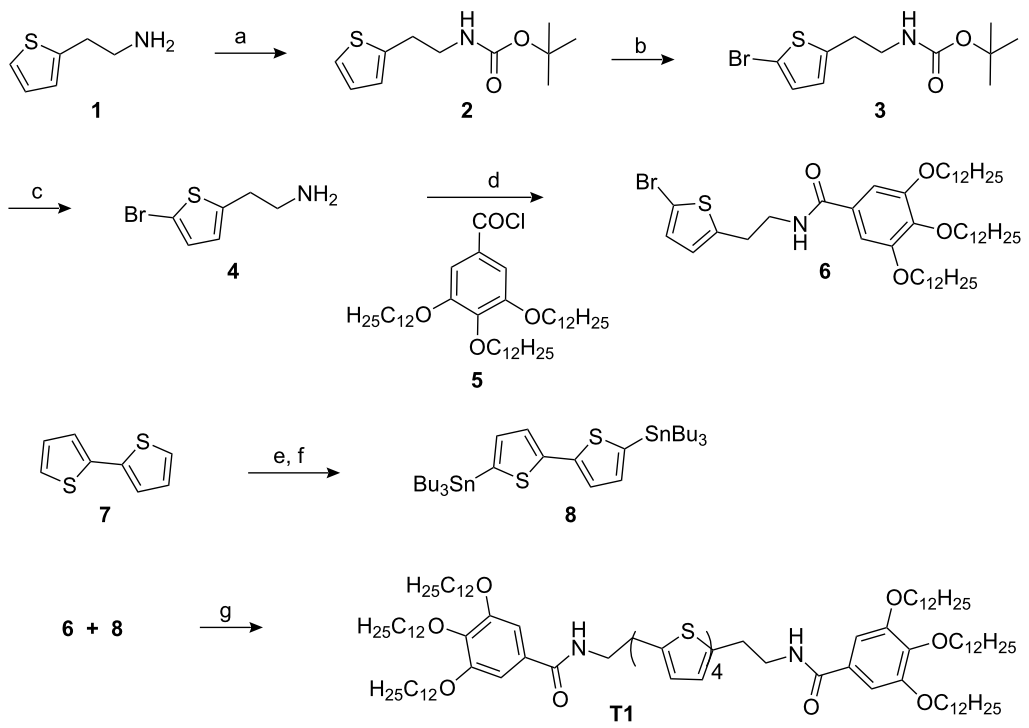

Scheme 2: Synthetic route to **T1**. Reagent and conditions: a) Boc anhydride, CH_2Cl_2, 6 h, 0 °C–rt, 97%; b) NBS, DMF, rt, 12 h, 89%; c) TFA, CH_2Cl_2, rt, 4 h, 99%; d) Et_3N, CH_2Cl_2, 0 °C–rt, 78%; e) BuLi, THF, 0 °C, 1 h; f) Bu_3SnCl, rt, 12 h; g) $Pd(PPh_3)_2Cl_2$, DMF, 80 °C, 8 h, 82%.

Table 1: Gelation studies of **T1** in various solvents.

Entry	Solvent	Observation	CGC (moles/lit.)	CGC (Wt %)
1	Toluene	G	1×10^{-3}	0.20
2	Benzene	G	1×10^{-3}	0.19
3	Methylcyclohexane	G	2×10^{-4}	**0.04**
4	Cyclohexane	G	4×10^{-4}	**0.08**
5	*n*-Heptane	G	3.75×10^{-4}	**0.09**
6	*n*-Hexane	G	0.4×10^{-3}	**0.10**
7	$CHCl_3$	soluble	–	–
8	CH_2Cl_2	soluble	–	–
9	Chlorobenzene	G	0.33×10^{-2}	0.51
10	Tetrachloroethylene	G	9.09×10^{-4}	**0.09**
11	1,2-Dichloroethylene	G	1.25×10^{-3}	0.17
12	1,4-Dioxan	G[a]	0.125×10^{-2}	0.26
13	THF	soluble	–	–
14	Dibutylether	G	1×10^{-3}	0.22
15	Acetone	G[a]	1.11×10^{-3}	0.24
16	Triethylamine	G	0.5×10^{-3}	0.12
17	Acetonitrile	not soluble	–	–
18	DMF	G	1×10^{-3}	0.18
19	DMSO	gel-like ppt.	–	–
20	Ethanol	G[a]	1×10^{-3}	0.21

[a]Opaque gel.

assembly propensity of the gelator and good solubility due to the presence of the trialkoxybenzamide groups.

AFM investigations

The topology of gels of quaterthiophene derivative **T1** was examined by atomic force microscopy (AFM) in the tapping mode. As an illustrative example, the AFM images of **T1** gel in MCH deposited on highly ordered pyrolytic graphite (HOPG) are shown in Figure 1. These images clearly show interconnected long fibers a few micrometers in length and bundles that are responsible for the gelation of the solvents. At nanometer to micrometer resolution, a fibrous network is observed that contains smaller fibers (indicated by yellow arrows in Figure 1C) with a mean height of 2.3±0.3 nm and width of 7.0±1.0 nm.

Self-assembly studies by UV-vis spectroscopy

Self-assembly of **T1** in solution was examined by UV-vis spectroscopy. Chloroform is known to be an excellent solvent for the study of rigid π-systems [20,21], and the oligothiophene chromophore **T1** has good solubility in this solvent. However, as noted above, in nonpolar solvents such as *n*-heptane, gelation was observed at extremely low CGC values. Thus, we compared the UV-vis spectra of **T1** in chloroform and *n*-heptane at 0.05 mM concentration (Figure 2a).

In chloroform the π-π* transition band appeared at 400 nm, whilst in *n*-heptane it was shifted significantly to a lower wavelength (374 nm). In *n*-heptane, additional shoulders appeared at 420, 461 and 513 nm that were absent in the spectrum recorded

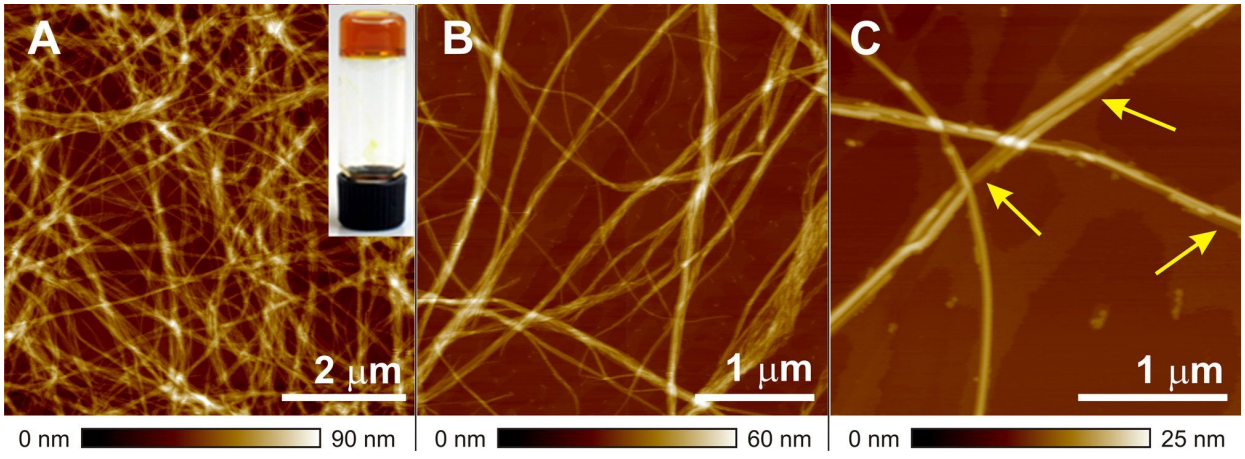

Figure 1: AFM height images of a film spin-coated from diluted gel solution of **T1** in MCH (2×10^{-3} M) onto HOPG (A, B and C). The z scale (90, 60 and 25 nm, respectively) is shown under the respective image. Inset in 1A: a photograph of gel in cyclohexane at 1.5 mM concentration.

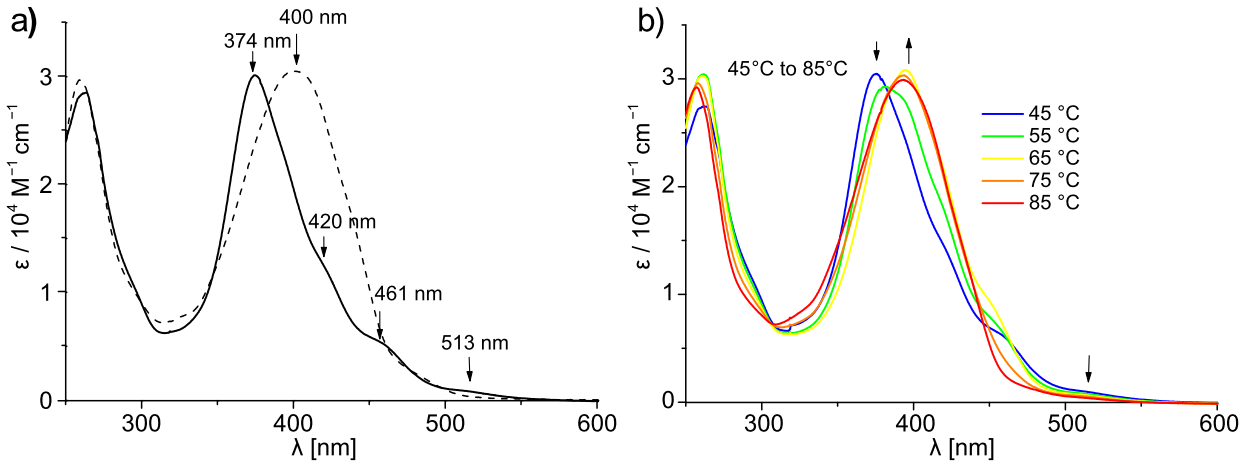

Figure 2: a) UV-vis spectra of **T1** in chloroform (dashed line) and *n*-heptane (solid line); b) UV-vis spectra of **T1** in *n*-heptane at different temperatures. Concentration of **T1** is 5×10^{-5} M.

in chloroform. These results are in accord with the literature reports for the formation of H-aggregates of oligothiophenes [19] and can be attributed to an excitonic interaction as well as an increase in the conformational order in the assembled state [23]. To test the reversibility of the self-assembly process, variable temperature UV-vis experiments were performed in *n*-heptane. These clearly showed that when the temperature was gradually raised from 45 °C to 85 °C, the spectral pattern changed significantly (Figure 2b). The λ_{max} value shifted from 374 nm to 400 nm and the shoulders at higher wavelengths (420, 461 and 513 nm) gradually disappeared. At the higher temperature, the spectrum resembles quite well that observed in chloroform solution (Figure 2a). These results suggest disassembly of the H-type aggregate to monomeric building blocks at elevated temperature. The self-assembly of **T1** at such low concentrations can be attributed to the synergistic effect of π-π-stacking among the oligothiophene chromophores and intermolecular hydrogen bonding between the amide groups of the neighbouring chromophores (Scheme 3). To ascertain the involvement of hydrogen bonding in the self-assembly, we examined the effect of a protic solvent, e.g. MeOH, on the self-assembly process by UV-vis spectroscopy. MeOH itself can be involved in H-bonding interaction with the amide groups, and thus expected to interfere with the inter-chromophoric hydrogen-bonding interaction and to disrupt the assembly. Note that, as methanol is not miscible with *n*-heptane, cyclohexane was used as nonpolar solvent for this experiment. It can be seen in Figure 3 that in the presence of 2.4% MeOH the absorption spectrum of **T1** in cyclohexane changed significantly. The shoulders at longer wavelength disappeared and the λ_{max} value shifted from 382 nm to 399 nm, suggesting disassembly of the aggregate into monomers. Thus, it is evident that hydrogen bonding is essential for the self-assembly of **T1**, particularly at such a low concentration of 5 x 10^{-5} M.

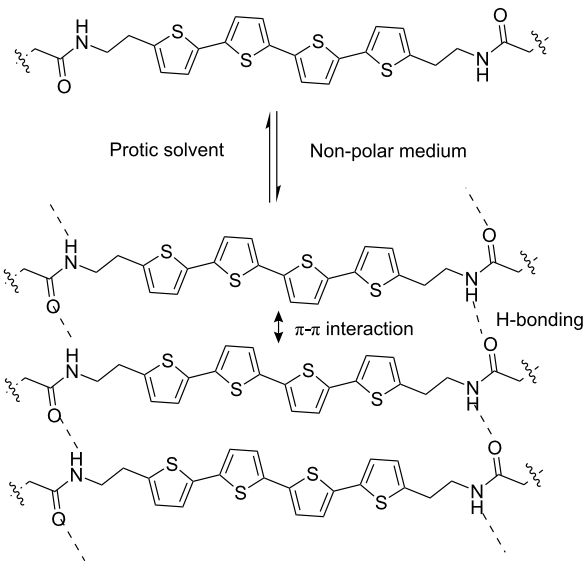

Scheme 3: Proposed mode of self-assembly of **T1**.

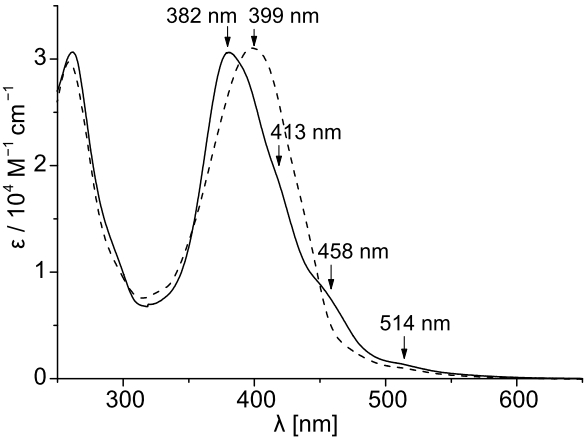

Figure 3: UV-vis spectra of **T1** (concentration 5 x 10^{-5} M) in cyclohexane (solid line) and 2.4% MeOH in cyclohexane (dashed line) at 25 °C.

Studies on blends of T1 with PCBM

The fullerene derivative [6,6]-phenyl-C_{61}-butyric acid methyl ester (PCBM) is a well-known n-type semiconductor and its blends with various electron-donor materials have been extensively used in solar cell devices [24]. The morphology of the blend of donor and acceptor materials plays a prominent role in device performance [25]. Recently, we reported that a n-type perylene bisimide organogelator exhibits photovoltaic activity with a p-type semiconducting polymer [26]. In this work, as an initial study we characterized the morphology of a mixture of PCBM with the p-type semiconducting oligothiophene-based gelator **T1** to elucidate the prospect of this system being used as a photovoltaic material. Figure 4 depicts the AFM images of a mixture of **T1** and PCBM on HOPG in which two types of aggregates are visible. The observed long fibers can be attributed to aggregates of **T1** and the spherical nano-objects can be related to PCBM aggregates. The height and width of the long fibers were estimated to be 2.4±0.3 nm and 6.0±01.0 nm, respectively, which very closely match with the values observed for the self-assembly of **T1** alone (Figure 1). This indicates that PCBM does not interfere in the self-assembly of **T1**.

Determination of charge carrier mobility

It was anticipated that the well-organized π-stacked assembly of oligothiophene chromophores would provide percolation pathways for charge transport, similar to the previously reported results for mono- and bithiophene bisurea compunds [18]. Therefore, the charge transport properties of **T1** in the solid

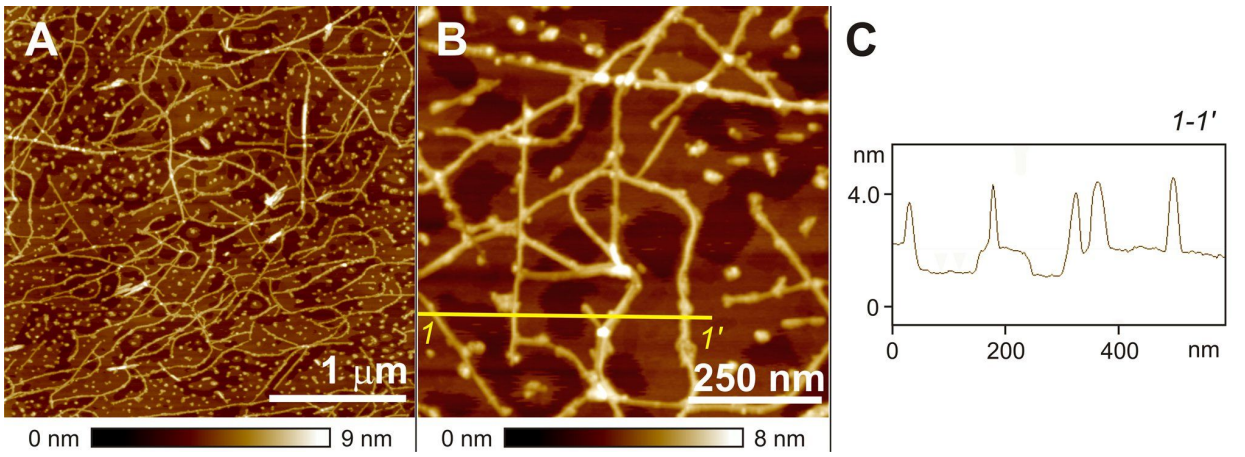

Figure 4: AFM height images (A and B) of a film spin-coated from MCH solution (concentration 5 x 10^{-4} M) of a 1:1 mixture of **T1** and PCBM onto HOPG. The z scale (9 nm and 8 nm, respectively) is shown under the respective image. Figure 4C depicts cross-section analysis along the yellow line 1-1' in image B.

state were investigated by pulse radiolysis time resolved microwave conductivity (PR-TRMC) measurements [27].

PR-TRMC measurements were performed with a solid (powder) sample of **T1** using the same methodology as reported previously [27,28]. The sample (~32.5 mg) was irradiated with a short pulse of 3 MeV electrons, which lead to the formation of charges in the material during the pulse. The conductivity was measured as a function of time by microwave conductivity measurements. The dose-normalized PR-TRMC transients for different irradiation doses at a temperature of 20 ºC are shown in Figure 5. The decay is the same for all irradiation doses, which indicates first order decay of the charge carriers. Such first order decay is typically observed for columnar materials and can be due to either trapping of charges or geminate recombination of electrons and holes [28].

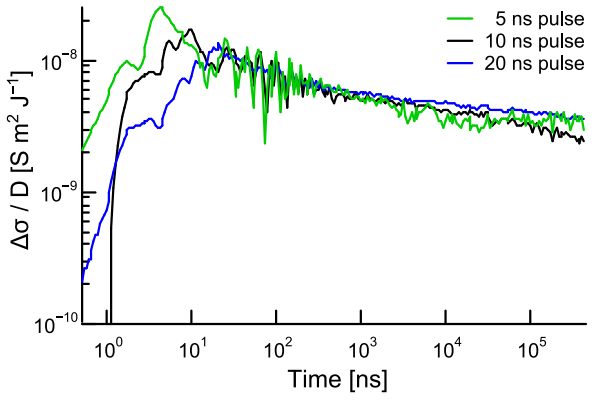

Figure 5: Variation of dose-normalized conductivity transients ($\Delta\sigma/D$) with time for **T1**.

The lower limits of $\Sigma\mu_{min}$ (the sum of the mobilities of the positive and negative charge carriers) were estimated from the relation $\Sigma\mu_{min} = E_p(\Delta\sigma/D)$, where E_p is the average electron-hole pair formation energy [28]. The mobility values obtained in this way at various temperatures are listed in Table 2. The charge carrier mobility of **T1** at 20 °C was found to be 2.9 × 10^{-3} cm^2 V^{-1} s^{-1}. When the sample was heated up to 110 °C, no significant difference was observed in the mobility value compared to that at 20 °C, indicating good thermal stability of the supramolecular assembly of **T1**. A repeat measurement of mobility at 20 °C after the sample was annealed revealed a slightly higher value (4.2 × 10^{-3} cm^2 V^{-1} s^{-1}), indicating an improvement of the supramolecular order in the material on annealing. It is interesting to note that the mobility value obtained for **T1** is very close to that reported for non-regio regular alkyl-substituted polythiophenes ($\Sigma\mu_{min}$ = 7 × 10^{-3} cm^2 V^{-1} s^{-1}) [29], suggesting similar electronic coupling between oligothiophenes in the gelated π-stacks.

Table 2: Charge carrier mobilities of **T1** at various temperatures in the sequence as measured in two experimental series.

T (°C)	$\Sigma\mu_{min}$ (cm^2 V^{-1} s^{-1})	T (°C)	$\Sigma\mu_{min}$ (cm^2 V^{-1} s^{-1})
20	0.0030	80	0.0024
0	0.0032	100	0.0021
−20	0.0031	110	0.0024
−40	0.0030	100	0.0027
−20	0.0030	80	0.0031
0	0.0032	60	0.0034
20	0.0029	40	0.0039
40	0.0028	20	0.0042
60	0.0026		

Conclusion

We have demonstrated the self-assembly and charge transport properties of a trialkoxybenzamide-functionalized quaterthiophene π-system. Our studies revealed the versatile and very effective gelation ability of the present system compared to the previously reported oligothiophene gelators. The critical gelation concentrations in numerous solvents are remarkably low and in few cases even in the range of supergelators. The impact of facile self-assembly of newly developed oligothiophene building block on its material properties is reflected in promising charge transport characteristics as revealed by PR-TRMC measurements. When compared with ordinary amorphous or crystalline organic semiconductors it should be taken into account that the oligothiophene moiety, which is responsible for charge transport, is only 19% of the total molecular weight of **T1** and the remainder being made up by long alkyl chains that do not contribute to charge carrier mobility. AFM studies revealed self-sorted assembly of p-type oligothiophene gelator and n-type **PCBM** in their blend which might offer some prospect for photocurrent generation [30].

Experimental

Materials and methods. All reagents and solvents were purchased from commercial sources and purified by standard protocols [31]. Spectroscopic grade solvents were used as received for spectroscopic studies. ^{1}H NMR spectra were recorded on a 400 MHz Bruker NMR spectrometer with tetramethylsilane (TMS) as the internal standard. UV-vis experiments were carried out on a Perkin-Elmer Lambda 40P spectrometer equipped with a Peltier system for temperature control.

Gelation tests. A measured amount of **T1** and the appropriate solvent were taken together in a sample vial, heated to dissolve the sample and then left at room temperature. After 30 minutes, the gelation was tested by the "stable to inversion" method.

UV-vis spectroscopic studies. A stock solution of **T1** was prepared in chloroform with 1 mM concentration. A measured amount of stock solution was transferred to another vial and the solvent removed by blowing argon gas over it. To this vial, a measured amount of solvent such as *n*-heptane or cyclohexane was added to give the desired concentration and the mixture then gently heated in a warm water-bath to yield a homogeneous solution. The solutions were allowed to equilibrate at room temperature for 2 h before performing UV-vis experiments. For variable temperature studies, the temperature was changed from lower to higher values and the sample equilibrated for 10 min prior to each measurement after the particular temperature was reached.

Atomic force microscopy (AFM) measurements. AFM measurements were carried out under ambient conditions with a Veeco MultiMode^{TM} Nanoscope IV system operating in the tapping mode in air. Silicon cantilevers (Olympus Corporation, Japan) with a resonance frequency of ~300 kHz and spring constant of ~42 N/m were used. A solution of **T1** in methylcyclohexane (MCH) with a concentration of 2×10^{-3} M was spin-coated onto highly oriented pyrolytic graphite (HOPG) at 6000 rpm. The sample of a **T1**-PCBM mixture was prepared by spin-coating of MCH solution with a concentration of 5×10^{-4} M onto HOPG at 4000 rpm. The height of the observed fibers was determined by statistical analysis on the premise that the fibers lay on a thin film. Note that, due to the AFM tip broadening effect, the actual width of aggregates is usually smaller than the apparent one.

Pulse radiolysis time resolved microwave conductivity (PR-TRMC) measurements. Conductivity measurements of quaterthiophene **T1** were performed on a solid (powder) sample (about 32.5 mg) that was manually compressed into a perspex container. The sample was placed in a microwave cell, consisting of a piece of rectangular waveguide with inner dimensions of 3.55×7.00 mm^2 and short circuited with a metal end plate. The materials were uniformly ionized with a nanosecond pulse of 3 MeV electrons from a Van de Graaff accelerator. The energy absorbed by the sample is accurately known from dosimetry and leads to the formation of a micromolar concentration of charge carriers (ca. 10^{-21} m^{-3}). The change in conductivity due to creation of these charges was measured by time resolved microwave conductivity (TRMC) measurements [27].

Synthesis and characterization. 3,4,5-Tris(dodecyloxy)-benzoyl chloride (**5**) and compounds **2**, **3**, **4** and **8** were prepared according to literature reported procedures and characterized by ^{1}H NMR and UV-vis spectroscopy. New compounds (**6** and **T1**) were characterized by ^{1}H NMR, UV-vis, HRMS (ESI) and elemental analysis.

***Tert*-butyl 2-(thiophen-2-yl)ethylcarbamate (2).** To a solution of 2-(thiophen-2-yl) ethylamine (1.63 g, 0.013 mol) in 10 mL $CHCl_3$, a solution of Boc-anhydride (2.8 g, 0.013 mol) in 10 mL $CHCl_3$ was added dropwise and the reaction mixture stirred under an inert atmosphere for 6 h at room temperature. The volatiles were then removed at reduced pressure to yield the crude **2** as a colourless oil (97%). ^{1}H NMR (400 MHz, $CDCl_3$, TMS, 300 K): δ (ppm) = 7.15 (d, 1H), 6.95–6.83 (m, 1H), 6.83 (m, 1H), 4.65 (broad peak, 1H), 3.38 (t, J = 6.24 Hz, 2H), 3.01(t, J = 6.68 Hz, 2H), 1.44 (s, 9H); UV-vis (CH_2Cl_2): λ_{max} (ε) = 235 nm (0.697×10^4 M^{-1}cm^{-1}).

***Tert*-butyl 2-(5-bromothiophen-2-yl)ethylcarbamate (3).** To an ice-cold solution of compound **2** (0.77 g, 3.38 mmol) in 10 mL DMF, a solution of NBS (0.603 g, 3.38 mmol) in 5 mL DMF was added dropwise. After the addition was complete, the reaction mixture was stirred at room temperature for a further 12 h, then poured into 100 mL water and extracted with (2 × 30) mL diethylether. The combined organic layer was dried over anhydrous Na_2SO_4 and solvent removed to give the crude product as a light brown oil (90%) which was used in the next step without further purification. ^{1}H NMR (400 MHz, $CDCl_3$, TMS, 300 K): δ (ppm) = 6.88 (d, J = 3.64 Hz, 1H), 6.59 (d, J = 3.72 Hz, 1H), 4.63 (broad peak, 1H), 3.35 (t, J = 5.44 Hz, 2H), 2.93 (t, J = 6.60 Hz, 2H), 1.44 (s, 9H); UV-vis (CH_2Cl_2): λ_{max} (ε) = 238 nm (0.735 × 10^4 $M^{-1}cm^{-1}$).

2-(5-Bromothiophen-2-yl)ethylamine (4). To a solution of *tert*-butyl 2-(5-bromothiophene-2-yl)ethylcarbamate (**3**) in 5 mL CH_2Cl_2, 5 mL TFA was added and the reaction mixture stirred at rt under an argon atmosphere for 2 h. The volatiles were then removed under reduced pressure to afford the crude product as a light brown oil (96%) which was used in the next step without further purification. ^{1}H NMR (400 MHz, $CDCl_3$, TMS, 300 K): δ (ppm) = 7.48 (broad s, 2H); 6.90 (d, J = 3.72 Hz, 1H), 6.67 (d, J = 3.64 Hz, 1H), 3.28 (m, 2H), 3.15 (t, J = 7.04 Hz, 2H); UV-vis (CH_2Cl_2): λ_{max} (ε) = 238 nm (0.741 × 10^4 $M^{-1}cm^{-1}$).

***N*-2-(5-Bromothiophen-2-yl)ethyl) 3,4,5-tris(dodecyloxy)-benzamide (6).** Compound **4** (2.94 mmol) was dissolved in 5 mL dry CH_2Cl_2 and cooled in an ice-bath. To this cold solution, 4 mL triethylamine was added slowly. The resulting mixture was ice-cooled for an additional 10 minutes and then a solution of compound **5** in 10 mL dry CH_2Cl_2 was added dropwise. The reaction mixture was stirred at rt for 12 h, diluted with a further 25 mL CH_2Cl_2 and washed successively with water (2 × 50 mL), dil. HCl (2 × 50 mL) and finally with 50 mL brine. The combined organic layer was dried over anhydrous Na_2SO_4 and solvent removed under reduced pressure to give the crude product as a light yellow solid which was purified by column chromatography on silica gel with CH_2Cl_2 as eluent. The product was further purified by dissolving it in 5 mL CH_2Cl_2 and re-precipitating from 200 mL *n*-hexane to yield a white solid (67%). M.p. 76–78 °C; ^{1}H NMR (400 MHz, $CDCl_3$, TMS, 300 K): δ (ppm) = 6.91–6.90 (m, 3H), 6.64 (d, J = 3.64 Hz, 1H), 6.13 (broad s, 1H), 4.00–3.96 (m, 6H), 3.69–3.63 (m, 2H), 3.07 (t, J = 6.44 Hz, 2H), 1.76–1.48 (m, 60H), 0.88 (t, J = 7.00 Hz, 9H); UV-vis (CH_2Cl_2): λ_{max} (ε) = 257 nm (1.381 × 10^4 M^{-1} cm^{-1}), 290 nm (0.296 × 10^4 M^{-1} cm^{-1}); HRMS (ESI): m/z calcd for $C_{49}H_{85}BrNO_4S$ $[M + 2H]^+$: 862.5372; found: 862.5377; elemental analysis: calcd for $C_{49}H_{85}BrNO_4S$: C, 68.18, H, 9.81, N, 1.62, found: C, 67.93, H, 9.70, N, 1.76.

Quaterthiophene gelator T1. *n*-BuLi (360 μL in 2 mL dry THF) was added to a round-bottomed flask, flushed with argon gas for 15 minutes, and then cooled to 0 °C in an ice-bath. To this solution, a solution of 2, 2′-bithiophene in dry THF (68.0 mg in 5 mL) was added dropwise under continuous flow of argon. A white solid precipitate was formed. The reaction mixture was stirred at room temperature for 1 h and then immersed in an ice-bath. To this cold solution, 400 μL Bu_3SnCl was added which caused the precipitate to dissolve immediately. The reaction mixture was stirred at room for further 12 h under an argon atmosphere. The volatiles were removed under reduced pressure to give the crude product as a white pasty mass. The crude product was dissolved in 20 mL dry DMF, compound **9** added and the flask evacuated, purged three times with argon and ~15 mg of the Pd-catalyst added under continuous flow of argon. The reaction mixture was then heated at 80 °C for 8 h under an argon atmosphere. It was observed that an orange precipitate appeared within first 30 min, which almost dissolved as the reaction progressed. After 8 h the reaction was stopped, cooled to rt and poured into 200 mL MeOH. A yellowish orange precipitate was separated by filtration and dried in vacuum to give the crude product as a yellow solid. The crude product was purified by column chromatography on silica gel with 2% methanol in chloroform as eluent to afford the pure product as a yellow solid (78%). M.p. 144 °C. ^{1}H NMR (400 MHz, $CDCl_3$, TMS, 300 K): δ (ppm) = 7.04–7.00 (m, 6H), 6.79 (s, 4H), 6.18 (s, 2H), 6.78–6.75 (m, 2H), 3.99–3.95 (m, 12H), 3.73–3.69 (m, 4H), 3.14–3.10 (m, 4H),1.81–1.25 (m, 120H), 0.89–0.85 (m, 18H); UV-vis (CH_2Cl_2): λ_{max} (ε) = 262 nm (1.76 × 10^4 M^{-1} cm^{-1}), 405 nm (2.90 × 10^4 M^{-1} cm^{-1}); HRMS (ESI): m/z calcd for $C_{106}H_{172}N_2Na_1O_8S_4$ $[M + Na]^+$:1752.1881; found: 1752.1920; MS (MALDI) m/z calcd for $C_{106}H_{172}N_2O_8S_4$ $[M + H]^+$ 1730.206, found: 1730.265; elemental analysis: calcd for $C_{106}H_{172}N_2Na_1O_8S_4$: C, 73.56, H, 10.02, N, 1.62, found: C, 73.32, H, 9.81, N, 1.73.

Acknowledgement

SG thanks the Alexander von Humboldt foundation for a post-doctoral fellowship.

References

1. Lehn, J.-M. *Supramolecular Chemistry - Concepts and Perspectives;* Wiley-VCH: Weinheim, 1995.
2. Hoeben, F. M.; Jonkheijm, P.; Meijer, E. W.; Schenning, A. P. H. J. *Chem. Rev.* **2005,** *105,* 1491–1546. doi:10.1021/cr030070z
3. Fages, F. *Low Molecular Mass Gelators;* Topics in Current Chemistry, Vol. 256; Springer: Berlin, Germany, 2005. doi:10.1007/b105250
4. Bouas-Laurent, H.; Desvergne, J.-P. In *Molecular Gels: Materials with Self-Assembled Fibrilla Networks;* Weiss, G. R.; Terech, P., Eds.; Chapter 12; Springer: Netherlands, 2006.
5. Ajayaghosh, A.; Praveen, V. K. *Acc. Chem. Res.* **2007,** *40,* 644–665. doi:10.1021/ar7000364

6. Prasanthkumar, S.; Saeki, A.; Seki, S.; Ajayaghosh, A. *J. Am. Chem. Soc.* **2010,** *132,* 8866–8867. doi:10.1021/ja103685j
7. Ajayaghosh, A.; Varghese, R.; Mahesh, S.; Praveen, V. K. *Angew. Chem., Int. Ed.* **2006,** *45,* 7729–7732. doi:10.1002/anie.200603238
8. Engelkamp, H.; Middelbeek, S.; Nolte, R. J. M. *Science* **1999,** *284,* 785–790. doi:10.1126/science.284.5415.785
9. Malik, S.; Kawano, S-i.; Fujita, N.; Shinkai, S. *Tetrahedron* **2007,** *63,* 7326–7333. doi:10.1016/j.tet.2007.05.027
10. Sugiyasu, K.; Fujita, N.; Shinkai, S. *Angew. Chem., Int. Ed.* **2004,** *43,* 1229–1233. doi:10.1002/anie.200352458
11. Mukhopadhyay, P.; Iwashita, Y.; Shirakawa, M.; Kawano, S-i.; Fujita, N.; Shinkai, S. *Angew. Chem., Int. Ed.* **2006,** *45,* 1592–1595. doi:10.1002/anie.200503158
12. Li, X.-Q.; Stepanenko, V.; Chen, Z.; Prins, P.; Siebbeles, L. D. A.; Würthner, F. *Chem. Commun.* **2006,** 3871–3873. doi:10.1039/b611422a
13. Del Guerzo, A.; Olive, A. G. L.; Reichwagen, J.; Hopf, H.; Desvergne, J.-P. *J. Am. Chem. Soc.* **2005,** *127,* 17984–17985. doi:10.1021/ja0566228
14. Desvergne, J. P.; Olive, A. G. L.; Sangeetha, N. M.; Reichwagen, J.; Hopf, H.; Del Guerzo, A. *Pure Appl. Chem.* **2006,** *78,* 2333–2339. doi:10.1351/pac200678122333
15. Yagai, S.; Ishii, M.; Karatsu, T.; Kitamura, A. *Angew. Chem., Int. Ed.* **2007,** *46,* 8005–8009. doi:10.1002/anie.200702263
16. Yao, S.; Beginn, U.; Greß, T.; Lysetska, M.; Würthner, F. *J. Am. Chem. Soc.* **2004,** *126,* 8336–8348. doi:10.1021/ja0496367
17. Mishra, A.; Ma, C.-Q.; Bäuerle, P. *Chem. Rev.* **2009,** *109,* 1141–1276. doi:10.1021/cr8004229
18. Schoonbeek, F. S.; Van Esch, J. H.; Wegewijs, B.; Rep, D. B. A.; De Haas, M. P.; Klapwijk, T. M.; Kellogg, R. M.; Feringa, B. L. *Angew. Chem., Int. Ed.* **1999,** *38,* 1393–1397. doi:10.1002/(SICI)1521-3773(19990517)38:10<1393::AID-ANIE1393>3.0.CO;2-H
19. Kawano, S.; Fujita, N.; Shinkai, S. *Chem.–Eur. J.* **2005,** *11,* 4735–4742. doi:10.1002/chem.200500274
20. Ghosh, S.; Li, X.-Q.; Stepanenko, V.; Würthner, F. *Chem.–Eur. J.* **2008,** *14,* 11343–11357. doi:10.1002/chem.200801454
21. Würthner, F.; Bauer, C.; Stepanenko, V.; Yagai, S. *Adv. Mater.* **2008,** *20,* 1695–1698. doi:10.1002/adma.200702935
22. Venkatachalam, T. K.; Sudbeck, E. A.; Uckun, F. M. *Tetrahedron Lett.* **2001,** *42,* 6629–6632. doi:10.1016/s0040-4039(01)01290-4
23. Langeveld-Voss, B. M. W.; Waterval, R. J. M.; Janssen, R. A. J.; Meijer, E. W. *Macromolecules* **1999,** *32,* 227–230. doi:10.1021/ma981349y
24. Nelson, J. *Curr. Opin. Solid State Mater. Sci.* **2002,** *6,* 87–95. doi:10.1016/s1359-0286(02)00006-2
25. Van Duren, J. K. J.; Yang, X.; Loos, J.; Bulle-Lieuwma, C. W. T.; Sieval, A. B.; Hummelen, J. C.; Janssen, R. A. J. *Adv. Funct. Mater.* **2004,** *14,* 425–434. doi:10.1002/adfm.200305049
26. Wicklein, A.; Ghosh, S.; Sommer, M.; Würthner, F.; Thelakkat, M. *ACS Nano* **2009,** *3,* 1107–1114. doi:10.1021/nn9001165
27. Warman, J. M.; de Haas, M. P.; Dicker, G.; Grozema, F. C.; Piris, J.; Debije, M. G. *Chem. Mater.* **2004,** *16,* 4600–4609. doi:10.1021/cm049577w
28. Warman, J. M.; Van de Craats, A. M. *Mol. Cryst. Liq. Cryst.* **2003,** *396,* 41–72. doi:10.1080/15421400390213186
29. Van der Laan, G. P.; Haas, M. P. D.; Buik, A.; De Ruiter, B. *Synth. Met.* **1993,** *55,* 4930–4935. doi:10.1016/0379-6779(93)90841-J
30. Yamamoto, Y.; Fukushima, T.; Suna, Y.; Ishii, N.; Saeki, A.; Seki, S.; Tagawa, S.; Taniguchi, M.; Kawai, T.; Aida, T. *Science* **2006,** *314,* 1761–1764. doi:10.1126/science.1134441
31. Perrin, D. D.; Armarego, W. L. F.; Perrin, D. R. *Purification of Laboratory chemicals,* 2nd ed.; Pergamon: Oxford, 1980.

License and Terms

Beilstein Journal of Organic Chemistry

Gelation or molecular recognition; is the *bis*-(α,β-dihydroxy ester)s motif an omnigelator?

Peter C. Griffiths[*1,§], David W. Knight[1], Ian R. Morgan[1], Amy Ford[1], James Brown[1], Ben Davies[1], Richard K. Heenan[2], Stephen M. King[2], Robert M. Dalgliesh[2], John Tomkinson[2], Stuart Prescott[3], Ralf Schweins[4] and Alison Paul[1]

Full Research Paper

Open Access

Address:
[1]School of Chemistry, Cardiff University, Main Building, Park Place, Cardiff CF10 3AT, U.K., [2]Rutherford Appleton Laboratory, Science and Technology Research Council, Didcot, Oxfordshire OX11 0QX U.K., [3]School of Chemistry, Bristol University, Cantock's Close, Bristol BS8 1TS U.K. and [4]Institut Laue Langevin, 6 rue Jules Horowitz, 38042 Grenoble, Cedex 9, France

Email:
Peter C. Griffiths[*] - griffithspc@cardiff.ac.uk; David W. Knight - knightdw@cardiff.ac.uk

* Corresponding author
§ Phone: +44(0)2920875858

Keywords:
gelation; inelastic neutron spectroscopy; low molar mass organogelator; neutron scattering; neutron spin-echo scattering; self-assembly

Beilstein J. Org. Chem. **2010,** *6,* 1079–1088.
doi:10.3762/bjoc.6.123

Received: 18 July 2010
Accepted: 02 November 2010
Published: 18 November 2010

Guest Editor: J.-P. Desvergne

Abstract

Understanding the gelation of liquids by low molecular weight solutes at low concentrations gives an insight into many molecular recognition phenomena and also offers a simple route to modifying the physical properties of the liquid. *Bis*-(α,β-dihydroxy ester)s are shown here to gel thermoreversibly a wide range of solvents, raising interesting questions as to the mechanism of gelation. At gelator concentrations of 5–50 mg ml^{-1}, gels were successfully formed in acetone, ethanol/water mixtures, toluene, cyclohexane and chloroform (the latter, albeit at a higher gelator concentration). A range of neutron techniques – in particular small-angle neutron scattering (SANS) – have been employed to probe the structure of a selection of these gels. The universality of gelation in a range of solvent types suggests the gelation mechanism is a feature of the *bis*-(α,β-dihydroxy ester) motif, with SANS demonstrating the presence of regular structures in the 30–40 Å range. A correlation between the apparent rodlike character of the structures formed and the polarity of the solvent is evident. Preliminary spin-echo neutron scattering studies (SESANS) indicated the absence of any larger scale structures. Inelastic neutron spectroscopy (INS) studies demonstrated that the solvent is largely unaffected by gelation, but does reveal insights into the thermal history of the samples. Further neutron studies of this kind (particularly SESANS and INS) are warranted, and it is hoped that this work will stimulate others to pursue this line of research.

Introduction

A detailed, molecular level understanding of the fundamental aspects of the spontaneous self-assembly and network formation of low molecular mass organogelators (LMOGS) is still elusive, although much research attempting to quantify the fundamental aspects of this fascinating phenomenon is underway [1-5]. A wide range of structurally diverse gelators have been identified, and in general, whilst a particular gelator functions for a small set of solvents, its gelling ability is not universal [3-11]. This lack of generality doubtless arises as there is generally no single unifying mechanism for gelation, which invariably involves a range of physical (non-covalent) interactions, such as hydrogen bonding, solvophobic effects and π–π interactions [11-34].

Our previous work has focused on the thermoreversible gelation of partially fluorinated liquids by a homologous series of chiral, non-racemic *bis*-(α,β-dihydroxy ester)s [35], in which the gelation character was found to depend on both solvent composition and the molecular structure of the gelator. The enthalpy of melting ΔH_m for a series of gelators was found to be positive, indicating an endothermic melting process, associated with the increase in entropy. Interestingly, the enthalpies were insensitive to both the solvent composition and the gelator chain length (G_n, where n corresponds to the number of CH_2-groups in the interheadgroup spacer less 2), suggesting that gelation is a feature dominated by the common end-group structural motif. A gelation mechanism based on hydrogen bonding of the end-group was confirmed by IR and circular dichroism (CD) spectroscopic characterisation. The specific stereochemistry of the gelator end-groups is a crucial factor, providing an obvious analogy to molecular recognition phenomena.

Small-angle neutron scattering provided a detailed insight into the gelator self-assembled structures, with data being best interpreted with a Kholodenko–Dirac worm model, comprising a flexible assembly of rodlike structures, in which the balance between flexibility and rigidity is defined by the parameter m. For the fluorinated systems, $m = 4$, indicating a rather rigid structure, with a Gaussian cross-section of 25–40 Å depending on gelator concentration and structure. The rodlike segments were typically hundreds of Å in length, suggesting a stacked geometry that was later confirmed with CD spectroscopy. With an increase in temperature, these structures simply "melt", i.e., the size of the structure is largely invariant until the gel temperature is reached. Interestingly, whereas the size and shape of the scatterers was not found to vary significantly with gelator concentration, the scattering intensity did increase with gelator concentration indicating that the number of scatterers increases, leading to the stiffer gels implied by the concomitant increase in $T_{gel–sol}$ observed.

These gelators form gels in a wide range of solvents, a rather serendipitous and unusual discovery. It is that observation that is elaborated here, and in particular, our focus is to probe the structures present in these gels. To this end, small-angle neutron scattering (SANS) has been used, supplemented in a small number of cases, with inelastic neutron spectroscopy (INS), spin-echo neutron scattering (SESANS), and pulsed-gradient spin-echo (PGSE-)NMR measurements.

Results and Discussion

A series of *bis*-(α,β-dihydroxy ester)s have been found to gel a wide range of solvents at a solvent-specific concentration ($C_{gelator}$), typically a few mg per ml, e.g., for G_6 3.8 mg ml^{-1} in toluene, 7.1 mg ml^{-1} in dichloromethane, 4.8 mg ml^{-1} cyclohexane, 4.1 mg ml^{-1} in chloroform/hexane (90% hexane) and 1.8 mg ml^{-1} in water-rich (75%) ethanol/water mixtures. The gels formed from water-rich systems and cyclohexane showed varying degrees of opacity, depending on the gelator concentration, but all other systems were transparent. Of the common solvents tested, the only non-gelling system was with acetonitrile. As is evident from this list, these liquids encompass highly polar liquids, nonpolar liquids, and those that are strongly hydrophobic, and at such low gelator concentrations (<10 mg ml^{-1}). It is surprising, therefore, that a single gelator can gel such a wide range of liquids. With the exception of the water/ethanol system, there is a clear correlation of the order of the minimum gelator concentration required (water/ethanol < cyclohexane ≈ toluene < dichloromethane ≤ acetonitrile) with the dielectric constants (hexane ≈ cyclohexane ≈ toluene < dichloromethane < ethanol < acetonitrile ≤ water), suggesting that the gelation mechanism is driven by the polarity (and therefore, the strength of the hydrogen bonding) sensed by the gelator headgroups.

Figure 1 presents a thermodynamic analysis of gelation for a selection of the gels examined here, focusing specifically on the toluene and ethanol/water gels for gelators G_6 and G_8 (see Scheme 1 in the Experimental section). In all cases, the gelation temperature increases with concentration, with the toluene gels melting at higher temperatures for the same concentration of gelator, a trend that is more pronounced for the G_6 gelator. The higher melting temperature of the toluene gels, typically 20 °C, indicates that the gel is considerably more stable. The slopes of the data in this Schröder–van Laar representation correspond to the enthalpy of melting, and these were found to be 70 (±5) kJ mol^{-1} and 55 (±5) kJ mol^{-1} for the toluene and ethanol/water cases, respectively, and consistent with multiple hydrogen bonds between the headgroups, as found previously in the case of the fluorinated solvents [35]. For the cyclohexane systems, only a fragile gel is observed (even after several

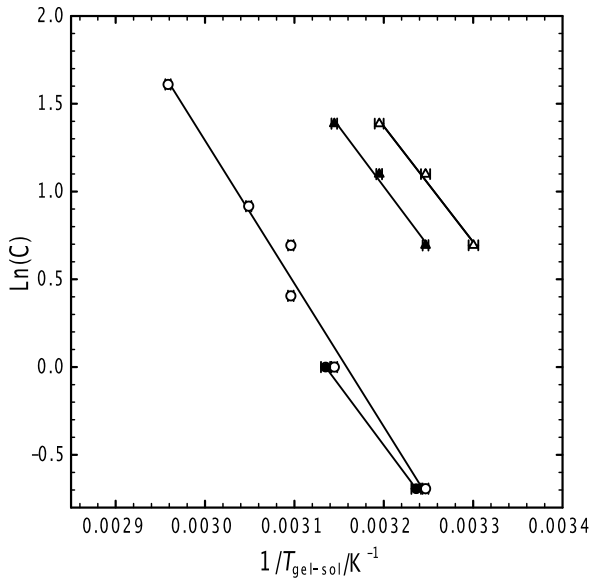

Figure 1: Schröder–van Laar analysis for the melting of toluene (open symbols) and ethanol/water (filled symbols) gels formed from G_6 (circles) and G_8 gelators (triangles).

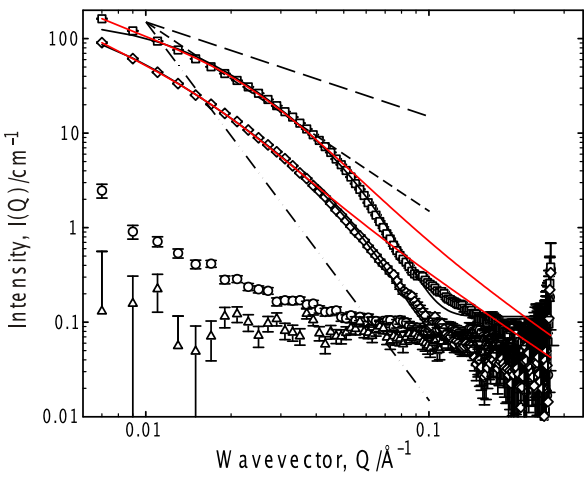

Figure 2: SANS from 50 mg ml^{-1} G_6 in a range of solvents, 25 °C; *d*-acetone (circles), *d*-chloroform (triangles), 50% *d*-ethanol/D_2O (squares) and *d*-toluene (diamonds). Fits to the Kholodenko–Dirac worm model are superimposed on the data as solid black lines, whereas the solid red lines are best attempts to describe the data by a two correlation length model. Limiting behaviors of Q^{-1}, Q^{-2} and Q^{-4} are also shown.

heat–cool cycles), over wide ranges of gelator concentration ($5 < C_{gelator} < 50$ mg ml^{-1}) and temperature ($25 < T < 55$ °C), this representing the poorest performance of the gelator.

Representative SANS data are presented in Figures 2–6 from which the morphology of the structures can be extracted in terms of the nature of the solvent (Figure 2), the gelator concentration (Figure 3) and the gelator chain length (Figure 4). These studies have focused on toluene and cyclohexane gels, in which a "contrast variation" approach has been adopted to probe the internal structure of the gels (Figure 5 and Figure 6). The chloroform sample, at this gelator concentration, was not gelled (Figure 2) and no scattering is evident. Thus, we may conclude that there is no aggregation in these solutions that leads to structures large enough to scatter neutrons, i.e., the gelator molecularly dissolves.

The most common macroscopic structural arrangement formed by (chiral) gelators are fibrils formed from a stacking of the gelator molecules [15,16,19,22,27,28,34,36-40], which exhibit "signature" intensity vs. wave–vector (Q) relationships, viz Q^{-1} (rod) at low Q becoming Q^{-4} (Porod scattering from smooth surfaces, characteristic of a well-defined aggregate) at higher Q in conjunction with local maxima or oscillations usually at higher Q arising from Bragg reflections or sharp interfaces, or a switch from a Q^{-1} to a Q^{-2} dependencies on a double logarithmic I(Q) versus Q plot [13,41-49]. With the exception of the acetone sample, which shows very weak scattering, all the

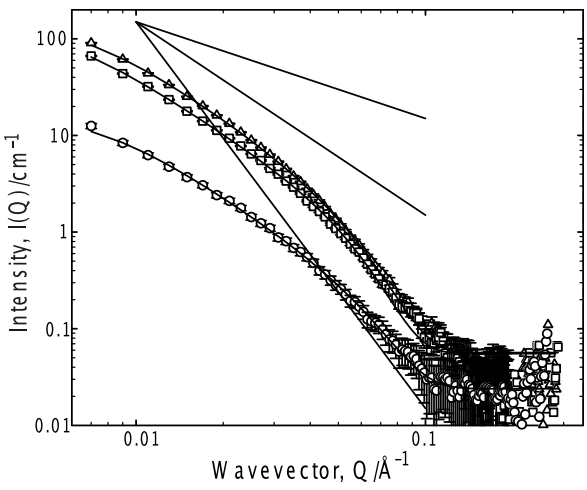

Figure 3: SANS from G_6 25 °C in *d*-toluene as a function of G_6 concentration; 5 mg ml^{-1} (circles), 10 mg ml^{-1} (squares) and 50 mg ml^{-1} (triangles). Fits to the Kholodenko–Dirac worm model are superimposed on the data. Limiting behaviors of Q^{-1}, Q^{-2} and Q^{-4} are also shown.

systems show a smooth transition from a simple Q^{-1} dependence indicative of rodlike structures, into the Q^{-4} expected for well-defined objects. This latter dependence (Q^{-4}) is most evident in 75% D_2O/*d*-ethanol, implying the structure in this case is more particle-like, consistent with the fragility (and appearance) of this gel. Clearly, existing frameworks for analyzing such data are not appropriate here.

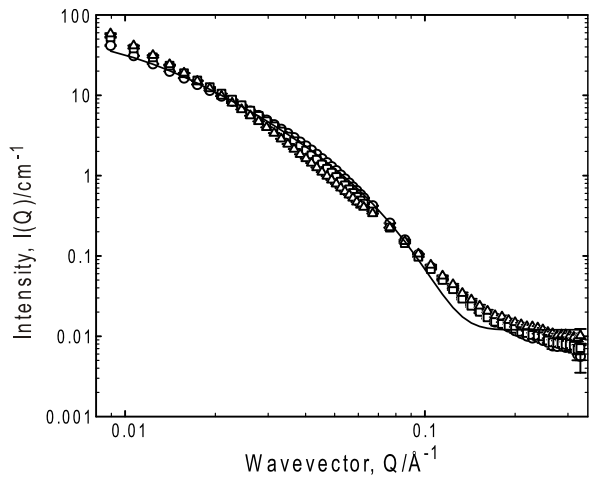

Figure 4: SANS from a series of homologous gelators, G_5 (circles), G_6 (squares) and G_8 (triangles) in *d*-toluene, all at 50 mg ml^{-1} and 25 °C. Selected fits to the Kholodenko–Dirac worm model are superimposed on the data.

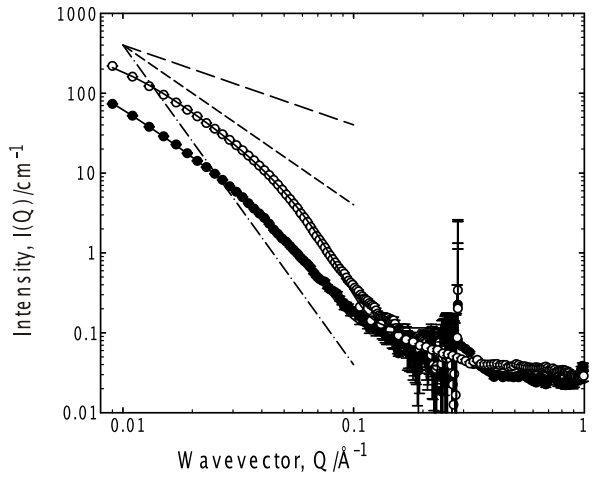

Figure 5: SANS from 50 mg ml^{-1} G_6 in *d*-toluene, 25 °C; hydrogenous gelator (empty symbols) and partially deuterated gelator (filled symbols). Fits to the Kholodenko–Dirac worm model are superimposed on the data. Limiting behaviors of Q^{-1}, Q^{-2} and Q^{-4} are also shown.

In order to identify an appropriate theoretical framework with which to analyze these data, it is important to probe for any interaction between the structures – to ascertain whether the data may be analyzed merely in terms of their morphology or if there is an additional contribution from inter aggregate correlations. This is most easily assessed by recording the scattering from a series of gels as a function of the gelator concentration. The concentration dependence of the scattering from G_6 was therefore studied over a wide range of concentration, and representative data is presented for the toluene system in

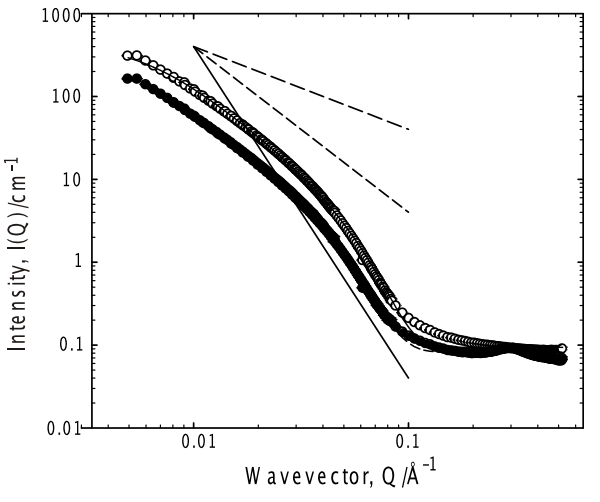

Figure 6: SANS from 35 mg ml^{-1} G_6 in 75% *d*-ethanol/25% D_2O, 37 °C; hydrogenous gelator (empty symbols) and partially deuterated gelator (filled symbols). Fits to the Kholodenko–Dirac worm model are superimposed on the data. Limiting behaviors of Q^{-1}, Q^{-2} and Q^{-4} are also shown.

Figure 3. The toluene system was chosen as there is appreciable scattering in this system, even just above the minimum gelation concentration.

From this system presentation, it is obvious that the functional form of the scattering does not follow a simple Q dependence at any concentration of gelator and that this complex functional form is invariant with concentration. This observation therefore, allows the data analysis to ignore incorporation of a term describing an interaction between the aggregates. Further, one may conclude that the changes in scattering arise from an increase in the number of structures, with perhaps subtle changes in their size or morphology (at least over this range), i.e., gelation is akin to the simple self-assembly process demonstrated by surfactants, and is a consequence of a cooperative process. Given the morphology of the scatterers, this is most likely to arise due to growth along the long axis (elongation) of the structures.

An analysis protocol has therefore been adopted that reflects the smooth transition in Q dependence observed in these systems, viz a flexible wormlike structure, parameterized by the Kholodenko–Dirac model. This model is based on a Gaussian coil comprising multiple (m) cylindrical elements of statistical length (ℓ) and radius (R_{Ax}). The parameter m can be considered a measure of the balance of the Gaussian to rigid rod character – when m is large, and both ℓ and R_{Ax} small, the limiting behavior of this model is effectively that of a Gaussian Debye coil, whereas when m is small and ℓ large, the limiting behavior is that of a rigid rod.

Representative fit parameters are given in Table 1, and the model predictions overlaid on the experimental scattering in all the figures. The fitting is most sensitive to the radial cross-section of the structure (R_{Ax}), invariably with a radius of 25–35 Å. Converting this Guinier radius to an equivalent cylindrical radius (multiply by √2), and if one considers a disc of thickness 1 Å and the volume of a gelator molecule to be 600 Å^3, that disc contains on average 6 ± 1 molecules, consistent with the proposed number of hydrogen bonds between the end-groups of the gelator molecules [35]. Further, the universality of the radius would seem to be a feature of the gelator structure rather than the solvent, i.e., self-association driven by a molecular recognition process, as opposed to a classical aggregation such as that observed in surfactants. There is a negligible variation in the scattering behavior with increasing gelator length, as might be expected were a bilayer structure present. In all cases, the fitting procedure was tested to ensure that the best fit observed was a global minimum, especially since there is some coupling of the parameters m and ℓ.

The internal morphology of the structures may be elaborated by considering a partially deuterated gelator, in which the end-groups no longer contribute to the scattering, an experimental approach known as "contrast variation". For both the toluene and 25% ethanol/water systems, there is no significant change in the form of the scattering (merely the intensity) when the partially (headgroup) deuterated gelator is used, although the relative change in intensity, typically a factor of 3 ± 0.5, is somewhat smaller than would be expected given a homogeneous structure. This indicates that the headgroups and the alkyl sections of the gelator exhibit a very similar morphology, but there is some spatial separation within the structure between the headgroups and the alkyl chain. Further, the deuterated gelator data show a weak peak at Q ≈ 0.3 Å^{-1}, corresponding to a dimension of approx. 20 Å. Given that the length of the alkyl spacer is approximately 10 Å, the simplest interpretation of this distance is the characteristic length associated with the correlation between the (deuterated) end-groups of two end-on gelator molecules. If this arrangement were heavily populated in the aggregate, one would also expect to see a feature on the SANS around a Q commensurate with the 10 Å distance, i.e., Q = 0.6 Å^{-1}, but the data are not of sufficient quality to state whether the features at this Q are significant or not. It should be noted that a core-shell morphology was also tested, but the peak could only be reproduced by assuming unphysical parameters – a 10 Å in length alkyl spacer and a 20 Å headgroup region – whilst the fit at low Q was poor.

If one considers the trends in the Gaussian coil-rigid rod character (m) and the length (ℓ) of the rods comprising the building blocks of the gelled structure, i.e., for m; fluorinated solvent ≈ acetone ≈ ethanol/water < chloroform < toluene, whereas for ℓ; chloroform ≈ fluorinated solvent ≈ toluene << ethanol/water ≈ acetone, it is clear that more Gaussian coil- or particlelike structures are evident when the hydrogen bonding is weaker.

The fitted parameters, combined with the absolute intensities, may be used to further elaborate the structure of the gelator assemblies. Taking the parameters listed in Table 1 and the absolute intensity, the number of worms per unit volume, N, may be calculated, along with the number of molecules per worm, and ultimately the number of gelator molecules per worm per unit length. For all the data presented here, this characteristic number is surprisingly invariant across the systems, typically 8 ± 2 molecules, not inconsistent with the estimate of the same parameter derived from the radius of the rodlike element (6 ± 1).

Table 1: Parameters describing the fit to the SANS data using the Kholodenko–Dirac worm model.

[Gelator]/wt %	Solvent	Number of links m	Length of link, l Å	Radial cross-section R_{Ax}/Å
[G_6] = 0.5	toluene	30 (±2)	90 (±5)	28 (±1)
[G_6] = 1.0	toluene	30 (±3)	110 (±8)	30 (±1)
[G_6] = 5.0	toluene	55 (±5)	100 (±10)	30 (±2)
[G_6] = 5.0	acetone	Does not fit to Kholodenko–Dirac worm model, simple rod Q dependence		
[G_6] = 5.0	50% ethanol/water	4 (±0.2)	200 (±20)	33 (±2)
[G_6] = 10.0	chloroform	13 (±2)	100 (±10)	25 (±1)
[G_6] = 10.0	acetone	4 (±1)	220 (±8)	30 (±2)
[G_6] = 10.0	ethanol	55 (±10)	85 (±10)	20 (±3)
d-[G_6] = 5.0	toluene	55 (±10)	100 (±10)	30 (±3)
h-[G_6] = 5.0	toluene	60 (±5)	80 (±10)	25 (±3)
d-[G_6] = 5.0	25% ethanol/water	480 (±3)	32 (±2)	27 (±2)
h-[G_6] = 5.0	25% ethanol/water	460 (±3)	30 (±2)	26 (±2)

A variation of the scattering experiment, SESANS, has been used to probe the existence of any structural order on a length scale greater than a few tens of nanometers up to several microns, Figure 7, for the toluene gels. In this experiment, polarized neutrons are used as a probe of long-range order. Polarized and nonpolarized neutrons probe structure differently, such that the ratio of their intensities is a measure of any structure present, over a distance scale defined by the evolution period used in the experiment. For the gels studied here, this ratio was constant at a value of unity, indicating a complete lack of higher order structure present in these systems, and one may conclude that there is no long-range ordering or association of the fibrils, i.e., they are randomly dispersed over these characteristic length scales.

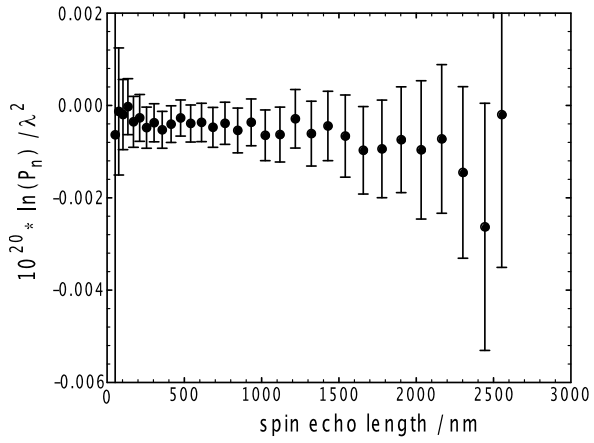

Figure 7: SESANS data for 50 mg ml^{-1} G_6 in deuterated toluene, 25 °C.

The characteristics of the solvent in these gels have been examined by inelastic neutron spectroscopy (INS), Figure 8 and Figure 9, for the toluene and cyclohexane gels, respectively. For the toluene gels, the observed gel spectra are dominated by the toluene spectrum (Figure 8). There are very subtle differences between the *h*- and *d*-gelator spectra, these being most obvious in the OH stretching region around 3000 cm^{-1} and in the low frequency region below 150 cm^{-1}. However, the data in these regions are too broad and statistically too poor to extract any detailed interpretation, but it is comforting that the spectra are

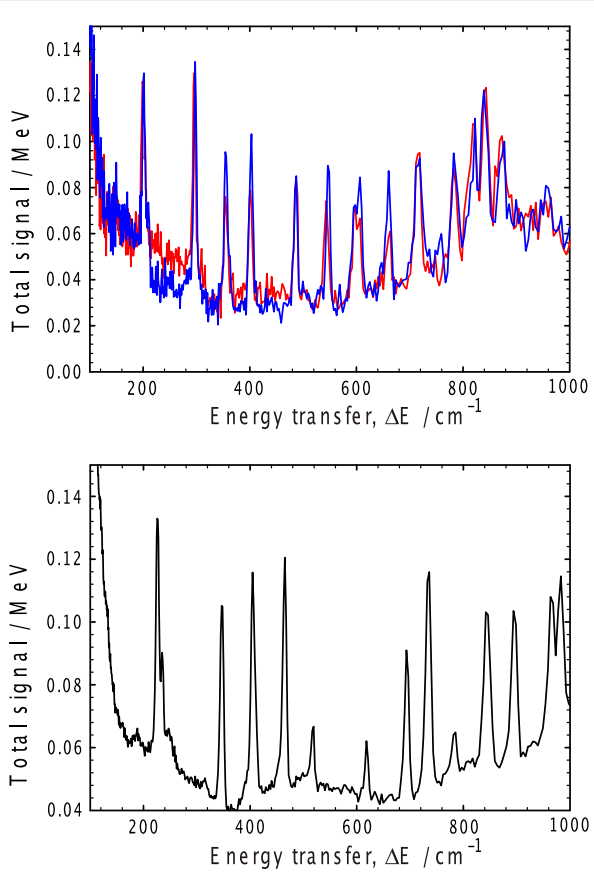

Figure 8: Inelastic neutron spectroscopy from toluene gels (upper Figure): red deuterated toluene/hydrogenous gelator, blue deuterated toluene/deuterated gelator, and the pure solvent (lower trace).

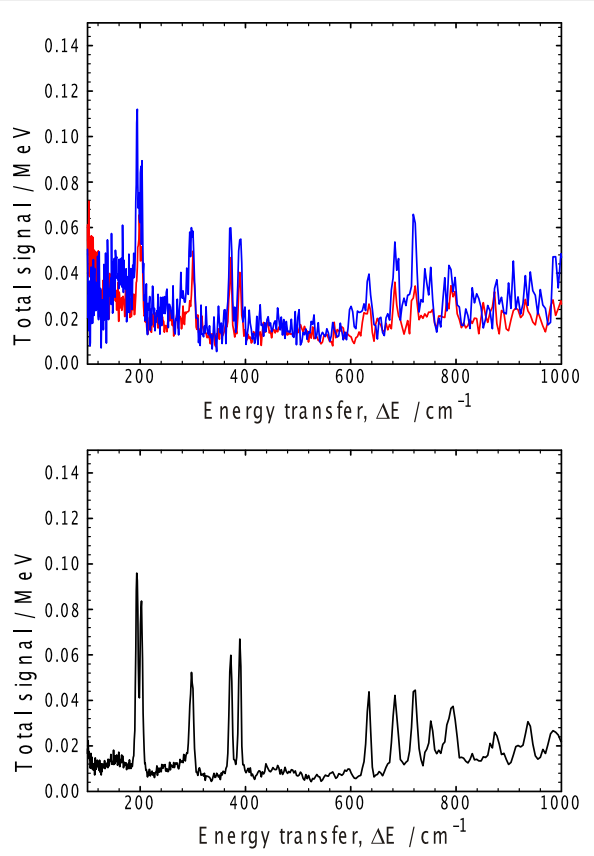

Figure 9: Inelastic neutron spectroscopy from cyclohexane gels (upper Figure): red deuterated cyclohexane/hydrogenous gelator, blue deuterated cyclohexane/deuterated gelator, and the pure solvent (lower Figure).

different in those regions of the spectrum where the peaks due to those functional groups that have been altered by deuteration would be expected.

The nine sharp features between 150 and 800 cm^{-1} arising from the *d*-toluene in the gelled samples are of considerably more interest, indicating that the average environment of the toluene methyl groups are significantly different. This difference may have a number of origins, one of which may be as a result of deuteration, but it is much more likely due to unavoidable thermal histories of the two samples (cooling rates, time elapsed since the initial freezing). Further, it is not possible to normalize the spectra such that all of these nine bands overlap completely with the same intensity in both spectra, again a consequence of differences in the samples rather than for example, spectrometer performance or gelation. Thus, it is probable that the differences in the spectra observed for the *d*-toluene gels arise as a result of two populations of coexisting solvent phases – the amorphous phase that has a structural arrangement of the molecules similar to that in the unstable β-toluene phase [50] and the more stable α-toluene phase – since the average barrier to methyl rotation in the amorphous phase is higher than the barrier heights in either the α- or β-phases [51]. Hence, when comparing two samples such as we do here, if the average barrier to methyl rotation is less in one sample than the second, the methyl group's Debye–Waller factors that control that portion of the intensities in the observed bands arising from the methyl groups will differ, thereby accounting for the observed variations in the intensity of those bands involving most methyl group vibrations. A similar conclusion – that the solvent does not participate in the gelation mechanism – may be drawn from the cyclohexane data; again, the two spectra are very similar, the key differences being in the bands relating to the isopropyl dynamics.

Finally, the self-diffusion coefficients of the solvents (toluene, cyclohexane, water/ethanol) in these gels (at 25 °C) have been measured by PGSE-NMR (data not presented), and compared with the self-diffusion coefficients in the appropriate bulk solutions. A very slight retardation in the diffusion of the solvent is observed, consistent with the obstruction effect introduced by the assemblies of the gelator molecules, as the solvent molecules must diffuse around the structures, thereby increasing their diffusion path length.

Conclusion

A diverse range of liquids has been successfully gelled with low concentrations of a low molecular weight gelator incorporating *bis*-(α,β-dihydroxy ester) end-group motifs. Gelation is caused by association of gelator molecules into stacks, due to intermolecular hydrogen bonding between the end-groups. The critical dimensions of these structures have been determined by analysis of neutron scattering data (SANS and SESANS), and are dependent on the strength of the intermolecular hydrogen bonding interaction. The strongest gels are formed in solvents where stronger intermolecular hydrogen bonds lead to longer segments and less flexible structures, whereas shorter, more flexible segments lead to a particlelike gelator structure which can only form weak gels. PGSE-NMR confirms retardation of solvent diffusion due to an obstruction effect. Preliminary INS data exhibit subtle differences providing an insight into the thermal history of the sample, but not the gelation mechanism.

Experimental

Materials

All solvents were of spectroscopic grade and used as received.

Synthesis of gelators

The omnigelator **4** was prepared as previously described [52] by sequential Grubbs double cross metathesis [53] between (*Z*)-cyclodecene (**1**) and two equivalents of isopropyl acrylate **2**, which routinely delivered 80–85% yields of the bisenoate **3**, exclusively as the (*E,E*)-isomer shown (Scheme 1), followed by an AD-mix double bishydroxylation with $(DHQD)_2PHAL$ as the chiral ligand [54].

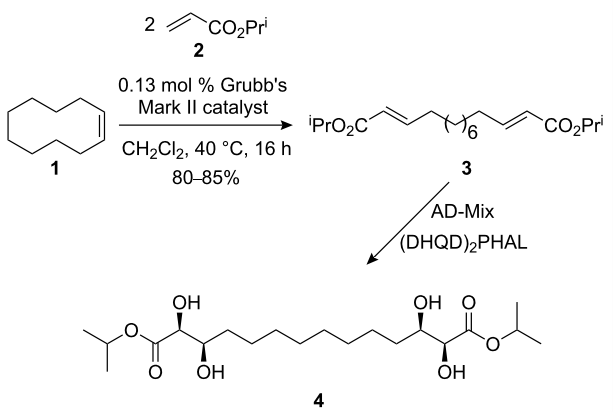

Scheme 1: Synthesis of hydrogenous gelators.

The deuterated analogue **6**, Scheme 2, was prepared by using d_7-isopropyl acrylate (**5**) in the initial cross metathesis step. The deuterated ester **5** was prepared from acryloyl chloride and d_7-isopropanol (Et_3N, CH_2Cl_2, 0→20 °C, 2 h); yields were essentially identical to the nondeuterated example, given that the deuterated acrylate **5** was carefully purified and was completely free of triethylamine, which is a very effective ligand and quench for the Grubbs Mark II metathesis catalyst. This was achieved by extensive washing during work-up (water, sat. aq NH_4Cl, 1 M HCl, sat. aq K_2CO_3, water and brine) followed by distillation, bp ~40 °C at 17 mm Hg.

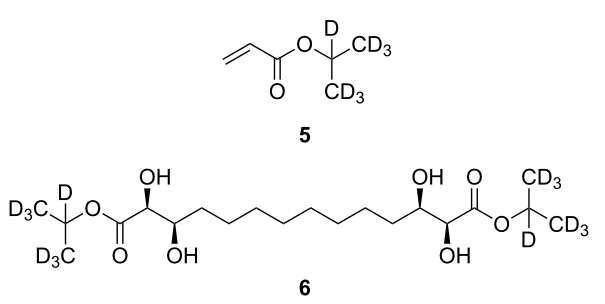

Scheme 2: Structure of partially deuterated gelators.

Gel formation

On a 0.5 g scale, the gelator and solvent were weighed directly into a screw top vial. A simple heat–cool cycle was necessary for several of these gels to ensure homogeneity, although several heterogeneous gels did form spontaneously at room temperature.

Determination of gelation temperature $T_{gel–sol}$

Glass vials containing the samples were equilibrated in a temperature-controlled water bath and the temperature increased from 15 °C initially in 2 °C steps with a 30 min equilibration time at each temperature. On approaching the gelation temperature, smaller increments (0.5 °C) were adopted. The simplest measure of gelation – that the gel be stable to inversion [3] – was used to quantify the gel–sol behavior.

Small-Angle Neutron Scattering (SANS)

Small-angle neutron scattering (SANS) measurements were performed on either (a) the fixed-geometry, time-of-flight LOQ diffractometer (ISIS Spallation Neutron Source, Oxfordshire, UK) or (b) on the D11 diffractometer at the ILL, Grenoble. On LOQ, a white beam of radiation with neutron wavelengths spanning 2.2 to 10 Å were used to access a Q [$Q = 4\pi\sin(\theta/2)/\lambda$] range of 0.008 to 0.25 $Å^{-1}$ (25 Hz), with a fixed sample-detector distance of 4.1 m. On D11, a neutron wavelength of 6 Å was employed to access a Q-range of approximately 0.005 to 0.50 $Å^{-1}$, requiring three separate instrument configurations (sample-detector distances and collimation).

On both instruments, the samples were contained in 2 mm path length, UV-spectrophotometer grade, quartz cuvettes (Hellma) and mounted in aluminium holders on top of an enclosed, computer-controlled, sample chamber. Sample volumes were approximately 0.4 cm^3. Temperature control was achieved through the use of a thermostatted circulating bath pumping fluid through the base of the sample chamber. Under these conditions a temperature stability of better than ±0.5 °C can be achieved. Experimental measuring times were approximately 40 min.

All scattering data were (a) normalized for the sample transmission, (b) background corrected using an empty quartz cell or one filled with the appropriate solvent (this also removes the inherent instrumental background arising from vacuum windows, etc) and (c) corrected for the linearity and efficiency of the detector response using the instrument-specific software package. The data were put onto an absolute scale by reference to the scattering from a partially deuterated polystyrene blend (LOQ) or 1 mm H_2O.

The Kholodenko–Dirac wormlike chain model [9] has been used to analyse the SANS data. This approach is derived from a Gaussian coil model, where long thin rods are made of a succession of m cylindrical elements of statistical length ℓ and radius R_{Ax}. The contour length of the chain, L, is equal to the product $m{\cdot}\ell$. The scattering intensity generated from Kholodenko–Dirac wormlike chains is proportional to two terms:

$$I(Q) = P_{Worm}(Q) * P_{Axial}(Q) + B_{inc} \quad (1)$$

where B_{inc} is the incoherent background. The Kholodenko–Dirac model therefore smoothly interpolates between the Gaussian coil and rigid rod predictions and the number of segments (m) forming the chain, and hence gives an indication regarding the flexibility of the chain. Smaller values of m correspond to stiffer chains. When m tends towards infinity, the scatterer adopts a flexible Gaussian random coil whereas when tending towards unity, a rigid rod is obtained.

For long thin rods

$$P_{Worm}(Q) = \frac{2}{3n}\int_0^{3n}\left(1-\frac{y}{3n}\right)f(y)dy \quad (2)$$

where for

$$Q \le \frac{3}{l},$$

$$f(y) = \frac{\sinh(Ey)}{E\sinh(y)}$$

with

$$E = \left[1-\left(\frac{Ql}{3}\right)^2\right]^{1/2}$$

whereas for

$$Q > \frac{3}{l},$$

$$f(y) = \frac{\sin(Fy)}{F\sinh(y)}$$

with

$$F = \left[\left(\frac{Ql}{3}\right)^2 - 1\right]^{1/2}$$

given that m is the number of chain elements, l the statistical chain element length (giving the total chain length L = $m \cdot l$).

P_{Axial} (Q) was adopted with a radial Guinier form, such as:

$$P_{Axial}(Q) = N(\rho_1 - \rho_3)^2 (AL)^2 \exp\left(-\frac{1}{2}Q^2 R_{Ax}^2\right) \quad (3)$$

with ρ_1 and ρ_3 the scattering length densities for the worm and solvent, N worms per unit volume, A the cross sectional area and R_{Ax} the cross sectional radius of the chain, assuming a Gaussian scattering density.

Inelastic Neutron Scattering (INS)

The samples, about 0.5 g each, were held in air-tight sample holders and rapidly cooled to 20 K in the TOSCA neutron spectrometer, ISIS Facility, the Rutherford Appleton Laboratory, Harwell Science and Innovation Campus, OX11 0QX, UK. TOSCA is a pulsed neutron, indirect geometry, low band-pass spectrometer with good spectral resolution ($\Delta E_t/E_t \approx$ 1–2%), further details are given elsewhere [55]. Data were collected for about 8 h and transformed into the conventional scattering law, S(Q,ω) (arbitrary units), vs. energy transfer, E_t (cm^{-1}), using standard programs.

Acknowledgements

EPSRC (EP/C013220/1), Cardiff and Bristol Universities are acknowledged for financial support. STFC is gratefully acknowledged for consumables support and access to neutron facilities.

References

1. Gronwald, O.; Snip, E.; Shinkai, S. *Curr. Opin. Colloid Interface Sci.* **2002,** *7,* 148–156. doi:10.1016/S1359-0294(02)00016-X
2. Abdallah, D. J.; Weiss, R. G. *J. Braz. Chem. Soc.* **2000,** *11,* 209–218.
3. Terech, P.; Weiss, R. G. *Chem. Rev.* **1997,** *97,* 3133–3159. doi:10.1021/cr9700282
4. Sangeetha, N. M.; Maitra, U. *Chem. Soc. Rev.* **2005,** *34,* 821–836. doi:10.1039/b417081b
5. Smith, D. K., Ed. *Tetrahedron Symposia-in-Print on Low molecular Weight Organic Gelators*, July 30, 2007; Elsevier, 2007.
6. Escuder, B.; Miravet, J. F. *Langmuir* **2006,** *22,* 7793–7797. doi:10.1021/la060499w
7. Luboradzki, R.; Gronwald, O.; Ikeda, M.; Shinkai, S.; Reinhoudt, D. N. *Tetrahedron* **2000,** *56,* 9595–9599. doi:10.1016/S0040-4020(00)00915-7
8. Mieden-Gundert, G.; Klein, L.; Fischer, M.; Vogtle, F.; Heuze, K.; Pozzo, J. L.; Vallier, M.; Fages, F. *Angew. Chem., Int. Ed.* **2001,** *40,* 3164–3166. doi:10.1002/1521-3773(20010903)40:17<3164::AID-ANIE3164>3.0.CO;2-B
9. Weiss, R. G.; Terech, P. *Molecular Gels – Materials with Self-Assembled Fibrillar Networks;* Springer: Dordrecht, The Netherlands, 2006.
10. Yoza, K.; Ono, Y.; Yoshihara, K.; Akao, T.; Shinmori, H.; Takeuchi, M.; Shinkai, S.; Reinhoudt, D. N. *Chem. Commun.* **1998,** 907–908. doi:10.1039/a800825f
11. Yoza, K.; Amanokura, N.; Ono, Y.; Akao, T.; Shinmori, H.; Takeuchi, M.; Shinkai, S.; Reinhoudt, D. N. *Chem.–Eur. J.* **1999,** *5,* 2722–2729. doi:10.1002/(SICI)1521-3765(19990903)5:9<2722::AID-CHEM2722>3.0.CO;2-N
12. Burkhardt, M.; Kinzel, S.; Gradzielski, M. *J. Colloid Interface Sci.* **2008,** *331,* 514–521. doi:10.1016/j.jcis.2008.11.078
13. George, M.; Snyder, S. L.; Terech, P.; Glinka, C. J.; Weiss, R. G. *J. Am. Chem. Soc.* **2003,** *125,* 10275–10283. doi:10.1021/ja0362407
14. George, M.; Snyder, S. L.; Terech, P.; Weiss, R. G. *Langmuir* **2005,** *21,* 9970–9977. doi:10.1021/la050371z
15. Bao, C. Y.; Jin, M.; Lu, R.; Song, Z. G.; Yang, X. C.; Song, D. P.; Xu, T. H.; Liu, G. F.; Zhao, Y. Y. *Tetrahedron* **2007,** *63,* 7443–7448. doi:10.1016/j.tet.2007.03.125
16. Bag, B. G.; Maity, G. C.; Pramanik, S. R. *Supramol. Chem.* **2005,** *17,* 383–385. doi:10.1080/10610270500114640
17. Brizard, A.; Oda, R.; Huc, I. *Top. Curr. Chem.* **2005,** *256,* 167–218.
18. Snijder, C. S.; deJong, J. C.; Meetsma, A.; van Bolhuis, F.; Feringa, B. L. *Chem.–Eur. J.* **1995,** *1,* 594–597. doi:10.1002/chem.19950010905
19. Haino, T.; Tanaka, M.; Fukazawa, Y. *Chem. Commun.* **2008,** 468–470. doi:10.1039/B715871H
20. Babu, P.; Sangeetha, N. M.; Maitra, U. *Macromol. Symp.* **2006,** *241,* 60–67. doi:10.1002/masy.200650909
21. Jung, J. H.; John, G.; Masuda, M.; Yoshida, K.; Shinkai, S.; Shimizu, T. *Langmuir* **2001,** *17,* 7229–7232. doi:10.1021/la0109516
22. Hanabusa, K.; Maesaka, Y.; Kimura, M.; Shirai, H. *Tetrahedron Lett.* **1999,** *40,* 2385–2388. doi:10.1016/S0040-4039(99)00195-1
23. Mukkamala, R.; Weiss, R. G. *Langmuir* **1996,** *12,* 1474–1482. doi:10.1021/la950666k
24. Watanabe, Y.; Miyasou, T.; Hayashi, M. *Org. Lett.* **2004,** *6,* 1547–1550. doi:10.1021/ol049737+
25. Hafkamp, R. J. H.; Feiters, M. C.; Nolte, R. J. M. *J. Org. Chem.* **1999,** *64,* 412–426. doi:10.1021/jo981158t
26. Sagawa, T.; Chowdhury, S.; Takafuji, M.; Ihara, H. *Macromol. Symp.* **2006,** *237,* 28–38. doi:10.1002/masy.200650504

27. Sumiyoshi, T.; Nishimura, K.; Nakano, M.; Handa, T.; Miwa, Y.; Tomioka, K. *J. Am. Chem. Soc.* **2003,** *125,* 12137–12142. doi:10.1021/ja035085t
28. Becerril, J.; Burguete, M. I.; Escuder, B.; Galindo, F.; Gavara, R.; Miravet, J. F.; Luis, S. V.; Peris, G. *Chem.–Eur. J.* **2004,** *10,* 3879–3890. doi:10.1002/chem.200400031
29. Doi, M.; Asano, A.; Yoshida, H.; Inouguchi, M.; Iwanaga, K.; Sasaki, M.; Katsuya, Y.; Taniguchi, T.; Yamamoto, D. *J. Pept. Res.* **2005,** *66,* 181–189. doi:10.1111/j.1399-3011.2005.00286.x
30. Caplar, V.; Zinic, M.; Pozzo, J. L.; Fages, F.; Mieden-Gundert, G.; Vogtle, F. *Eur. J. Org. Chem.* **2004,** *19,* 4048–4059. doi:10.1002/ejoc.200400105
31. Makarevic, J.; Jokic, M.; Raza, Z.; Stefanic, Z.; Kojic-Prodic, B.; Zinic, M. *Chem.–Eur. J.* **2003,** *9,* 5567–5580. doi:10.1002/chem.200304573
32. Friggeri, A.; van der pol, C.; van Bommel, K. J. C.; Heeres, A.; Stuart, M. C. A.; Feringa, B. L.; van Esch, J. *Chem.–Eur. J.* **2005,** *11,* 5353–5361. doi:10.1002/chem.200500007
33. Ihara, H.; Sakurai, T.; Yamada, T.; Hashimoto, T.; Takafuji, M.; Sagawa, T.; Hachisako, H. *Langmuir* **2002,** *18,* 7120–7123. doi:10.1021/la025535f
34. Becerril, J.; Escuder, B.; Miravet, J. F.; Gavara, R.; Luis, S. V. *Eur. J. Org. Chem.* **2005,** *3,* 481–485. doi:10.1002/ejoc.200400629
35. Griffiths, P. C.; Cote, M.; James, R.; Rogueda, P. G.; Morgan, I. R.; Knight, D. W. *Chem. Commun.* **2005,** 3998–4000. doi:10.1039/b505938k
36. Fu, X. J.; Yang, Y.; Wang, N. X.; Wang, H.; Yang, Y. J. *J. Mol. Recognit.* **2007,** *20,* 238–244. doi:10.1002/jmr.831
37. Das, D.; Dasgupta, A.; Roy, S.; Mitra, R. N.; Debnath, S.; Das, P. K. *Chem.–Eur. J.* **2006,** *12,* 5068–5074. doi:10.1002/chem.200501638
38. Smith, J. M.; Katsoulis, D. E. *J. Mater. Chem.* **1995,** *5,* 1899–1903. doi:10.1039/jm9950501899
39. Pantos, G. D.; Pengo, P.; Sanders, J. K. M. *Angew. Chem., Int. Ed.* **2007,** *46,* 194–197. doi:10.1002/anie.200603348
40. Zhan, C. L.; Gao, P.; Liu, M. H. *Chem. Commun.* **2005,** 462–464. doi:10.1039/b413259a
41. George, M.; Funkhouser, G. P.; Terech, P.; Weiss, R. G. *Langmuir* **2006,** *22,* 7885–7893. doi:10.1021/la0610405
42. Okabe, S.; Ando, K.; Hanabusa, K.; Shibayama, M. *J. Polym. Sci., Part B: Polym. Phys.* **2004,** *42,* 1841–1848. doi:10.1002/polb.20067
43. Okabe, S.; Hanabusa, K.; Shibayama, M. *J. Polym. Sci., Part B: Polym. Phys.* **2005,** *43,* 3567–3574. doi:10.1002/polb.20620
44. Terech, P.; Bouaslaurent, H.; Desvergne, J. P. *J. Colloid Interface Sci.* **1995,** *174,* 258–263. doi:10.1006/jcis.1995.1389
45. Terech, P.; Clavier, G.; Bouas-Laurent, H.; Desvergne, J. P.; Deme, B.; Pozzo, J. L. *J. Colloid Interface Sci.* **2006,** *302,* 633–642. doi:10.1016/j.jcis.2006.06.056
46. Dastidar, P.; Okabe, S.; Nakano, K.; Iida, K.; Miyata, M.; Tohnai, N.; Shibayama, M. *Chem. Mater.* **2005,** *17,* 741–748. doi:10.1021/cm048210o
47. Terech, P.; Furman, I.; Weiss, R. G. *J. Phys. Chem.* **1995,** *99,* 9558–9566. doi:10.1021/j100023a038
48. Terech, P.; Allegraud, J. J.; Garner, C. M. *Langmuir* **1998,** *14,* 3991–3998. doi:10.1021/la980160c
49. Willemen, H. M.; Marcelis, A. T. M.; Sudholter, E. J. R.; Bouwman, W. G.; Deme, B.; Terech, P. *Langmuir* **2004,** *20,* 2075–2080. doi:10.1021/la035041y
50. Andre, D.; Fourme, R.; Bruneauxpoulle, J.; Bosio, L. *J. Mol. Struct.* **1982,** *81,* 253–255. doi:10.1016/0022-2860(82)85338-6
51. Moreno, A.; Alegria, A.; Colmenero, J.; Prager, M.; Grimm, H.; Frick, B. *J. Chem. Phys.* **2001,** *115,* 8958–8966. doi:10.1063/1.1413742
52. Knight, D. W.; Morgan, I. R. *Tetrahedron Lett.* **2009,** *50,* 6610–6612. doi:10.1016/j.tetlet.2009.09.070
53. Chatterjee, A.; Grubbs, R. *Angew. Chem., Int. Ed.* **2002,** *41,* 3171. doi:10.1002/1521-3773(20020902)41:17<3171::AID-ANIE3171>3.0.CO;2-O
54. Kolb, H. C.; Vannieuwenhze, M. S.; Sharpless, K. B. *Chem. Rev.* **1994,** *94,* 2483–2547. doi:10.1021/cr00032a009
55. Mitchell, P. C. H.; Parker, S. F.; Ramirez-Cuesta, A. J.; Tomkinson, J., Eds. *Vibrational Spectroscopy with Neutrons;* Series on Neutron Techniques and Applications, Vol. 3; World Scientific Press: Singapore, 2005.

License and Terms

Beilstein Journal of Organic Chemistry

Exceptionally small supramolecular hydrogelators based on aromatic–aromatic interactions

Junfeng Shi[1], Yuan Gao[1], Zhimou Yang[2] and Bing Xu[*1]

Full Research Paper

Open Access

Address:
[1]Department of Chemistry, Brandeis University, 415 South Street, Waltham, Massachusetts 02453 and [2]The Key Laboratory of Bioactive Materials, Ministry of Education, College of Life Science, NanKai University, Tianjin 300071, People's Republic of China

Email:
Bing Xu* - bxu@brandeis.edu

* Corresponding author

Keywords:
aromatic–aromatic interaction; cinnamoyl; hydrogel; hydrogelator; supramolecular

Beilstein J. Org. Chem. **2011,** *7,* 167–172.
doi:10.3762/bjoc.7.23

Received: 08 November 2010
Accepted: 07 January 2011
Published: 07 February 2011

Guest Editor: J.-P. Desvergne

Abstract

We report herein the use of an aromatic–aromatic interaction to produce small molecule hydrogelators that self-assemble in water and form molecular nanofibers in the resulting hydrogels. Among these hydrogelators, a hydrogelator (**6**) made from a phenylalanine and a cinnamoyl group represents the lowest molecular weight (MW = 295.33 g/mol) peptide-based hydrogelator prepared to date. The supramolecular hydrogels were characterized by transmission electron micrograph (TEM) and fluorescence spectroscopy, and the results obtained by both techniques correlate well with their rheological properties. Notably, compound **6** can undergo *cis*/*trans*-isomerization upon UV irradiation.

Introduction

Gels formed by three-dimensional, elastic networks to encapsulate a liquid [1], have many useful properties (e.g., response to external stimuli and flow in response to shear force [2]) and applications in several areas (e.g., bioanalysis [3,4], chemical sensing [5-7], food processing [8], cosmetics [9], drug delivery [10,11], and tissue engineering [12,13]). Inspired by the existing and potential applications of gel materials, research on supramolecular gels [14-19] has rapidly expanded. Amongst these, self-assembled oligopeptides [20-23], which self-assemble in water to form nanofibers and provide hydrogels for biomedical applications, have stimulated the recent research efforts on low molecular weight hydrogelators [24-29]. Despite the intensive research and rapid advances in the design and synthesis of low molecular weight hydrogelators, the minimum structural requirement for a small molecule to act as a hydrogelator to form supramolecular hydrogels has been less explored. We have shown that aromatic–aromatic interactions induce the self-assembly of glycopeptides [30] or pentapeptidic derivatives [31] in water to form nanofibers and supramolecular hydrogels. These results, together with the supramolecular hydrogelators made from dipeptide conjugates with fluorenyl or naphthyl groups, clearly support the simple notion that

aromatic–aromatic interactions in water may direct the formation of hydrogen bonding and would be useful for the supramolecular self-assembly of small molecules in water.

However, despite the progress noted above, an important question still remains to be answered: What is the minimal set of aromatic–aromatic interactions and hydrogen bonding for molecular self-assembly in water to produce supramolecular nanofibers and hydrogels? About a decade ago, Menger [32] and coworkers showed that an aroyl L-cystine derivative, which has a molecular weight as low as 448.51 g/mol, can form a hydrogel at a concentration as low as 0.2 mM and elucidated the molecular structure of the hydrogel based on the crystal structure of the gelator. During that gelation experiment, dimethyl sulfoxide (DMSO) was required in the gel, however, this might complicate the accurate assessment of the aromatic–aromatic interactions and hydrogen bonding since DMSO is prone to form hydrogen bonds with hydrogen bond donors. Therefore, it is necessary to explore small supramolecular hydrogelators for correlating the molecular structure (e.g., numbers of hydrogen bond donors and acceptors and aromatic groups) and the capability of self-assembly without the inclusion of DMSO. Recently, Dastidar and Das [33] reported that *N*-(4-pyridyl)-isonicotinamide (MW = 199.21 g/mol) can act as a non-polymeric hydrogelator at the concentration of 0.37 wt %, which further suggests the possibility of peptide-based hydrogelators that are smaller than the aroyl L-cystine noted above.

Here, we reported the systematic synthesis and examination of a series of phenylalanine derivatives and the identification of the lowest molecular weight peptide-based hydrogelator (MW = 295.33 g/mol) produced to date. Since phenylalanine derivatives belong to a class of insulin absorption promoters [34], this work not only provides a possible benchmark for low-molecular weight hydrogelators, but also a simple system to help in understanding the self-assembly of these phenylalanine based molecules in water and this may offer insights to address side effects, polymorphrism, and efficacy of drug candidates that share common molecular features with these hydrogelators.

Results and Discussion

Scheme 1 shows the structures of the phenylalanines investigated in this work. We chose four types of aromatic moiety, fluorenyl, naphthyl, naphthalenoxyl, and cinnamoyl groups, to covalently attach to the phenylalanine via a simple amide bond. On treatment with 1N NaOH solution, all the prepared compounds dissolve. However, when the pH of the solution is changed from basic to slightly acidic, compounds **1**, **3**, **4** and **6** form hydrogels. Compared with compound **3**, compound **2** fails to form a gel due to the conjugation between the carbonyl group and the naphthyl group, which partial reduces the rotational freedom of the naphthyl group that is necessary for self-assembly. As shown in Table 1, all gels (gels **I**, **II**, **III** and **IV** formed by compounds **1**, **3**, **4** and **6**, respectively) are thermally and pH reversible. For example, heating the gel formed by 0.3 wt % of compound **1** in water to 56 °C or changing its pH from 6.6 to 9.0 leads to a gel–sol phase transition. The gel forms again after restoring the previous conditions, and this cycle can be repeated several times.

Table 1: Typical conditions for the hydrogelation of the phenylalanine derivatives.

Gel#	Compound	Conc. (wt %)[a]	pH[b]	Temp. (°C)[b]	γ_0 (%)[c]	G_0 (Pa)[d]
I	**1**	0.3	6.6	55	0.20	50199
II	**3**	0.5	5.7	45	0.26	4849
III	**4**	0.7	5.9	48	0.56	7820
VI	**6**	1.0	4.6	41	0.85	2519

[a]The minimum concentration of the gelator needed for gelation, [b]the gel–sol phase transition pH/temperature at concentration of 1.0%, [c]critical strain [35], [d]elastic constant.

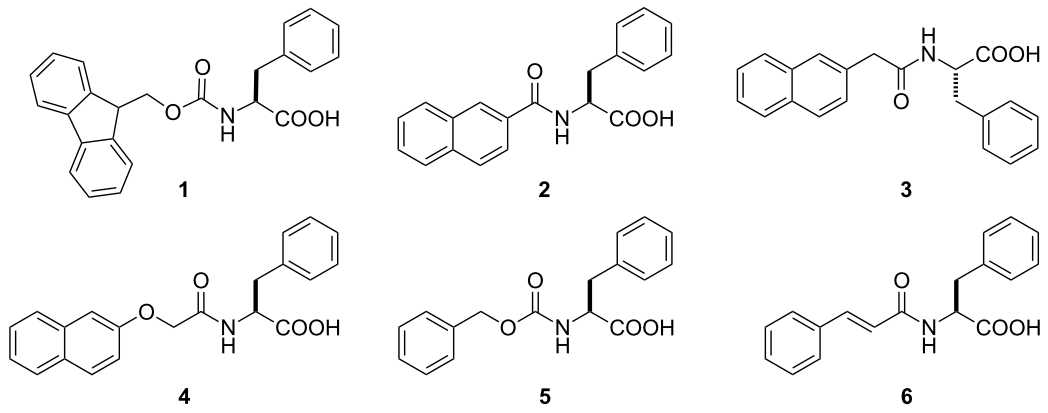

Scheme 1: The chemical structures of the phenylalanine derivatives.

We noted that the gel **IV** exists in two phases (Figure 1B) when it was irradiated by 254 nm UV light for 2 hours: One phase appears solid like, whilst the other phase flows. Two layers of gels are formed after 2 hours aging (Figure 1C). In order to understand the reason for phase separation, compound **6** was placed in a UV reactor for the same duration. As revealed by the ^{1}H NMR (Figure 1F), a new set of peaks at 5.9 ppm and 6.6 ppm appears after UV irradiation, indicating that *cis*-**6** forms upon the photo-excitation [36]. Since there was no new peak in the range of 2.5 to 2.9 ppm (Figure S1, Supporting Information File 1), photopolymerization or photodimerization are unlikely. Furthermore, the result shown in Figure S2 (Supporting Information File S2) also supports the contention that heating is insufficient to cause conversion of the *trans*-isomer to the *cis*-isomer during UV irradiation. Thus, we infer that the formation of two layers in the gel **IV** after UV irradiation originates from geometric (*cis*/*trans*-) isomerism.

Compound **6** also exhibits another interesting phenomenon. On acidification by 1N HCl solution, the solution of **6** (Figure 2A, 2.0 wt %) first turns from a clear solution into a suspension (Figure 2B). The suspension becomes an opaque gel (Figure 2C) when the pH reaches 4.6, which finally turns into a clear hydrogel after aging for ten days (Figure 2D): The aging process apparently helps the small molecules of **6** to disperse evenly and self-assemble again. This behavior seems unique to **6** in these phenylalanine derivatives because solutions of the other compounds on acidification change directly to either gels or suspensions, and the suspensions are unable to become gels spontaneously. This interesting gelation process suggests that the reversible *cis*/*trans*-isomerization provides an additional pathway for rearranging the supramolecular structures and achieving ordered supramolecular structures to produce well-dispersed nanofibers as the matrices of the hydrogels. The fact that compound **6** has the lowest molecular weight amongst the peptide-based hydrogelators suggests that a single amino acid molecule is unlikely to be able to provide an adequate amount of supramolecular interactions to form nanofibers, entrap the solvent, and result in hydrogelation. Apparently, the cinnamoyl

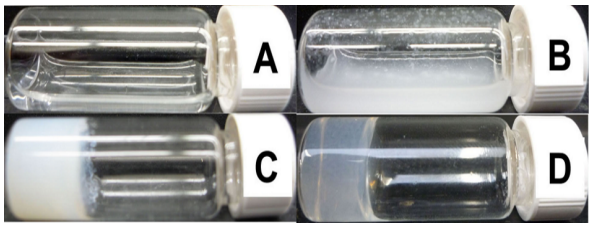

Figure 2: The optical images of (A) solution of **6** (2 wt %, pH = 9.0), (B) suspension of **6** (2 wt %, pH = 6.5), (C) opaque gel of **6** (2 wt %, pH = 4.6), (D) transparent gel of **6** (2 wt %, pH = 4.6, aging for 10 days).

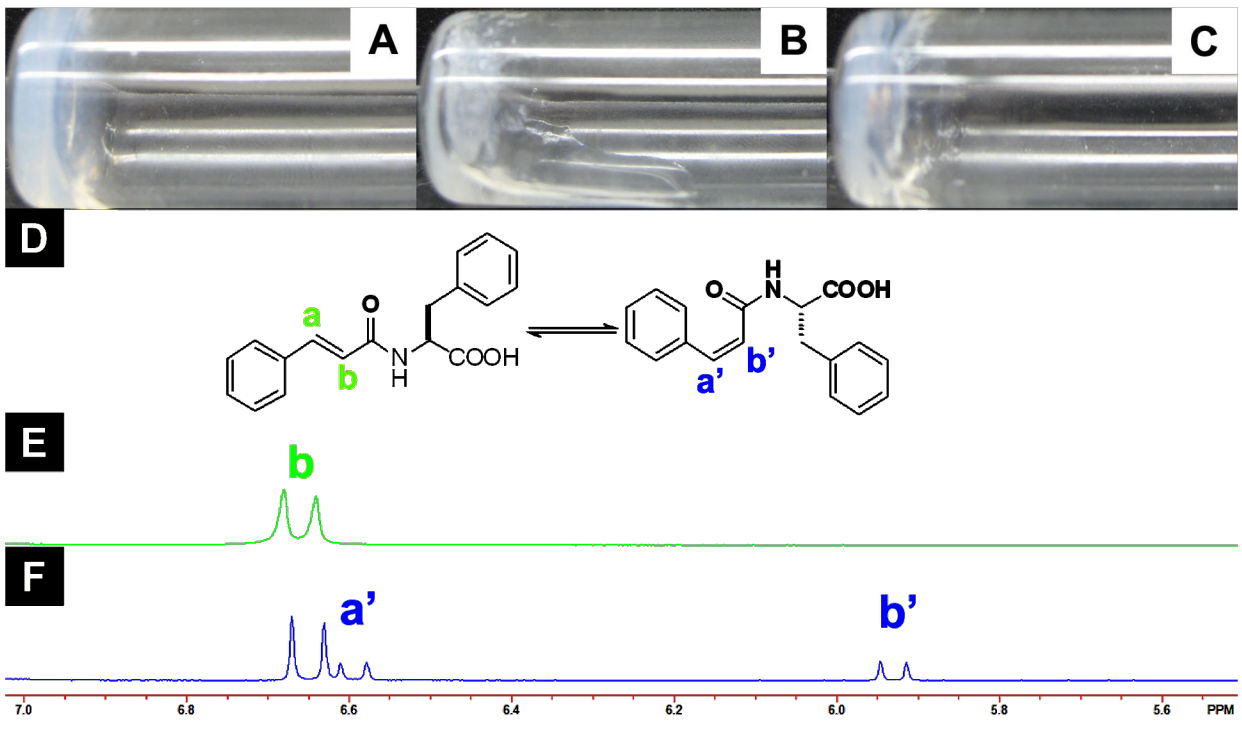

Figure 1: Optical images of (A) gel **IV** (1.5 wt %, pH = 4.6), (B) gel **IV** after UV irradiation (no aging), (C) gel **IV** after UV irradiation (aging 2 hours), (D) the structure of compound **6** in *trans*- and *cis*-isomers, (E) the NMR spectra of compound **6** before and (F) after UV irradiation for 2 hours.

group is the minimum structure motif to provide sufficient aromatic–aromatic interactions for a phenylalanine derivative to act as a hydrogelator.

Figure 3 shows the frequency dependence of storage modulus (*G*') and loss modulus (*G*'') for gels **I** to **IV** at a concentration of 1.0 wt %. The values of the dynamic storage moduli (*G*') of all gels are higher than those of their dynamic loss moduli (*G*"), indicating that all samples behave as viscoelastic materials. The values of *G*' of the hydrogels exhibit little dependence on the frequency (from 0.1 to 200 rad/s), suggesting that the matrices of gels have good tolerance to external shear force. Gel **IV**, which formed by the lowest molecular weight hydrogelator among the phenylalanine derivatives prepared, has the lowest storage modulus. Gel **I**, which was formed by a hydrogelator with the highest molecular weight among compounds **1**–**6**, exhibits the strongest mechanical strength among the gels reported in this work. This is in agreement with the fact that the interactions between fluorenyl and phenyl groups are stronger than the interactions among phenyl groups. Figure 3B shows the modulus (*G*' and *G*'')-strain profiles of gels **I** to **IV**, which provide the maximum *G*' values in the linear region and values of critical strain. The *G*' remained almost constant when the strain increased and then suddenly decreased, indicating the loss of crosslinking within the gel network. Obviously, the critical strain of gel **IV** is greater than the others. These results suggest that gel **IV** can form a more complex network structure, which agrees with the morphology as revealed by TEM (Figure 4).

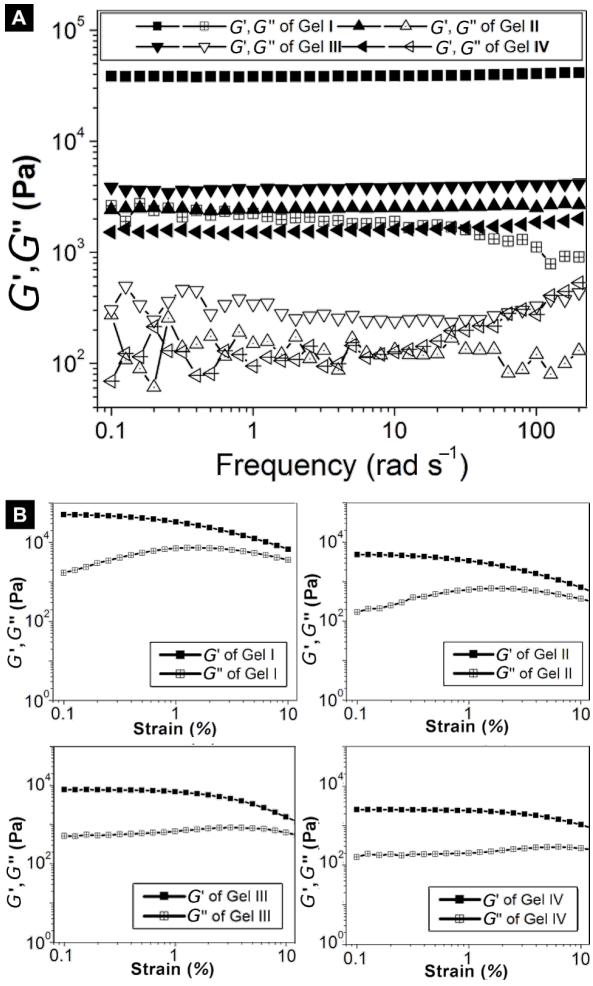

Figure 3: (A) Frequency dependence of dynamic storage modulus (*G*') and loss modulus (*G*") of gels **I** to **IV** at 1.0 wt % concentration. (B) Dynamic storage modulus (*G*') and loss modulus (*G*'') versus strain for the gels **I** to **IV**.

Figure 4 shows the TEM images of the matrices of gels **I** to **IV**. The phenylalanine based hydrogelator self-assemble into nanofibers that physically cross-link to form a fibrous network as the matrix of hydrogel. For example, the fibers in gel **III** (Figure 4C) are longer and larger than those in gel **II** (Figure 4B), agreeing with the fact that gel **III** has a larger critical strain and higher storage modulus. In the TEM image of gel **IV** (Figure 4D), the fibers are smaller and longer than other gels, which could contribute to its relative high critical strain and low storage module values. Unlike other gels, nanoparticles (20–80 nm) string together to constitute the matrices for gel **I**, indicating a high tendency for aggregation. This result also supports the fact that the fluorenyl and phenyl groups have the strongest interactions among those hydrogelators and result in the highest storage moduli among the gels **I**–**IV**.

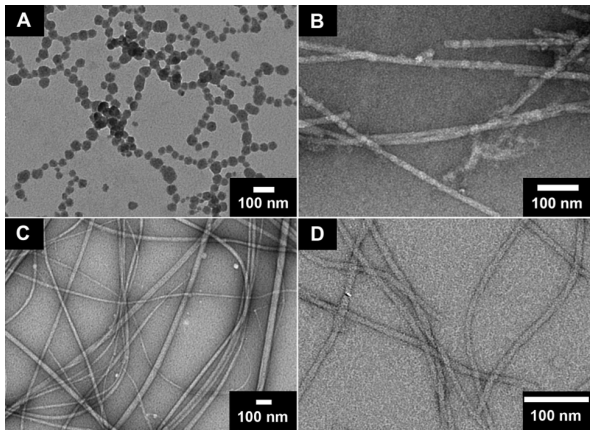

Figure 4: TEM images of the nanofibers that act as the matrices of gel **I** (A), gel **II** (B), gel **III** (C) and gel **IV** (D).

Based on emission spectra of the hydrogels (Figure 5), aromatic–aromatic interactions increase in the gel state, evidenced by the fact that most of bands in the gel phase show red shift. In gel **I**, the band centers at about 309 nm in solution and shift to about 329 nm in the gel phase, suggesting that Fmoc group overlaps with the phenyl group; the shoulder at 363 nm

likely originates from the antiparallel dimerization of the fluorenyl group whilst the small broad bands above 400 nm apparently relate to trimeric or tetrameric aggregates of the Fmoc groups. In gel **II** and gel **III**, the red shifts are smaller than that of gel **I** (from 332 to 333 nm in gel **II**, from 345 to 360 nm in gel **III**), suggesting that the interactions between naphthyl groups and phenyl groups in compounds **3** and **4** result in less overlap than that of fluorenyl and phenyl groups.

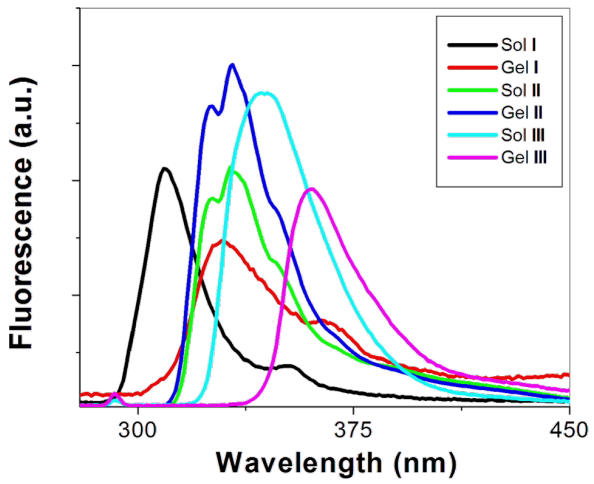

Figure 5: The emission spectra (slit width = 3.0 nm) of the gels **I–III** and their solutions (**I**: λ_{ex}= 265 nm; **II**, **III**: λ_{ex}= 292 nm).

Conclusion

In summary, we have demonstrated that an aromatic group (fluorenyl, naphthyl, naphthalenoxyl, or cinnamoyl) covalently attached to phenylalanine gives rise to a series of new low molecular weight hydrogelators and the identification of the lowest molecular weight peptide-based hydrogelator prepared to date. Obviously, the cinnamoyl group is the minimum structure motif to provide sufficient aromatic–aromatic interactions for a phenylalanine derivative to be a hydrogelator. It not only provides a useful experimental system for further elucidating the relationship between hydrogelation and molecular structure, but also offers a small molecular building block for the development of enzyme based molecular self-assembly. Furthermore, *cis*/*trans*-isomerization offers a novel pathway for achieving well-dispersed nanofibers, which could be used in drug separation, drug release and other fields.

Supporting Information

Supporting Information File 1

Experimental part.
[http://www.beilstein-journals.org/bjoc/content/supplementary/1860-5397-7-23-S1.pdf]

Acknowledgements

This work was partially supported by start-up funds from Brandeis University and National Institute of Health. Junfeng Shi thanks the Scholarship from Chinese Scholarship Council (2008638092).

References

1. Estroff, L. A.; Hamilton, A. D. *Chem. Rev.* **2004,** *104,* 1201. doi:10.1021/cr0302049
2. Yoshinobu, M.; Morita, M.; Sakata, I. *J. Appl. Polym. Sci.* **1992,** *45,* 805. doi:10.1002/app.1992.070450506
3. Heller, A.; Feldman, B. *Acc. Chem. Res.* **2010,** *43,* 963. doi:10.1021/ar9002015
4. Moorthy, J.; Mensing, G. A.; Kim, D.; Mohanty, S.; Eddington, D. T.; Tepp, W. H.; Johnson, E. A.; Beebe, D. J. *Electrophoresis* **2004,** *25,* 1705. doi:10.1002/elps.200405888
5. Sangeetha, N. M.; Maitra, U. *Chem. Soc. Rev.* **2005,** *34,* 821. doi:10.1039/b417081b
6. Holtz, J. H.; Asher, S. A. *Nature* **1997,** *389,* 829. doi:10.1038/39834
7. Chen, J.; McNeil, A. J. *J. Am. Chem. Soc.* **2008,** *130,* 16496. doi:10.1021/ja807651a
8. Ladet, S.; David, L.; Domard, A. *Nature* **2008,** *452,* 76. doi:10.1038/nature06619
9. Jenning, V.; Gysler, A.; Schafer-Korting, M.; Gohla, S. H. *Eur. J. Pharm. Biopharm.* **2000,** *49,* 211. doi:10.1016/S0939-6411(99)00075-2
10. Ma, D.; Tu, K.; Zhang, L. M. *Biomacromolecules* **2010,** *11,* 2204. doi:10.1021/bm100676a
11. Qiu, Y.; Park, K. *Adv. Drug Delivery Rev.* **2001,** *53,* 321. doi:10.1016/S0169-409X(01)00203-4
12. Lee, K. Y.; Mooney, D. J. *Chem. Rev.* **2001,** *101,* 1869. doi:10.1021/cr000108x
13. Langer, R.; Vacanti, J. P. *Science* **1993,** *260,* 920. doi:10.1126/science.8493529
14. Kiyonaka, S.; Sugiyasu, K.; Shinkai, S.; Hamachi, I. *J. Am. Chem. Soc.* **2002,** *124,* 10954. doi:10.1021/ja027277e
15. Gao, Y.; Kuang, Y.; Guo, Z. F.; Guo, Z. H.; Krauss, I. J.; Xu, B. *J. Am. Chem. Soc.* **2009,** *131,* 13576. doi:10.1021/ja904411z
16. Edwards, A. A.; Birchall, L. S.; Jayawarna, V.; Roy, S.; Hughes, M.; Tuttle, T.; Saudi, N.; Okorgheye, G.; Ulijn, R. V. *J. Pharm. Pharmacol.* **2010,** *62,* 1331. doi:10.1111/j.2042-7158.2010.01178.x
17. Schneider, J. P.; Pochan, D. J.; Ozbas, B.; Rajagopal, K.; Pakstis, L.; Kretsinger, J. *J. Am. Chem. Soc.* **2002,** *124,* 15030. doi:10.1021/ja027993g
18. Tam, A. Y. Y.; Wong, K. M. C.; Wang, G. X.; Yam, V. W. W. *Chem. Commun.* **2007,** 2028. doi:10.1039/b705062c
19. Pozzo, J. L.; Clavier, G. M.; Desvergne, J. P. *J. Mater. Chem.* **1998,** *8,* 2575. doi:10.1039/a807237j
20. Hartgerink, J. D.; Beniash, E.; Stupp, S. I. *Science* **2001,** *294,* 1684. doi:10.1126/science.1063187
21. Hartgerink, J. D.; Beniash, E.; Stupp, S. I. *Proc. Natl. Acad. Sci. U. S. A.* **2002,** *99,* 5133. doi:10.1073/pnas.072699999
22. Zhang, S. G.; Holmes, T. C.; Dipersio, C. M.; Hynes, R. O.; Su, X.; Rich, A. *Biomaterials* **1995,** *16,* 1385. doi:10.1016/0142-9612(95)96874-Y
23. Zhao, X. J.; Zhang, S. G. *Chem. Soc. Rev.* **2006,** *35,* 1105. doi:10.1039/b511336a

24. Estroff, L. A.; Hamilton, A. D. *Angew. Chem., Int. Ed.* **2000,** *39,* 3447. doi:10.1002/1521-3773(20001002)39:19<3447::AID-ANIE3447>3.0.CO;2-X
25. Kiyonaka, S.; Sada, K.; Yoshimura, I.; Shinkai, S.; Kato, N.; Hamachi, I. *Nat. Mater.* **2004,** *3,* 58. doi:10.1038/nmat1034
26. Jung, J. H.; John, G.; Masuda, M.; Yoshida, K.; Shinkai, S.; Shimizu, T. *Langmuir* **2001,** *17,* 7229. doi:10.1021/la0109516
27. Vauthey, S.; Santoso, S.; Gong, H. Y.; Watson, N.; Zhang, S. G. *Proc. Natl. Acad. Sci. U. S. A.* **2002,** *99,* 5355. doi:10.1073/pnas.072089599
28. van Esch, J. H.; Feringa, B. L. *Angew. Chem., Int. Ed.* **2000,** *39,* 2263. doi:10.1002/1521-3773(20000703)39:13<2263::AID-ANIE2263>3.0.CO;2-V
29. Terech, P.; Weiss, R. G. *Chem. Rev.* **1997,** *97,* 3133. doi:10.1021/cr9700282
30. Xing, B. G.; Yu, C. W.; Chow, K. H.; Ho, P. L.; Fu, D. G.; Xu, B. *J. Am. Chem. Soc.* **2002,** *124,* 14846. doi:10.1021/ja028539f
31. Ma, M. L.; Kuang, Y.; Gao, Y.; Zhang, Y.; Gao, P.; Xu, B. *J. Am. Chem. Soc.* **2010,** *132,* 2719. doi:10.1021/ja9088764
32. Menger, F. M.; Caran, K. L. *J. Am. Chem. Soc.* **2000,** *122,* 11679. doi:10.1021/ja0016811
33. Kumar, D. K.; Jose, D. A.; Dastidar, P.; Das, A. *Langmuir* **2004,** *20,* 10413. doi:10.1021/la049097j
34. Lustig, N.; Spiegels, H.; Schneide, E.; Lichtens, N. *Isr. J. Chem.* **1974,** *12,* 757.
35. Song, F.; Zhang, L. M.; Li, N. N.; Shi, J. F. *Biomacromolecules* **2009,** *10,* 959. doi:10.1021/bm801500w
36. Danylec, B.; Iskander, M. N. *J. Chem. Educ.* **2002,** *79,* 1000. doi:10.1021/ed079p1000

License and Terms

Beilstein Journal of Organic Chemistry

Synthesis and self-assembly of 1-deoxyglucose derivatives as low molecular weight organogelators

Guijun Wang*[1], Hao Yang[1], Sherwin Cheuk[1] and Sherman Coleman[2]

Full Research Paper

Open Access

Address:
[1]Department of Chemistry, University of New Orleans, New Orleans, LA 70148, Phone: 504 280-1258, Fax: 504 280-6860 and [2]Dillard University, 2601 Gentilly Boulevard, New Orleans, Louisiana 70122

Email:
Guijun Wang* - gwang2@uno.edu

* Corresponding author

Keywords:
1,5-anhydroglucitol; carbohydrate; hydrogelator; organogelator; self-assembly

Beilstein J. Org. Chem. **2011,** *7,* 234–242.
doi:10.3762/bjoc.7.31

Received: 13 July 2010
Accepted: 19 January 2011
Published: 21 February 2011

Guest Editor: J.-P. Desvergne

Abstract

Low molecular weight gelators are an important class of molecules. The supramolecular gels formed by carbohydrate derived low molecular weight gelators are interesting soft materials that show great potential for many applications. Previously, we have synthesized a series of methyl 4,6-*O*-benzylidene-α-D-glucopyranoside derivatives and found that several of them are good gelators for water, aqueous mixtures of DMSO, or aqueous mixtures of ethanol. The gelation efficiency of these glycolipid derivatives is dependent upon the structures of their acyl chains. In order to understand the influence of the anomeric position of the sugar headgroup towards self-assembly, we synthesized a series of 1-deoxyglucose analogs, and examined their gelation properties in several solvents. Several long chain esters, including diacetylene containing esters, and aryl esters exhibited gelation in ethanol, aqueous ethanol, or aqueous DMSO. The synthesis and characterization of these novel analogs are reported.

Introduction

In recent years, the field of low molecular weight gelators (LMWGs) has received a great deal of attention. LMWGs are an interesting class of small molecules that can form reversible supramolecular gels in organic solvents or aqueous solutions [1-9]. Non-covalent interactions such as hydrogen bonding, hydrophobic interactions, and π–π stacking are the main driving forces for the self-assembly of the gelators into 3-dimensional networks. The resulting gels may find applications as soft materials for drug delivery, enzyme immobilization, scaffolds for tissue engineering, etc. [10-14]. The structures of LMWGs span a diverse range; carbohydrates have frequently been used in the synthesis of LMWGs because they are naturally abundant and possess multiple chiral centers that can be selectively functionalized [15-37]. Sugar-based supramolecular hydrogels are being explored as biocompatible soft materials and as matrices for enzymes, DNA, and drug delivery systems [22-28]. Glucose, in

particular, is a versatile building block for the preparation of various small molecule gelators [30-37], as it is relatively easy to obtain substituted products by selective functionalization of the anomeric position and the 4- and 6-hydroxy groups. We have found that further derivatization of the glucose headgroup to form different glycolipids can result in organogelators [34-37].

Previously, we have systematically synthesized and studied the self-assembling properties of a series of methyl 4,6-*O*-benzylidene-α-D-glucopyranoside (**1**) derivatives (Figure 1), including esters and carbamates with different functional groups. Several of these compounds proved to be effective gelators for organic solvents and aqueous solutions [34-37]. We found that the structures of the acyl chains of diester **2**, and monoesters **3** and **4,** are important for gelation. This result also indicates that the ester linked derivatives require more specific structures and many substituents are not tolerated. Typically, monoesters with alkynyl groups containing 5–7 carbons (Figure 2, **5–7**) are good gelators for water or aqueous ethanol mixtures. The monoesters presumably form an extended hydrogen bonding array between the ring oxygen and the free hydroxy groups [36].

For these compounds, the main forces that influence gelation include phenyl ring π–π interactions, hydrogen bonding, and hydrophobic interactions of the acyl chains, etc. To further understand the structural influence of the anomeric position of the sugar headgroup on self-assembly, we synthesized analogs using head group **8** [38] (Figure 2), in which the anomeric methoxy group was replaced with a hydrogen atom and contained a similar series of acyl chains to those in compounds **2–4**. These can potentially lead to novel classes of organogelators.

Results and Discussion

In order to better understand the importance of the anomeric substituent of the sugar headgroup for self-assembly, we synthesized a series of esters of the headgroup **8** by a one pot reaction of the acid chloride with the headgroup (Scheme 1). In general, three products were obtained, which could be separated by flash chromatography. Our previous results had shown that esterification of headgroup **1** typically gave the 2-monoester as the major product, but when the headgroup **8** was used, the selectivity of the acylation diminished significantly. The 2- and 3-esters were obtained in similar quantities and, in some cases, the 3-ester was the major product. The difference in the acylation selectivity was possibly because of the configurations of C-1 and C-2 positions. The α-methoxy group allows intramolecular hydrogen bonding to the C-2 hydroxy to take place, which can make the 2-hydroxy group relatively more nucleophilic than the 3 position. In compound **8**, there is no α-methoxy group available for hydrogen bonding to the 2-hydroxy, so the 2- and 3-hydroxy groups were more or less equally nucleophilic [39]. The amount of diester was significantly less than the amounts of the 2- and 3-esters. Diester formation mirrors the synthesis of the diesters of compound **1**.

The selection of the R groups used in this series was based on our previous results [34-36]. We synthesized the terminal acetylenes **9–11**, saturated hydrocarbons **12–14**, aryl derivatives **15**,**16**, and two long chain diacetylene containing glycolipids **17**,**18**. After we obtained these compounds, we then screened them for gelation in several solvents. These results are shown in Table 1.

From the gelation test results shown in Table 1, quite a few of the diesters were good gelators for the solvents tested. In

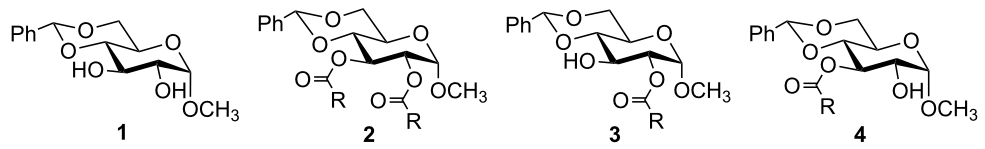

Figure 1: Structures of three ester derivatives of compound **1**.

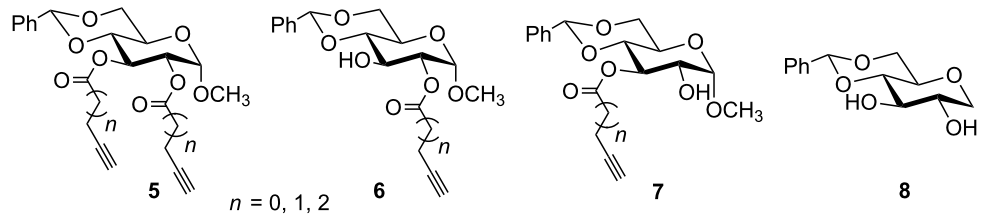

Figure 2: Structures of ester analogs **5–7** and headgroup **8**.

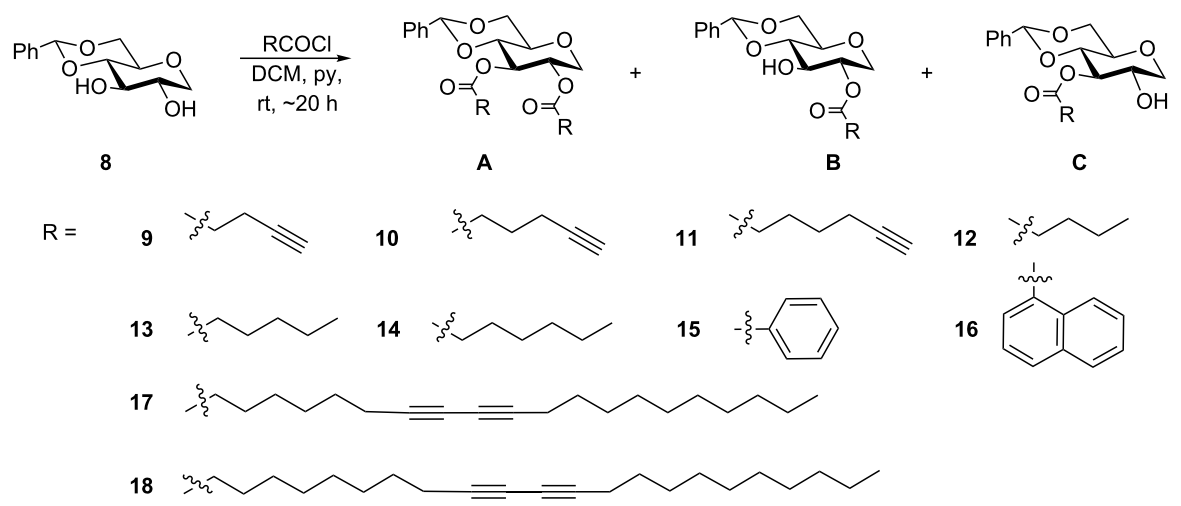

Scheme 1: Synthesis of a series of esters **9A–18C**.

Table 1: The gelation test results of the compounds synthesized[a].

Compound	Hexane	H_2O	EtOH	EtOH:H_2O (1:2)	DMSO:H_2O (1:2)
9A	G 15	I	P	P	P
10A	G 20	I	S	P	P
11A	P	I	S	P	P
12A	S	P	S	P	P
13A	S	P	S	S	P
14A	S	P	S	P	P
15A	I	P	G 5	P	G 5
16A	I	P	P	P	G 20
17A	S	P	G 7	P	P
18A	P	P	G 3	P	P
9B	P	I	S	S	G 20
10B	P	P	S	P	P
11B	P	P	S	P	P
12B	P	P	S	P	P
13B	P	P	S	P	P
14B	P	P	S	P	P
15B	I	P	S	G 4	P
16B	I	P	S	P	P
17B	P	P	S	P	P
18B	P	P	S	P	P
9C	I	P	S	S	S
10C	P	I	S	P	P
11C	P	P	S	P	S
12C	P	P	S	S	P
13C	P	P	S	P	P
14C	P	P	S	P	P
15C	I	P	S	G 10	G 20
17C	P	P	S	P	P
18C	P	S	S	P	P

[a]All concentrations are in mg/mL; G, gel at room temperature; the numbers after G are minimum gelation concentrations; P, precipitation; S, soluble at ~20 mg/mL; the ratio of solvents in parenthesis.

hexane, only the two short chain terminal acetylene compounds **9A** and **10A** formed gels. Several diesters were effective gelators for ethanol, including the benzoate **15A** and the long chain diacetylene compounds **17A** and **18A**. The two diaryl esters **15A** and **16A** were also able to form gels in aqueous DMSO solution. Compared to the diesters, the monoesters were not as effective as organogelators; only the 2-pentynoate **9B** was able to gelate aqueous DMSO, and the 2-benzoate **15B** was able to form a gel in ethanol. The rest of the 2-monoesters did not gelate any of the other solvents. For the 3-monoesters, compound **15C** was able to form gels in aqueous DMSO and aqueous ethanol, but none of the other esters and solvents formed gels.

The morphologies of several gels are shown in Figure 3. The hexane gel of compound **9A** formed fibrous assemblies (Figure 3A, Figure 3B). Compound **9B** showed tubular assemblies (Figure 3C) and more straight cylindrical tube or ribbons (Figure 3D) at different areas. Compound **15B** formed gels more efficiently at 4 mg/mL in the ethanol/water mixture. The morphology of the assembly showed uniform, long and narrow fibers (Figure 3E, Figure 3F).

It is interesting to see that the gelation trends of the diester derivatives of compound **8** are quite different compared to the corresponding compounds derived from headgroup **1**. The gelation of the long chain diacetylene compounds were not affected adversely by changing the headgroup. For the monoesters, the deoxy sugar derivatives are somewhat less effective gelators in comparison to the α-methoxy sugar derivatives. The terminal alkynyl esters were among the most efficient gelators from the ester library derived from compound **1**. The removal of the

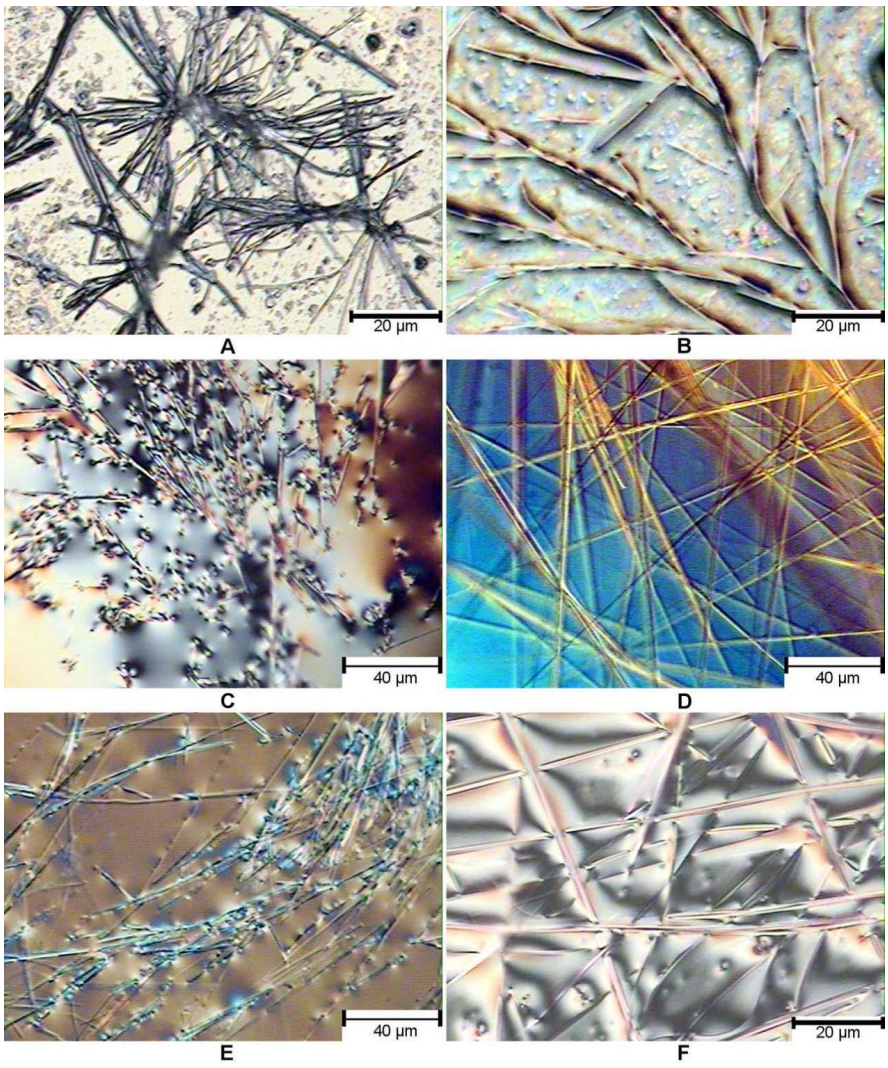

Figure 3: Optical micrographs of the gels formed by compound **9A** in hexane at 15 mg/mL (**A**, **B**), **9B** in DMSO/water (1:2) at 20 mg/mL (**C**, **D**), and **15B** in EtOH/H_2O (1:2) at 4 mg/mL (**E**, **F**). The images were taken with gels containing solvents (not dried gels).

methoxy group resulted in a sharp reduction in gelation, but these compounds did exhibit some gelation ability. This observation indicated that the α-methoxy group is useful in the formation of a fibrillar network and may or may not be involved in the hydrogen bonding array. However, terminal alkynyl groups did show more promise than saturated hydrocarbons.

Polydiacetylenes have interesting optical and electronic properties, and diacetylene containing gels may have useful applications as advanced sensing materials [35,40,41]. The morphologies of the self-assembled structures can be retained by cross linking the diacetylene functional groups. Therefore, we have also synthesized and studied several diacetylene containing sugar lipids. Esterification of sugar headgroups with diacetylene containing long chain carboxylic acids can give the desired diacetylene containing lipids. Previously we had used headgroup **1** to synthesize a library of diacetylene containing lipids, and found that many of them are effective gelators [35]. Using the headgroup **8**, we also synthesized six long chain diacetylene containing glycolipids **17A–17C** and **18A–18C**. We found that the diesters are effective gelators for ethanol. Further characterization of the gel formed by compound **18A** in ethanol proved it to be a very efficient gelator, forming gels in ethanol at concentrations lower than 1 wt %/v. In addition, the gels can also be readily polymerized with a 6 W TLC illuminating UV lamp (Figure 4) to give the typically blue colored product. The glass vial is not UV transparent, therefore the polymerization only occurred from the top of the gel (Figure 4c). When a quartz tube was used as the container, the gel turned light blue homogeneously after one min of exposure to UV light (254 nm) (Figure 4d). After three min of UV treatment, it produced a dark blue colored gel (Figure 4e). The blue gel also exhibited interesting color transition properties upon heating (Figure 4f). For a comparison of the two sugar headgroups, the lipid **19** [35] was able gelate ethanol at 7 mg/mL, but it cannot be polymerized as easily with the 6 W UV lamp. This indicates that the two diacetylene chains in **19** are not aligned favorably for polymerization because of the presence of the methoxy group at the anomeric position. The ethanol gels of compound **19** formed long rods or cylindrical tubules, which may require stronger UV

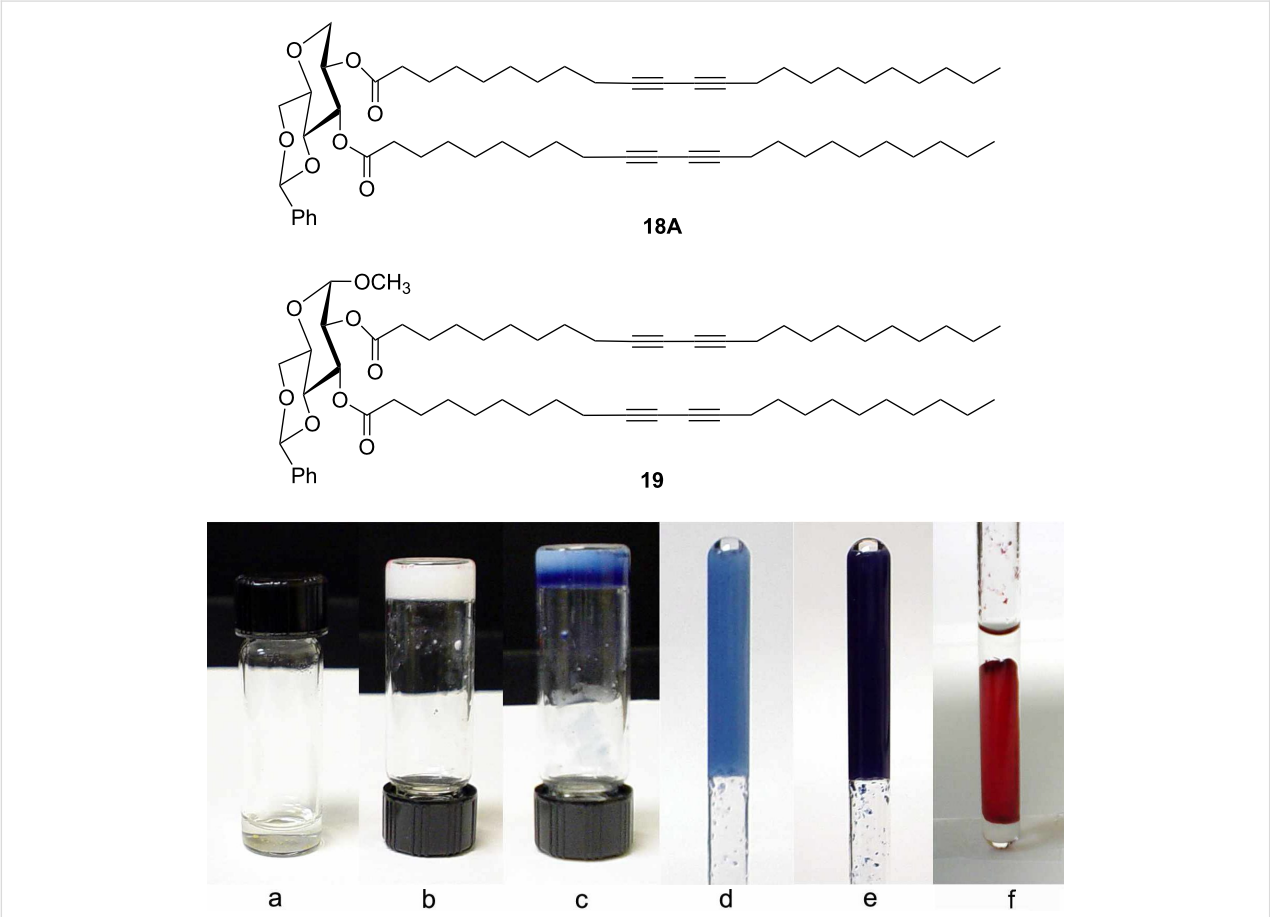

Figure 4: An ethanol gel formed by compound **18A** at <10 mg/mL. a) A clear solution when heated above 70 °C; b) a stable gel after cooling to room temperature; c) a blue gel after illuminating with UV lamp from the top of the vial in b; d) a light blue gel inside quartz tube after UV treatment for 1 min; e) a dark blue gel in quartz tube after UV treatment for 3 min; f) the blue gel in e) turned red after heating.

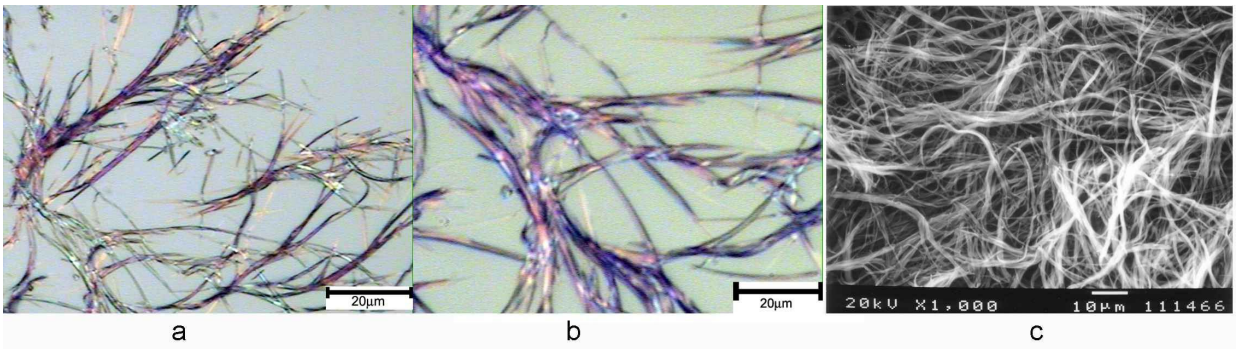

Figure 5: Optical micrographs under bright field (a, b) and scanning electron micrograph (c) of the gel formed by compound **18A** in ethanol after exposure to UV light for 3 min. Blue-purple fibers were observed in (a) and (b), and an entangled fibrous network was observed in (c).

energy to polymerize. The optical micrographs of **18A** showed fibrous assemblies composed of long intertwined thin fibers (Figure 5). The topological cross-link of the diacetylenes allowed the fibrous morphologies to be preserved.

We also carried out UV–vis studies to monitor the color transition of compound **18A** as shown in Figure 6. The gel formed by **18A** in ethanol (10 mg/mL) was treated with a 6 W UV lamp with 254 nm light for 1 min from the top of the uncovered plate. The absorption of the gel was very strong and exceeded the detection limit. The sample was split into two cells, and a small amount of ethanol was added to avoid drying. The UV–vis spectra showed two peaks at 646 nm (λ_{max}) and 590 nm, which is in agreement with the observed purple-blue color of the gel. This plate was then treated with the same UV light for another 2 min. The absorption peaks became more intense, and no new signals were observed (Figure 6A). The plate was covered with a matching glass lid and then incubated in an incubator at 35, 40, 50, and 60 °C for 10–15 min. Below 50 °C, there was a small red shift of the λ_{max}, which increased with increasing temperature. At 50 °C, the λ_{max} shifted from 650 nm to 634 nm. A short incubation at 60 °C also gave a similar spectrum but a new broad absorption at 530 nm began to appear (Figure 6B). The 530 nm absorption corresponds to the red phase of the gel. After incubating at 60 °C for 90 min, only part of the gel turned red, and the red signal at 530 nm increased significantly as shown in Figure 6C. Upon heating briefly to a higher temperature with a heat gun, the gel turned completely red, and the UV–vis spectrum (Figure 6D) showed two new strong peaks at 486 nm and 528 nm. After cooling the samples, part of the gel turned back to blue whilst the remainder stayed red.

From these observations, we can see that the side chain alignment of compound **18A** is quite favorable in providing long range order for the polymerization of the diacetylene groups. Typically polydiacetylenes exhibit absorptions near 530 nm and

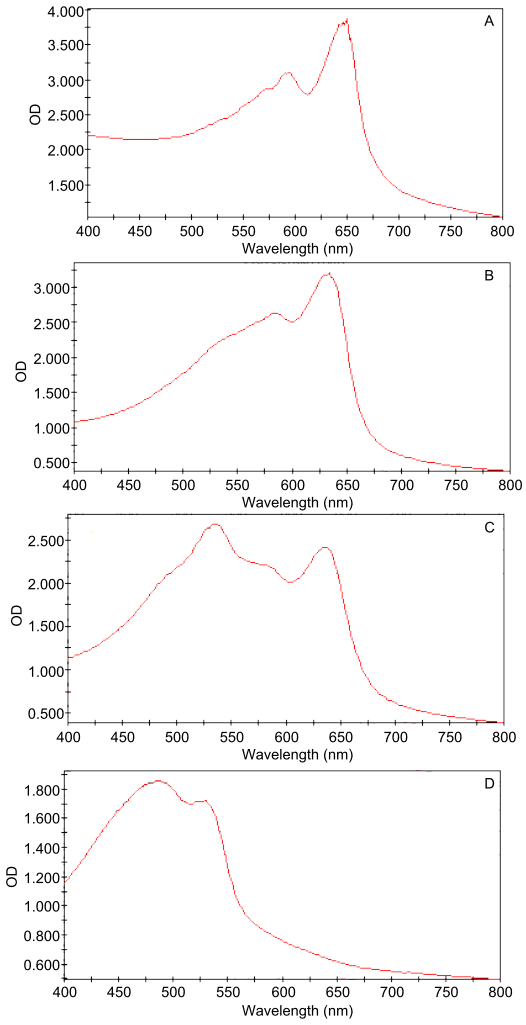

Figure 6: The UV–vis absorption spectra of the polymerized gel formed by compound **18A** in ethanol (10 mg/mL): A, at room temperature after 3 min UV irradiation (λ_{max} = 650 nm); B, at 50 °C (λ_{max} = 634 nm); C, at 60 °C incubation for 90 min (λ_{max} = 534 nm, other peaks are 582, 636 nm); D, after heating at above 60 °C till complete color change to red (λ_{max} = 486 nm together with 534 nm).

630 nm depending on the side chain structures, and the color transition from blue to red has also been well studied [42,43]. Our gelator **18A** polymerized readily with a TLC UV lamp and the cross linked gels only exhibited absorptions at longer wavelengths. The thermo induced color transition is probably due to an annealing effect of the blue-purple polydiacetylene gels into another stable conformation. The study indicated that the formation of diacetylene gel is an effective method to obtain polydiacetylenes with interesting optical properties.

Conclusion

We have synthesized a series of 1-deoxy glucose derived esters, and screened their gelation in several solvents. In comparison with the α-methoxy series with the same acyl chains, the deoxy sugar analogs, and the monoesters in particular, are less effective gelators. It appears that the presence of the α-methoxy group assists in the formation of hydrogen bonds among the compounds and with solvents. However, several diester derivatives are effective gelators, and for both the diesters and the monoesters, terminal acetylene and aromatic functional groups seemed to facilitate gelation. Therefore, even though it was found to be less effective than the α-methoxy headgroup **1**, the deoxy sugar headgroup **8** can be used for the preparation of self assembling gelators when the hydrophobic tails are chosen judicially. For instance, long chain diacetylene containing diester derivatives of **8** are effective gelators, and they can be polymerized using a TLC lamp more readily than the corresponding diesters of **1**. The polymerized diacetylene gels were dark blue with long wavelengths absorptions, these compounds may be useful as advanced stimuli responsive materials.

Experimental

General methods and materials

Materials and instrumentation. General chemicals and reagents were purchased from Aldrich, or VWR. The diacetylene containing fatty acids were purchased from GFS chemicals. Optical microscope images were recorded with an Olympus BX60 microscope and CCD camera. The samples were prepared as thin slices of gels placed on a cleaned glass slide, and the gels were imaged directly under the microscope. NMR spectra were recorded using a 400 MHz Varian NMR spectrometer. High resolution mass spectrometry data were measured on the Q-Tof of the Mass Spectrometry lab at the University of Illinois after the low resolution masses were confirmed. The ionization technique used was ESI (electrospray ionization). Melting points were measured using a Fisher-Jones melting point apparatus.

Optical microscopy. Optical micrographs were recorded with an Olympus BX60 microscope and CCD camera. The sample was prepared as a small piece of gel placed on a clean microscope glass slide, and the gel was imaged directly under the microscope. The program used to acquire and store the photos was Corel Photo-Paint 7.

Scanning electron microscopy. A piece of the gel was deposited on an aluminum sample holder and allowed to dry in a desiccator. The dried gel sample was coated with a thin layer of platinum (~100–150 Å) by a Denton Vacuum (model Desk II) at a reduced pressure of ~30 mTorr and a current of 45 mA for 60 sec. The sample was analyzed using a JEOL JSM 5410 scanning electron microscope with an EDAX Detecting Unit PV9757/05 ME (Model 204B+, active area = 10 mm^2).

Gelation testing. The compounds were typically tested for gelation in a 1 dram glass vial. The diacetylene containing compounds were tested in brown vials to avoid polymerization. A starting concentration of 20 mg/mL was used. The mixture was heated and sonicated until the sample was fully dissolved. The solution was then allowed to cool to room temperature for 15–20 min. If a gel is formed, then the vial is inverted; if no solvent flows while the gel is inverted, then it is called a stable gel. If the gel falls apart during inversion and by gentle shaking, then it is called an unstable gel or gel-like particulate. If a stable gel is formed, serial dilution is performed until the resulting gel is no longer stable. The concentration prior to formation of the unstable gel was recorded as the minimum gelation concentration (MGC).

UV–vis spectroscopy. The UV–vis spectra were recorded on a Bio-Tek PowerWave Microplate Spectrophotometer using a 96-well microplate (Corning's UV transparent microplate #3635). A sample (about 50–100 μL) of the gel of compound **18A** in ethanol (10 mg/mL) was transferred into a cell of the plate. The plate was covered with its matching lid when not inside the plate holder. Heating was carried out using the internal incubator of the spectrophotometer (temperature range 25–50 °C) and Max 4000 incubator (temperature range 25–60 °C) from Barnstead.

General procedure for the synthesis of ester derivatives of compound **8**

The three ester derivatives **A**, **B**, and **C** were synthesized in a one pot reaction by reacting the corresponding acid chloride (1.2 equiv) with headgroup **8** (1.0 equiv). Compound **8** was prepared according to literature procedure [38]. If the acid chloride was not commercially available, it was prepared by converting the corresponding terminal alkynyl carboxylic acid (1.2 equiv) to the acyl chloride using excess oxalyl chloride [35]. After confirming complete conversion to the acyl chloride, hexane was used to co-distill and remove the excess oxalyl chloride. The acyl chloride was added to compound **8** (1 equiv)

in DCM and 4 equiv of pyridine. The reaction mixture was left stirring under an anhydrous atmosphere for 14–20 h. The crude product was concentrated, extracted with DCM, washed with water, then brine, and the combined organic phase dried over anhydrous sodium sulfate. The crude product was isolated and purified using a gradient solvent system (hexanes and acetone), starting with 5% acetone. All yields reported are pure isolated yields, and were calculated based on compound **8**; the yields were not optimized. The following sections include the characterization data for three compounds, the rest are shown in the Supporting Information section.

Synthesis of 4-pentynoates **9A**, **9B**, and **9C**

Compound 9A. This product was isolated as a white crystalline solid in 9.1% yield. M.p. 97–98 °C. ^{1}H NMR (400 MHz, $CDCl_3$) δ (ppm) 7.39–7.46 (m, 2H), 7.29–7.37 (m, 3H), 5.49 (s, 1H), 5.37 (t, 1H, *J* = 9.5 Hz), 5.08 (ddd~dt, 1H, *J* = 5.9, 9.5, 10.3 Hz), 4.33 (dd, 1H, *J* = 5.1, 10.3 Hz), 4.13 (dd, 1H, *J* = 5.9, 11.4 Hz), 3.71 (t, 1H, *J* = 10.3 Hz), 3.64 (t, 1H, *J* = 9.5 Hz), 3.46 (dt, 1H, *J* = 5.1, 9.5 Hz), 3.40 (t, 1H, *J* = 11.0 Hz), 2.51–2.59 (m, 4H), 2.43–2.50 (m, 4H), 1.99 (t, 1H, *J* = 2.6 Hz), 1.89 (t, 1H, *J* = 2.6 Hz). ^{13}C NMR (100 MHz, $CDCl_3$) δ (ppm) 170.8, 170.7, 136.8, 129.0, 128.1, 126.1, 101.4, 82.2, 82.0, 78.6, 72.5, 71.4, 69.8, 69.3, 68.5, 67.3, 33.2, 33.1, 14.3, 14.2. HRMS ESI calcd for $C_{23}H_{24}O_7Na$ [M + Na^+] 435.1420, found 435.1406.

Compound 9B. This product was isolated as a white crystalline solid in 14.6% yield. M.p. 100–101 °C. ^{1}H NMR (400 MHz, $CDCl_3$) δ (ppm) 7.46–7.53 (m, 2H), 7.33–7.42 (m, 3H), 5.51 (s, 1H), 4.93 (ddd~dt, 1H, *J* = 5.9, 9.5, 10.3 Hz), 4.30 (dd, 1H, *J* = 4.8, 10.6 Hz), 4.09 (dd, 1H, *J* = 5.9, 11.0 Hz), 3.85 (t, 1H, *J* = 9.2 Hz), 3.67 (t, 1H, *J* = 10.3 Hz), 3.49 (t, 1H, *J* = 9.2 Hz), 3.35 (dt, 1H, *J* = 5.1, 9.9 Hz), 3.26 (dd~t, 1H, *J* = 10.6, 11.0 Hz), 2.54–2.64 (m, 2H), 2.45–2.54 (m, 2H), 2.01 (t, 1H, *J* = 2.6 Hz). ^{13}C NMR (100 MHz, $CDCl_3$) δ (ppm) 171.1, 136.8, 129.2, 128.2, 126.2, 101.8, 82.2, 81.0, 72.4, 71.9, 70.9, 69.3, 68.5, 67.0, 33.1, 14.3. HRMS ESI calcd for $C_{18}H_{20}O_6Na$ [M + Na^+] 355.1158, found 355.1166.

Compound 9C. This product was isolated as a white crystalline solid in 23.0% yield. M.p. 148–150 °C. ^{1}H NMR (400 MHz, $CDCl_3$) δ (ppm) 7.40–7.47 (m, 2H), 7.28–7.36 (m, 3H), 5.46 (s, 1H), 5.16 (dd~t, 1H, *J* = 9.2, 9.5 Hz), 4.30 (dd, 1H, *J* = 5.1, 10.6 Hz), 4.07 (dd, 1H, *J* = 5.9, 11.4 Hz), 3.86 (m, 1H), 3.67 (dd~t, 1H, *J* = 10.1 Hz), 3.56 (dd~t, 1H, *J* = 9.3 Hz, 1H), 3.34–3.47 (m, 2H), 2.54–2.64 (m, 2H), 2.42–2.52 (m, 2H), 1.88 (m, 1H). ^{13}C NMR (100 MHz, $CDCl_3$) δ (ppm) 172.0, 136.9, 128.9, 128.1, 126.0, 101.2, 82.3, 78.7, 76.6, 71.2, 70.6, 69.14, 69.09, 68.7, 33.3, 14.3. HRMS calcd for $C_{18}H_{20}O_7Na$ [M + Na^+] 355.1158, found 355.1147.

Supporting Information

Supporting Information File 1

Yields and characterization data for compounds **10A–10C** to **18A–18C**.
[http://www.beilstein-journals.org/bjoc/content/supplementary/1860-5397-7-31-S1.pdf]

Supporting Information File 2

^{1}H and ^{13}C NMR spectra of compounds **9A–18C**.
[http://www.beilstein-journals.org/bjoc/content/supplementary/1860-5397-7-31-S2.pdf]

Acknowledgements

This research was supported by the National Science Foundation CHE#518283 and in part by the NSF REU program of AMRI at UNO for Mr. Sherman Coleman (2008 summer). We also thank the assistance of Navneet Goyal and Kristopher Williams with the preparation of the manuscript.

References

1. Terech, P.; Weiss, R. G. *Chem. Rev.* **1997,** *97,* 3133–3160. doi:10.1021/cr9700282
2. Abdallah, D. J.; Weiss, R. G. *Adv. Mater.* **2000,** *12,* 1237–1247. doi:10.1002/1521-4095(200009)12:17<1237::AID-ADMA1237>3.0.CO;2-B
3. Meléndez, R. E.; Carr, A. J.; Linton, B. R.; Hamilton, A. D. *Struct. Bonding* **2000,** *96,* 31–61. doi:10.1007/3-540-46591-X_2
4. Estroff, L. A.; Hamilton, A. D. *Chem. Rev.* **2004,** *104,* 1201–1218. doi:10.1021/cr0302049
5. Gronwald, O.; Snip, E.; Shinkai, S. *Curr. Opin. Colloid Interface Sci.* **2002,** *7,* 148–156. doi:10.1016/S1359-0294(02)00016-X
6. George, M.; Weiss, R. G. *Acc. Chem. Res.* **2006,** *39,* 489–497. doi:10.1021/ar0500923
7. Carretti, E.; Bonini, M.; Dei, L.; Berrie, B. H.; Angelova, L. V.; Baglioni, P.; Weiss, R. G. *Acc. Chem. Res.* **2010,** *43,* 751–760. doi:10.1021/ar900282h
8. Yang, Z.; Liang, G.; Xu, B. *Acc. Chem. Res.* **2008,** *41,* 315–326. doi:10.1021/ar7001914
9. Yang, Z.; Liang, G.; Xu, B. *Soft Matter* **2007,** *3,* 515–520. doi:10.1039/b700138j
10. Shah, C.; Patel, R.; Mazumder, R.; Bhattacharya, S.; Mazumder, A.; Gupta, R. N. *Pharma Rev.* **2009,** *7,* 164–166.
11. Zhao, F.; Ma, M. L.; Xu, B. *Chem. Soc. Rev.* **2009,** *38,* 883–891. doi:10.1039/b806410p
12. Fujita, N.; Mukhopadhyay, P.; Shinkai, S. *Annu. Rev. Nano Res.* **2006,** *1,* 385–428. doi:10.1142/9789812772374_0009
13. Vintiloiu, A.; Leroux, J.-C. *J. Controlled Release* **2008,** *125,* 179–192. doi:10.1016/j.jconrel.2007.09.014
14. Nonappa, N.; Maitra, U. *Org. Biomol. Chem.* **2008,** *6,* 657–669. doi:10.1039/B714475J
15. Hafkamp, R. J. H.; Feiters, M. C.; Nolte, R. J. M. *J. Org. Chem.* **1999,** *64,* 412–426. doi:10.1021/jo981158t
16. Ajayaghosh, A.; Praveen, V. K.; Vijayakumar, C. *Chem. Soc. Rev.* **2008,** *37,* 109–122. doi:10.1039/b704456a

17. Vemula, P. K.; John, G. *Acc. Chem. Res,* **2008,** *41,* 769–782. doi:10.1021/ar7002682
18. John, G.; Vemula, P. K. *Soft Matter* **2006,** *2,* 909–914. doi:10.1039/b609422h
19. Ghosh, R.; Chakraborty, A.; Maiti, D. K.; Puranik, V. G. *Org. Lett.* **2006,** *8,* 1061–1064. doi:10.1021/ol052963e
20. Friggeri, A.; Gronwald, O.; Van Bommel, K. J. C.; Shinkai, S.; Reinhoudt, D. N. *J. Am. Chem. Soc.* **2002,** *124,* 10754–10758. doi:10.1021/ja012585i
21. Chakraborty, T. K.; Jayaprakash, S.; Srinivasu, P.; Madhavendra, S. S.; Ravi Sankar, A.; Kunwar, A. C. *Tetrahedron* **2002,** *58,* 2853–2859. doi:10.1016/S0040-4020(02)00158-8
22. Koshi, Y.; Nakata, E.; Yamane, H.; Hamachi, I. *J. Am. Chem. Soc.* **2006,** *128,* 10413–10422. doi:10.1021/ja0613963
23. Kiyonaka, S.; Sada, K.; Yoshimura, I.; Shinkai, S.; Kato, N.; Hamachi, I. *Nat. Mater.* **2004,** *3,* 58–64. doi:10.1038/nmat1034
24. Yang, Z.; Liang, G.; Ma, M.; Abbah, A. S.; Lu, W. W.; Xu, B. *Chem. Commun.* **2007,** 843–845. doi:10.1039/b616563j
25. Vemula, P. K.; Li, J.; John, G. *J. Am. Chem. Soc.* **2006,** *128,* 8932–8938. doi:10.1021/ja062650u
26. Jung, J. H.; Amaike, M.; Nakashima, K.; Shinkai, S. *J. Chem. Soc., Perkin Trans. 2* **2001,** 1938–1943. doi:10.1039/B104190H
27. Bhat, S.; Maitra, U. *Tetrahedron* **2007,** *63,* 7309–7320. doi:10.1016/j.tet.2007.03.118
28. Suzuki, M.; Owa, S.; Shirai, H.; Hanabusa, K. *Tetrahedron* **2007,** *63,* 7302–7308. doi:10.1016/j.tet.2007.02.065
29. Goyal, N.; Cheuk, S.; Wang, G. *Tetrahedron* **2010,** *66,* 5962–5971. doi:10.1016/j.tet.2010.05.071
30. Bielejewski, M.; Łapiński, A.; Luboradzki, R.; Tritt-Goc, J. *Langmuir* **2009,** *25,* 8274–8279. doi:10.1021/la900467d
31. Kobayashi, H.; Friggeri, A.; Koumoto, K.; Amaike, M.; Shinkai, S.; Reinhoudt, D. N. *Org. Lett.* **2002,** *4,* 1423–1426. doi:10.1021/ol025519+
32. Luboradzki, R.; Gronwald, O.; Ikeda, A.; Shinkai, S. *Chem. Lett.* **2000,** *29,* 1148–1149. doi:10.1246/cl.2000.1148
33. Jung, J. H.; John, G.; Masuda, M.; Yoshida, K.; Shinkai, S.; Shimizu, T. *Langmuir* **2001,** *17,* 7229–7232. doi:10.1021/la0109516
34. Wang, G.; Cheuk, S.; Williams, K.; Sharma, V.; Dakessian, L.; Thorton, Z. *Carbohydr. Res.* **2006,** *341,* 705–716. doi:10.1016/j.carres.2006.01.023
35. Nie, X.; Wang, G. *J. Org. Chem.* **2006,** *71,* 4734–4741. doi:10.1021/jo052317t
36. Cheuk, S.; Stevens, E. D.; Wang, G. *Carbohydr. Res.* **2009,** *344,* 417–425. doi:10.1016/j.carres.2008.12.006
37. Wang, G.; Cheuk, S.; Yang, H.; Goyal, N.; Reddy, P. V. N.; Hopkinson, B. *Langmuir* **2009,** *25,* 8696–8705. doi:10.1021/la804337g
38. Nie, X.; Wang, G. *J. Org. Chem.* **2005,** *70,* 8687–8692. doi:10.1021/jo0507901
39. Wang, G.; Ella-Menye, J.-R.; St. Martin, M.; Yang, H.; Williams, K. *Org. Lett.* **2008,** *10,* 4203–4206. doi:10.1021/ol801316f
40. Dautel, O. J.; Robitzer, M.; Lère-Porte, J.-P.; Serein-Spirau, F.; Moreau, J. J. E. *J. Am. Chem. Soc.* **2006,** *128,* 16213–16223. doi:10.1021/ja065434u
41. Sada, K.; Takeuchi, M.; Fujita, N.; Numata, M.; Shinkai, S. *Chem. Soc. Rev.* **2007,** *36,* 415–435. doi:10.1039/b603555h
42. Fujita, N.; Sakamoto, Y.; Shirakawa, M.; Ojima, M.; Fujii, A.; Ozaki, M.; Shinkai, S. *J. Am. Chem. Soc.* **2007,** *129,* 4134–4135. doi:10.1021/ja069307+
43. Schott, M. *J. Phys. Chem. B* **2006,** *110,* 15864–15868. doi:10.1021/jp0638437

License and Terms

Beilstein Journal of Organic Chemistry

Protonation and deprotonation induced organo/hydrogelation: Bile acid derived gelators containing a basic side chain

Uday Maitra* and Arkajyoti Chakrabarty

Full Research Paper

Open Access

Address:
Department of Organic Chemistry, Indian Institute of Science, Bangalore-560012, India

Email:
Uday Maitra* - maitra@orgchem.iisc.ernet.in; Arkajyoti Chakrabarty - arkajyoti82@yahoo.co.in

* Corresponding author

Keywords:
bile acid derived amines; organogelator and hydrogelator; protonation and deprotonation induced gelation; SEM and POM; thermal stability

Beilstein J. Org. Chem. **2011,** *7,* 304–309.
doi:10.3762/bjoc.7.40

Received: 19 January 2011
Accepted: 02 March 2011
Published: 10 March 2011

Guest Editor: J.-P. Desvergne

Abstract

Two bile acid derived molecules containing basic amino groups are reported to be efficient and unusual gelators of organic and aqueous solvents.

Introduction

Low molecular mass organo- and hydrogelators (LMOG) have attracted considerable attention in recent years due to their tunable physical properties, such as stimuli sensitivity. Their self-assembly in nanoscale superstructures are likely to have important implications in accessing functional nanomaterials [1]. The types of superstructures generated by the SAFINs (Self-Assembled Fibrillar Networks) include fibres, rods, and ribbons. Such self-assembled structures form mainly due to weak non-covalent interactions such as hydrogen-bonding, van der Waals forces, π–π interactions, charge-transfer interactions etc. in organogels, whereas, in aqueous gels, the major driving force for aggregation is hydrophobic interaction [2]. A number of hydrogelators derived from the bile acid backbone have been described in the literature [3-5]. The earliest reports include sodium deoxycholate which forms a gel in water at pH 6.9 [6] and calcium cholate which gels water at pH 7 [7-9]. The facial amphiphilicity of the bile acid derivatives appears to be primarily responsible for their aggregation in water. Unlike conventional surfactant molecules, bile acid salts possess a rigid steroidal backbone, with polar hydroxyl groups on the concave α-face and methyl groups on the convex β-face. On the other hand, relatively few bile acid derived organogelators have been reported [10-15]. Our group has previously reported charge-transfer interaction driven organogelation based on bile acid derived, and other donor molecules [16].

The present work describes efficient organo/hydrogelation by two bile acid-derived low molecular mass gelators **1** and **2** (Scheme 1) having remarkably simple structures with amino groups in the side-chain.

Scheme 1: Gelators **1** and **2**.

Results and Discussion

Compound **1** was found to be a super gelator of organic solvents such as 1,2-dichlorobenzene and chlorobenzene and gelled these solvents at very low concentrations (0.05% w/v). In contrast, **2** was found to gel mixtures of aqueous organic solvents such as DMSO/water and DMF/water. Interestingly, it is the protonated amine **1** which has the organogelation property; whilst **2** must be in the neutral form for hydrogelation (Figure 1).

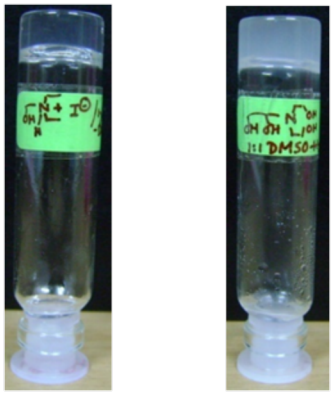

Figure 1: Photographs of the gels: **1** in 1,2-dichlorobenzene (0.2% w/v, left); **2** in 1:1 DMSO/water (0.3% w/v, right).

(A) Gelation behaviour of **1** and **2**

The gelation tests were carried out with compounds **1** and **2** in various organic and mixtures of aqueous organic solvents (Experimental section); the results of the gelation studies are summarized in Table 1.

Table 1: Gelation behaviour of 1 and 2[a].

	1	2
Chloroform	S	S
Mesitylene	S	P
1,2-Dichlorobenzene	TG (CGC 2 mM)	TG (W)
Chlorobenzene	TG (CGC 2 mM)	GP
Benzene	I	P
Toluene	I	GP
Isopropanol	S	S
DMSO/water	P	TG (CGC 5 mM)[b]
DMF/water	S	TG
MeOH/water	P	GP
AcOH/water	S	S
Acetone/water	S	GP
Dioxane/water	S	TLG
CH_3CN/water	S	OG
Water	I	I

[a]TG, transparent gel; TLG, translucent gel; GP, gelatinous precipitate; S, solution; I, insoluble; P, precipitate; OG, opaque gel; W, weak.
[b]**2** formed gel in mixtures of DMSO/water (1:2 to 3:2), DMF/water (2:3 to 3:2), 1,4-dioxane/water (1:4) and acetonitrile/water (1:3).

(B) Protonation–deprotonation induced gelation

The organogelator **1** was found to be a non-gelator in its neutral form, whereas when it was used as its iodide salt it formed strong gels in 1,2-dichlorobenzene and chlorobenzene. To illustrate the acid-base switching of this gel, a simple experiment was designed to show the reversible switching from gel→sol→gel of **1** in 1,2-dichlorobenzene using cresol red sodium salt as the acid–base indicator.

Upon exposure to ammonia vapour, the gel (Figure 2a) formed a solution (Figure 2b, the solution did not form a gel on heating and cooling) with a concomitant colour change (yellow to pink). When this pink solution was exposed to HI vapour, the gel was reformed (Figure 2c, heating was required to dissolve the salt formed and the gel formed upon cooling to room temperature) with the colour turning yellow again (Figure 2d). It is important to note that cresol red turns yellow in water below pH 7.2 and pink above pH 8.8 [17,18]. If the pink solution (Figure 2b) was heated at 120 °C and exposed to HI vapour (this was done by keeping the test tube containing the hot solution inside a sealed chamber containing conc. HI), sol to gel conversion did not require further heating and cooling.

However, for the hydrogel derived from **2**, the situation was reversed. The neutral amine **2** formed a gel in 1:1 DMSO/water (0.5% w/v). When the gel was doped with cresol red, it developed a red colour (Figure 3a), indicating a "pH" of 7.2. However, when 10 µl of HI (conc. HI (7 M, 57%) was diluted

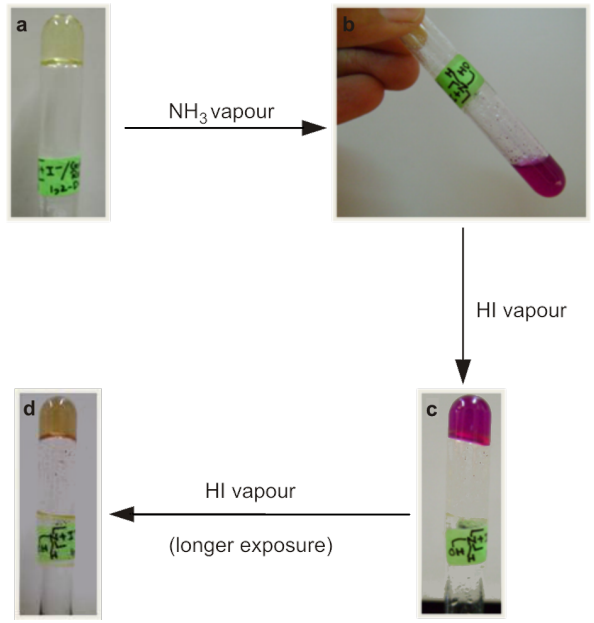

Figure 2: Illustration of base-instability and acid-stability of the organogel of **1** in 1,2-dichlorobenzene.

20-fold and ~0.6 equiv of acid was used with respect to the amine) was added to the gel, the gel framework was disrupted and the solution turned yellow (Figure 3b, the gel did not reform upon heating and cooling/sonication) indicating the solution has "pH" <7.2. The addition of 10 µl of 25% aq. ammonia (13 M, ~30 equiv of ammonia was used with respect to the protonated amine) triggered the sol to gel transition and this time the gel turned pink colour (Figure 3c, heating and cooling reformed the gel).

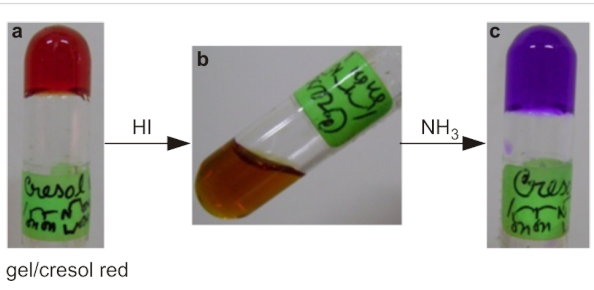

Figure 3: Acid-instability and base-stability of the hydrogel of **2** in 1:1 DMSO/water.

(C) SEM and POM characterization of the gels

The gels showed birefringent textures under a polarizing optical microscope [19]. The organogel showed spherulitic structures [20] (where the fibres originated from nucleation centres, Figure 4a) and a highly entangled fibrillar network (Figure 4b) at higher (1.25% w/v) and lower (0.25% w/v) concentrations of gelator, respectively. SEM images showed the presence of fine fibres (diameter <1µm) in the organogel (Figure 4c, Figure 4d).

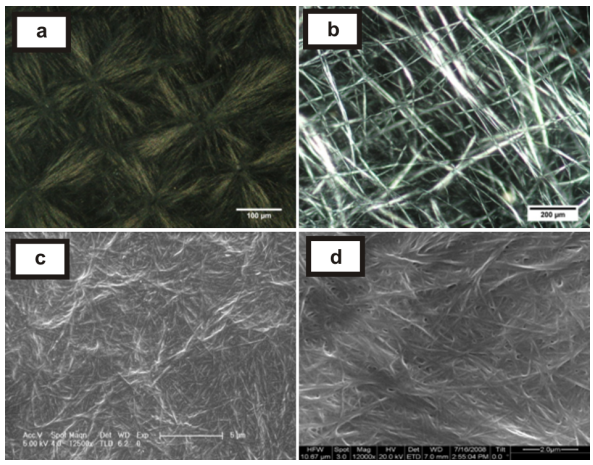

Figure 4: (a) and (b) POM images of the gels of diethylaminolitho-cholyl iodide **1** in 1,2-dichlorobenzene (1.25 and 0.25% w/v of gelator, respectively); (c) and (d) SEM images of xerogels of **1** in 1,2-dichlorobenzene (0.5 and 1% w/v, respectively).

However, for the DMSO/water hydrogel (normally cooled), inter-connected fibres (Figure 5a) and some needle-like micro-crystallites (Figure 5b) were observed under a polarizing optical microscope. Interestingly, there were two types of morphology observed in the SEM micrographs: Normally-cooled gels showed finer fibres as compared to the sonication-induced gel. The arrangement of the fibres were found to be different in the normally cooled gel (Figure 5c, 5e, 5g) in comparison to the sonication induced gel (Figure 5d, 5f, 5h) [21].

(D) Thermal stability of the gels

The concentration dependence of the thermal stability of **1**/1,2-dichlorobenzene gel was carried out by the "inverted test-tube" method [22]. The sharp increase in melting point of the gels (Figure 6) containing 0.2 to 0.6% w/v of gelator could be due to the maximal interaction between solvent and gelator molecules leading to gelation [23]. There were also observable changes in the POM images as the gelator concentration was varied from 0.25 to 1.25% w/v (Figure 4a and 4b).

Thermal stability studies on the gels obtained from **2** in 1:1 DMSO/water (Figure 7) showed that normally cooled gels melted from 51–66 °C (gelator concentration 0.75 to 1.75% w/v, 12–38 mM). The melting profile of the sonicated samples was found to be very similar to that of the normally cooled gels. This suggests that while the sonication process after heating led to different structures of the SAFIN as illustrated in the SEM images, *thermal stabilities were unaffected.*

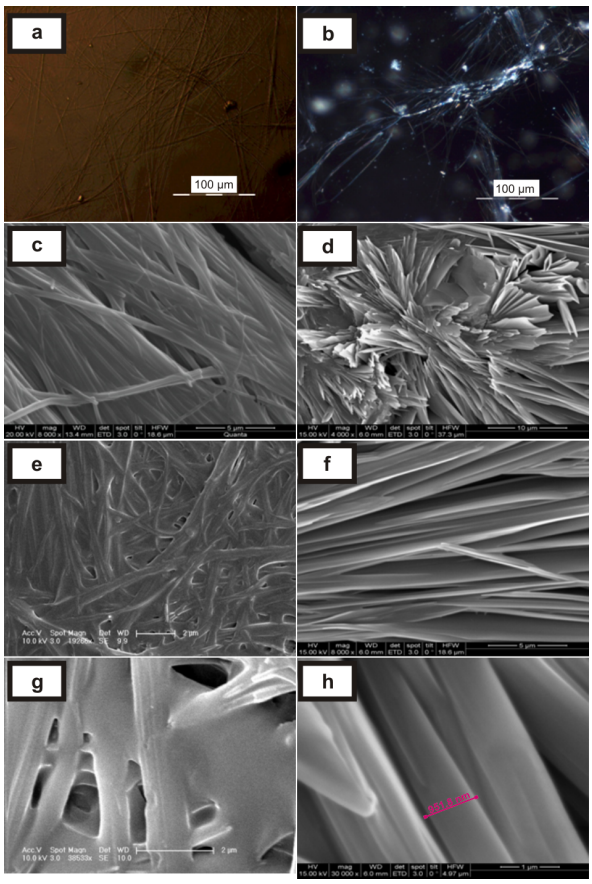

Figure 5: (a) and (b) POM images of bis(2-hydroxyethyl)aminodeoxycholane **2** gel in 1:1 DMSO/water (normally-cooled gel); (c), (e) and (g) SEM images of the xerogels (normally cooled gels); (d), (f) and (h) SEM images of the xerogels (heated and sonicated).

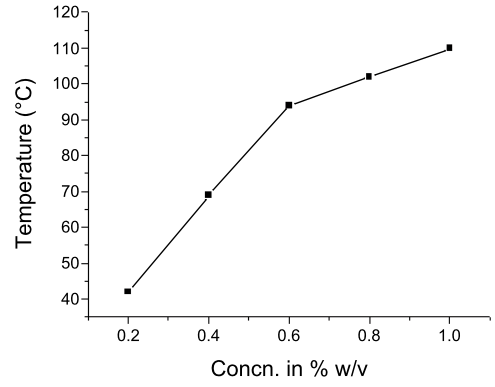

Figure 6: Gel melting profile of diethylaminolithocholyl iodide **1** gel in 1,2-dichlorobenzene.

Conclusion

In conclusion, we have demonstrated an interesting protonation and deprotonation induced gelation of an organogelator and a hydrogelator, respectively. Using cresol red as an indicator, it was possible to illustrate the acid-stability and base-instability of the organogel and the acid-instability and base-stability of the hydrogel.

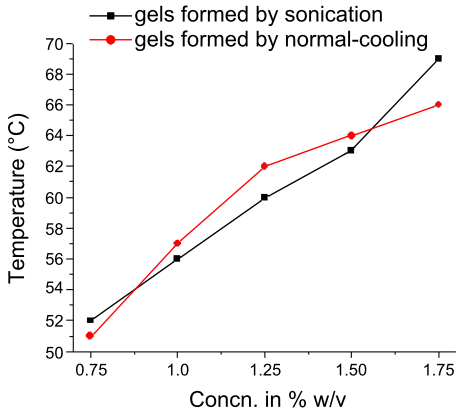

Figure 7: Gel melting profile of bis(2-hydroxyethyl)aminodeoxycholane **2** gel in 1:1 DMSO/water (normally cooled (red) and sonication-induced (black) gels).

However, it was also found that the organogel showed high thermal stability and the nanoscale morphology represented fibres of diameters ranging from 80 nm to 1 µm. The hydrogel had comparatively lower thermal stability and showed different morphologies on sonication induced gelation and normally cooled gelation phenomenon. The hydrogel consisted of fine fibres and birefringent textures when investigated under a polarizing optical microscope.

Finally, these low molecular mass gelators which gel organic and aqueous organic solvents, represent a new class of gelators which have the ability to respond to acid-base stimuli and are potentially useful in emerging fields [24-26].

Experimental

Materials

The syntheses of gelators were carried out starting from lithocholic and 7-deoxycholic acids supplied by Sigma. Diethylamine was purchased from Aldrich and diethanolamine was obtained from a local supplier. Solvents were distilled prior to use.

Instruments

Olympus BX 51 polarizing optical microscope was used for recording POM images of the gels. SEM images were recorded using E-SEM Quanta machine operating at 10–20 kV and xerogels were gold-coated with 10 nm thickness before recording images. For recording gel melting temperatures a Heidolph stirrer-heater was used and test tubes were sealed at the top after preparing the gels. The test tubes containing the gels were kept

upside down in a water bath/paraffin oil bath. Temperature was increased at a controlled rate (~2 °C/min). The temperature at which the gels fell under gravity was noted as the gel melting temperatures. In preparing POM samples, the gels were carefully scooped up and placed over a clean microscope slide covering the sample with a thin cover slip. In case of SEM, scooped up gels were placed over carbon tapes pasted on aluminium stubs and allowed to dry at room temperature in a desiccator connected to vacuum pump.

Brief synthetic procedure

Organogelator **1** and hydrogelator **2** were synthesized starting from lithocholic acid and deoxycholic acid, respectively, as shown in Scheme 2. Formylated lithocholic, deoxycholic acid and formyliodolithocholane, diformyliododeoxycholane were synthesized according to reported procedures [27,28].

Synthesis of compound **1**

3α-Formyloxy-5β-23-iodo-24-norcholane (0.50 g, 1.03 mmol) was dissolved in diethylamine (10 mL, 96 mmol) and stirred at 50 °C for 18 h. After removing the volatiles, the crude product was purified by column chromatography on silica gel (2.5 cm × 10.0 cm) with 5–10% EtOH/$CHCl_3$ as eluent to yield 0.53 g (97%) of the salt. The product was re-precipitated with $CHCl_3$/hexane (1:20) and separated by centrifugation. This process was repeated twice to obtain the pure salt (0.40 g, 74%). m.p. 272–276 °C. $[\alpha]_D^{24}$: 36 (*c* 2.00, EtOH).^{1}H NMR (400 MHz, $CDCl_3$): δ 3.64 (m, 1H), 3.23–2.97 (br m, 6H), 2.03–1.52 (steroidal CH_2), 1.48 (t, 6H, *J* = 7.2 Hz), 1.42–1.10 (steroidal CH_2), 0.99 (d, 3H, *J* = 5.6 Hz), 0.92 (s, 3H), 0.65 (s, 3H). ^{13}C NMR (75 MHz, $CDCl_3$): δ 71.7, 56.4, 55.6, 49.4, 47.3, 42.8, 42.0, 40.3, 40.1, 36.4, 35.8, 35.3, 34.5, 34.3, 30.5, 28.8, 28.5, 27.1, 26.3, 24.1, 23.3, 20.7, 18.7, 12.0, 8.8. IR (KBr): $\tilde{\nu}_{max}$ 3457, 2927, 2860, 1457, 1040 cm^{-1}. HRMS (ESI): Calcd. for $C_{27}H_{50}NO^+$ $[M + H]^+$ 404.3887; Found 404.3892. Anal. calcd. for $C_{27}H_{50}NOI$: C, 61.00, H 9.48, N, 2.63. Found: C, 61.14, H, 9.50, N, 3.10.

^{1}H NMR of the neutral form of compound **1** i.e. $C_{27}H_{49}NO$ showed the following pattern: ^{1}H NMR (400 MHz, $CDCl_3$): δ 3.63 (m, 1H), 2.57–2.36 (br m, 6H), 1.98–1.10 (steroidal CH_2), 1.04 (t, 6H, *J* = 7.2 Hz), 0.94–0.92 (s, d merged, 6H), 0.64 (s, 3H).

Synthesis of compound **2**

3α,12α-Diformyloxy-5β-23-iodo-24-norcholane (0.74 g, 1.56 mmol) was stirred with diethanolamine (15 mL, 157 mmol) at 80 °C for 24 h. The reaction mixture was diluted with 150 mL of $CHCl_3$ and washed with water (2 × 50 mL) in a separatory funnel (250 mL). The organic layer was dried over anhydrous Na_2SO_4. The crude product was purified by column chromatography on silica gel (2.5 cm × 10.0 cm) with 20–40% EtOH/$CHCl_3$ as eluent. The column purified product was passed through a column of basic alumina (0.7 cm × 16 cm) to remove traces of acidic impurities. The neutral amine was obtained in 66% yield (0.46 g). m.p.: 155–156 °C. $[\alpha]_D^{29}$: 44

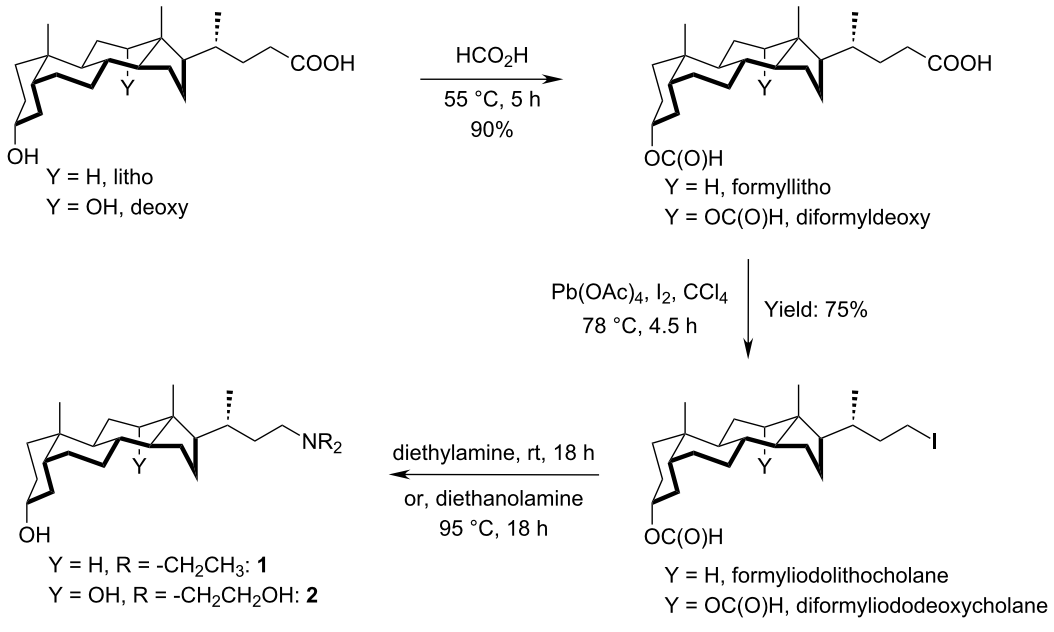

Scheme 2: General method of synthesis of bile acid derived amines **1** and **2**.

(*c* 2.00, EtOH). ^{1}H NMR (300 MHz, $CDCl_3$): δ 3.98 (br s, 1H), 3.65–3.58 (m, 5H), 2.74–2.47 (m, 6H), 1.00 (d, J = 6.6 Hz, 3H), 0.91 (s, 3H), 0.68 (s, 3H). ^{13}C NMR (75 MHz, $CDCl_3$): δ 73.1, 71.7, 59.4, 56.1, 52.0, 48.2, 47.2, 46.5, 42.1, 36.4, 36.0, 35.2, 34.1, 33.6, 32.4, 30.4, 29.6, 28.6, 27.7, 27.1, 26.1, 23.6, 23.1, 17.9, 12.7. IR (KBr): $\tilde{\nu}_{max}$ 3375, 2935, 2863, 1470, 1448, 1045 cm^{-1}. LRMS (ESI): Calcd. for $C_{27}H_{49}NO_4Na$ 474. Found 474. Anal. calcd. for $C_{27}H_{49}NO_4$: C, 71.80, H, 10.93, N 3.10. Found: C, 71.45, H, 10.82, N, 3.20.

Gelation procedure

The gelation tests were performed by dissolving compound **1** in 1,2-dichlorobenzene by heating at 120 °C and then allowing to cool to room temperature to form the gel. The gels formed very fast (2–15 min depending upon the gelator concentration). A translucent gel formed when the gelator **2** was dissolved in DMSO followed by addition of water at rt. If the resulting solution was heated at 110 °C to yield a transparent solution, it took 5–10 min to form an almost transparent gel upon cooling to rt. However, a transparent gel was obtained when the hot solution was sonicated for 35–40 s.

Acknowledgements

We thank the department of Science & Technology, New Delhi for financial assistance (J. C. Bose Fellowship to UM). AC thanks the CSIR, New Delhi for a fellowship. The Institute Nanoscience Initiative is thanked for providing electron microscope facilities.

References

1. Banerjee, S.; Das, R. K.; Maitra, U. *J. Mater. Chem.* **2009,** *19,* 6649. doi:10.1039/b819218a
2. Weiss, R.; Terech, P. *Molecular Gels: Materials with Self-Assembled Fibrillar Networks;* Springer, 2006. See pp 449–450 and pp 613–614.
3. Maitra, U.; Mukhopadhyay, S.; Sarkar, A.; Rao, P.; Indi, S. S. *Angew. Chem., Int. Ed.* **2001,** *40,* 2281. doi:10.1002/1521-3773(20010618)40:12<2281::AID-ANIE2281>3.0.CO;2-L
4. Sangeetha, N. M.; Balasubramanian, R.; Maitra, U.; Ghosh, S.; Raju, A. R. *Langmuir* **2002,** *18,* 7154. doi:10.1021/la025569n
5. Maitra, U.; Babu, P. *Steroids* **2003,** *68,* 459. doi:10.1016/S0039-128X(03)00051-5
6. Rich, A.; Blow, D. M. *Nature* **1958,** *182,* 423. doi:10.1038/182423a0
7. Schryver, S. B. *Proc. R. Soc. London, Ser. B* **1914,** *87,* 366. doi:10.1098/rspb.1914.0023
8. Schryver, S. B. *Proc. R. Soc. London, Ser. B* **1916,** *89,* 176. doi:10.1098/rspb.1916.0004
9. Schryver, S. B.; Hewlett, M. *Proc. R. Soc. London, Ser. B* **1916,** *89,* 361. doi:10.1098/rspb.1916.0022
10. Nonappa; Maitra, U. *Soft Matter* **2007,** *3,* 1428. doi:10.1039/b711010c
11. Hishikawa, Y.; Sada, K.; Watanabe, R.; Miyata, M.; Hanabusa, K. *Chem. Lett.* **1998,** *27,* 795. doi:10.1246/cl.1998.795
12. Nakano, K.; Hishikawa, Y.; Sada, K.; Miyata, M.; Hanabusa, K. *Chem. Lett.* **2000,** *29,* 1170. doi:10.1246/cl.2000.1170
13. Willemen, H. N.; Vermonden, T.; Marcelis, A. T. M.; Sudhölter, E. J. R. *Eur. J. Org. Chem.* **2001,** 2329. doi:10.1002/1099-0690(200106)2001:12<2329::AID-EJOC2329>3.0.CO;2-N
14. Willemen, H. N.; Vermonden, T.; Marcelis, A. T. M.; Sudhölter, E. J. R. *Langmuir* **2002,** *18,* 7102. doi:10.1021/la025514l
15. Willemen, H. M.; Marcelis, A. T. M.; Sudhölter, E. J. R.; Bouwman, W. G.; Demé, B.; Terech, P. *Langmuir* **2004,** *20,* 2075. doi:10.1021/la035041y
16. Maitra, U.; Kumar, P. V.; Chandra, N.; D'Souza, L. J.; Prasanna, M. D.; Raju, A. R. *Chem. Commun.* **1999,** 595. doi:10.1039/A809821B
17. Greenwood, N. N.; Earnshaw, A. *Chemistry of the Elements,* 2nd ed.; Butterworth-Heinemann: Oxford, UK, 1997.
18. *The Merck Index,* 7th ed.; Merck & Co: Rahway, New Jersey, USA, 1960; pp 370 ff.
19. Sangeetha, N. M.; Bhat, S.; Choudhury, A. R.; Maitra, U.; Terech, P. *J. Phys. Chem. B* **2004,** *108,* 16056. doi:10.1021/jp047272z
20. Huang, X.; Terech, P.; Raghavan, S. R.; Weiss, R. G. *J. Am. Chem. Soc.* **2005,** *127,* 4336. doi:10.1021/ja0426544
21. Bardelang, D.; Camerel, F.; Margeson, J. C.; Leek, D. M.; Schmutz, M.; Zaman, B.; Yu, K.; Soldatov, D. V.; Ziessel, R.; Ratcliffe, C. I.; Ripmeester, J. A. *J. Am. Chem. Soc.* **2008,** *130,* 3313. doi:10.1021/ja711342y
22. Clavier, G. M.; Brugger, J.-F.; Bouas-Laurent, H.; Pozzo, J.-L. *J. Chem. Soc., Perkin Trans. 2* **1998,** 2527. doi:10.1039/a803302a
23. Tata, M.; John, V. T.; Waguespack, Y. Y.; McPherson, G. L. *J. Am. Chem. Soc.* **1994,** *116,* 9464. doi:10.1021/ja00100a008
24. Ishi-i, T.; Shinkai, S. *Top. Curr. Chem.* **2005,** *258,* 119. doi:10.1007/b135554
25. Palui, G.; Banerjee, A. *J. Phys. Chem. B* **2008,** *112,* 10107. doi:10.1021/jp801657h
26. Chung, J. W.; An, B.; Park, S. Y. *Chem. Mater.* **2008,** *20,* 6750. doi:10.1021/cm8019186
27. Babu, P.; Maitra, U. *Steroids* **2005,** *70,* 681. doi:10.1016/j.steroids.2005.03.008
28. Bhat, S.; Maitra, U. *Tetrahedron* **2007,** *63,* 7309. doi:10.1016/j.tet.2007.03.118

License and Terms

Beilstein Journal of Organic Chemistry

Self-assembly of 2,3-dihydroxycholestane steroids into supramolecular organogels as a soft template for the in-situ generation of silicate nanomaterials

Valeria C. Edelsztein, Andrea S. Mac Cormack, Matías Ciarlantini and Pablo H. Di Chenna*

Full Research Paper

Open Access

Address:
Departamento de Química Orgánica and UMYMFOR (CONICET-FCEN), Facultad de Ciencias Exactas y Naturales, Universidad de Buenos Aires, Ciudad Universitaria, Pabellón II, Buenos Aires, C1428EGA, Argentina

Email:
Pablo H. Di Chenna* - dichenna@qo.fcen.uba.ar

* Corresponding author

Keywords:
Hansen parameters; nanotube; organogel; self-assembly; supramolecular gel

Beilstein J. Org. Chem. **2013,** *9,* 1826–1836.
doi:10.3762/bjoc.9.213

Received: 15 May 2013
Accepted: 12 August 2013
Published: 09 September 2013

Associate Editor: S. C. Zimmerman

Abstract

Supramolecular gels are an important and interesting class of soft materials that show great potential for many applications. Most of them have been discovered serendipitously, and understanding the supramolecular self-assembly that leads to the formation of the gel superstructure is the key to the directed design of new organogels. We report herein the organogelating property of four stereoisomers of the simple steroid 2,3-dihydroxycholestane. Only the isomer with the *trans*-diaxial hydroxy groups had the ability to gelate a broad variety of liquids and, thus, to be a super-organogelator for hydrocarbons. The scope of solvent gelation was analysed with regard to two solvent parameters, namely the Kamlet–Taft and the Hansen solubility parameters. The best correlation was observed with the Hansen approach that revealed the existence of two clear gelation zones. We propose a general model of self-assembly through multiple intermolecular hydrogen bonds between the 1,2-dihydroxy system, which is based on experimental data and computational simulations revealing the importance of the di-axial orientation of the hydroxy groups for the one-dimensional self-assembly. Under controlled conditions, the fibrillar superstructure of the organogel was successfully used as a template for the in-situ sol–gel polymerization of tetraethoxysilane and the further preparation of silica nanotubes. We propose that the driving forces for templating are hydrogen bonding and electrostatic interactions between the anionic silicate intermediate species and the self-assembled fibrillar network.

Introduction

Low molecular mass organogelators (LMOGs) have received increasing attention during the last two decades because of their unique properties and numerous potential applications in fields such as the stabilization of organic photochromatic materials, the templated synthesis of nanostructured and functional materials, the controlled release drugs systems, the capture of

spilled pollutants in the environment, electrochemistry, light-harvesting materials and so on [1-6]. These small molecules self-assemble into regular supramolecular structures through non covalent interactions such as ion–ion, dipole–dipole, hydrogen bonding, π–π stacking, van der Waals, host–guest, and ion coordination, and in so doing trap the solvent molecules in the supramolecular network to form supramolecular gels. The non-covalent nature of these interactions makes it possible for the supramolecular gel systems to achieve a reversible sol–gel phase transition by the simple application of an external stimulus. Intrinsically, supramolecular gels are thermosensitive and can be transformed reversibly to a fluid (sol) by heating. A small number of novel LMOGs, however, undergo a sol–gel transition as the temperature increases, which is called thermogelling [7]. Many other LMOG molecules form gels that are sensitive to other physical stimuli such as light, ultrasound or chemical stimuli [8-12]. A wide variety of structurally diverse molecules have the ability to form physical gels (e.g., saccharides, peptides, ureas, nucleobases, steroids, dendrimers, etc. [13]). Although a great effort has been made to investigate the structure–property relationships, it is still impossible to design a new LMOG de novo. For those reasons most of the known LMOGs have been discovered serendipitously. Nevertheless, with the knowledge gained about the mode of aggregation of LMOG molecules some of the structural features necessary for gelation are known. The presence of a supramolecular synthon to promote the one-dimensional (1D) self-assembly is a necessary feature in order to form the fibrillar entangled network that entraps the solvent [14]. The strongest and most important supramolecular synthons involve functional groups that possess a complementary donor–acceptor hydrogen bond motif, such as for instance amides, ureas, carbamates, saccharides, ammonium carboxylate salts, etc. A rod-like molecular shape is also a general structural requirement for steroid derived LMOGs because it allows a good face to face molecular contact to promote the one-dimensional growth. These concepts have been recently exploited to design new LMOGs [15,16]. Nevertheless, the presence of a supramolecular synthon in a molecule is a necessary but not a sufficient feature to become an organogelator. The formation of the gel involves a delicate balance of cooperative forces between the directional self-assembly that promotes the 1D aggregation and the solubility and insolubility in a given solvent, which is based on the specific interactions between solvent and gelator molecules [17]. Numerous attempts have been made to correlate solvent parameters to gelation ability. The most promising technique was recently presented in the works of Bouteiller et al. and Rogers et al., in which they apply the Hansen solubility parameters (HSP) to evaluate the gelation behavior of LMOGs in different solvents [18,19]. The Kamlet–Taft solvatochromic parameters, which consider separately the hydrogen-bond donor (HBD, α), hydrogen-bond acceptor (HBA, β), and polarizability (π*) properties as contributions to the overall solvent polarity had also been occasionally used to study solvent–gelator specific interactions [20,21].

LMOGs based on cholesterol and bile acids offered the most versatile units on which to base the systematic design of functional LMOGs for the gelation of organic solvents. Neither cholesterol nor cholestanol are gelator molecules, and although a variety of steroid derivatives has been analyzed over the years only a few simple analogues are known to be organogelators [22]. The steroidal LMOGs usually have substituents attached to the 3β-OH of the cholestane A ring and synthetic variations at the steroidal skeleton are scarce. Cholesterol-based LMOGs build mesophases in which steroid–steroid stacking is controlled by van der Waals forces. These interactions, including the additional intermolecular contacts from the pending moieties linked at C-3 (usually hydrogen bond and π–π stacking), lead to a primarily one-dimensional long-range growth and finally produce the interconnected 3D self-assembled fibrillar network (SAFIN), which traps the solvent and turns into a self-supporting gel. There are several types of cholesterol-based LMOGs grafted on hydrophilic heads such as saccharides, chromophores, ligands, peptides, etc. The first study on rational syntheses of cholesterol derived organogels was made by Weiss et al. [23] on a family of molecules containing an aromatic moiety (A) connected to a steroidal group (S) through a linker (L). Since then a great number of ALS molecules have been discovered constituting the most systematically investigated family of LMOGs [24].

Recently we have reported a new steroid-based organogelator with a non-conventional bridged pregnane skeleton and its use as template for the preparation of nanotubes and fluorescent nanospheres of silica via the in-situ sol-gel polymerization of tetraethyl orthosilicate (TEOS) [25,26]. In our search for new LMOGs analogues with structural variations in the steroidal nucleus and new properties we prepared steroid **1** as a synthetic intermediate (Figure 1). This known steroid, which is widely used in medicinal chemistry as a precursor in the synthesis of cholesteryl derived bioactive analogues [27,28], gelated *n*-hexane during concentrating the fractions from a chromatographic column. Although this simple steroid has been synthesized for the first time decades ago, its gelation property has never been described in the literature.

In this paper, we report the broad scope and super-organogelating ability of steroid **1** and the use of their gels as template for the in situ polymerization of TEOS. A general self-assembly model with multiple intermolecular hydrogen bond interactions is proposed based on experimental and computational data. In

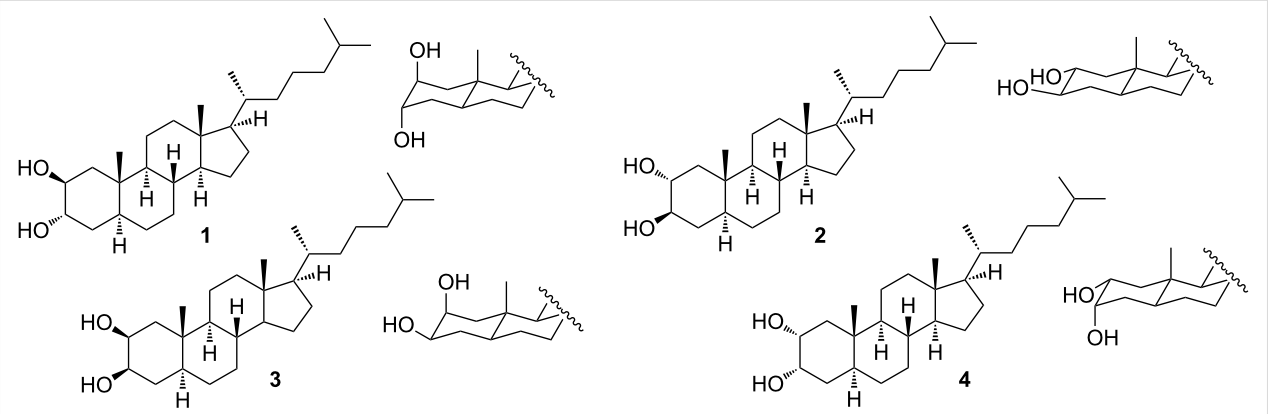

Figure 1: Structures of the 2,3-dihydroxycholestane isomers studied in this work.

order to understand the role of the *trans*-diaxial orientation of the vicinal dihydroxy moiety we have also studied the organogelating properties of the stereoisomers **2**–**4** bearing equatorial hydroxy groups (Figure 1). The gelation ability of **1** is discussed in terms of the Hansen solubility parameters and Kamlet–Taft parameters based on its behavior in a set of 33 solvents. We also report on the sol–gel polymerization of TEOS carried out with gels of **1** demonstrating that templated silica nanotubes are obtained only under controlled conditions. Considering that the design of new LMOGs with predictable gelation properties is still a challenge nowadays, we consider that the *trans*-diaxial dihydroxy supramolecular synthon studied herein is a valuable contribution towards the development and design of new LMOGs molecules with potential applications.

Results and Discussion

As mentioned before, steroid **1** showed an excellent gelation ability in *n*-hexane during concentrating a solution on a rotatory evaporator. Preliminary qualitative tests with cyclohexane and dichloromethane also showed a good gelling ability. These remarkable properties for such a simple steroid molecule prompted us to study the gelation scope, morphology, mode of self-assembly and the potential use of the gels to prepare silica nanoparticles through a bottom-up approach.

Gelation scope and thermal stability

To assess the scope of the gelation ability of steroids **1**–**4** in a simple way, the test tube method was first used with 28 selected organic solvents ranging from hydrocarbons to alcohols (Table 1, entries 1–28). While steroids **2**–**4** were unable to gelate any of these solvents, steroid **1** showed a good to excellent gelation ability over a wide variety of solvents.

Given these results we directed our analysis towards the scope of solvent gelation of **1** by using the HSP approach described by Boutellier [18]. A tridimensional plot of the dispersive interac-

Table 1: Gelation test for LMOG **1**.

entry	solvent	test[a]	CCG[b] (wt %)
1	1,2-dicloroethane	G	1.4
2	1,4-dioxane	G	7.0
3	1-hexanol	S	—
4	acetic acid	S	—
5	acetone	I	—
6	acetonitrile	I	—
7	aniline	G	2,0
8	CCl_4	G	0.8
9	chloroform	G	2.5
10	pyridine	S	—
11	dichloromethane	G	0.8
12	DMF	S	—
13	DMSO	G	5.0
14	ethanol	I	—
15	ethyl acetate	S	—
16	isopropyl ether	I	—
17	methanol	I	—
18	*n*-butanol	I	—
19	*n*-heptane	TG	0.06
20	*n*-hexane	TG	0.06
21	cyclohexane	TG	0.13
22	TEA	I	—
23	TEOS	S	—
24	THF	S	—
25	toluene	G	2.5
26	water	I	—
27	xylene	G	0.8
28	methyl acrylate	G	4.0
29	nitrobenzene	G	3.3
30	methylcyclohexane	TG	0.16
31	decane	TG	0.04
32	styrene	G	2.5
33	*o*-dichlorobenzene	G	5.0

[a]G: gel, TG: turbid gel, S: soluble I: insoluble; [b]critical concentration for gelation.

tions (δ_d), the dipolar-interactions (δ_p) and the hydrogen-bonding (δ_H) parameters of LMOG **1** showed a complex correlation between the gelation ability and the HSP of the solvents (Figure 2, see Supporting Information File 1 for full data). Two gelation zones were clearly identified graphically. The first gelation space (zone A), with a cylindrical, almost linear profile, involves solvents with zero or very low δ_H and δ_p parameters and a δ_d parameter between 14 and 18 (hydrocarbons). Gelation zone B includes polar, non-protic solvents with higher dispersive interaction parameters δ_d (from 17.5 to 20). In contrast to the results obtained by Boutellier et al. [18], it was not possible to define a gelation sphere in either zone in this case. Nevertheless, in order to corroborate the tendency observed we chose a new set of solvents with HSP between the gelation spaces (Table 1, entries 29–33), all of them could be gelated by **1** showing that, although spherical spaces cannot be defined, prediction is possible by selecting solvents with HSP inside the gelation zones. Figure 2 qualitative shows that there is a good correlation between the HSP and the gelated solvents, pyridine and methyl acrylate are the only solvents that visible lay outside the corresponding zones. It is clear from the graphic analysis that the higher the δ_H, the higher the δ_p, of the gelated solvent with a limit of about 10 for the former. Non-gelled solvents are clustered in zones with high δ_H and low δ_d. This makes sense, because a solvent, which acts as either a strong hydrogen-bond donor or a strong hydrogen-bond acceptor, will significantly interact with the hydroxy groups of **1** and thus impede the supramolecular self-assembly and the formation of the gel. This way it will prevent gelation or will make a higher concentration of gelator necessary. This effect is higher for solvents with smaller dispersive interaction parameters. For solvents in zone A steroid **1** is a supergelator with critical concentrations for gelation (CCG) below 0.1 wt % for linear hydrocarbons (entries 19, 20 and 31) and of about 1% for cyclic hydrocarbons and carbon tetrachloride (entries 8, 21 and 30). The second zone comprises aromatic and polar solvents bearing nitrogen or oxygen atoms with CCG values between 2 and 7 wt %. The presence of two gelation zones is indicative of a difference in the molecular packing of the gel fibers and will be discussed in the following section.

Next we considered the Kamlet–Taft parameters for the tested solvents and compared these results to the Hansen approach [29]. The 3D plot did not show clear zones of gelation (Figure 2b) although it is evident from the analysis that solvents with very high α parameters (α > 0.5, such as alcohols, water and formic acid) cannot be gelated. The same tendency is observed for the β parameter but with some exceptions, such as DMSO, which is a very strong hydrogen-bond acceptor but still capable of forming gels. The effect of π* seems to be less important since solvents with both high and low polarizability can be gelled (see π*-vs-α and π*-vs-β plots in Supporting Information File 1). We assume that the bad correlation between the Kamlet–Taft parameters and the gelation behavior of LMOG **1** is connected to the solvatochromic origin of the scale [29]. The Hansen solubility parameters with a scale based on solubility seems to be more suitable for solvent–gelation analysis.

All gels were stable, thermoreversible and non-thixotropic. Gels from hydrocarbons were turbid, depending on the concentration of gelator, indicating a low solubility. To estimate the relationship between thermal stability, concentration of gelator, and solvent we studied the variation of the gelation temperature (*T*g) with the concentration of **1** in gels of cyclohexane, dichloromethane, carbon tetrachloride, dioxane, aniline and nitrobenzene. Tube inversion experiments were performed to measure T_g. This method was selected because of its simplicity and

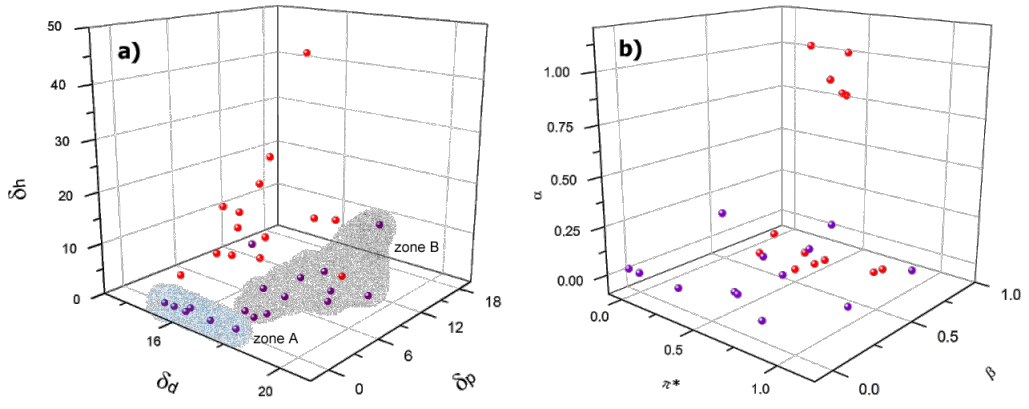

Figure 2: 3D plots for LMOG **1** and solvent parameters of the tested solvents a) Hansen solubility parameters (δ_d dispersive interactions, δ_p dipolar interactions, δ_H hydrogen bonding) and b) Kamlet–Taft parameters (α hydrogen bond donor, β hydrogen bond acceptor, π^* polarizability). Purple: gelated solvents. Red: non-gelated solvents. (For more details see Table S1 in Supporting Information File 1.)

widespread use in the field of gel-phase materials. Typically, as the concentration of **1** was increased, T_g also increased until a plateau region was reached. Cyclohexane gave the most stable gel with a T_g of 64 °C at the CCG, and a maximum T_g value of 99 °C for a 2-wt-% gel (Figure 3). Carbon tetrachloride and dichloromethane reached the plateau region at the same concentration, but with T_g values of 75 and 45 °C, respectively, which shows that more polar solvents gives thermally less stable gels. On the other hand, dioxane, nitrobenzene and aniline, capable of hydrogen bonding, had a maximum T_g of 72 °C, 77 °C and 66 °C, respectively, but at considerably higher concentrations of 26, 6 and 8 wt % (see Supporting Information File 1). LMOG **1** could also selectively gelate the organic layer from a water/organic solvent mixture after a heating–cooling process.

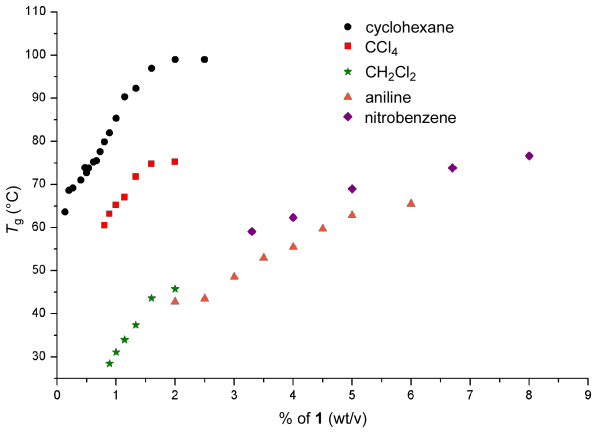

Figure 3: *T*g-vs-concentration plots for gels of **1**.

Morphology and self-assembly

The FTIR spectra of the gel and the solution of LMOG **1** provided evidence that the interactions leading to self-assembly is primarily hydrogen bonding between the hydroxy groups. In dichloromethane (DCM) solution, at a concentration of LMOG **1** below the CCG, a broad band was observed at ν_{O-H} = 3608.2 cm^{-1} (O–H stretching). In the gel state this band was widened and shifted to 3363.3 cm^{-1}, which is typical for an intermolecular hydroxy hydrogen-bond. The FTIR spectrum of the gel still showed the band of free hydroxy groups at ν_{O-H} = 3610.1 cm^{-1} and may be associated with molecules of LMOG **1** in the liquid-like solution phase trapped within the SAFIN (see Supporting Information File 1 for IR spectra) [17].

The microscopic morphology of the xerogel of **1** from DCM, *n*-hexane and dioxane was analyzed by SEM. The images showed an entangled fibrillar network for all solvents. Particularly the images of the dichloromethane xerogel (Figure 4a and Figure 4b) showed left handed helical fibers with a fiber width

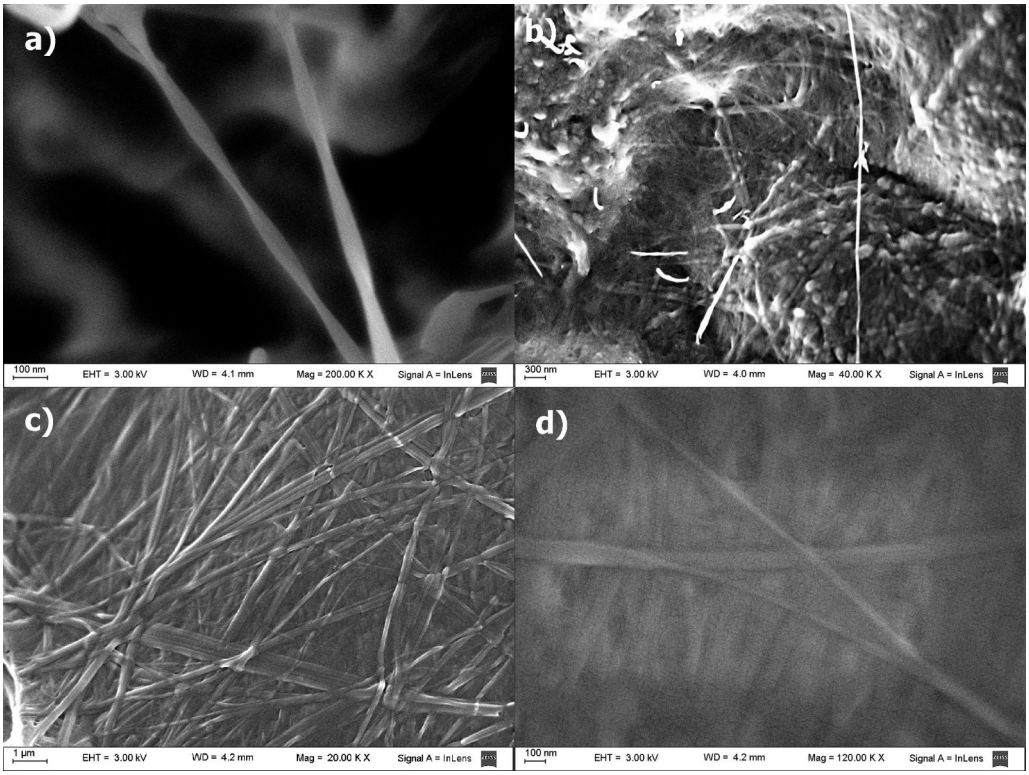

Figure 4: SEM images of xerogels from a,b) dichloromethane, and c,d) from dioxane.

ranging from 20 to 75 nm, and a helicoidal period of about 750 nm. The helical shape is clearly observed in the isolated fibers (Figure 4a), but these are difficult to find in the bulk due to the collapsed fibrillar network. For *n*-hexane and dioxane simple straight entangled fibers were observed with a minimum width of 20 nm. In all cases fibers with lengths of up to several micrometers were clearly visible. SEM images of the xerogel from dioxane showed a tighter SAFIN compared to *n*-hexane and dichloromethane xerogels. This is indicative of a more compact assembly in this polar solvent. Due to the lack of a chromophore in **1**, it was not possible to use circular dichroism to prove the helicoidal nature of the fibrillar network, but images suggest that, at least in dichloromethane, the one dimensional self-assembly is directed helicoidally by the inherently asymmetric steroid molecule.

To gain a better insight into the packing of the material, X-ray powder diffractograms (XRPD) of xerogels from dichloromethane (DCM) and *n*-hexane were performed (Figure 5). The X-ray pattern of the xerogel of **1** from *n*-hexane showed an intense scattering peak at d = 35.0 Å with a small shoulder at 27.6 Å and two smaller and broader peaks at d= 6.0 and 5.0 Å (Figure 5a). The larger d value can be associated to the repeating distance of the aggregates. In the case of the xerogel from DCM this peak appears at d = 29.4 Å, and the generally less sharp peaks indicate a less ordered self-assembly (Figure 5b). As shown in Figure 6, the scattering peak at d = 35 Å of the *n*-hexane gel perfectly correlates with the distance of two molecules of **1** arranged head-to-head with

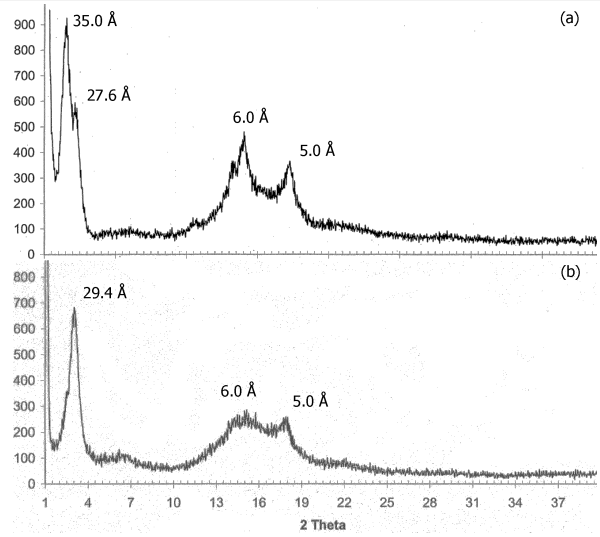

Figure 5: Powder X-ray diffraction pattern of the xerogels of **1** from a) *n*-hexane and b) dichloromethane.

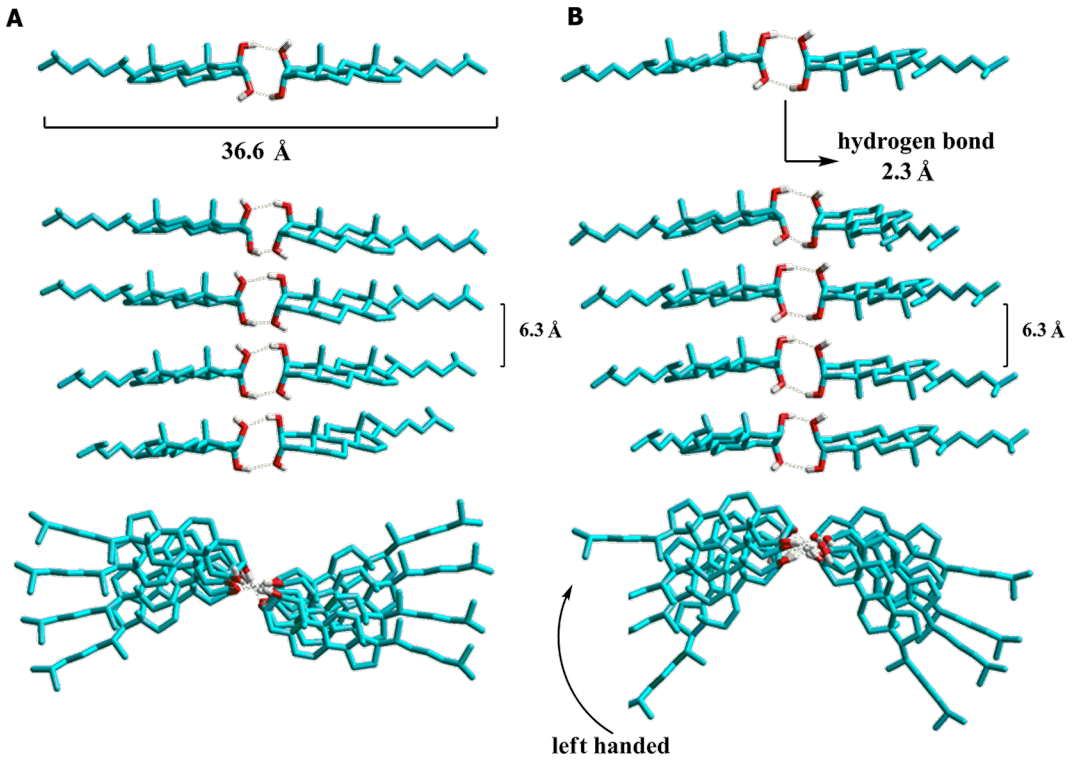

Figure 6: Self-assembly models proposed for LMOG **1**, only the left handed helix is shown, head to head hydrogen bonds are shown in dotted lines, hydrogen atoms have been removed for clarity. System **A**: hydrogen bonds at C2–OH/C2′-OH and C3–OH/C3′–OH; system **B**: C2–OH/C3′–OH and C2′–OH/C3–OH.

completely elongated side chains. Taking this into account the specific molecular packing of gels of **1** may be understood from its molecular structure itself. Steroid **1** is a typical amphiphilic compound in which the dihydroxy moiety defines a hydrophilic head while the rest of the skeleton (tail) is hydrophobic. The amphiphilic property causes molecules to aggregate into structures that avoid the unfavorable head-to-tail contact, and so, head-to-head and tail-to-tail contacts are directing the self-assembly. In more polar solvents such as DCM, the side chain of the steroid is not fully elongated to avoid the interaction of DCM molecules with the polar head. This is evidenced by the shift of *d* from 35.0 Å (*n*-hexane) to 29.4 Å (DCM). On the other hand, the spatial orientation of the hydroxy groups is critical since only steroid **1**, with both hydroxy groups at axial positions, has the ability of a long range self-assembly to promote gelation. To get an insight of the necessary molecular spatial requirements for the 2,3-dihydroxy moiety to reach an optimal hydrogen bonding, we studied the possible mode of self-assembly of the four isomers by a molecular modeling simulation in vacuum (semiempirical AM1).

A conformational study of a single molecule of LMOG **1** (semi-empirical, AM1) showed a distance of 18.0 Å for the molecule with the elongated side chain (Figure 6) suggesting a repetitive unit involving a head-to-head self-assembly between two molecules, as explained above. Next, we minimized different modes of head-to-head interactions and found two possible arrangements with minimal energies. In the first one, both molecules interact with the α faces of the steroids pointing to the same side (Figure 6, system **A**). In the second case the α faces are oriented to opposite sides (Figure 6, system **B**). Both dimers were similar in energy with stabilizations of 9.7 and 10.0 kcal/mol compared to the isolated molecules. This stabilization energy arises from the two intermolecular hydrogen bonds between the hydroxy groups with a H–OH distance of 2.4 Å. We then analyzed the one-dimensional arrangements of the dimers described above by an α- and β-helix self-assembly. We placed the dimers in a way so that the central hydrophilic zones can interact with each other with a distance of 2.7 Å between the hydroxy groups (to allow hydrogen bond interactions) and a rotation angle around the hydrogen bond axis of ±18 degrees (corresponding to left- and right-handed helices, respectively). After minimization, the left handed assemblies were slightly more stable than the right handed, but with no significant differences (0.2–0.3 kcal/mol). For this reason we will only discuss the energy of the left-handed systems. The stabilization energy for each dimer–dimer interface for the β-octamer **A** was 8.1 kcal/mol and for the β-octamer **B** 8.3 kcal/mol. This stabilization between the dimers arises from hydrogen bonding between the dimers with H–OH distances of about 2.8 Å, and van der Waals interactions between the hydrocarbonated skeletons of the steroid.

A structural analysis of the steroids **2**, **3** and **4**, with hydroxy groups at equatorial positions, showed that angles and distances between the hydroxy groups are inadequate to give the intermolecular hydrogen bonding necessary for the one-dimensional self-assembly. These results led to the conclusion that for LMOG **1**, the arrangements proposed are valid modes of self-assembly in agreement with the experimental results. Both, left- and right-handed self-assembled systems, are stable at the conditions of the calculations and this stabilization arises from the multiple hydrogen bonds that are only allowed for the *trans*-diaxial dihydroxy system present in organogelator **1**. As mentioned before, the existence of two clearly differentiated gelation zones in the HSP plot is indicative for a difference in the molecular packing of the gel fibers in non-polar and non-protic polar solvents. In the last case the packing is tight enough to prevent the polar solvent molecules to interact with the polar head of the steroid breaking the hydrogen bonds that lead to the SAFIN.

Templated preparation of silica nanoparticles

Even though LMOG **1** does not gelate tetraethoxysilane (TEOS), in-situ sol–gel polymerization experiments were performed with dioxane and dichloromethane gels containing 16.6% of TEOS with benzylamine as a catalyst. The morphology of the nanostructured silica obtained was analyzed by SEM microscopy (Figure 7). A first polymerization attempt using 3 μL of catalyst and 15 μL of water showed a mixture of amorphous silica with nanotubes in a 3/2 ratio reflecting a partial template polymerization process (Figure 7a). Since high reaction rates usually disfavor the template process for the sol–gel polymerization of TEOS, we decided to slow down the reaction rate by lowering the water concentration and the catalyst load. In the first case (Figure 7b) a highly amorphous material was observed, while lowering the benzylamine load to a third rendered only nanotubes of silica with external diameters between 50 and 175 nm and lengths of several micrometers (Figure 7c,d). Lowering the catalyst load down to a tenth rendered a higher amount of amorphous material. To assess the role of the fibrillar network in the templating process we repeated the experiment under the same conditions, in which nanotubes were obtained, but in absence of gelator. In this case only amorphous silica was observed by SEM microscopy of the product (see Supporting Information File 1), which proves the directing role of the fibers during the polymerization of TEOS. Next we performed the polymerization of TEOS in dichloromethane gels to confirm the helicoidally nature of the fibers by templation. The SEM images of the product obtained showed spherical nanoparticles of irregular size (see Supporting Information File 1). In this solvent the templated sol–gel polymerization failed, but the formation of spherical particles indicates some control effect on the growth of the silica nucleus by the

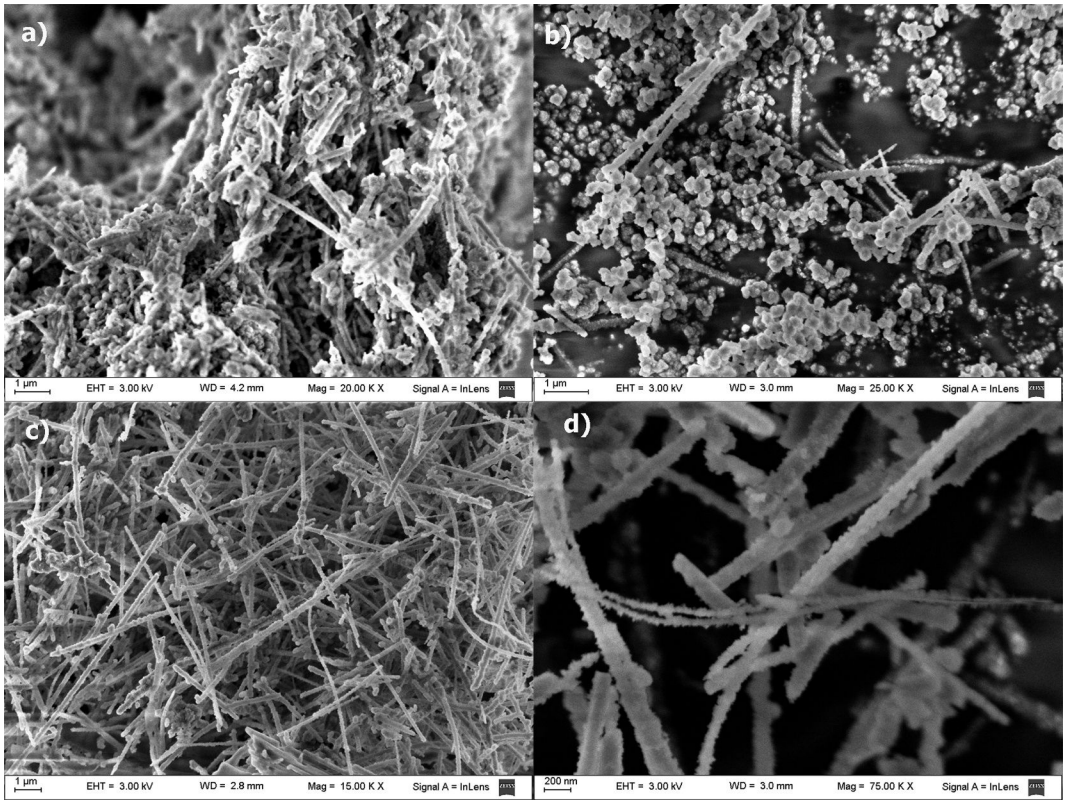

Figure 7: SEM images of nanostructured silica obtained from gels of LMOG **1** under the following conditions: 0.5 mL of dioxane, 0.1 mL TEOS, 35 mg of **1**, and (a) 3 µL of benzylamine and 15 µL of water, (b) 3 µL of benzylamine and 3 µL of water (c,d) 1 µL of benzylamine and 15 µL of water.

fibrillar network of the gel. Tubular nanostructured materials, such as these presented here, may offer alternatives over spherical nanoparticles for some biomedical and biotechnological applications [30,31].

Conclusion

In summary, we have studied the organogelating behavior of the four stereoisomers of the structurally simple 2,3-dihydroxycholestane. The theoretical and experimental results on the four stereoisomers indicate that the *trans*-diaxial orientation of the hydroxy groups on this supramolecular synthon is essential for the gelating property. Only the isomer with the *trans*-diaxial dihydroxy group had the ability to gelate a wide variety of organic solvents and to be a superorganogelator for hydrocarbons with a minimal concentration for gelation of 0.04 wt %. From the analysis of the solvent parameters we conclude that the Hansen solubility parameter (HSP) approach is more suitable to study the solvent–gelation relationship than the solvatochromic Kamlet–Taft scale. The HSP analysis showed two gelating zones indicative of different packing in polar and nonpolar solvents. In contrast to the results obtained by Boutellier et al., it was not possible to define a gelation sphere in either zone, but a qualitative analysis showed that predictions are still possible for this complex system. The FTIR, XRPD, and semi-empirical molecular modeling studies allowed us to propose a packing mode in which the amphiphilic steroid self-assembles in a head-to-head mode through two hydrogen bonds between the dihydroxylic system. The resulting dimers can then form 1D aggregates, in which multiple hydrogen bonding plays an important role together with van der Waals interaction stabilization. In case of polar solvents, capable of hydrogen bond formation, the packing of LMOG **1** is tighter in order to prevent the solvent molecules to interact with the polar head of the steroids, which would break the self-assembled fibrillar network. Finally, the dioxane gel was successfully used as template to grow silica nanotubes through sol–gel polymerization of TEOS under basic catalysis. We conclude that the success of the template on dioxane strongly depends on the catalyst load. Usually the structural motif or element enabling the more efficient transcription for template synthesis of inorganic oxides involves a covalently attached positive charge. For neutral organogelator **1**, electrostatic or hydrogen-bond interactions between the intermediate anionic silicate species and the fibrillar network may be proposed as the only driving force directing the template. Such

nanostructured materials may have biomedical and biotechnological applications that offer alternatives over spherical nanoparticles. Among the solvents gelled by steroid **1**, styrene and methyl acrylate offer great potential in the preparation of mesoporous polymers. We are currently exploring these materials and their potential applications.

Experimental

Materials

Cholesterol (94%) was purchased from Sigma-Aldrich. *n*-Hexane, ethyl acetate, dichloromethane and THF were fractionally distilled, and the remaining solvents were used as supplied by the manufactures.

Methods

Synthesis*:* 2β,3α-dihydroxycholestane (**1**), 2α,3β-dihydroxycholestane(**2**), 2β,3β-dihydroxycholestane(**3**) and 2α,3α-dihydroxycholestane (**4**) were prepared from cholesterol following the procedures described in the literature [27]. The identities of compounds **1**, **3** and **4** were confirmed by comparing the NMR spectra with those found in the literature. ^{13}C NMR spectra of compound **2** did not match the literature data [27,28] and was completely characterized to confirm its identity concluding that the ^{13}C NMR data reported in literature was mistaken (see Supporting Information File 1).

Gelation Tests: The test were carried out in a similar manner as described in [25]. The gelation ability was investigated by a typical test tube experiment. A mixture of a defined amount of gelator and a volume of the solvent (10% wt/v) in a closed flask was heated and shaken until the solid was dissolved and then slowly cooled to room temperature. If a stable gel was observed after inversion of the flask, it was considered a gel (G). When gelation was not observed at room temperature, the sample was cooled at 5 °C. The critical concentration for gelation (CCG) was determined by subsequent dilution of the original organogel followed by a heating–cooling process until gel formation was not observed at room temperature (20 °C)

The reversible gel–sol transition temperatures (T_g) were measured using the classical inverted tube method [32].

Phase-selective gelation experiment: Compound **1** (8 mg) was added to a flask with a mixture of 1 mL of dichloromethane and 1 mL of water, the flask was closed, shaken and heated until the solid was dissolved. Then, the solution was cooled and left at room temperature. After ca.15 min the dichloromethane phase became a gel and the water layer was still fluid.

Xerogel preparation: The preparation was carried out in a similar manner as described in [25]. The xerogels were prepared by cooling the gels in a bath at −90 °C, evaporating the solvent under high vacuum over 6 h and then slowly letting the gels get to room temperature under vacuum.

FTIR measurements: The measurements were carried in a similar manner as described in [25]. Fourier transform infrared (FTIR) measurements of the solution and the gels of **1** were performed on a Nicolet Magna IR 550 FTIR spectrometer in a demountable liquid cell with two NaBr disks, 32 mm in diameter and a 0.5 mm thick Teflon spacer. For the dichloromethane gel, a warm solution of **1** (0.25 wt %) was injected into the cell and allowed to cool down for 10 min at room temperature before measuring the spectra.

X-ray powder diffraction measurements: Diffraction patterns were obtained by using a Siemens D5000 diffractometer with Cu Kα radiation (λ = 1.54056 Å), the stepsize was 0.025° with a measurement time of 6 s per step.

Scanning electron microscopy: SEM measurements were performed in a similar manner as described in [25]. SEM pictures of the xerogel and silica nanoparticles were taken on a Carl Zeiss NTS SUPRA 40FEG scanning electron microscope. A small portion of the solid sample (xerogel or silica) was attached to the holder by using a conductive adhesive carbon tape. Prior to examination the xerogels were coated with a thin layer of gold.

Sol–Gel polymerization of TEOS in dioxane: Compound **1** (35 mg) was dissolved by heating and shaking in dioxane (0.5 mL) and TEOS (0.1 mL) with an addition of benzylamine (0.1–3.0 μL) and water (3–15 μL). The solution was cooled down to room temperature until gelation was observed and then left at room temperature for 6 days. Subsequently, the sample was diluted in dichloromethane, the solid was centrifuged, and washed once with dichloromethane. The silica was heated at 200 °C for 2 h and 600 °C for 4 h in air.

Molecular modeling experiment: These experiments were conducted in a similar manner as described in [25]. The computational experiments were performed with HyperChem 8.0.4, semiempirical optimization, AM1 method in vacuum. Algorithm: Fletcher–Reeves. Termination condition, RMS gradient: 0.05 kcal/(Å·mol). No bond or distance restrictions were imposed. The interaction energies were estimated from the difference between the heats of formation of the different arrangements divided by the number of molecule–molecule interfaces. To have an insight in the stabilization energy of the 1D self-assembled models proposed we carried out the following experiments: Experiment I: an isolated molecule of LMOG **1** was minimized using the above conditions;

$\Delta H_f = -201.46$ kcal/mol. Experiment II: head-to-head dimers of LMOG **1** were minimized, the molecules were placed facing the hydroxy groups at a distance typical for hydrogen bonds: Dimeric system **A**: C2-OH/C2′–OH and C3–OH/C3′–OH; $\Delta H_f = -412.60$ kcal/mol. Dimeric system **B**: C2–OH/C3′–OH and C2′–OH/C3–OH; $\Delta H_f = -412.91$ kcal/mol. Experiment III: four dimers from experiments II were placed in a 1D arrangement facing the α- and β-faces of the steroids with a separation of about 6 Å between the steroid skeleton, and a rotation angle around the hydrogen bond axis of +18° and −18° (α- and β-helix). No bond or distance restrictions were imposed. The right and left handed helix of systems **A** and **B** gave similar heats of formation with no significant differences. Octameric system **A** (left handed helix): $\Delta H_f = -1674.52$ kcal/mol; octameric system **B** (left handed helix): $\Delta H_f = -1676.62$ kcal/mol. The stabilization energy for the head-to-head interaction in each molecule–molecule interface was estimated from the difference between the heats of formation of the dimers and the isolated molecules. The stabilization energy for the dimer–dimer interaction in the one dimensional arrangement interface was estimated from the difference between the heats of formation of the octamers and the dimers.

Supporting Information

Supporting Information features additional experimental data, i.e. characterization data of steroid **2**, SEM images, T_g-vs-concentration plots, FTIR spectra, and HSP plots.

Supporting Information File 1

Additional experimental data.
[http://www.beilstein-journals.org/bjoc/content/supplementary/1860-5397-9-213-S1.pdf]

Acknowledgements

The authors are grateful to ANPCyT (Argentina), CONICET (Argentina) and the University of Buenos Aires for financial support.

References

1. Shahmburo, A.; Biewer, M. C. *Chem. Mater.* **2002,** *14,* 3745–3750. doi:10.1021/cm020421a
2. Llusar, M.; Sanchez, C. *Chem. Mater.* **2008,** *20,* 782–820. doi:10.1021/cm702141e
3. Wang, X.; Zhou, L.; Wang, H.; Luo, Q.; Xu, J.; Liu, J. *J. Colloid Interface Sci.* **2011,** *353,* 412–419. doi:10.1016/j.jcis.2010.09.089
4. Prathap, A.; Sureshman, K. M. *Chem. Commun.* **2012,** *48,* 5250–5252. doi:10.1039/c2cc31631e
5. Shibata, Y.; Kato, T.; Kado, T.; Shiratuchi, R.; Takashima, R.; Kaneto, W.; Hayase, S. *Chem. Commun.* **2003,** 2730–2731. doi:10.1039/b305368g
6. Ajayaghosh, A.; Praveen, V. K.; Vijayakumar, C. *Chem. Soc. Rev.* **2008,** *37,* 109–122. doi:10.1039/b704456a
7. Li, Y.; Liu, J.; Du, G.; Yan, H.; Wang, H.; Zhang, H.; An, W.; Zhao, W.; Sun, T.; Xin, F.; Kong, L.; Li, Y.; Hao, A.; Hao, J. *J. Phys. Chem. B* **2010,** *114,* 10321–10326. doi:10.1021/jp1017373
8. Murata, K.; Aoki, M.; Suzuki, T.; Harada, T.; Kawabata, H.; Komori, T.; Ohseto, F.; Ueda, K.; Shinkai, S. *J. Am. Chem. Soc.* **1994,** *116,* 6664–6676. doi:10.1021/ja00094a023
9. Yu, X.; Liu, Q.; Wu, J.; Zhang, M.; Cao, X.; Zhang, S.; Wang, Q.; Chen, L.; Yi, T. *Chem.–Eur. J.* **2010,** *16,* 9099–9106. doi:10.1002/chem.201000187
10. Maitra, U.; Chakrabarty, A. *Beilstein J. Org. Chem.* **2011,** *7,* 304–309. doi:10.3762/bjoc.7.40
11. Chen, J.; Wu, W.; Mc Neil, A. J. *Chem. Commun.* **2012,** *48,* 7310–7312. doi:10.1039/c2cc33486k
12. Díaz Díaz, D.; Kühbeck, D.; Koopmans, R. J. *Chem. Soc. Rev.* **2011,** *40,* 427–448. doi:10.1039/c005401c
13. Weiss, R. G.; Terech, P. *Molecular Gels: Materials with Self-Assembled Fibrillar Networks;* Springer: The Netherlands, 2006.
14. Desiraju, G. R. *Angew. Chem., Int. Ed. Engl.* **1995,** *34,* 2311–2327. doi:10.1002/anie.199523111
15. Sahoo, P.; Chakraborty, I.; Dastidar, P. *Soft Matter* **2012,** *8,* 2595–2598. doi:10.1039/c2sm06957a
16. Adalder, T. K.; Adarsh, N. N.; Sankolli, R.; Dastidar, P. *Beilstein J. Org. Chem.* **2010,** *6,* 848–858. doi:10.3762/bjoc.6.100
17. Hirst, A. R.; Coates, I. A.; Boucheteau, T. R.; Miravet, J. F.; Escuder, B.; Castelletto, V.; Hamley, I. W.; Smith, D. K. *J. Am. Chem. Soc.* **2008,** *130,* 9113–9121. doi:10.1021/ja801804c
18. Raynal, M.; Bouteiller, L. *Chem. Commun.* **2011,** *47,* 8271–8273. doi:10.1039/c1cc13244j
19. Gao, J.; Wu, S.; Rogers, M. A. *J. Mater. Chem.* **2012,** *22,* 12651–12658. doi:10.1039/c2jm32056h
20. Edwards, W.; Lagadec, C. A.; Smith, D. K. *Soft Matter* **2011,** *7,* 110–117. doi:10.1039/c0sm00843e
21. Löfman, M.; Koivukorpi, J.; Noponen, V.; Salo, H.; Sievänen, E. *J. Colloid Interface Sci.* **2011,** *360,* 633–644. doi:10.1016/j.jcis.2011.04.112
22. Zinic, M.; Vögtle, F.; Fages, F. In *Gelation with Small Molecules;* Fages, F., Ed.; Springer Verlag: Berlin, Germany, 2005; pp 39–63.
23. Lin, Y. C.; Kachar, B.; Weiss, R. G. *J. Am. Chem. Soc.* **1989,** *111,* 5542–5551. doi:10.1021/ja00197a005
24. Svobodová, H.; Noponen, V.; Kolehmainen, E.; Sievänen, E. *RSC Adv.* **2012,** *2,* 4985–5007. doi:10.1039/c2ra01343f
25. Edelsztein, V. C.; Burton, G.; Di Chenna, P. H. *Tetrahedron* **2010,** *66,* 2162–2167. doi:10.1016/j.tet.2010.01.065
26. Edelsztein, V. C.; Jares-Erijman, E. A.; Müllen, K.; Di Chenna, P. H.; Spagnuolo, C. C. *J. Mater. Chem.* **2012,** *22,* 21857–21861. doi:10.1039/c2jm34891h
27. Cruz Silva, M. M.; Riva, S.; Sá e Melo, M. L. *Tetrahedron* **2005,** *61,* 3065–3073. doi:10.1016/j.tet.2005.01.104
28. Jursic, B. S.; Upadhyay, S. K.; Creech, C. C.; Neumann, D. M. *Bioorg. Med. Chem. Lett.* **2010,** *24,* 7372–7375. doi:10.1016/j.bmcl.2010.10.044
29. Kamlet, M. J.; Abboud, J. L. M.; Abraham, M. H.; Taft, R. W. *J. Org. Chem.* **1983,** *48,* 2877–2887. doi:10.1021/jo00165a018
30. Martin, C. R.; Kohli, P. *Nat. Rev. Drug Discovery* **2003,** *2,* 29–37. doi:10.1038/nrd988

31. Bae, S. W.; Tan, W.; Hong, J.-I. *Chem. Commun.* **2012,** *48,* 2270–2282. doi:10.1039/c2cc16306c
32. Raghavan, S. R.; Cipriano, B. H. Gel formation: Phase Diagrams using table top Rheology and Calorimetry. In *Molecular Gels: Materials with Self-Assembled Fibrillar Networks;* Weiss, R. G.; Terech, P., Eds.; Springer Verlag: The Netherlands, 2006.

License and Terms